



University of HUDDERSFIELD

University of Huddersfield Repository

Mohamed, Hamd

Partial Discharge Detection and localization Using Software Defined Radio in the future smart grid

Original Citation

Mohamed, Hamd (2018) Partial Discharge Detection and localization Using Software Defined Radio in the future smart grid. Doctoral thesis, University of Huddersfield.

This version is available at <http://eprints.hud.ac.uk/id/eprint/34801/>

The University Repository is a digital collection of the research output of the University, available on Open Access. Copyright and Moral Rights for the items on this site are retained by the individual author and/or other copyright owners. Users may access full items free of charge; copies of full text items generally can be reproduced, displayed or performed and given to third parties in any format or medium for personal research or study, educational or not-for-profit purposes without prior permission or charge, provided:

- The authors, title and full bibliographic details is credited in any copy;
- A hyperlink and/or URL is included for the original metadata page; and
- The content is not changed in any way.

For more information, including our policy and submission procedure, please contact the Repository Team at: E.mailbox@hud.ac.uk.

<http://eprints.hud.ac.uk/>

Partial Discharge Detection and localization Using Software Defined Radio in the future smart grid

HAMD MOHAMED

A thesis submitted to the University of Huddersfield in partial fulfilment of the requirements
for
the degree of Doctor of Philosophy

The University of Huddersfield
Submission date. February 2018

Copyright statement.

- I. The author of this thesis (including any appendices and/or schedules to this thesis) owns any copyright in it (the “Copyright”) and s/he has given The University of Huddersfield the right to use such copyright for any administrative, promotional, educational and/or teaching purposes.
- II. Copies of this thesis, either in full or in extracts, may be made only in accordance with the regulations of the University Library. Details of these regulations may be obtained from the Librarian. This page must form part of any such copies made.
- III. The ownership of any patents, designs, trademarks and any and all other intellectual property rights except for the Copyright (the “Intellectual Property Rights”) and any reproductions of copyright works, for example graphs and tables (“Reproductions”), which may be described in this thesis, may not be owned by the author and may be owned by third parties. Such Intellectual Property Rights and Reproductions cannot and must not be made available for use without the prior written permission of the owner(s) of the relevant Intellectual Property Rights and/or Reproductions.

DEDICATION

To my parents, my brothers and sisters, my wife, and my son and daughter who supported me incredibly.

Acknowledgements

First of all, all praise and thanks to Allah who endowed me with will, strength, and means to complete this thesis. Without His bounty, grace and mercy this work would have never been accomplished.

I take this opportunity to express my sincere thanks to my supervisor Dr Pavlos Lazaridis. I am deeply grateful for his genuine guidance without his generous help my thesis would not have taken the final shape. I would also like to thank my co-supervisor Prof Ian Glover for his guidance and encouragement over the duration of my research.

Quite naturally I also wish to thank both my Mother and Father, brothers and sisters who instilled in me the belief to pursue my education. I am grateful for the guidance, love and confidence they invested in me.

Special thanks to my Wife without whom this work would not have been possible.

Lastly but not least, I would like to thank all my brothers and sisters back home who supported me throughout my study and many thanks to all my other relatives and friends back home.

Abstract

Partial discharge (PD) occurs if a high voltage is applied to insulation that contains voids. PD is one of the predominant factors to be controlled to ensure reliability and undisrupted functions of power generators, motors, Gas Insulated Switchgear (GIS) and grid connected power distribution equipment. PD can degrade insulation and if left untreated can cause catastrophic insulation failure. However, PD pulse monitoring and detection can save cost and life prior to plant failure. PD is detected using traditional methods such as galvanic contact methods or UHF PD detection methods.

Recently, an alternative method for PD detection and monitoring using wireless technology has become possible. Software Defined Radio has opened new opportunities to detect and monitor PD activity. This research makes use of SDR technology for PD detection and monitoring. The main advantages of SDR technology are that it is cost-effective and it is relatively immune against environmental noise. This is because the noise at electrical power stations is from around a few KHz to a few MHz and this is well below the SDR frequency range and PD frequency band (50-800 MHz). However, noise or interference also exists in the PD frequency band. These interferences are narrow band and mainly from FM, TV broadcasting and mobile telephony signals whose frequencies are well known, thus these interferences can be possibly processed and removed.

In this research two SDR products (Realtek software defined radio RTL-SDR / Universal software radio peripheral USRP N200) are used to detect PD signals emitted by a PD source that was located at a distance of 1 m in case of RTL-SDR device while in case of USRP N200 the PD source was located at a distance of 3 m. These PD signals once received by an SDR device are recorded and processed offline in order to localize the PD source. The detected PD signal was around 20 dB above background noise in case of the RTL-SDR device and 25 dB above background noise in case of using the USRP N200. Selecting the appropriate SDR device depends on factors such as high sensitivity and selectivity. Furthermore, although USRP N200 is more expensive than RTL-SDR dongles, USRP N200 was preferred over RTL-SDR as it demonstrates higher sensitivity and overall better results. PD detection using SDR devices was conducted in the frequency domain. These result were validated using a high-end costly device, i.e. spectrum analyzer. Generally, SDR devices demonstrate satisfactory results when compared to spectrum analyzers. Considering that spectrum analyzers cost around £10,000, while a USRP N200 SRD device costs less than £1000, SDR technology seems to be cost-effective.

Following PD detection, PD localization was performed using USRP N200 results, and a localization algorithm based on Received Signal Strength (RSS) was adopted. The localization result was within a 1.3-meter accuracy and this can be considered as a relatively good result. In addition, and for the purpose of evaluating the proposed scheme, more experiments were conducted using another system that is based on radiometric sensors which is WSN PD system. The estimated error was 1m in case of using the SDR-USRP N200 system and 0.8 m in case of using the WSN PD system. Results of both systems were very satisfactory, although some results at the corners of the detection grid were not good and the error was higher than 3 meters due to the fact that the RSS algorithm performs poorly at corners. These experiments were used to validate both systems for PD detection and localization in industrial environments.

Publications from this research:

1. H. Mohamed, P. Lazaridis, U. Khan, D. Upton, B. Saeed, A. Japer, P. Mather, D. Atkinson, K. Barlee, M. Vieira and I. Glover, "Partial discharge detection using software defined radio" in International Conference for Students on Applied Engineering (ISCAE 2016) IEEE, Newcastle, UK, October 2016, (pp. 373-376).
2. H. Mohamed, P. Lazaridis, U. Khan, D. Upton, B. Saeed, A. Japer, P. Mather, D. Atkinson, K. Barlee, M. Vieira and I. Glover, "Partial discharge detection using low cost RTL-SDR model for wideband spectrum sensing". In 23rd International Conference on Telecommunications (ICT 2016), Thessaloniki, Greece, May 2016 IEEE, (pp. 1-5).
3. H. Mohamed, P. Lazaridis, U. Khan, D. Upton, B. Saeed, A. Japer, P. Mather, D. Atkinson, K. Barlee, M. Vieira and I. Glover, "Partial Discharge Localization Based on Received Signal Strength" in 21st International Conference on Automation and Computing (ICAC 2017), Huddersfield, England, September 2017.
4. H. Mohamed, P. Lazaridis, U. Khan, D. Upton, B. Saeed, A. Japer, P. Mather, D. Atkinson, K. Barlee, M. Vieira and I. Glover, "The use of Software Defined Radio for Partial Discharge and Localization in the future smart grid" in 25th TELFOR conference; Belgrade, Serbia, November 2017.
5. H. Ahmed, P. Lazaridis, U. Khan, D W Upton, P J Mather, Y Zhang, A Jaber, , U Khan, B Saeed, M F Q Vieira, R Atkinson and I A Glover, " Partial Discharge Detection Using Low-cost Real-time Software Defined Radio Technology" in 2015 URSI UK Festival of Radio Science Science Conference, Manchester, UK, 2015, pp. 1-1.
6. H. Ahmed, P. Lazaridis, U. Khan, D W Upton, P J Mather, Y Zhang, A Jaber, , U Khan, B Saeed, M F Q Vieira, R Atkinson and I A Glover, " Partial Discharge Detection Using Medium-cost Software Defined Radio Technology" in 2016 URSI UK Festival of Radio Science Science Conference, Manchester, UK, 2016, pp. 1-1.
7. H. Mohamed, P. Lazaridis, U. Khan, D. Upton, B. Saeed, A. Japer, P. Mather, D. Atkinson, K. Barlee, M. Vieira and I. Glover, "A comparative study Partial Discharge detection using Software Defined Radio" in 26th TELFOR conference; Belgrade, Serbia, November 2018.

Magazine article under review:

1. H. Mohamed, P. Lazaridis, P. Mather, M. Judd, R. Atkinson, M. Vieira and I. Glover, "Partial discharge detection and localization using software defined radio" in IEEE IEM Magazine, May 2018.
2. Umar Khan, Pavlos I Lazaridis, Hamd Mohamed, Ricardo Albarracín, Zaharias D Zaharis, Robert C Atkinson, Christos Tachtatzis, and Ian A Glover, "A comparative study of partial discharge localization in high voltage systems using received signal strength" in Sensors Open access Journal, MDPI.

The author of the thesis also contributed as a co-author on the papers listed below:

1. Y. Zhang, D. Upton, A. Jaber, H. Ahmed, B. Saeed, P. Mather, P. Lazaridis, A. Mopty, C. Tachtatzis, R. Atkinson, M. Judd, M F Q Vieira, and I A Glover, "Radiometric wireless sensor network monitoring of partial discharge sources in electrical substations," International Journal of Distributed Sensor Networks, vol. 2015, p. 179.
2. Y. Zhang, J. M. Neto, D. Upton, A. Jaber, U. Khan, B. Saeed, H. Ahmed, P. Mather, R. Atkinson, J.S. Neto, M.F. Q Vieira, P. Lazaridis and I.A. Glover, "Radiometer monitoring system for artil discharge detection in substation," in Radio Science Conference (URSI AT-RASC), 1st URSI Atlantic Gran Canaria, Spain, 2015, pp. 1-1.
3. Y. Zhang, D. Upton, A. Jaber, U. Khan, B. Saeed, H. Ahmed, P. Mather, R. Atkinson, P. Lazaridis, M.F. Q Vieira and I.A. Glover, "An Ultrawideband Patch Antenna for UHF Detection of Partial Discharge," in Radio Science Conference (URSI AT-RASC), 2015 1st URSI Atlantic, Gran Canaria, Spain, 2015, pp. 1-1.
4. Y. Zhang, D. Upton, A. Jaber, H. Ahmed, U. Khan, B. Saeed, P. Mather, P. Lazaridis, R. Atkinson, M.F. Q Vieira, I.A. Glover, "Multiple source localization for partial discharge monitoring in electrical substation," in Antennas & Propagation Conference (LAPC), Loughborough, UK, 2015, pp. 1-4.
5. D. Upton, B. Saeed, Umar Khan, A. Japer, P. Lazaridis, H. Mohamed, K. Mistry, P. Mather, E. Iorkyase, C.Tachtatzis, M. Judd, D. Atkinson, K. Barlee, M. Vieira and I. Glover "Wireless Sensor Network for Radiometric Detection and Assessment of Partial Discharge in HV Equipment" 32nd URSI GASS, Montreal, 19-26 August 2017.
6. U. Khan, P. Lazaridis, H. Mohamed, D. Upton, B. Saeed, K. Mistry, P. Mather, E. Iorkyase, C.Tachtatzis, M. Judd, D. Atkinson, K. Barlee, M. Vieira and I. Glover"

- Localization of Partial Discharge by Using Received Signal Strength” in Radio Science Conference (URSI AT-RASC), 2018 2nd URSI Atlantic, Gran Canaria, Spain, 2018.
7. D. Upton, B. Saeed, Umar Khan, H. Mohamed, K. Mistry, P. Lazaridis, P. Mather, E. Iorkyase, C.Tachtatzis, M. Judd, D. Atkinson, K. Barlee, M. Vieira and I. Glover “ Low Power High-Speed Folding ADC based Partial Discharge Sensor for Wireless Fault Detection in Substations” in Radio Science Conference (URSI AT-RASC), 2018 2nd URSI Atlantic, Gran Canaria, Spain, 2018.
 8. B. Saeed, D. Upton, Umar Khan, H. Mohamed, K. Mistry, P. Lazaridis, P. Mather, E. Iorkyase, C.Tachtatzis, M. Judd, D. Atkinson, K. Barlee, M. Vieira and I. Glover “ A Supervisory System for Partial Discharge Monitoring “ in Radio Science Conference (URSI AT-RASC), 2018 2nd URSI Atlantic, Gran Canaria, Spain, 2018.
 9. U. Khan, P. Lazaridis, H. Mohamed, D. Upton, B. Saeed, K. Mistry, P. Mather, E. Iorkyase, C.Tachtatzis, M. Judd, D. Atkinson, K. Barlee, M. Vieira and I. Glover “ Received Signal Strength Intensity Based Localization of Partial Discharge in High Voltage Systems “ in Proceedings of the 24th International Conference on Automation & Computing, (ICAC) Newcastle University, Newcastle upon Tyne, UK, 6-7 September 2018.
 10. D W Upton, P J Mather, Y Zhang, A Jaber, H Ahmed, U Khan, B Saeed, M F Q Vieira, R Atkinson and I A Glover, "Signal Conditioning Electronics for UHF Partial Discharge Detection and Location System" in 2014 URSI UK Festival of Radio Science Science Conference, Manchester, UK, 2014, pp. 1-1.

Table of Contents

1	Introduction	1
1.1	Overview	2
1.2	Motivation and Problem Statement	4
1.3	Research aim	7
1.4	Research Objectives	7
1.5	Methodology and Project Design	8
1.6	Original Contributions	8
1.7	Thesis Organization	9
2	Literature view	11
2.1	The smart grid	12
2.2	Partial Discharge	15
2.2.1	PD activity and its mechanism	15
2.2.2	PD activity and electromagnetic wave radiation	16
2.2.3	PD pulse	18
2.2.4	The detection of PD pulses	22
2.2.5	Partial discharge generation and modelling	23
2.2.6	PD classification	23
2.3	Software Defined Radio (SDR)	26
2.3.1	SDR architecture	26
2.3.2	SDR architecture evolution	28
2.3.3	Desktop real time (RTL) Software Defined Radio	28
2.3.4	System requirements for Realtek RTL-SDR hardware	33
2.3.5	RTL-SDR hardware support package and USRP hardware support package	33
2.3.6	Challenges of using SDR on low cost PCs	33
2.3.7	Wireless Sensor Networks	34
2.4	Substation Electromagnetic Environment	35
2.5	Partial Discharge Detection	35
2.5.1	Partial Discharge Detection using Electromagnetic waves	35
2.5.2	Partial discharge detection using wireless technologies	36
2.6	Partial discharge localization	43
2.7	Software Defined Radio (SDR technology)	46
2.8	The research gap	47

3	The description of the system	49
3.1	Introduction.....	50
3.2	The use of Software Defined Radio	50
3.3	Analysis of existing platforms	51
3.3.1	Spectrum analysers	51
3.3.2	SDR devices (Hardware/Software overview).....	52
3.3.3	Summary.....	57
3.4	USRP as a wide band spectrum analyzer	58
3.5	The description of the code	59
3.6	Summary.....	64
4	Partial discharge detection results	65
4.1	Partial discharge detection using SDR technology	66
4.1.1	Partial discharge detection using RTL-SDR dongles	66
4.1.2	Partial discharge detection using USRP N200.....	72
4.2	Partial discharge analysis.....	76
4.2.1	The filtering algorithms.....	76
4.2.2	Median filter	76
4.3	Performance Evaluation.....	82
4.3.1	Limited Sensing Sensitivity	83
4.3.2	Limited Sensing Bandwidth	83
4.3.3	Impact on Sensing Sensitivity	83
4.3.4	Signal and Noise Measurements	83
4.4	Summary.....	84
5	Partial discharge localization based on received signal strength ..85	
5.1	Introduction.....	86
5.2	Received Signal Strength algorithm	87
5.3	RSS Localization algorithm description	89
5.4	The experimental Set-Up.....	94
5.5	The localization results	97
5.6	Summary of the chapter	99
6	Chapter Wireless Sensor Networks WSNs.....	100
6.1	Introduction.....	101
6.2	Wireless Sensor Networks	101

6.3	Requirements for industrial wireless sensor network applications (IWSN).....	101
6.4	PD detection system based on Radiometric sensor	102
6.4.1	PD Radiometer sensor architecture	103
6.5	PD Measurements	107
6.6	Summary.....	111
7	Conclusion and future work.....	112
7.1	Conclusion	113
	The RTL-SDR device.....	114
	The USRP N200.....	115
7.1.1	PD detection using software defined radio	116
7.1.2	PD localization using RSS algorithm.....	117
7.2	Future work.....	118
8	References.....	119
9	Appendices.....	124
	Network mote.....	137
	Preparing the system.....	138
	Installation of SDK Software.....	138
	Establishing connection to the manager and mote.....	140
	Establishing connection to the mote CLI.....	140
	Connecting with the Manager through CLI	146
	Connecting with the manager through API.....	151
	Admin Toolset and Smart Mesh SDK Applications	153
	Admin Toolset	153

List of Figures

Figure 1. Traditional power system (Gellings, 2011)	2
Figure 2. Future smart power system (Gellings, 2011).....	2
Figure 3. PD within Insulation system (Paoletti, 1999).....	4
Figure 4. PD equivalent circuit (Zhang, 2015)	4
Figure 5. Examples of PD activity in HV power system.	5
Figure 6. PD activity and protection activation	6
Figure 7 Smart Grid communication infrastructures (Rahimi & Ipakchi, 2010).....	13
Figure 8 Electric and magnetic field phenomenon of moving charged (Sinaga, 2012) (Sheffield et al., 2010).	17
Figure 9 field patterns and their adjustment (Sinaga, 2012).	17
Figure 10 Pulse modelling by using the Gaussian function from the radiated field strength (Sheffield et al., 2010).	18
Figure11. (a)Typical PD current pulse and (b) Typical signal arising from radiated PD energy (Zhang et al., 2015).	19
Figure 12. A typical PD frequency spectrum: lower trace is a reference in the absence of PD (Zhang et al., 2015)	20
Figure 13. Different Gaussian pulses of different pulse rise times (Sinaga, 2012).....	21
Figure 14. Normalized spectra of Gaussian pulses (Sinaga, 2012).....	21
Figure 15 shows methods of PD detection.....	22
Figure 16. Gemant and Philippoff 's capacitive model (Paoletti, 1999)	23
Figure 17. An example of internal discharge (Sinaga, 2012).	24
Figure 18. The equivalent capacitance circuit.	24
Figure 19 Surface discharge(Sinaga, 2012).	25
Figure 20 Corona discharge	25
Figure 21. SDR architecture.	27
Figure 22. Direct conversion receiver with I/Q sampling (Isomäki, 2004).	28
Figure 23. Block diagram of the RTL-SDR receiver chain (Stewart et al., 2015).....	29
Figure 24. Block diagram show a detailed architecture (Stewart et al., 2015).	30
Figure 25 Structure of the PD location system (He et al., 2011).	37
Figure 26. The physical model (Samat et al., 2012).	38
Figure 27. The equivalent circuit of a void in a solid (Samat et al., 2012).	38
Figure 28. externally mounted RF sensor on a power transformer inspection hatch (Baker et al., 2010).	39
Figure 29. Principles of a RF PD Monitoring System (Baker et al., 2010).	39
Figure 30 Block diagram of PD measurement experiment (Chang et al., 2011).	40
Figure 31 Partial Discharge measurement circuit (Khayam & Vauzia, 2014).....	40
Figure 32. Enhanced bowtie antenna fabricated on a printed circuit board (Muslim et al., 2013).	41
Figure 33 Experimental set up (Muslim et al., 2013).	41
Figure 34. The block diagram of the emulated sensor (Neto et al., 2014).	42
Figure 35. USRP Block diagram.....	52
Figure 36. USRP N200 hardware.	53
Figure 37. Key components of the NooElec NESDR Mini RTL-SDR.....	54
Figure 38. Block diagram of the RTL-SDR receiver chain.	56

Figure 39. The proposed system.	57
Figure 40. Flowchart of USRP N200 for detecting signal energy.....	58
Figure 41. Swept-FFT in spectrum analysis.	61
Figure 42. RTL-SDR dongle connected to the laptop via USB port and PD emulator.	67
Figure 43. Measured spectrum using the dongle for FM band 85-110 MHz.....	67
Figure 44. Measured spectrum using an FSH-8 spectrum analyser for the FM band 85-110 MHz.	68
Figure 45. Measured UHF TV band spectrum using the RTL-SDR 600-700 MHz.	69
Figure 46. Measured UHF TV band Spectrum using FSH-8 spectrum analyzer 600-700 MHz.	69
Figure 47. Measured spectrum using the RTL-SDR dongle in absence of PD.....	70
Figure 48. Measured spectrum using the RTL-SDR dongle in presence of PD.	70
Figure 49. Measured spectrum using a FSV 13.6 GHz R&S Spectrum analyzer in absence of PD.....	71
Figure 50. Measured spectrum using a FSV 13.6 GHz R&S Spectrum analyzer in presence of PD. ..	71
Figure 51. Experimental set up and schematic.....	72
Figure 52. Antenna gain.....	73
Figure 53. The measured spectra using USRP N200 transceiver.	74
Figure 54 The measured spectra using the FSH-8 spectrum analyzer.	74
Figure 55 The measured spectra using USRP transceiver (outside the lab).	76
Figure 56. Flowchart of the median filter implementation.	77
Figure 57. Flowchart of the moving average filter implementation.	78
Figure 58. The output of the median filter.	79
Figure 59. The output of the median filter.	80
Figure 60. The output of the median filter on the noise signal.	81
Figure 61. The output of the moving average filter on the noise signal.	81
Figure 62 The signals after being filtered.	82
Figure 63. The difference between the PD signal and noise in a linear scale.....	82
Figure 64. Flowchart of the RSS localization algorithm.....	89
Figure 65. Experimental setup.	94
Figure 66. The measured spectra using USRP N200 transceiver (outside the lab.)	95
Figure 67. PD signal and noise floor after filtering.	95
Figure 68. PD signal and background noise plus interference after removing TV interference.....	96
Figure 69. The difference between the PD signal and background noise plus interference.	97
Figure 70. PD source localization set-up and results.....	98
Figure 71. PD source localization set-up and results.....	98
Figure 72 PD detection system based on Radiometric sensor.	102
Figure 73. The PD radiometer sensor node block diagram.....	103
Figure 74. RF front end circuit diagram.	103
Figure 75. The supervisory system.	107
Figure 76. PD measurements using two systems. (SDR and radiometric).	108
Figure 77. PD results using SDR system at PD source 1 position.....	108
Figure 78. PD results using radiometric sensor system at PD source 1 position.	109
Figure 79. PD results using SDR system at PD source 2 position.....	110
Figure 80. PD results using radiometric system at PD source 2 position	110

List of tables

Table 1 Specifications of the USRP N200.....	53
Table 2 RTL SDR features.	55
Table 3 comparison of existing sensing solutions.....	57
Table 4 Comparison between the measured spectrum using the spectrum analyser and the RTL-SDR dongle and USRP N200.....	75
Table 5 Power values at the receiver locations (uncalibrated).....	96
Table 6 Comparison of WSN technologies.....	105

A list of Abbreviation

ADC	Analogue to digital Converter.
AES	Advanced Encryption Standard.
ANN	Artificial Neural Network.
AOA	Angle of arrival.
BAN	Business Area Network
BPSK	Binary Phase Shift Keying
CFAR	Constant False Alarm Rate
CMOS	Complementary Metal-Oxide-Semiconductor
COTS	Commercial Off-The Shelf
CWC	Cognitive Wireless Cloud
DAC	Digital to Analogue Converter
DCR	Direct Conversion Receiver
DMS	Distribution Management System
DSI	Discreet Spectral Interference
DSP	Digital Signal Processing
DVB-T	Digital Video Broadcasting- Terrestrial
EM	Electromagnetic
EMS	Energy Management Systems
ERP	Enterprise Resource Planning
FFT	Fats Fourier Transform
FM	Frequency Modulation
FPGA	Field Programmable Gate Array
FDTD	Finite Difference Time Domain
GIS	Gas Insulated Switchgear
GLONASS	Global Orbiting Navigation Satellite System

GSM	Global System Mobile
HAN	Home Area Network
HV	High Voltage
IC	Integrated Circuit
IETF	Internet Engineering Task Force
IWSN	Industrial Wireless Sensor Network
LiNbO3	Lithium Niobate
LOS	Line of Sight
LNA	Low Noise Amplifier
MAC	Medium Access Control
MCX	Micro Coaxial
MME	Maximum and Minimum Value of the Eigenvalue
M-PSK	M-array phase shift keying
NAN	Neighborhood Area Network
NFFT	Number of Fats Fourier Transform
OFDM	Orthogonal Frequency Division Multiple Access
OQPSK	Offset Phase Shift Keying
PD	Partial Discharge
PCB	Printed Circuit Board
PLC	Power Line Communication
QAM	Quadrature Amplitude Modulation
RSS	Received Signal Strength
RBW	Resolution bandwidth
RF	Radio Frequency Signals
RTL-SDR	Realtek Software Defined Radio
SA	Spectrum Analyzer
SDR	Software Defined Radio

SDCR	Software Defined Cognitive Radio
SCADA	Supervisory Control and Data Acquisition
SFDR	Spurious Free Dynamic Range
SNR	Signal to Noise Ratio
TDMA	Time Division Multiple Access
TDOA	Time Difference of Arrival
TOA	Time of Arrival
TV	Television
UHD USRP	Hardware Driver
UHF	Ultra High Frequency
USB	Universal Serial Bus
USRP	Universal Software Radio Peripheral
VHF	Very High Frequency
WAN	Wide Area Network
WSN	Wireless Sensor Networks
WiMAX	Worldwide Interoperability for Microwave Access
Wi-Fi	Wireless Fidelity
WirelessHART	Highway addressable remote transduce protocol
WPAN	Wireless Personal Area Network
W-CDMA	Wideband Code Division Multiple Access

1 Introduction

Power failure in electrical power stations can be caused by many reasons, one of these reasons is partial discharge. Hence partial discharge detection is of great significance in electrical power stations. This chapter introduces partial discharge and clarifies the problem, then states the research aims and objectives in addition to the original contribution including published papers. Finally, the thesis organization is described.

1.1 Overview

Smart grid is the term used to describe the next generation power grid in which the management of electricity distribution is enhanced by advanced two-way communications, so that it monitors, protects, and takes decisions automatically to optimize the operation of its interconnected elements. The present electric power delivery infrastructure cannot provide such advantages effectively. The smart grid consists of large-scale and small-scale distributed generation which is connected by high voltage HV network of transmission lines. As can be seen from Figure 1, the flow of power in the traditional power system distribution is principally in one direction.

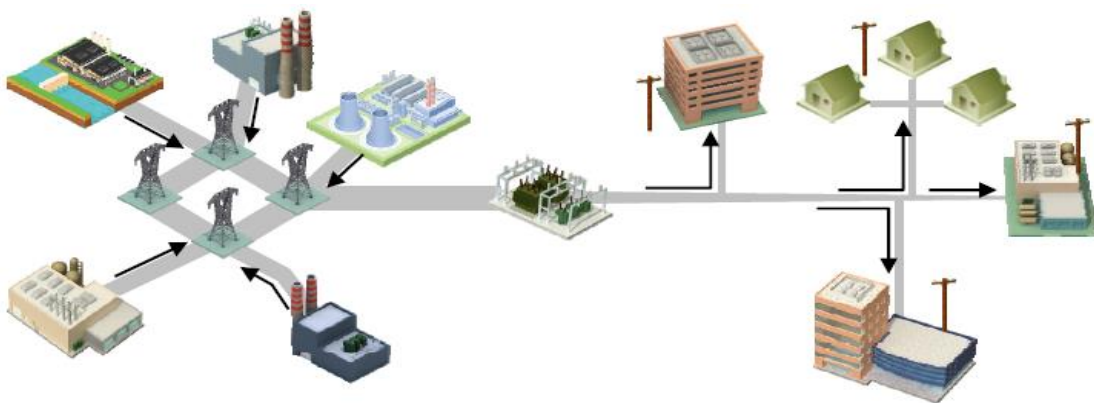


Figure 1. Traditional power system (Gellings, 2011).

Figure 2 shows that in the smart grid, the direction of power flow may be in either direction. The smart grid does not depend only on the support of large central-station generation but incorporates significant electric energy storage and distributed energy generation.

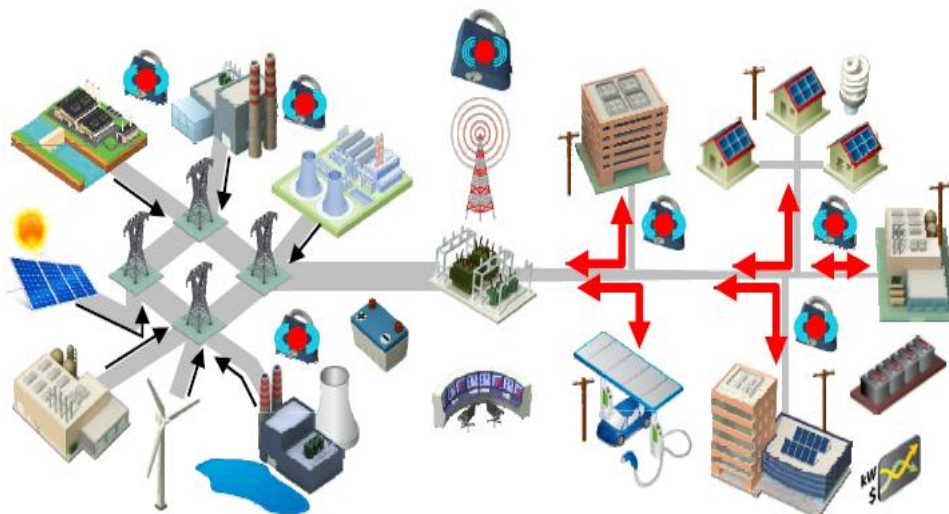


Figure 2. Future smart power system (Gellings, 2011).

The smart grid communication infrastructure can be supported by several technologies, e.g. WiMAX, power line carrier, traditional twisted-copper phone line, microwave radio relay, satellite, cellular, fiber optic cable, as well as the short range technologies such as Wi-Fi, ZigBee and Wireless HART.

In order to add intelligence to the current power system, a smarter asset monitoring infrastructure is required. Wireless sensor networks have made it possible to monitor, measure, and detect changes in physical phenomena in electric power systems. One important such phenomenon is partial discharges (PD). IEC 60270 defined Partial Discharge as a localized electrical discharge that only partially bridges the insulation between conductors and which can or cannot occur adjacent to a conductor. PD can be stated as an electrical discharge or the pulse generated in a dielectric solid or liquid insulation system. The failures caused due to electrical insulation are one of the vital and generic reasons of unexpected disruption in power systems and associated electrical machineries and power cables. In general, the power generation, transmission and distribution are the most expensive electrical assets in HV power systems, which are subjected to numerous electrical, thermal, environmental and mechanical stresses (IEC, 2000). Among them, the PD issues are the most general and common cause leading to power system failure. PD can also degrade other associated functional components. Especially, in the HV system, a number of materials such as, liquid, solid, and gaseous materials are employed to insulate certain components in HV power environment. PD within insulation system and its equivalent circuit are shown in figure 3 and figure 4 respectively.

PD in electrical systems indicates the presence of foreign material inside insulation. The majority of insulating materials are not perfect and often comprise impurities such as air bubbles that cause local weak zones inside the insulator. So PD occurs if a HV was applied on two materials with different permittivity (or dielectric constant) are subject to a voltage, the electric field is greatest in the region of smallest permittivity. In this region, electrical breakdown is possible to occur and not elsewhere. PD events thus weaken and degrade the insulation capability of HV power equipment due to the cumulative effect of electrical, chemical and thermal stress (IEC-TS, 2016). Because of the HV stress, the insulator (mainly the weak zone inside the insulator) causes PD and the insulation properties of such materials is enormously degraded. Hence power system reliability is reduced. In fact, the quality of insulation has a very significant impact on HV power equipment reliability (Zhang et al., 2015).

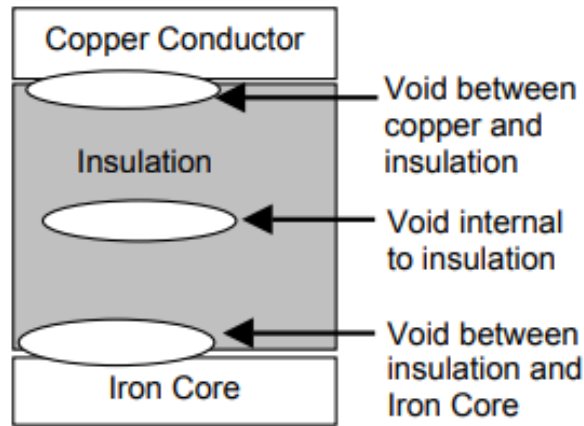


Figure 3. PD within Insulation system (Paoletti, 1999).

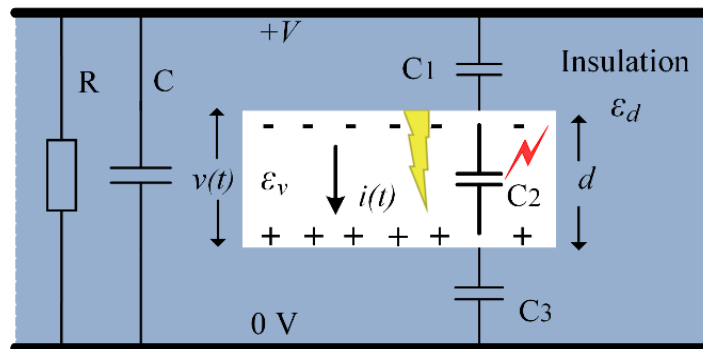


Figure 4. PD equivalent circuit (Zhang, 2015).

1.2 Motivation and Problem Statement

Partial discharges occur due to degradation in the dielectric insulation surrounding the plant equipment. These defects may occur during its operational lifetime or may be present during the manufacturing process, and can increase in both intensity and frequency, eventually leading to internal arcing which in some cases can lead to loss of the asset. It is observed that with the increase in applied voltage the PD activity also increases, (Zhang et al., 2015) (Karmakar, 2012). PD activity in a cable depends upon applied voltage, dielectric constant of material and size of the void. These are considered as the main factors affecting partial discharge in transformer components and distribution systems.

In general, partial discharge detection and efficient monitoring can play a significant role in the ongoing maintenance of high-voltage plants and power generation systems. Because of the increased regulatory and operational requirements and the large capital value of equipment, the need for efficient condition monitoring systems has become an inevitable need so as to avoid

power equipment failure. Figure 5 shows an example of PD activity in electrical power plants and Figure 6 shows the PD activity and when protection should be activated.

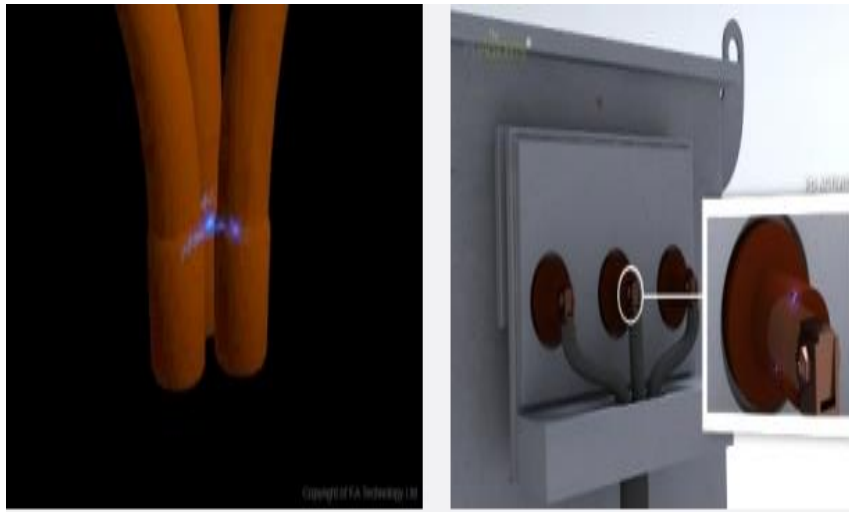


Figure 5. Examples of PD activity in HV power system.

There are a number of sensing devices available for spectrum sensing. Some of the solutions, like spectrum analysers are capable of scanning a wide spectrum range, but are too costly. A spectrum analyser can not perform continuous recording for a time period more than a few seconds, and furthermore, the recorded spectrum requires higher frequency resolution for better visualization. On the other hand, low-cost spectrum analysers are trimmed for simple and steady recording but are deficient of the flexibility and expected performance, which confines their efficiency to obtain the seamless spectrum sensing for partial discharge and possess non-configurable frequency span and resolution bandwidth. The predominant requirement for spectrum sensing and assessment in frequency spectrum sensing are reliability, flexibility, continuous recording capability. Energy per channel is the expected output format; a very good frequency resolution is not usually required. In order to facilitate the cooperative or distributed spectrum sensing, the measurement must be accomplished with a relatively low-cost sensing platform. Recently, Realtek RTL2832U demodulator based low-cost USB digital TV tuners have attracted radio scientists and researchers to SDR. In this work, it has been intended to achieve a low cost spectrum sensing platform based on multiple SDR devices (i.e. USRPs and RTL-SDRs) for wideband spectrum sensing utilities. Compared to traditional hardware implementations, SDR gives the possibility of implementing various radios on the same hardware, or changing the configuration by adjusting software parameters. Thus, it can be significant for sensing to alter the resolution bandwidth and MaxHold settings.

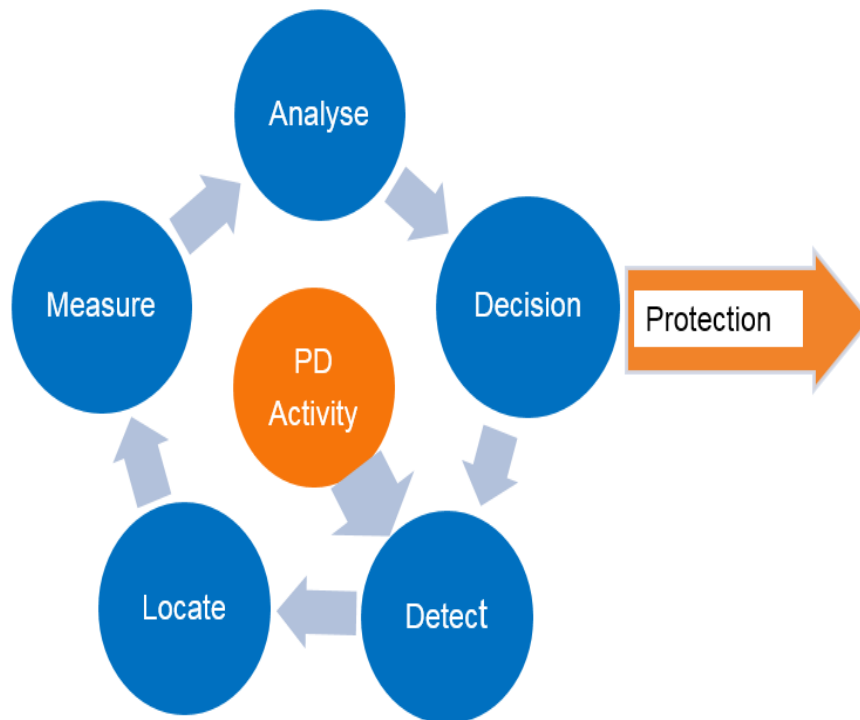


Figure 6. PD activity and protection activation.

The predominant requirement for spectrum sensing and assessment in frequency spectrum sensing are reliability, flexibility, continuous recording capability. Energy per channel is the expected output format; a very good frequency resolution is not usually required. In order to facilitate the cooperative or distributed spectrum sensing, the measurement must be accomplished with a relatively low-cost sensing platform. Recently, Realtek RTL2832U demodulator based low-cost USB digital TV tuners have attracted radio scientists and researchers to SDR. In this work, it has been intended to achieve a low cost spectrum sensing platform based on multiple SDR devices (i.e. USRPs and RTL-SDRs) for wideband spectrum sensing utilities. Compared to traditional hardware implementations, SDR gives the possibility of implementing various radios on the same hardware, or changing the configuration by adjusting software parameters. Thus, it can be significant for sensing to alter the resolution bandwidth and MaxHold settings. In this study a MATLAB based simulation framework has been developed that provides the feasibility to alter the resolution bandwidth and MaxHold settings and to achieve optimal accuracy and efficiency for wideband spectrum sensing (H Mohamed et al., 2016b). The work reported here considers the use of recently developed, low-cost, Software Defined Radio (SDR) technology configured as a spectrum analyser to measure

the radio power spectral density across the frequency band that PD energy might be expected to reside. The study has been conducted using the USRP N200 and the RTL-SDR dongle which is an SDR device designed primarily as a DVB-T tuner. The device uses RTL2832 ICs and has been configured to function as a radio scanner. The RTL-SDR receiver employs a Realtek RTL2832 quadrature sampling detector and a programmable frequency oscillator. It has a frequency range of 25 MHz to 1.75 GHz. The maximum sampling rate at the output of the decimator is 2.8MHz (H Mohamed et al., 2016b).

1.3 Research aim

To develop a robust and efficient partial discharge detection system based on SDR technology for efficient power system monitoring and control.

1.4 Research Objectives

Taking into consideration of the significance of partial discharge detection using low cost devices, in this research work certain objectives have been defined.

Some of the predominant objectives are given as follows:

1. To study the popular condition monitoring techniques and select the most appropriate technique for PD detection and monitoring.
2. To investigate the fundamental design and implementation of SDR systems.
3. To learn about the core components of an SDR system, and how Digital Signal Processing DSP and Physical PHY layer algorithms allow signals to be extracted and received.
4. To be able to design and run, MATLAB code and Simulink models, and work with associated toolboxes and support packages.
5. To develop an efficient remote monitoring and control mechanism for partial discharge detection at ultra-high frequency (UHF).
6. To validate the PD detection results with high end spectrum analyzers.
7. To develop a highly robust, efficient and low cost partial discharge detector for power system reliability and effective monitoring.
8. To develop a MATLAB based software interface model/algorithm to change spectrum sensing parameters so as to examine the variations of the resolution bandwidth, MaxHold and sampling parameters on the detection efficiency of the proposed RTL SDR based PD detector.

9. To develop an algorithm for PD source localization.
10. To make a comparison test between SDR technology and WSN systems for PD detection and localization.

Here, the prime objective of the proposed research work is to propose and develop such a low cost system that can enable reliable, efficient and cost effective solution for spectrum analysis and precise partial discharge detection and localization.

1.5 Methodology and Project Design

The project plans to explore the possibility of Partial Discharge detection and localization in the future smart grid. The project will make use of Software Defined Radio in order to compare and contrast various algorithms and protocols and their impact on power consumption.

Based on the experimental results using SDR, the project will contrast and analyse whether the approach would be the best fit for partial discharge detection in the future smart grid. The methodology used can be summarised as:

1. Partial discharge detection requirements will be established using the existing literature.
2. Investigation on Software Defined Radio and how to employ it for partial discharge detection.
3. A suitable hardware system for partial discharge detection will be identified and/or developed.
4. Analytical and/or numerical models of the software defined radio will be used to investigate relative performance of candidate SDR products.
5. A small number of candidate technologies will be selected for detailed practical work.
6. The configuration of selected products will be optimized using analytical and/or numerical modelling for a range of partial discharge detection constraints.
7. The results will be validated using well know approaches for partial discharge detection.

1.6 Original Contributions

This research contributes in the field of PD detection and localization and the use of SDR technology in the following aspects:

- 1- Provides a detailed description on how the SDR technology was used and developed for the purpose of PD detection (Chapter 3).
- 2- Implements and optimizes PD detection using SDR technology which varies from medium to low cost. Validates the results by a comparison to high end spectrum analyzer (Chapter4).
- 3- Employs an RSS algorithm for PD localization using SDR technology (Chapter 5)
- 4- It opens the opportunity for the researcher to use a very inexpensive device (RTL-SDR devices).
- 5- Performs experimental tests in order to examine the SDR system performance in a real environment. Compares it to different technologies. The SDR system has been compared to WSN system (Chapter 6).

1.7 Thesis Organization

Chapter 1

In the introduction PD is defined, introduced, analyzed and classified and the problem statement is clarified. Then it states the research aims and objectives in addition to the original contributions including published papers and ends with the thesis organization description.

Chapter2

This chapter firstly reviews the partial discharge activity and its mechanism in addition to the PD pulse shapes and PD classification, then discusses some of the predominant researches performed for partial discharge (PD) detection and localization where various techniques employed for PD detection and localization with their respective strengths and limitations are discussed.

This chapter also presents a number of electromagnetic (EM) approaches that have been proposed for partial discharge detection and monitoring in HV infrastructure. These approaches which have been proposed and demonstrated in the last and recent years are described and discussed.

Chapter 3

In this chapter a detailed description of software defined radio is presented and then the use of Software Defined Radio (SDR) technology for PD detection and localization is proposed. The proposed technology is compared to high end spectrum analyzers. The comparison shows that

SDR technology is a promising technology when considering the cost, flexibility, availability, portability and the ease of use. Then, the MATLAB PD detection algorithm is explained and analyzed.

Chapter4

In this chapter PD detection is introduced and discussed. Initially, a portable spectrum analyzer has been used for PD detection that was later replaced by USRP N200 and an RTL-SDR device. Then a comparison is made. The proposed schemes exhibit promising results for spectral detection within the VHF and UHF bands.

Chapter5

This chapter gives an introduction to PD detection and localization using SDR technology then presents the received signal strength (RSS) algorithm followed by a description to another location algorithm by means of a flowchart. Also the experimental set-up is presented. At the end the localization results for the PD industrial are demonstrated and discussed. Considering the noisy environment and the simplicity of the system, the estimation error obtained by the selected localization system is acceptable.

Chapter6

This chapter compares experimental results obtained using a radiometric PD detection system with results that were obtained using the SDR system. Both systems make use of the received signal strength (RSS) algorithm and this chapter concludes with a summary comparing different technologies.

Chapter 7

This chapter concludes the whole work and reviews the achievements of the project against the aims and objectives. It also provides the contributions to knowledge made by the work and suggests some possible further work.

2 Literature view

Being an important part of the condition monitoring in electrical power stations, partial discharge detection plays a vital role in saving costs of equipment and people life. Partial discharge if left untreated can cause a degradation of the insulation material until power failure occurs, which can be a catastrophic. This chapter primarily discusses some of the predominant researches performed for partial discharge (PD) detection and localization where various techniques have been employed and their respective strengths and limitations are discussed. A number of electromagnetic (EM) approaches have been proposed for partial discharge detection and monitoring in HV infrastructure. These approaches are described and discussed in this chapter.

2.1 The smart grid

Today's households are already host to industrial and smart home appliances, which can detect energy consumption increases. Consumers nonetheless, can be advised to adjust their usage in order to cut back on costs, such as by using renewable energy and avoid consuming energy on peak hours. Conventional carbon fuel-based power plants work together with developing distributed renewable energy resources such as wind and solar energy. Renewable resources lessen the consumption of carbon fuel and subsequent emissions of greenhouse gases.

An essential component of the smart grid is an accessible and universal communication infrastructure. The improvement in performance, reliability, security and economy that a smart grid enjoys over a conventional grid relies on and derives from its communication infrastructure. This chapter describes the communication infrastructures in a smart grid and the prerequisites of that infrastructure.

Smart grid refers to the next generation power grid with upgraded electricity distribution and management. The smart grid is made possible by combining two-way communications and computing capabilities, to enhance control, efficiency, reliability, and safety. Using two-way digital technologies, a smart grid can transport electricity between suppliers and consumers. Such technology allows consumers to save energy, reduce cost and increase their smart appliances' efficiency, reliability and transparency (Energy, Feb 2012).

The smart grid provides control, protection and automatic optimization to operate its interconnected elements effectively and efficiently. The smart grid technology ranges from traditional central generator and/or emerging renewal distributed generator, which reflects transmission network and distribution system through industrial consumers to domestic users with their thermostats, electric vehicles, and intelligent appliances (Rahimi & Ipakchi, 2010). Bi-directional connection of electricity and information flows characterizes a smart grid. The information flows establish an automatic and widely distributed delivery network. Through these, the benefits of real-time information enables the near-instantaneous balancing/management of supply and demand (U.S. Department of Energy). Smart grid communication technologies can be grouped into five areas, namely: advanced components, sensing and measurement, improved interfaces and decision support, standards and groups, and integrated communications.

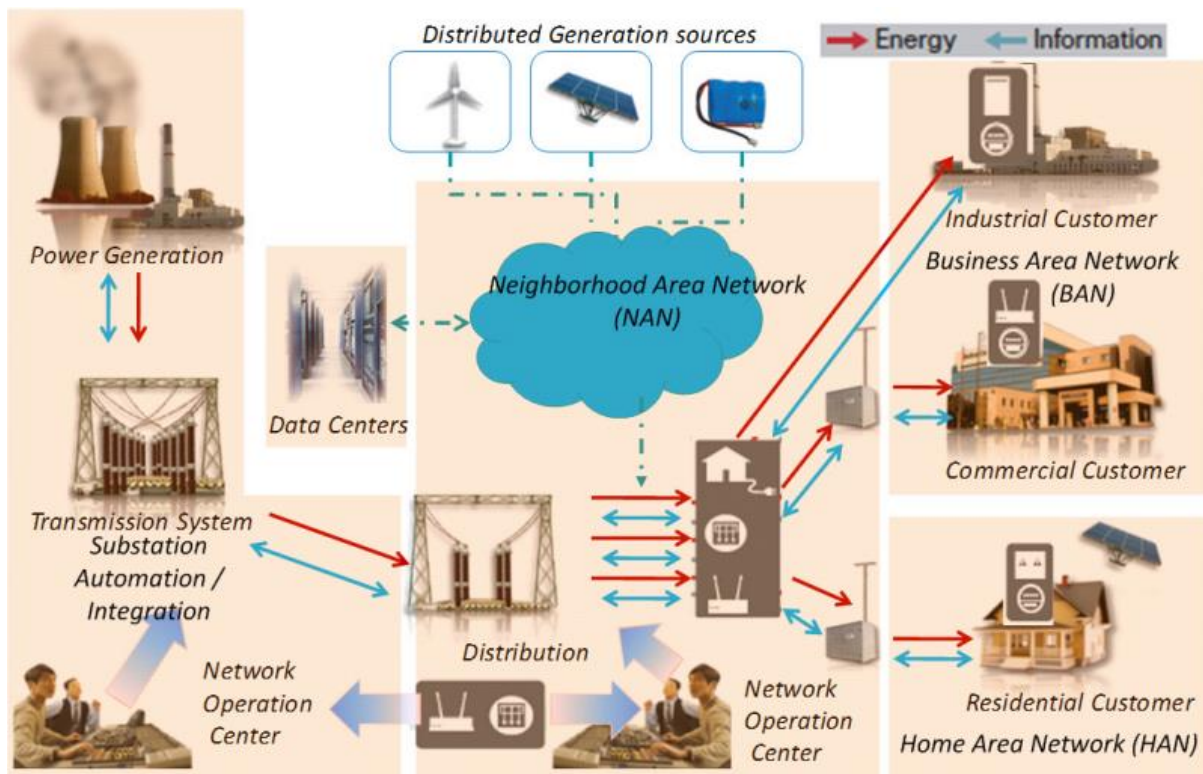


Figure 7. Smart Grid communication infrastructures (Rahimi & Ipakchi, 2010).

Figure 7 is an illustration of smart grid communications infrastructures. It is divided into home area networks (HANs), business area networks (BANs), and neighborhood area networks (NANs), data centres, and substation automation integration systems (Yu et al., 2011). Smart grids distribute electricity between generators and end users. The generators refer to both the traditional power generation and distributed generation sources, while the end users are the industrial, commercial and residential consumers. The distribution is made possible through bi-directional information flow, which will control the consumers' smart appliances and allow them to save on energy consumption and reduce costs, while increasing the system reliability and operation transparency. The network operation centre retrieves customer power usage data and online market pricing from data centers to facilitate optimization of electricity generation and distribution based on energy consumption.

Through extensive deployment of new smart grid components, convergence of existing information and control technologies applied in the legacy power grid, the complex smart grid system can offer sustainable operations to both customers and utilities (Yu et al., 2011). The efficiency of legacy power generation, transmission and distribution systems is enhanced and the usage of clean renewable energy is increased.

The smart grid has the ability for multiple entities to interact through a communication infrastructure. These multiple entities include intelligent devices, dedicated software, processes, control centers, and many others. Consequently, critical issues are also present in the structure and operation of smart grid communication systems, prior to the development of a pervasive and reliable communication infrastructure (Vaccaro & Villacci, 2005), (Baigent, Adamiak, Mackiewicz, & SISCO, 2004). This emphasizes the need to develop a reliable communication infrastructure as a strategic requirement to support the process. Such infrastructure will aid the establishment of robust real-time data transportation through the Wide Area Networks (WANs) to the distribution feeder and customer level (Cupp & Beehler, 2008).

Meanwhile, the present existing electrical utility WANs are adopted from hybrid communication technologies that include wired technologies, such as fiber optics, power line communication (PLC) systems, copper-wire lines, and a variety of wireless technologies (Ghassemi, Bavarian, & Lampe, 2010). These technologies are structured to support some monitoring or controlling applications as Supervisory Control and Data Acquisition (SCADA)/Energy Management Systems (EMS), Distribution Management Systems (DMS), Enterprise Resource Planning (ERP) systems, generation plant automation, distribution feeder automation and physical security for facilities in wide range areas with very limited bandwidth and capacity in closed networks.

Several applications on the smart grid have developed from decades of wireless sensor networks research. One of these smart grid applications is energy metering. However, sensor networks were precluded from interoperating with the Internet because of the lack of IP-based network architecture. This limits the real world impacts of the sensor networks. To address this, the wireless personal area network WPAN and routing over low power and lossy networks ROLL working groups were chartered by the Internet Engineering Task Force (IETF) in order to stipulate the standards at several protocols stack layers, with the aim of connecting low-power devices to the Internet. These standards, as proposed by the mentioned working group are presented in (Ko et al., 2011), along with the description of how the research community actively participated in the process, through influencing their design and providing open source implementations.

The current communication infrastructure should develop and advance towards nearly universal data transport networks. These data transport networks must have the capacity to

handle power delivery applications, together with large amounts of new data from the smart grid applications. Also, these networks should be accessible and highly pervasive, so that the current and present set of emerging smart grid communication technological functions and platforms, along with the deployment of last-mile communications will be supported (Madani, Vaccaro, Villacci, & King, 2007). These are described below.

2.2 Partial Discharge

(EA Technology) defines and describes PD as 'a discharge that does not completely bridge the space between the conductors causing it. It occurs in power systems insulation that is inhomogeneous in dielectric constant due, for example, to voids or cracks in solid insulation and gas bubbles or particulate contaminants in oil insulation'.

PD can lead to insulation failure which in return will cause catastrophic power failure. The detection of PD current pulses, however, can allow incipient insulation faults to be identified, located and repaired prior to plant failure. Traditionally PD is detected using galvanic contact methods or sensors that use capacitive/inductive coupling (IEC-TS, 2016). Recently, however, the use of wireless technology has provided an alternative method to detect and monitor PD. Wireless reception of PD energy has, until now, involved receiving the radiated broadband signals using a broadband receiver. The emergence of wireless network technology and software defined radio has opened new opportunities in PD monitoring.

The term PD as defined earlier refers to an electrical discharge that only partially bridges the insulations between conductors. Discharge can be of various types including internal, external or surface discharge. The discharge can also be of different natures varying from small to extensive. An extensive discharge will cause full breakdown. As a consequence of continuous and extensive PD activity in HV systems, a breakdown can take place.

2.2.1 PD activity and its mechanism

Two main categories of PD activity include the Townsend discharge and streamer discharge. Townsend discharge represents the PD activity where the increase in ionization results in an increase of gap current. Townsend emission occurs due to cathode discharge (F. H. Kreuger, 1989) (Bartnikas, 2002). There are various types of pulses that occur due to Townsend discharge including glow, true and pseudo glow pulses. Rise time and duration of all these PD

pulses can range from a hundred to several thousands of nanoseconds. This means that PD pulse duration ranges from nanoseconds to microseconds (F. Kreuger, 1991).

The steamer discharge in contrast to Townsend discharge is independent of cathode discharge. It depends on the process of photoionisation of the gas atoms in the HV transformers and systems. It occurs in a high field region and this requires larger gaps in contrast to the Townsend discharge that can occur in smaller gaps (Bartnikas, 2002).

Whether it is Townsend or steamer discharges, they both represent PD activity. Thus a PD pulse is a current or a voltage pulse that lasts in the range of nanoseconds and has risen and fall times that can vary. For detection of such pulses, modern equipment is used that mainly measures such pulses periodically, although progress has been made in recent times to detect them autonomously (Kuffel & Kuffel, 2000). PD activity leads to the generation of radio waves, i.e. electromagnetic waves that have a frequency range from 20 MHz to 1GHz. The next section will focus on PD activity and the generation of electromagnetic waves from it.

2.2.2 PD activity and electromagnetic wave radiation

A PD activity takes place as a result of movement of free electrons that are accelerated due to an external force. At the same time a change in external force will cause deceleration as well. As a result of accelerating and decelerating of free electrons that were at rest initially, a time varying electric field is produced. The production of the electric field results in the emission of electromagnetic radiations from the location of PD source (Sheffield, Froula, Glenzer, & Luhmann Jr, 2010) (Lonngren, Savov, & Jost, 2007).

If a charge remains stationary, it will possess an electric field that is radiated only radially. A moving charge will have both electric and magnetic fields. The strength of electric field depends upon the distance between the observer and the radial displacement. The equation below can be used to calculate the electric field strength of a moving charge when a partial discharge (PD) activity occurs (Sinaga, 2012).

$$E = \frac{Q}{4\pi\epsilon R^2} \quad (2.1)$$

Where Q is the total moving charge and R is the total displacement from the observer. ϵ is the permittivity of free space and has a fixed value. Electrical field strength is a vector.

On the other hand side, the magnetic field strength can be expressed by using the equation 2.2 (Sinaga, 2012):

$$B = \frac{\mu_0 Qc}{4\pi\epsilon R^2} \quad (2.2)$$

Where μ is the permeability of free space and again has a fixed value. c is the speed of light i.e. 2.99×10^8 m/s

The electric and magnetic field phenomenon can be understood if we assume that the charge Q initially at rest is moving towards the direction x as shown in the figure below.

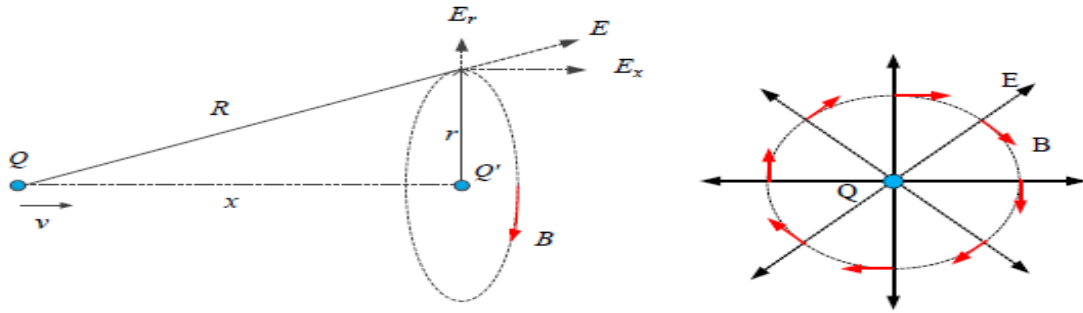


Figure 8. Electric and magnetic field phenomenon of moving charged (Sinaga, 2012). (Sheffield et al., 2010).

The Figure above shows that the electric field is radial. From the position of the charge when it is moving with a velocity at a speed of light, the field is radial and both fields are at right angles to each other lines. Lines of the electric field will always update their position depending upon the acceleration or deceleration they will come under. The electric field lines will be misaligned because they will require time to adjust (Lonngren et al., 2007). This can be seen in the Figure 9.

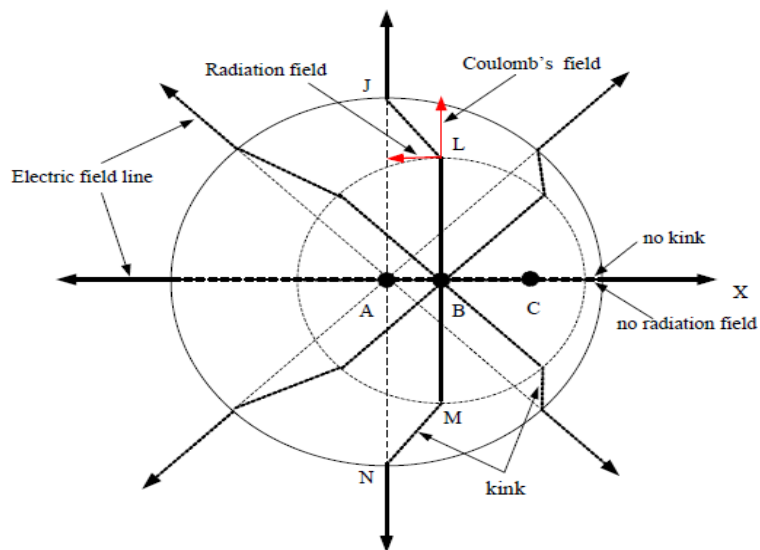


Figure 9. field patterns and their adjustment (Sinaga, 2012).

The previous figure illustrates electric and magnetic field patterns and how both fields are aligned with respect to each other. From the next figure, it is clear that when charges accelerate, electric field line updates themselves. Due to time requirements for electric field line adjustments, the misalignment between electric field lines takes place (Lonngren et al., 2007). The process is termed as kink as shown in figure 9 above. The acceleration and the maximum field are transverse to each other since the kink has both electric and magnetic field patterns that are transverse. To model the pulse from the radiated field, the Gaussian function can be utilised. The figure below shows the pulse modelled by using the Gaussian function.

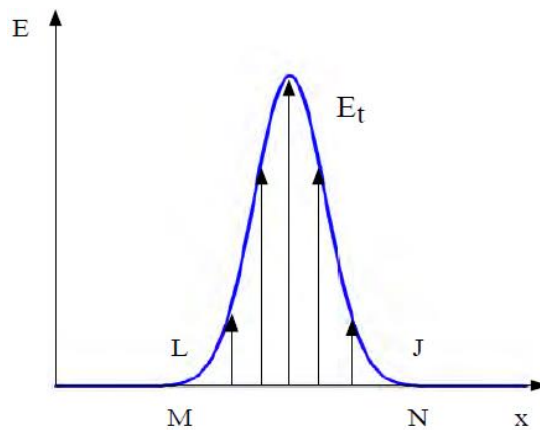


Figure 10 Pulse modelling by using the Gaussian function from the radiated field strength (Sheffield et al., 2010).

The figure above shows how a PD pulse can be modelled from the radiated field strength by using the Gaussian function. The radiated field points are from M-N and L-J.

2.2.3 PD pulse

The generation of PD pulse as mentioned above is based on the transverse electric field and Coulomb component that is based on the kink. The characteristics of partial discharge are based on key variables. Key variables include the type of the discharge source, i.e. HV transformer or any other material and location of the PD source within the HV system, e.g. surface or corona discharge. Also, the discharge has the key variable that is based on the type of sensor used for the detection system, due to the frequency range of the PD activity, it is imperative to use the detection sensors that operate within the entire bandwidth. Over the entire bandwidth, the PD activity may remain there but have different pulse characteristics depending upon the type of discharge (Agoris, 2009). For various discharge types, the rise and fall time will vary. For example in a GIS rise time will be shorter whereas, if a discharge occurs in a transformer oil,

the rise time will be longer due to the higher permittivity value of the oil (M. Judd & Farish, 1998).

The type of PD source and the electromagnetic medium where the waves propagate play a vital role in determining the PD pulse characteristics. For a free metallic discharge, the rise time of a PD pulse will be around 3ns. In contrast the rise time from a transformer oil will be around 20ns, which is a lot longer than that of metallic discharge (M. Judd & Farish, 1998) .

Within HV systems and transformers, PD signals are produced and propagated inside the systems and reflected or refracted the medium as well as the components of the HV systems including transformers. PD signals are electromagnetic signals in nature and are captured using a measuring unit connected to sensors. The recording of PD signals can be conducted in either the time domain or in the frequency domain (Bartnikas, 2002).

In the time domain PD signals are recorded with the use of an oscilloscope. The shape of PD signal in the time domain consists of the magnitude versus time over the entire band.

In the frequency domain PD signals are recorded using spectrum analyzer (SA). The PD spectrum consists of magnitude versus frequency.

PD pulse shape depends upon the source where the pulses are generated. For various types of sources, there will be varying PD pulse shapes. The pulse duration can vary from 10ns to 100ns depending upon the source of PD (Reid, Judd, Stewart, & Fouracre, 2006). Figure 11 shows the typical PD current pulse and typical signal arising from radiated PD energy. Figure 12 shows a typical PD frequency spectrum.

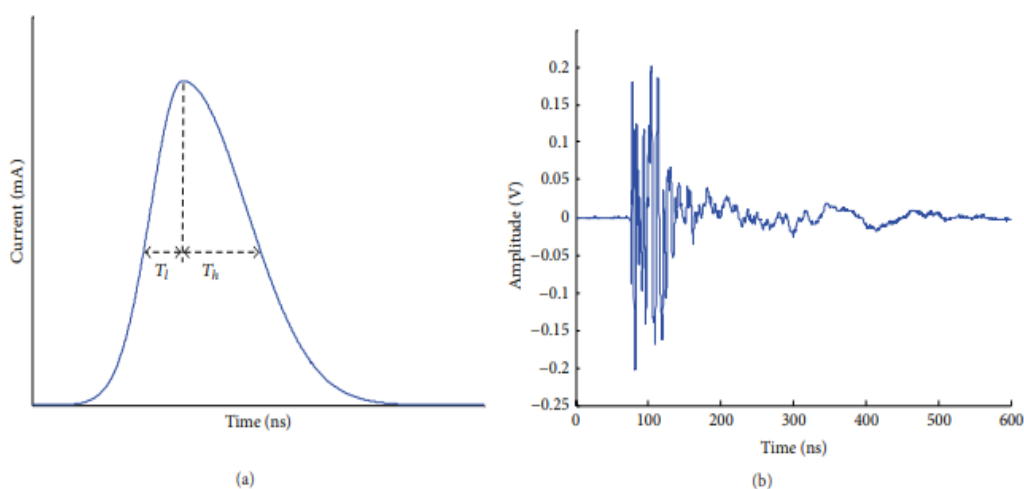


Figure 11. (a) Typical PD current pulse and (b) Typical signal arising from radiated PD energy (Zhang et al., 2015).

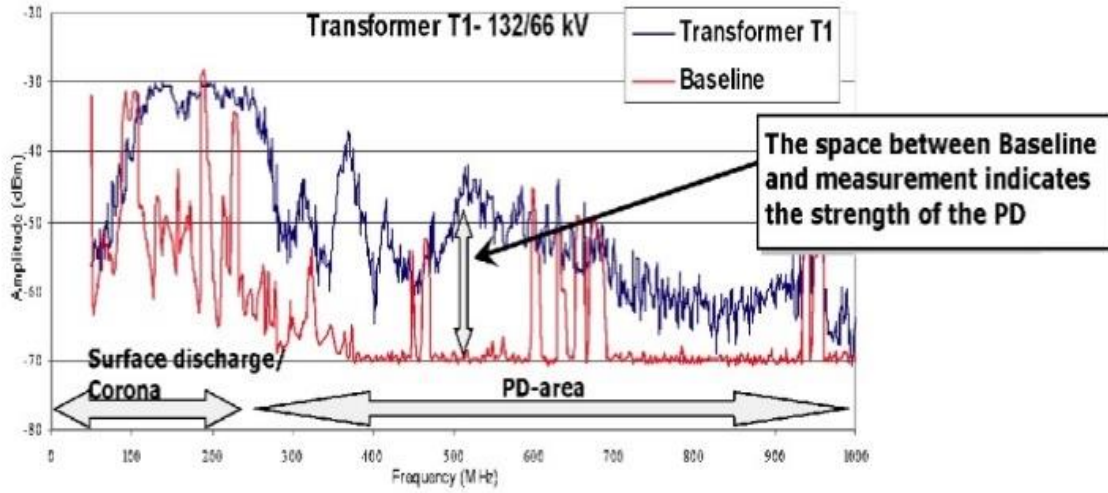


Figure 12. A typical PD frequency spectrum: lower trace is a reference in the absence of PD (Zhang et al., 2015).

As mentioned above that a PD pulse is modeled by using the Gaussian function, and the equation below defines the pulse (Sinaga, 2012):

$$i(t) = I_{MAX} e^{-\frac{t^2}{2\sigma^2}} \quad (2.3)$$

Where $i(t)$ is the current that is function of time.

I_{MAX} is the peak current magnitude

σ is the proportional to the width of the pulse and it is chosen to fit with the shape of the pulse.

It can be seen that when time is 0, the current will be maximum.

To get the spectrum of the above equation the Fourier transform is used (Sinaga, 2012).

$$F\{ I(t) \} = \int_{-\infty}^{\infty} I_{MAX} e^{-\frac{t^2}{2\sigma^2}} e^{-j\omega t} dt = I(\omega) \quad (2.4)$$

The Fourier transformation of the above equation will generate the spectrum that is also a Gaussian pulse (Sinaga, 2012).

$$I(\omega) = I_{MAX} \sigma \sqrt{2\pi} e^{-\frac{\omega^2 \sigma^2}{2}} \quad (2.5)$$

For the Gaussian pulse, the time required to reach from 10% to 90 % of the pulse is called the rise time, and it can be calculated by using the equation 2.6 given below (Sinaga, 2012) :

$$T = \frac{3.2}{\sigma} \operatorname{erf}^{-1} \quad (2.6)$$

Figure 13 shows different Gaussian pulses, while their spectra are shown in Figure 14 using the above equations 2.4 and 2.6

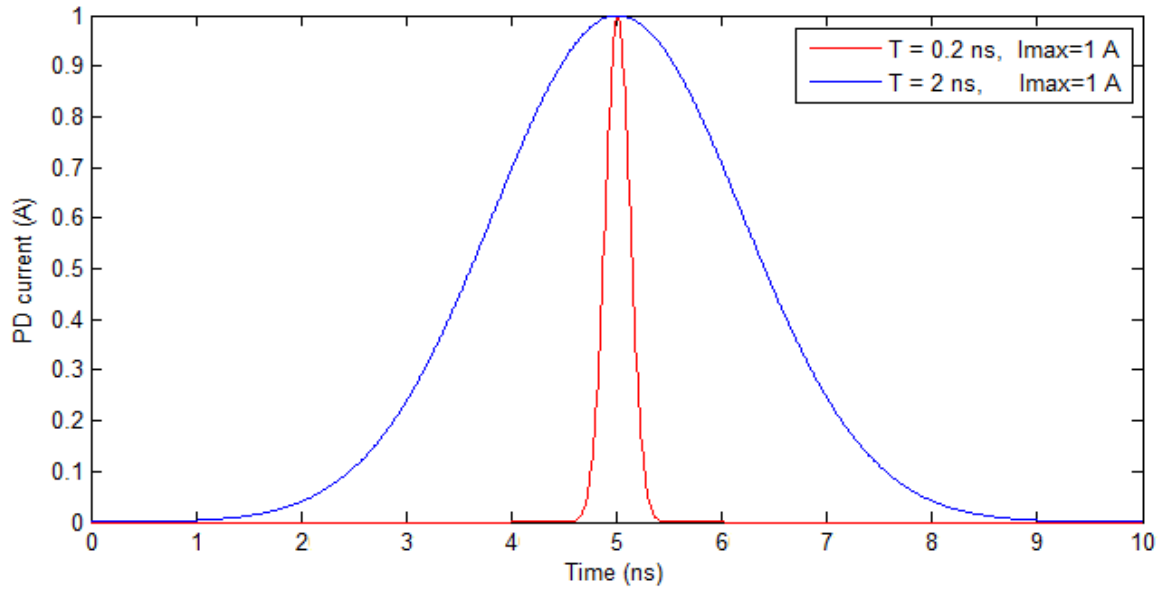


Figure 13. Different Gaussian pulses of different pulse rise times (Sinaga, 2012).

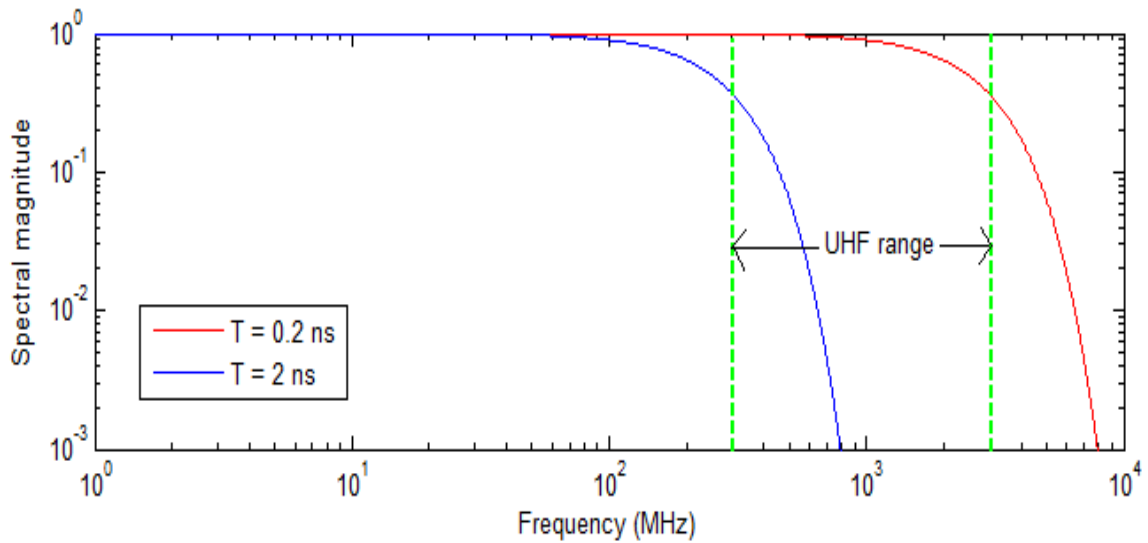


Figure 14. Normalized spectra of Gaussian pulses (Sinaga, 2012).

2.2.4 The detection of PD pulses

A HV power system including power transformers is critical in electricity generation and distributions. Its reliability depends on the insulation condition. It is essential to detect symptoms that lead to catastrophic failures to avoid disruptions and economic losses (Muhr et al., 2006). The biggest drawback associated with PD presence is that its long term persistence may result in failure in the insulation systems of the equipment such as power transformers. A long term PD may lead to deterioration of the equipment and can lead to an ultimate breakdown of the insulation system of the transformer. The heat generation due to PD activity can initiate chemical reactions that can also lead to accelerating the ageing of the insulation systems of power transformers (Lokhanin, Shneider, Sokolov, Chornogotsky, & Morozova, 2002) (Hampton & Meats, 1988). Figure 15 shows methods of PD detection.

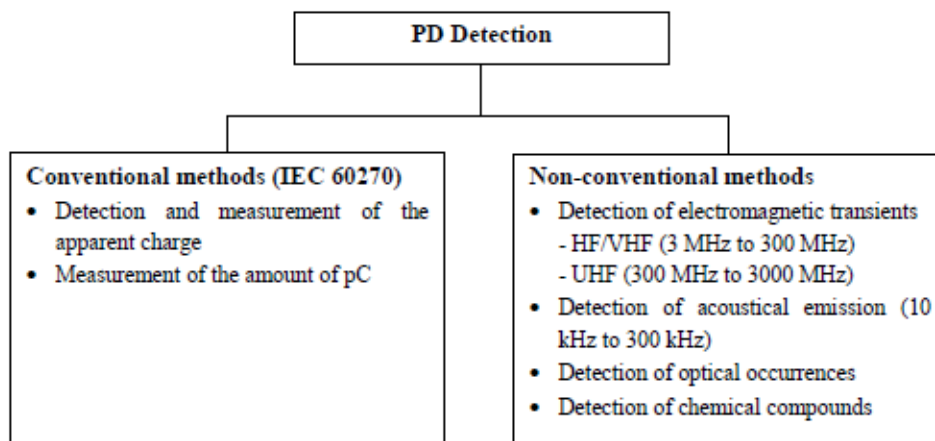


Figure 15. Methods of PD detection (Sinaga, 2012)

Two major techniques are quite common in PD detection, these include:

1. Electromagnetic detection
2. Acoustic detection

The above two techniques do not conform to IEC 60270. Both techniques mainly detect the signal rather than the quantity of charge. For this reason, several conventional and non-conventional methods are used for PD detection and are quite common. Conventional methods include measurement of charge in pico coulombs (pC) (Muhr et al., 2006). Non-conventional methods include the use of detection of EM transients, and detection of signals from 10KHz to 10MHz.

2.2.5 Partial discharge generation and modelling

Researchers over the past developed and proposed several models. PD is simulated in its simplest form by using three-capacitances, this model was proposed by Gemant and Philippoff in 1932. Figure 16 shows Gemant and Philippoff model. Three capacitors, C_a , C_b and C_c was used to model or represent the void and other parts of the insulation. Void in electrical insulation systems is regarded as one of the major causes of PD. It is assumed to increase the energy storing capacity of the electric field between the conductors thus influencing the dielectric capacitance of the equipment. Voids could be accidentally introduced during the manufacturing process or during breakdown of the equipment due to reaching its lifetime limit.

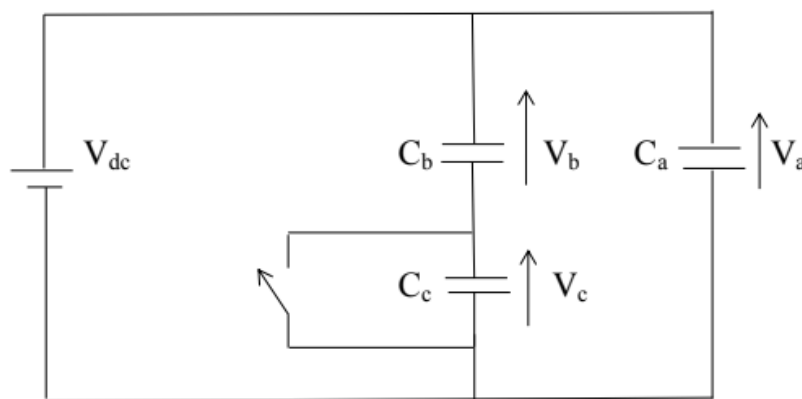


Figure 16. Gemant and Philippoff 's capacitive model (Paoletti, 1999)

2.2.6 PD classification

The classification of PD depends upon the nature of the signal and the type of the HV signal system (F. H. Kreuger, 1989). The discharge can be classified into three broad types that are:

- I. Internal discharge
- II. Surface discharge
- III. Corona discharge

2.2.6.1 Internal discharge

Internal discharge occurs when there are cavities, or there is the presence of an inclusion within the insulation of HV systems. During the fabrication process, these cavities become filled by materials that have a lower dielectric strength. Common materials include liquids or gasses (Sinaga, 2012) (Johnson, 2009). Figure 17 illustrates an example of internal discharge or the cavity present within the system and a cross section of the insulation. The equivalent capacitance circuit is shown in the figure 18.

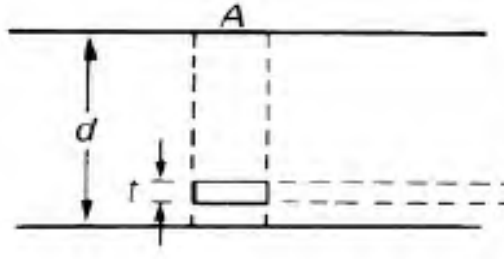


Figure 17. An example of internal discharge (Sinaga, 2012).

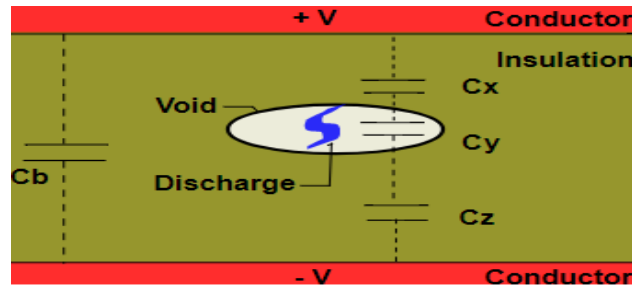


Figure 18. The equivalent capacitance circuit.

In figure 15, a voltage divider is present in the form of C_X , C_Y and C_Z . A small current flows through the conductor when a spark is created within the gap in the void that is filled by the gas atoms. The bulk capacitance C_B is in parallel to the voltage divider and the signal is attenuated by the voltage divider. The total capacitance of the voltage divider circuit depends on the permittivity of the material. The capacitance can be expressed by using the equation 2.7 below:

$$C_T = \frac{\epsilon_0 \epsilon_r A}{d} \quad (2.7)$$

Where ϵ_0 and ϵ_r are the permittivity of free space and permittivity of dielectric material respectively. The area is expressed as A and distance between the plates is expressed as d . The overall capacitance of the voltage divider circuit is expressed as C_T . Hence the voltage across the insulation that will initiate PD activity will depend on the breakdown strength of the cavity material and voltage presence across the insulation.

2.2.6.2 Surface discharge

A surface discharge occurs when a conducting layer is generated at the surface of the insulator and because of the conducting layer a leakage current is produced. The Figure below illustrates how surface discharge will cause a leakage current at the surface of an insulator (Sinaga, 2012) (Gallagher & Pearmain, 1983).

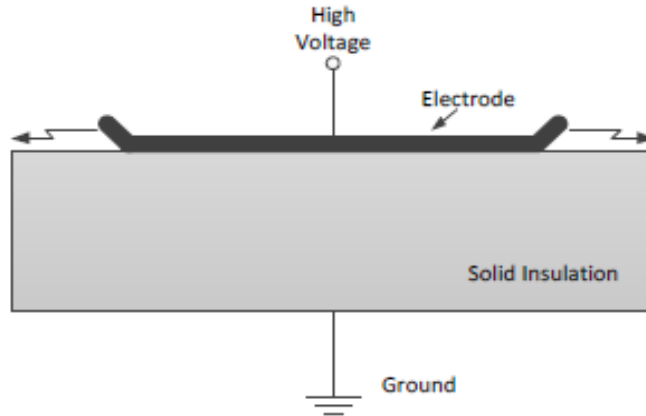


Figure 19 Surface discharge(Sinaga, 2012).

Figure 19 shows that a high-stress value at the edge of the insulation will trigger a surface discharge. In certain cases, if the insulator is weak or paper is used as an insulator, it can easily ignite and can easily cause a catastrophic situation (Kuffel & Kuffel, 2000).

2.2.6.3 Corona discharge

Corona discharge is another type of discharge that occurs in HV systems but is not regarded as dangerous as internal or surface discharge. It occurs due to the presence of rough surfaces or sharp edges. Because of such edges or surfaces, a strong electric field will be produced. Under such situations, the insulators will experience the stress that will be many times greater than the stress under normal conditions. Ionization process can be initiated due to such a high level of stress and can easily initiate a discharge termed as corona discharge (Gallagher & Pearmain, 1983) (Sinaga, 2012) . The figure below shows the phenomenon of corona discharge.

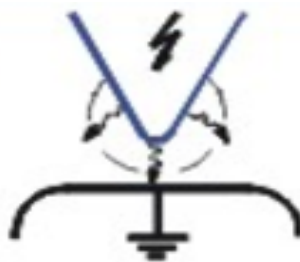


Figure 20 Corona discharge

Figure 20 illustrates how corona discharge is initiated. As it is evident from the Figure, the phenomenon is initiated at the vicinity of a point between the nearest electrodes. The corona phenomenon is quite common and is not considered as severe as other PD types.

2.3 Software Defined Radio (SDR)

In this section the SDR system that is used in this research is described and explained.

2.3.1 SDR architecture

SDR systems present novel demands on architecture in order to give multi-mode operation, configurability and multi-band that is required for air interface standard configurations. Also in the transmitter section of SDR systems, the waveforms are generated in the software as sampled digital signals converted from digital to analog through a wideband Digital to Analogue Converter (DAC). They are then up-converted from intermediate frequency (IF) to radio frequency (RF). A wideband ADC converter is employed in the receiver section to down convert and demodulate the received signal through the channels of the ADC. Figure 21 shows SDR architecture. One of the requirements for a good SDR device is that the ADC is as close to the antenna as possible (Isomäki & Avessta, 2004).

It can be observed that the SDR is made up of the RF section (antenna, filters and amplifiers), ADC and DAC interfaced with a DSP processor. The first generation SDR in the mid-1990's operated based on analogue processing. RF signals received from the antenna were down converted to an intermediate frequency (IF) signal. The baseband signal was then sampled and digitized utilizing an ADC. A DSP block was then used to recover the transmitted information through carrying out the necessary processing techniques. Most GSM mobile phones in the 1990's (2G) used this kind of architecture. However, as SDRs began to evolve, Direct Conversion Receiver (DCR) became more prevalent. Figure 22 shows a DCR receiver. The advantage of using the DCR is that it requires the least amount of parts to build thereby making it more attractive in particular for a broadband receiver due its simplicity and low cost. The disadvantage is that it needs an accurate phase shifter, a technique called six-port may solve such a problem. Also a signal leakage from the oscillator to the antenna may occur through the mixer and that will reflect into the mixer thus causing a DC offset. The DCR has over the years gained popularity and is most widely used now in SDR systems (Isomäki, 2004). In this process, the first stage of the baseband signals down converted the IF signals to baseband using decimation filters and demodulation techniques (Gibson, 2012). This method encouraged more flexibility since the filter was designed in the digital domain. In this project, the real time desktop (RTL) software defined radio will be used. This will be discussed in the next section (Isomäki & Avessta, 2004).

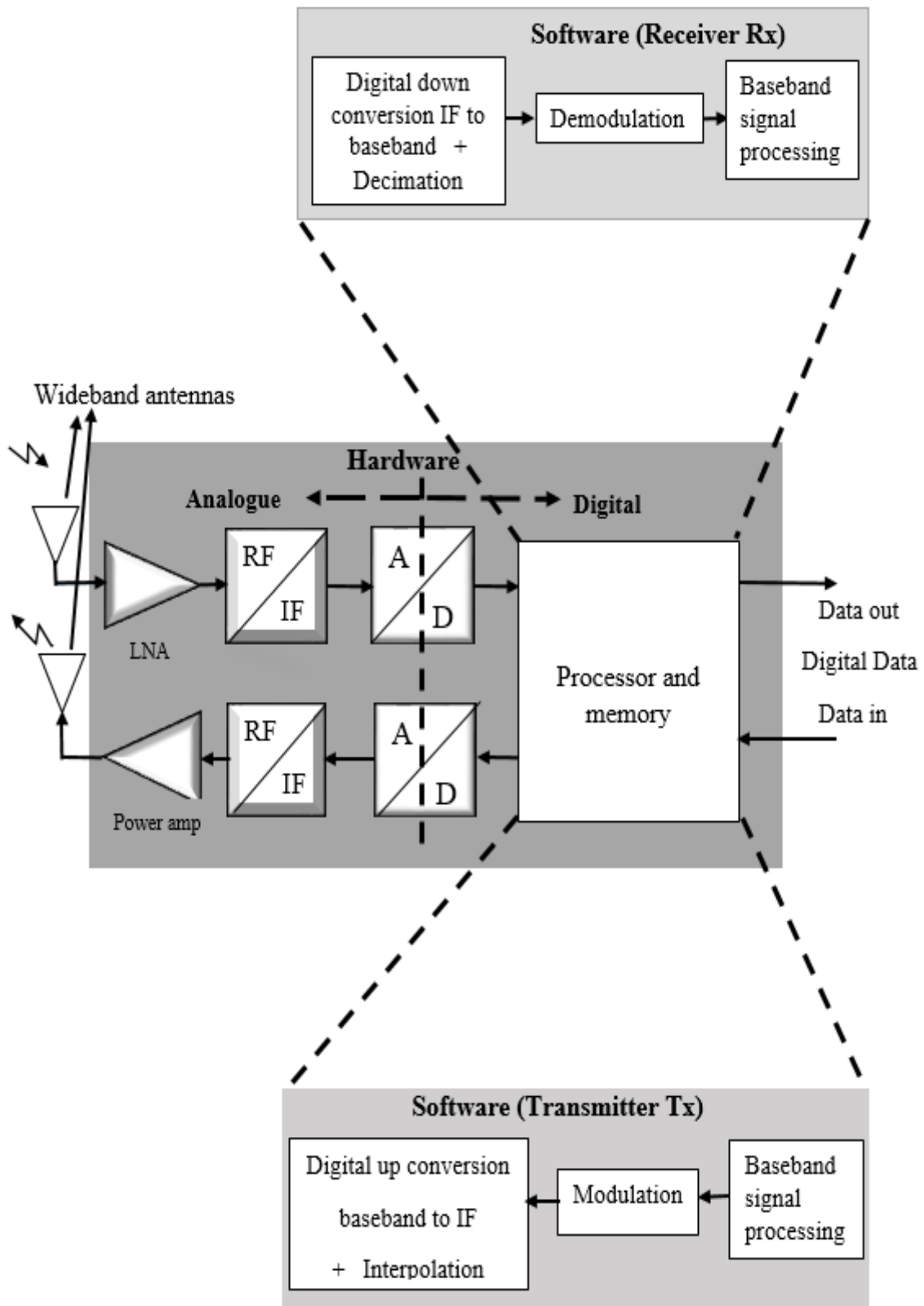


Figure 21. SDR architecture.

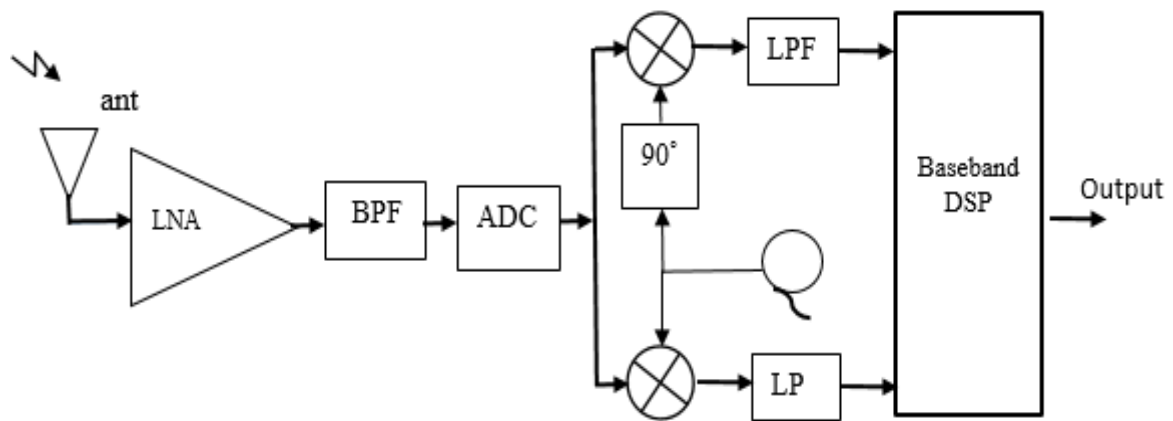


Figure 22. Direct conversion receiver with I/Q sampling (Isomäki, 2004).

2.3.2 SDR architecture evolution

Since the early 1990's SDR has often been regarded as the future design solution. Implementing SDR has become cheap thanks to the very low cost desktop PC's now available. This has made SDR technology available to the society at a low cost unlike before when it was only used in military and research applications (Machado-Fernández, 2015).

2.3.3 Desktop real time (RTL) Software Defined Radio

Real time (RTL) SDR can be defined as an inexpensive USB device that has the capability to receive radio signals (RF). It was recently discovered that this type of device can be used as SDR receivers by configuring it in a different mode unlike its previous application whereby it was used in Digital Video Broadcast – Terrestrial (DVB-T). When configured in this mode, this type of receiver is able to receive signals within the operating range of the tuner. Depending on the components used, this range changes from device to device. The most widely used frequency range for the RTL-SDR is 25MHz to 1.75GHz. This type of radio has functions based on the DCR scheme. In a typical DCR system, the received signal is first down converted to baseband. An anti-aliasing filter is then used to prefilter the variable and the desired channels are selected using filter design in software. Due to the flexibility and simplicity of designing especially the receiver section of SDR systems, DCR's have proven to be commercially usable and cheaper than other schemes such as the Tuned RF receiver and the Super-heterodyne receiver schemes (Stewart, Barlee, & Atkinson, 2015).

RTL-SDR is an example of a typical DCR system. RTL-SDR systems functions by first receiving the RF signal from the environment, converting it to baseband signal, converting

analog to digital, and finally sending the converted signal samples through the interface of the USB device. MATLAB and SIMULINK can be used to control the RTL-SDR device through the hardware support package released by Math Works. Users can implement and simulate virtually any kind of DSP receiver in a SIMULINK model in MATLAB to analyze the captured data. Since the entire process of processing and demodulating the data is carried out on in software on a laptop or pc, the entire process is called Software Defined Radio implementation.

RTL-SDR permits the reception of virtually all types of RF signals from the electromagnetic spectrum. They include, FM radio (87.5 – 108 MHz), Aeronautical (108 – 117MHz), 4G LTE-Advanced (800 MHz bands), GSM-R band (921 – 925 MHz), GPS Systems (1227 MHz – 1575 MHz) and other frequency ranges within the spectrum. Several hardware and software systems are required to get started with the RTL-SDR receiver (Stewart et al., 2015). They will be discussed in detail in subsequent chapters.

Hardware for RTL-SDR system

In this project, the hardware that will be used to implement the RTL-SDR is the NooElec receiver. They are of various sizes and shapes but all of them have basically the same functionality and are utilized in this application. This device has an antenna port called the Micro Coaxial (MCX) port whereby an omnidirectional antenna can be connected. The advantage of using this device is that it can be tuned to receive virtually any type of signal in the electromagnetic spectrum for baseband DSP processing in MATLAB and SIMULINK. However, in the UHF TV band, this device has been designed to function at its best. The device functions at a range of 25 MHz to 1.75 GHz (Stewart et al., 2015). A simple block diagram and the detailed block diagram of the RTL-SDR receiver is shown in Figure 23 and Figure 24 respectively. As can be observed from the figure, the demodulation process can be implemented in both hardware and software.

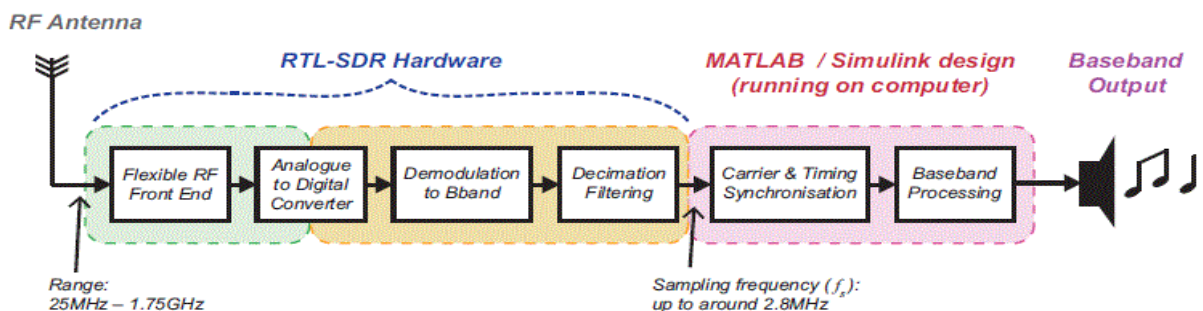


Figure 23. Block diagram of the RTL-SDR receiver chain (Stewart et al., 2015).

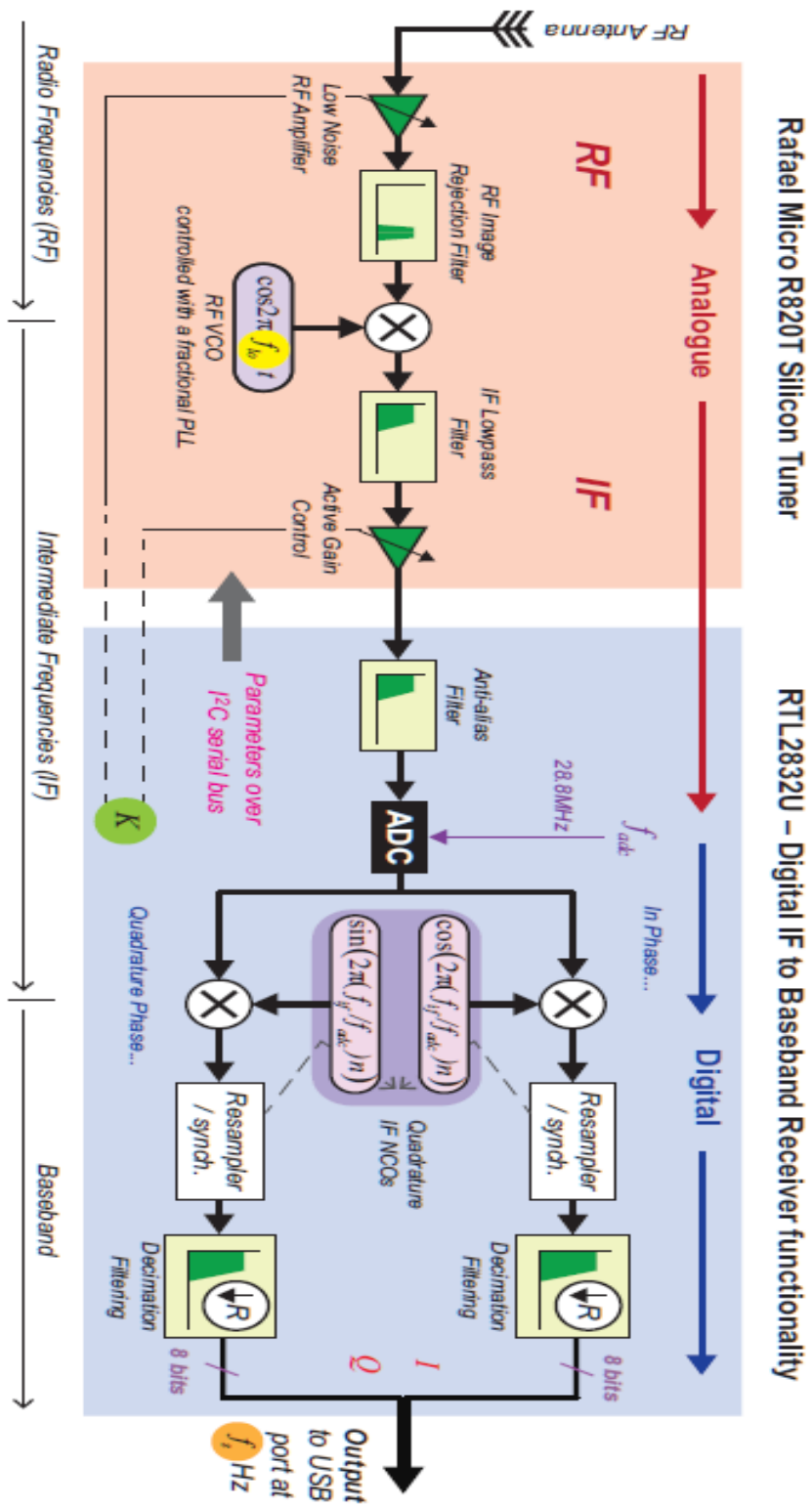


Figure 24. Block diagram show a detailed architecture (Stewart et al., 2015).

2.3.3.1 Analogue to Digital Converter (ADC)

Analog to digital Converter (ADC) are one of the most vital components used in the design of SDR systems. They determine the power consumption, bandwidth and dynamic range of the SDR. Most SDR systems make use of RF data converters that have bandwidths in GHz, high effective dynamic range and high bandwidth. The maximum frequency that the ADC can function is determined by the Nyquist rate. Since most SDRs are sampled with high frequencies, an anti-aliasing filter is used after the ADC to minimize the aliasing effects. It is important to note that the dynamic range of the ADC is determined by the number of bits the ADC can handle. However, most ADC's for SDR use over 14 bits' resolution with a bandwidth of about 100MHz and 100 dB dynamic range. Most ADCs in SDRs are prone to spurious free dynamic range (SFDR) problems. This problem is defined as the difference between the third order intermodulation distortion and the minimum detectable input (noise floor) signal. This problem is due to the fact that various applications required different dynamic ranges. This is one of the main challenges of ADCs in SDRs. Also of great concern in most ADC architectures is distortion and noise. These include overload distortion, quantization noise, non-linear errors, thermal noise, linear errors etc. From all the problems associated with ADC conversion, quantization noise seems to be prevalent. This type of noise is caused by approximation errors of the continuous signal into digital levels. To mitigate this problem noise shaping and oversampling methods can be used. In some situations, in SDR usage, the input signals can exceed the permitted ADC range. This is called overload distortion. This type of problem is difficult to neglect and therefore in most cases affects the signal to noise ratio (SNR). Also automatic gain control is a critical parameter for the performance of ADCs in SDR systems. To avoid overload distortion and allow full-scale utilization range, an optimal automatic gain control strategy is required. Thermal noise in ADC's is in most cases unavoidable. It can reduce the dynamic range of the ADC. To avoid this problem, the ADC should be used at a suitable environmental temperature. Dithering is also a problem in most ADCs since they increase SFDR in the SDR systems. It could be beneficial in reducing differential non-linearity errors, and correlated noise harmonics. Aperture jitter could also pose a problem in ADC conversion in SDR systems. It leads to poor noise performance, creates uncertainty in phase and introduces intersymbol interference to the signal (Stewart et al., 2015).

Having discussed ADC and the possible noise and distortion that can occur, it is necessary to investigate the sampling methods that can be used in SDR systems. Since the Nyquist theory needs the sampling rate to be at least twice the highest frequency component of the analog

signal, anti-aliasing filters are used before the ADC in most SDR system designs. However most anti-aliasing filters oversample the signal leading to increased data rate. Therefore, in SDR systems, quadrature sampling is mostly used whereby the signal is divided into quadrature and in-phase components. This implies that the sampling rate is reduced by half of the required bandwidth. This makes it an attractive and less expensive option for SDR system implementation. However, the downside of using this sampling method is the requirement for two synchronized phase converters (Isomäki, 2004) (Bilén et al., 2014).

2.3.3.2 Baseband Demodulation methods

Baseband demodulation methods are vital to SDR systems. Baseband is defined as the actual frequency band of the information signal. In SDR systems several frequency bands such as RF, UHF, are all supported. There are several baseband demodulation schemes that are available for demodulating a signal. Some of the baseband demodulation methods include FM baseband demodulator, BPSK demodulator, OQPSK demodulator, M-PSK baseband demodulator, rectangular QAM baseband demodulator and several others. However, SDR systems usually employ digital baseband demodulation techniques (Bilén et al., 2014).

2.3.3.3 Decimation filters

Decimation filters are multirate processing filters that are used at the output of ADC converters in SDR systems. They are used to increase computational efficiency and improve performance. Decimation filters are converting a discrete time signal to another form of discrete time signal made up of sub-samples. Decimation filters are used to reduce the sampling rate of ADCs by a factor of N. For instance, consider a decimation filter with N times decimation, then the sampling rate is reduced from f_s to f_s/N . Given data $x[n]$, the output from the decimated filter $y[n]$ can be expressed as:

$$y[n] = v[nN] = \sum_{k=-\infty}^{\infty} h[k]x[nN - k] \quad (2.8)$$

As discussed in the previous section, the ADC's anti-aliasing filter is preceded by the sampling rate compressor or down sampler. This prevents aliasing from happening as a result of the lower sampling rate. In real time in most SDR systems, the decimated signal as has been explained is observed at a reduced rate than the original signal by a factor of N (Bilén et al., 2014).

2.3.4 System requirements for Realtek RTL-SDR hardware

The NooElec RTL-SDR receiver is designed to operate in Windows 7, 8 and 10, 32 and 64 bit versions. It can also function in mac OS X 10.7.4+ and Linux versions. For optimal operation of the RTL-SDR hardware, it is necessary to use a AMD FX-8k or Intel (i5 and i7) series processor with a minimum of 8 GB RAM. A minimum allowable hard disk storage of 30 GB is also required. Also as part of the system requirements, it is necessary to have suitable sound cards where audio signals can be received and processed (Stewart et al., 2015).

2.3.5 RTL-SDR hardware support package and USRP hardware support package

The NooElec RTL-SDR receiver has its own software package which can be downloaded and installed by MATLAB and SIMULINK users. Also additional MATLAB toolboxes that provide added extra functions such as filter design tools are required. They include DSP system toolbox, Signal processing toolbox and the Communications Systems toolbox.

Universal Software Radio Peripheral (USRP) is a high speed device that is suitable for implementing SDR applications in real time. Just like RTL-SDR, USRP contains ADC and DAC converters, FPGA (for high speed operations such as decimation, down conversion and interpolation) and an RF front end. The USRP board also has the capability of performing baseband demodulation. It requires a desktop PC and USB interface to function. USRP Open-Source Toolchain (UHD and GNU Radio) software is used to simulate and configure USRP N200 hardware. It can be installed on Windows, Linux or OS X desktop system. Once the software has been installed on the PC, LIVE SDR environment is then used to verify the operation of the USRP software running on the PC.

2.3.6 Challenges of using SDR on low cost PCs

The challenges of implementing SDR on low cost PC are influenced from several factors, software or hardware issues, antenna and RF problems. Some of these concerns could be expanded (Stewart et al., 2015):

- (a) Frequency offset error in the RTL-SDR hardware tuner. This error increases as the device warms up.
- (b) Timing circuits and synchronization issues.
- (c) Environmental issues where there are a weak few RF signals between very strong RF signals.

- (d) Low performance of the omnidirectional antenna such as low sensitivity and low gain issues.
- (e) Saturation of automatic gain control (AGC) of the RTL-SDR due to inconsistencies in the gain of the front end and also for the USRPs. They can get saturated from very strong signals.
- (f) Low performance desktop PC issues. This includes for instance the inability of some PCs to run DSP and Communication algorithms in real-time.

2.3.7 Wireless Sensor Networks

A Wireless Sensor Network (WSN) can be defined as “a network of devices, denoted as nodes, which can sense the environment and communicate the information gathered from the monitored field (e.g., an area or volume) through wireless links.” (Buratti, Conti, Dardari, & Verdone, 2009), the same authors noted that WSNs can include single-sink or multiple-sink scenarios in terms of routing information within various conditions.

(Desai, Jain, & Merchant, 2007a) asserted that WSNs consist of four major components – radio, processor, sensor and battery. In addition, the same authors noted that WSNs can be regarded to as the ultimate enablers of technology that can “revolutionize information and communication” (Desai, Jain, & Merchant, 2007b). WSN applications have now become an emerging development in technological advancements mostly within the industries of healthcare, utilities, industrial and remote monitoring among others due to its offering of low-cost methods for data collection, reduced usage of energy and promotion of better management of resources. WSNs technology applications include Infrared, Wi-Fi, Bluetooth, IEEE 802.15.4 or ZigBee and WirelessHART among others. Whilst the Wireless Sensor Network prompted numerous benefits and advantages to its end-users, certain challenges need to be overcome. These issues have been identified by (Sohraby, Minoli, & Znati, 2007) as:

- “Limited functional capabilities, including problems of size”
- “Power factors”
- “Node Costs”
- “Environmental factors”
- “Transmission Channel factors”
- “Topology management complexity and node distribution”
- “Standards versus proprietary solutions”

2.4 Substation Electromagnetic Environment

PD detection plays a vital role in electrical power stations. It can help protect the HV equipment, it can prevent explosion of the equipment and hence prevent a catastrophic failure. PD detection can be performed in two modes, i.e. frequency domain and time domain. This section primarily discusses some of the predominant researches performed for partial discharge (PD) detection and localization where various techniques employed for PD detection with their respective strengths and limitations are discussed.

In general, it is also found that the operation of switching devices makes the power system cause electromagnetic emissions thus representing itself as a potential sources of broadband interference to a network of partial discharge detection. These kinds of emissions are found to be infrequent in nature and with limited duration and hence in some cases might be considered mistakenly as PD. Narrowband communication signals inside the partial discharge detection band such as the TV band and radio broadcast band can also cause significant interference. Such narrowband interferences are generally alleviated by the fact that such signals would approximately emerge from a distant transmitter and hence “biases” the radiometric measurements equally for all the sensors in the considered network or substation.

2.5 Partial Discharge Detection

The majority of existing systems employ conventional approaches of partial discharge detection such as electric parameters analysis based schemes, chemical analysis, acoustic analysis, and other sensing node (sensors) based approaches (Shan et al., 2008).

2.5.1 Partial Discharge Detection using Electromagnetic waves

Some methods employ electromagnetic EM sensors to detect the radiation emitted from PD activity and it has been shown to provide valuable information on the condition of insulators. The interest in the routine and continuous detection and estimation of RFI for defect diagnosis in power transmission and distribution network has gained immense attraction because of high pace decreasing costs of RF digital signal processing tools. There is also increased interest towards smart grids that are required to be strengthened with self-diagnosing abilities (Moore, Portugues, & Glover, 2006). The implementation of radiometric approaches for power line insulator defects has also confirmed the significance of partial discharge detection (Shihab & Wong, 2000). The prompt monitoring and control can enable power systems to identify equipment with severely degraded insulation and associated fault probability that might

ultimately avoid failure. The effective partial discharge analysis and interpretation can be of great significance for efficient power system monitoring and failure avoidance.

In addition, the partial discharge signals are characterised in terms of the amplitude and spectral distribution of electromagnetic signal. Such characterizing parameters together with the rate of discharge can be significantly employed for the PD caused fault identification in HV power instruments or transmission network. In general, the sources of partial discharge are considered to be of stochastic nature. In general, this stochastic nature makes it intricate to achieve an accurate mathematical model for the electromagnetic signal transmitted by partial discharge. The conventional partial discharge signals can be approximated mathematically using a Gaussian pulse shape (Shan et al., 2008). frequently, the Gaussian pulse model has been employed for detecting partial discharge detection based on EM radiation detection (Tian, Kawada, & Isaka, 2009) (M. D. Judd, Yang, & Hunter, 2005) (Oussalah, Zebboudj, & Boggs, 2007). The existing literature advocate that a better understanding of EM radiation in power networks can significantly help in the development of the fault avoidance and fault localization.

2.5.2 Partial discharge detection using wireless technologies

A partial discharge detection using WSN encompasses a network possessing PD radiometer sensors, individually interfaced to a WSN node. The two EM compatibility issues for WSN based PD detection need to be considered. These are: the possible interference of PD signals with the communications signals of the WSN causing poor communication in WSN network, and the increase of the measured radiometric PD power by the WSN signals might that cause the overestimation of the partial discharge intensity. The predominant approaches for alleviating such issues are the selection of a certain optimal frequency band and radio operating band. In general, the majority of radiated PD energy resides at frequencies below 800 MHz and the frequency band for the PD wireless sensor network WSN is 2.45GHz ISM band (Taove et al., 2000) (Taflove & Hagness, 2005). Literature also suggests that the substation electromagnetic environment has no significant adverse impact on the wireless sensor network performance for partial discharge detection. The optimal signal filtering at the front-end of the PD radiometer may ensure that the presence of a WSN communications signals does not significantly influence the PD intensity estimation. Along the same line, (He, Xie, & Jiang, 2011). proposed an online monitoring system for detecting and locating PDs using Wireless Sensor Network (WSN), whose schematic is given in Figure 25. Their proposed system exhibited better PD detection. Research developed a low cost detection system using CC2430

chip as a control unit and deployed the developed mechanism for RF communication in the sensing node. They developed an algorithm called SimpliciTI protocol for WSN to get good accuracy for time synchronization. Authors tested their system in a simulated environment and based on the results obtained, the system was able to locate the PD source within a certain error range.

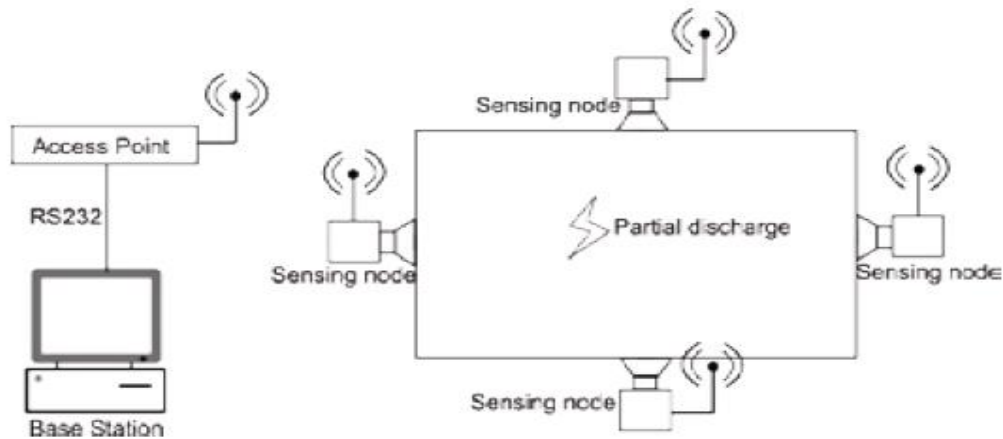


Figure 25 Structure of the PD location system (He et al., 2011).

In existing literature, the electromagnetic radiation in isotropic media has been studied extensively, (Oughstun & Sherman, 2012). In addition, the development of the Finite Difference Time Domain (FDTD) approaches permits precise EM investigation in diverse dielectric media (Taove et al., 2000). Recently FDTD mechanisms have been employed for simulating the propagation of EM radiation emitted from PD on a distribution power line (Tian et al., 2009). (Samat, Musirin, & Kusim, 2012) presented the effect of supply voltage on properties of partial discharge in a solid dielectric, and they characterised a pre-developed model which represents a void in a solid dielectric. This can be used for the investigation of discharges and in such a void in a solid dielectric when high AC voltage is applied. Figure 26 and 27 show the physical model of a void in a solid and its equivalent circuit respectively. (Bojovschi, Rowe, & Wong, 2009) investigated the partial discharge detection using the radiation spectra along a transmission line. The electromagnetic radiation spectra of partial discharge have shown that the EM radiation does propagate in HV insulating materials as dipoles or multi poles. Generally, the enhancement of the partial discharge detection depends on the precise interpretation of the EM spectra emitted from discharge zones.

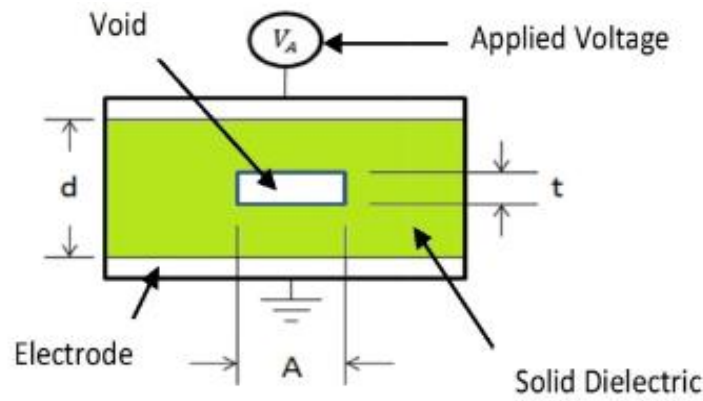


Figure 26. The physical model (Samat et al., 2012).

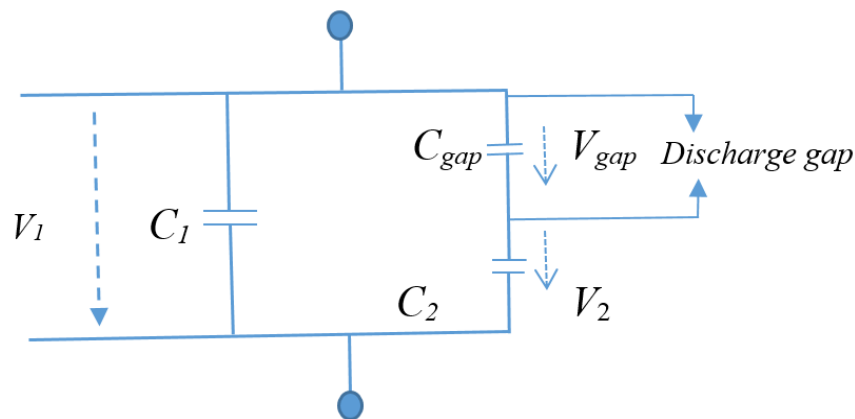


Figure 27. The equivalent circuit of a void in a solid (Samat et al., 2012).

(Wong, 2007), performed the investigation for the coupling between the EM radiation, generated by PD, and electric or electronic systems and found it to be of great significance for HV power infrastructure to detect electrical faults.

The electromagnetic radiation transmitted from partial discharge can be characterized in terms of amplitude, frequency band and time of occurrence. These parameters can be estimated in terms of the rate of ionization process and the dimensions of the cavities in which the partial discharge takes place (Bojovschi et al., 2009). Researchers have found that the iterative breakdown of gas within dielectric cavities in insulation material can be considered as the predominant source of intense electromagnetic radiation.

In the existing literature, (M. D. Judd et al., 2005) have proved that RF techniques can enable efficient ‘detection, location, analysis, and monitoring of partial discharge in both GIS and oil-filled transformers functional at higher voltage and frequency. Thus, radio frequency (RF) monitoring can be an effective tool for fault diagnosing (Agoris, 2009) (Coenen, Tenbohlen, & Markalous). Recent RF monitoring approaches encompass a wide-band ultra-high frequency (UHF) signal capture and conditioning unit, interfaced with the personal computer so as to

perform analysis and provide data visualization. Considering the specific cases where HV machines in a plant are undergoing certain unknown faults, the advantages of using a wideband on-line RF monitoring system are significant (Portugues, Moore, Glover, & Watson, 2008). Similarly, (Baker, Judd, & McArthur, 2010) presented a novel approach to partial discharge monitoring, their approach is a frequency based RF PD detector for low power wireless sensing using a frequency-based technique. They employed the detector in a way that could differentiate between the events of the partial discharge and other unwanted signals sources within a plant, however their detector could also track the insulation condition over time and provide information about the plant health. They designed the detector to operate as part of a wireless condition monitoring network, which presents a means to deploy wide-scale RF monitoring without the associated costs of wide-band monitoring systems. Figure 28 shows their RF sensor. Figure29 shows their RF PD Monitoring System.

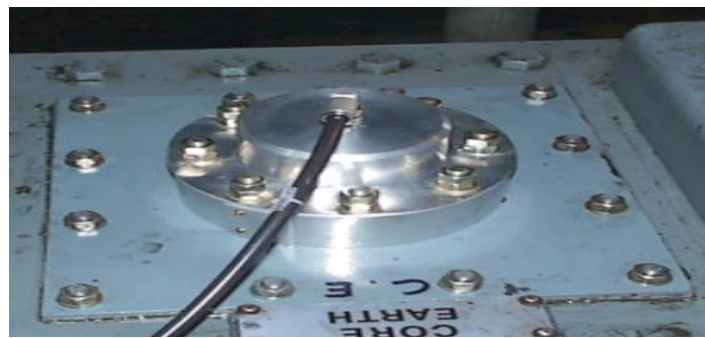


Figure 28. externally mounted RF sensor on a power transformer inspection hatch (Baker et al., 2010).

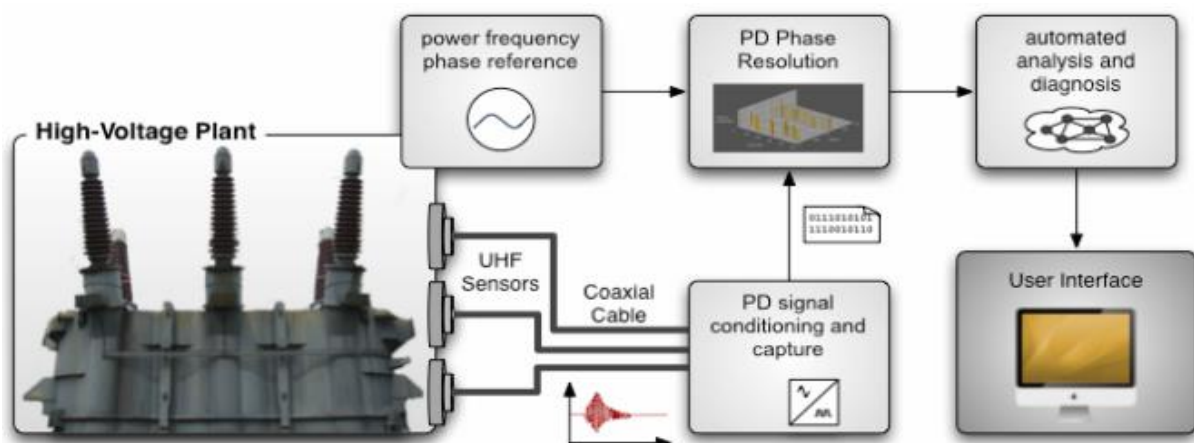


Figure 29. Principles of a RF PD Monitoring System (Baker et al., 2010).

Furthermore, (Chang, Gu, Chen, & Kuo, 2011) measured PD in GIS by establishing four defect types of 15kV switchgears and commercial inductive sensors and the current signals were classified using Artificial Neural Network (ANN). The authors stated that this detection could determine types of failures. Figure 30 shows the block diagram of their PD measurement experiment.

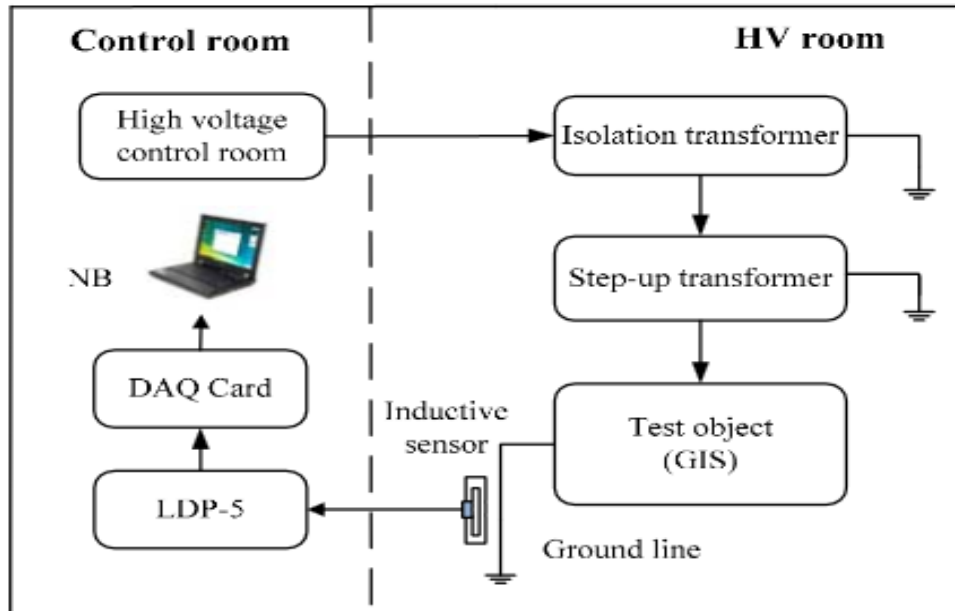


Figure 30 Block diagram of PD measurement experiment (Chang et al., 2011).

Similar work was done by (Khayam & Vauzia, 2014) where authors focused on designing and employing a bow-tie antenna as UHF sensor to achieve a 300 MHz bandwidth. This ‘‘optimum’’ antenna was fabricated on a double-layer PCB with FR4-epoxy substrate. The authors employed three antennas with different flare angles, and a spectrum analyser was used to measure the PD signal characteristics in two voltage levels, 26kV and 28kV. Figure 31 shows the partial discharge measurement circuit.



Figure 31 Partial Discharge measurement circuit (Khayam & Vauzia, 2014).

The authors found that all antennas detected the PD activity inside GIS. The best antenna is a bow-tie with 60° angle with substrate thickness of 2.8mm. The bowtie antenna is considered to be accurate, sensitive and easily designed and fabricated. (Muslim et al., 2013) designed a bow-tie antenna to work in the frequency range of 300MHz -3GHz. PD detection was performed with a GIS with a protrusion on the conductor as PD source and an antenna located at different positions with a voltage range of 20-25 KV. The PD activity was captured by enhanced antenna shown in figure 32. Figure 33 shows the experiment setup.

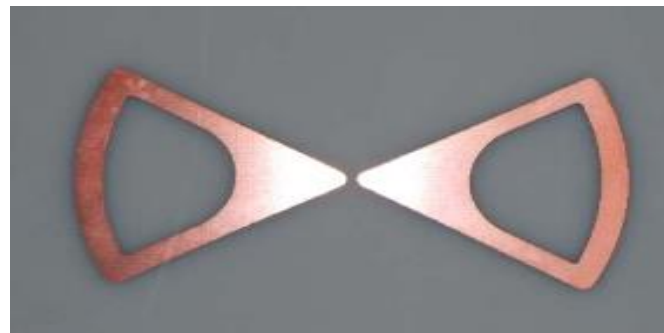


Figure 32. Enhanced bowtie antenna fabricated on a printed circuit board (Muslim et al., 2013).

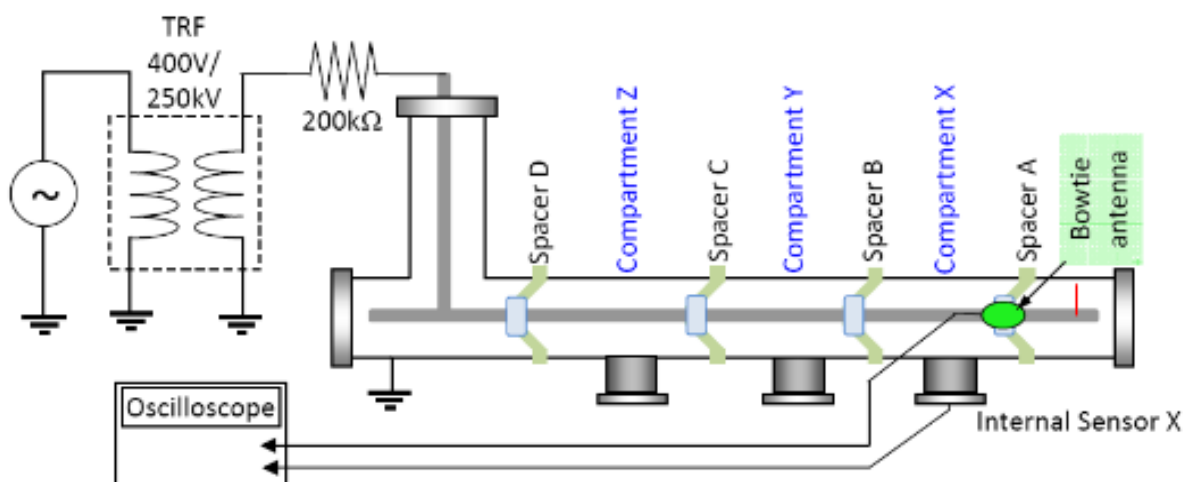


Figure 33 Experimental set up (Muslim et al., 2013).

As opposed to this point of view, Tian, et.al (2004) developed an online PD detection system using electro-optic modulators for HV cable systems. The authors employed a LiNbO3 modulator for modulating the transmitter laser intensity in proportion to the voltage applied across the modulator, where optical fiber was used to transmit the laser light and a capacitive coupler was employed for PD detection. Their system performed better in terms of immunity to electromagnetic interference. In another study (Neto et al., 2014) used an RF energy detector and an envelope energy detector to measure the PD signal and locate it. Their approach was

based on amplitude-only free-space radiometric measurements. Figure 34 shows the block diagram of the emulated sensor.

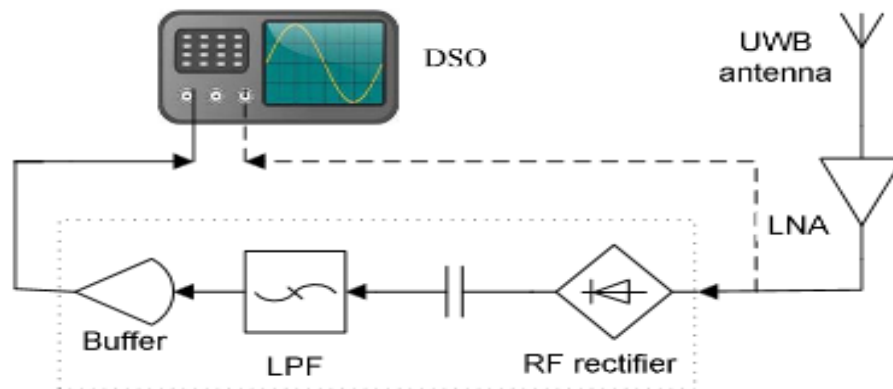


Figure 34. The block diagram of the emulated sensor (Neto et al., 2014).

Their measurements were inside two similar laboratories in terms of environment. There was a difference between measurements of the two laboratories as well as between the two sensor types. Measurements of one of the labs revealed that there was an earthed conducting mesh inside the walls and floor. Authors used a path-loss index to model the transmission loss which in case of the intensive multipath, it is inappropriate. It is worth mentioning here that the performance of the envelope detector was better and it has significant technological and cost benefits over RF energy detection. The authors suggested that their approach can be the basis of a low-cost wireless sensor network for PD detection and location in electrical power plants.

(Meijer, Agoris, Seitz, & Hermans, 2006) introduced a scheme for PD detection in power cable equipment using a wireless communication network. These researches exhibit that the implementation of RF techniques such as spectrum analysis or detection for PD detection can be a potential solution. However, spectrum sensing for a wideband spectrum is a highly intricate issue (Yucek & Arslan, 2009). To achieve it, higher end ADCs can be an alternative solution but they are very expensive they also require substantial computations for signal processing (Le, Rondeau, Reed, & Bostian, 2005). To abridge such problems, small scale sensing can be an option by employing multiple narrow bands for sensing a wideband spectrum.

Some solutions based on compressed sensing have been proposed but these schemes function only for sparse spectrum occupancy, (Paysarvi-Hoseini & Beaulieu, 2011), (Rokni & Ghasemzadeh, 2017), while major applications the access to dedicated hardware is required,

and, to the best of our knowledge, there is currently no research found presents simple wideband monitoring technique based on compressed sensing that runs on a low cost readily available technology. In (Tabassam, Suleman, Khan, & Tirmazi, 2011) cross correlation techniques were used for spectrum sensing using low cost SDR receivers and a phase-domain detection scheme was used for radio detection without any signal feature extraction overheads. In (Liu, Pareit, De Poorter, & Moerman, 2013) a statistical auto-regressive and moving average predictive model for grey-hole spectrum sensing was explored. Authors used SDR with USRP2 and RFX2400 boards for spectrum sensing and analysis. (Liu et al., 2013) a proposed substitute for channel assessment with commercial SDR to provide a seamless spectrum sensing over a wide spectrum band. Combining the GNU Radio and USRP in (Harada, 2008) an SDR based wireless system was developed. (Huang et al., 2009) employed SDR for spectrum sensing that explored the white spectrum in the TV band (490-700 MHz) and used a chi-square test with cyclostationary features for spectrum sensing. (Chen, Yen, & Chang, 2015) designed a 400-800 MHz spectrum sensing system using 0.18- μm CMOS for the UHF TV band. Recently, Realtek RTL2832 demodulator based low-cost USB digital TV tuners have attracted radio scientists and researchers because of software-defined radio (SDR) utilities that can be employed for spectrum sensing of wideband signals. Furthermore, researchers from the University of Strathclyde have showed in their work how SDR devices can be used to perform automated sweeps of the RF spectrum. Wideband sensing devices called Universal Software Radio Peripheral USRP, and RTL-SDR have been developed that possesses better sensing capabilities at higher frequencies and hence they can be a potential candidate for partial discharge detection. Practically the use of USRP SDR can enable low cost and accurate PD detection, (Stewart et al., 2015).

2.6 Partial discharge localization

Improvements and advancements in wireless technology have made it possible to use wireless based localization of partial discharge (PD) activity autonomously. Some of the key technologies available include GLONASS, Galileo and GPS, but to implement the existing solutions, some other technologies are required as well (Bruno, Adesso, & Restaino, 2014). Low-cost, reliable, efficient, autonomous and continuous monitoring of substations is made possible due to advancements in wireless technology.

Some of the key localization approaches used in the past include time of arrival (TOA), time difference of arrival (TDOA) and angle of arrival (AOA), (Xiong, Chen, An, & Yang, 2015) (Hettiwatte, Wang, & Crossley, 2014). Each of the localization techniques mentioned above

has its strengths and weaknesses. The methods are all classed based on the range where they estimate the location of the PD source by using a database or matrix of the locations.

The TOA approach is based on the location estimation of the time of arrival of the pulse transmitted to a receiving node. The advantage of the TOA approach is that it relies on measurements rather than relying on the transmitted wave information (L. Lin & So, 2011) (So & Lin, 2011). Within the TOA mechanism of localization, the lead time is observed as well as the arrival time of the pulse. In real applications, the signal undergoes various diffractions and reflections due to buildings, trees, vehicles or any other obstacles. In TOA, the path taken by the signal may be longer in comparison to the line of sight (LOS) propagation.

The major problem associated with TOA is that it relies on the one-way propagation time of a travelling signal i.e. there is a need for synchronization between the receiving nodes of a network. The accuracy is dependent on the arrival time of the pulse which means the longer the time of arrival less will be the location accuracy. This may well be overcome by increasing the number of receiving nodes for detecting PD pulses, but that means increasing the complexity and more importantly the cost (Hettiwatte et al., 2014) (Krivda, 1995).

The time difference of arrival (TDOA) is an extension of TOA. Again TDOA is a mechanism that is based on synchronization of all the receiving nodes. The way TDOA is different from TOA is that in contrast to TOA, the TDOA relies on a relative measurement which eliminates the need for source synchronization. By the time of arrival, the time difference of arrival is calculated between the node pairs. Although the TDOA scheme is better than TOA because source synchronization is eliminated, still synchronization amongst the receiving nodes is the requirement here as well. Whether it is TOA or TDOA, an array of antennas is used and the differences in the times of arrival are calculated between the node pairs (Moore et al., 2006) (Krivda, 1995).

The TOA mentioned above and TDOA are both based on the lateration technique i.e. measurement of the difference in the distance between locations that are known. The angle of arrival (AOA) works on the angle rather than the distance. The source location can be estimated in AOA by drawing lines from the source to the receiver with the requirement that at least two lines intersect each other. This seems a useful technique and it can be useful for localizing PD sources (Xu, Zhou, & Zhang, 2014a).

The main issue with the AOA technique is that in real environments there may be complex Propagation environments. AOA can work nearly perfect under an environment where there is a direct line of sight. This is not the case when dealing with PD localization. Where there are multipath interferences, it is a technique that is less effective. Pulse originating from a PD source is susceptible to multiple path interferences. AOA works very well for indoor applications but it is less powerful as a standalone technique for outdoor applications (Shuhong, Xicai, & Fanru, 1998) (Kaemarungsi & Krishnamurthy, 2004).

Whether it is TOA, TDOA or AOA, all these techniques have issues that restrict their use for localizing PD sources in real environments. In TOA and TDOA the synchronisation is the key requirement, and this makes the systems complex and time dependent. The accuracy may also be compromised in real environments because of the time dependency. In AOA, a technique that is based on the angle of arrival, an outdoor environment for PD pulse transmission, with rich multipath is very different. On this basis, another technique that can be useful for this environment is the Received Signal Strength (RSS) technique (Shuhong et al., 1998) (Xiong et al., 2015) (Xu et al., 2014a).

Recently, the received signal strength (RSS) approach has gained vital importance for indoor and outdoor localization. A primary reason for its popularity is its ability to exploit the features of the communications systems that already exist. It implies that there is no need to install additional hardware and software system that ultimately reduces the cost and complexity. Also, there is an important connection between the quality of communication and the RSS i.e. RSS is normally encapsulated within the measurements that are based on wireless communications (So & Lin, 2011) (Adhikary & Daigle, 2016; Kaemarungsi & Krishnamurthy, 2004).

When using the RSS for localization purposes, it proves extremely useful because it provides information about the distance between the source and the receiver that can be exploited to locate the source by converting the received power into distance. Multiple locations can be approximated by using the multiple receiver nodes that allow trilateration or even multilateration. The main issue that can be associated is the accuracy of the estimated location because of the heterogeneous nature of the radio propagation environment. The major challenge that is faced in PD localisation is the anonymity of the propagation parameters i.e. the source transmitted power is unknown as well as the path loss power is environment dependent and can vary from node to node due to the heterogeneous nature of the propagation environment (Orr, Reid, & Judd, 2008).

2.7 Software Defined Radio (SDR technology)

Spectrum sensing in narrow bandwidth has been found to be an easy task, but spectrum sensing for a wideband spectrum is highly challenging, where the assessment of white spaces can be of great significance for optimal resource utilization. Some recent studies on compressed sensing for wideband spectrum sensing have been performed but these schemes function for the situation when the occupation of the spectrum is sparse, (Paysarvi-Hoseini & Beaulieu, 2011), (Rokni & Ghasemzadeh, 2017) However majority of applications requires an access to dedicated hardware, and on the other hand, major applications of compressed sensing (Kitsunezuka & Pister, 2015), need access to dedicated hardware, and, to the best of this author's knowledge, there is currently no simple wideband monitoring technique based on compressed sensing that runs on unsophisticated low-cost hardware. (Mate, Lee, & Lu, 2011), implemented spectrum sensing in a real environment and verified two algorithms based on the time-covariance matrix and SDR and GNU radio interface. Combining the GNU Radio and USRP they developed SDR based wireless communication systems. To combat noise uncertainty, they employed COV with the ratio between the time correlation and the signal energy as the signal detection indicator; and MME which uses the ratio of maximum to minimum eigen-values of the covariance matrix to detect signal presence. (Dantas, Figueredo, & da Cruz, 2013), presented a comparison between real time and non-real time simulation methodologies for implementing some cooperative spectrum sensing algorithms. Their tools and their results are compared aiming at demonstrating pros and cons of the evaluation methodologies. There is a clear trade-off among development cost, simulation flexibility and execution time, especially considering the choice of prototyping methodology and the target application. (Huang et al., 2009) employed SDR for spectrum sensing using SDR which explored the white spectrum in the TV band 490-700 MHz and used a chi-square test with cyclostationary features for assessing spectrum presence. In addition, a discontinuous spectrum transmission approach was implemented in spectrum holes which has two independent OFDM links on two separated carriers. The valid data sub-carriers in each OFDM link was configured in a flexible way to perform sensing. (Harada, 2008), developed a small-size SDR equipment containing a multiband/tenable RF unit with switching facilities to sense RSSI signal over 400 MHz-6 GHz bands.

Later (Harada et al., 2007), developed a Cognitive Wireless Cloud (CWC) that can realize user-centric and scalable networks based on unique cognitive spectrum access, cross-network signaling, network optimization, and fast reconfiguration methods. Further the signal spectrum sensing was performed using software defined cognitive radio (SDCR) for feasibility assessment

for spectrum sensing period and reconfiguration period by using software packages of W-CDMA and IEEE802.11a. (Kim, Xin, & Rangarajan, 2010), explored noise power in spectrum detection using SDR for a cognitive radio network. For estimation of the threshold in energy detection a histogram approach was employed. (D. T. Lin, Chae, Li, & Flynn, 2012) implemented a flexible spectrum-sensing receiver in 65nm CMOS comprising a wideband front-end, spectrum-adaptive (SA) filtering, switched-capacitor amplifiers, and a filtering SAR ADC where the SA filter employed a DT spectrum-analyser and a reconfigurable DT notch filter to detect and suppress large interferers over a 55MHz range. (Chen et al., 2015), designed a 400--800 MHz spectrum sensing system using 0.18- μ m CMOS technology for CR in the UHF TV band. (Sarijari et al., 2009), analyzed the performance of spectrum sensing on GNU Radio system with USRP and investigated spectrum scarcity and proposed algorithm for energy detection at Rx signal in a fixed bandwidth, 'W', over an observation time window, 'T'. Their results showed that it can detected of primary user signal over a fixed bandwidth. An enhanced system for a wideband spectrum sensing FFT-based constant false alarm rate (CFAR) detector was developed in (Sarijari et al., 2009) that possesses a detection threshold that is independent of the noise variance and windowing sequence that facilitates monitoring of multiple frequency bands without false alarms. (Liu et al., 2013), proposed an alternative for channel assessment on top of a commercial SDR platform to provide a seamless spectrum sensing over a wide spectrum band and a flexible configuration. Solutions such as spectrum analysers are capable of scanning a wide spectrum range, but are not dedicated for channel occupation assessment because they are extremely costly and not able to perform continuous recording for a time period longer than a few seconds. On the other hand, low-cost solutions lack the flexibility and required performance in terms of configuration and sensing efficiency. To remedy the situation, this research presents an alternative for PD detection in the electrical power plants using a commercial software-defined radio platform. This thesis proposes a pioneering solution that is capable of seamless spectrum sensing over a wide spectrum band and guarantees sufficient flexibility in terms of configurations.

2.8 The research gap

A number of studies have been conducted so far for effective partial discharge detection, but still not much effort has been made on developing certain cost effective or low cost PD detection schemes. Recently a wideband sensing device called RTL SDR has been developed that possesses a better sensing capability at higher frequencies and hence it can be a potential candidate for a sensing system development for partial discharge detection. Unfortunately, until

now there is no research exploring RTL-SDR for partial discharge detection at higher frequencies or higher voltage applications. The implementation of RTL-SDR can enable low-cost PD detection. Thus, considering this, research gap in this research the efficiency of RTL-SDR has been explored for partial discharge detection at ultra-high frequency (UHF). Despite being a low cost device, RTL-SDR has exhibited better performance for sensing applications at higher frequencies. The detection of partial discharge at ultra-high frequencies using RTL-SDR can lead towards an energy efficient solution for power system monitoring. This research intends to explore the feasibility of RTL-SDR dongle based PD detection at higher frequency applications. Here it has been intended to examine the impacts of the variation in the key functional parameters such as resolution bandwidth (RBW), MaxHold and sampling parameters so as to enhance detection efficiency. As per our current knowledge and literature study, such approaches have not been implemented and hence these factors motivate us to develop a low cost RTL-SDR based partial discharge detection unit for power systems.

3 The description of the system

The emergence of wireless technology has provided numerous opportunities to optimize remote monitoring of facilities and can play a significant role in ensuring swift control and restoration of HV plant equipment. This chapter firstly describes in details the Software Defined Radio technology, including the technology evolution, the technology architecture existing platforms, followed by a description of the MATLAB code used to access the SDR devices.

3.1 Introduction

There has been great enthusiasm on the prospects of software radios by the digital signal processing (DSP), RF/radio and digital communications sectors over the past twenty years. The term software defined radio (SDR), in recent years, has somehow diverged between different engineering groups. This thesis is aimed at detecting PD signals at electrical substations using SDR that is in the form of radio systems enabled with DSP functions.

SDR in the past five years or less, has been achieved in the laboratory and at a very reasonable and fair cost in the area of around \$1500 or less for a hardware with ADC and DAC that is enabled by FPGA. Some products, for example the Universal Radio Software Peripheral URSP, which is an SDR device, has been used on many occasions to stream samples of down-converted RF signals to a PC where they are processed by software such as MATLAB, Simulink and Lab View for real time processing or recorded off-line for off-line use. In addition to this, a real-time DSP software algorithm could be easily implemented in situations where the required drivers are available and the PC itself is fast enough. SDR is currently established in a number of institutions if not most of them, as a part of their curriculum. In May 2014, a special issue on software defined radio (SDR) was published in the IEEE communications Magazine, and several authors reviewed the rate of success of the introduction of SDR based on USRP into already integrated laboratory sessions and course curricula for EE students. The advent of the USRP device however, comes with many positives, and it reduces the cost of a device down to a level that is similar to that of a laptop (Machado-Fernández, 2015).

3.2 The use of Software Defined Radio

The DSP community has many people who consider that SDR was in effect the engineering of radio stations that are DSP-enabled, by virtue of DACs (digital to analogue converters) and ADCs that are designed to have very high speed. The other communications engineering groups use SDR as a middleware, which is a software that acts as a bridge between the computer operating systems and their application or between the electronic devices in a radio network. Both the SDR interpretations are closely related i.e. the middleware and the radio that is DSP enabled, had a promise and concept that was easy to understand, but the software, and hardware that 20 years was mostly needed or required, was really expensive and not affordable(Stewart et al., 2015) .

3.3 Analysis of existing platforms

This section presents some of the most representative sensing solutions, starting from powerful but expensive spectrum analysers followed by cheaper ones. The processing mechanisms of high-end spectrum analysers are discussed in detail, as a way of understanding the technology adopted in this thesis.

3.3.1 Spectrum analysers

Most of spectrum analysers nowadays have two main modes: Fast Fourier Transform (FFT) and swept mode. In the swept mode a retune occurs in each single step by incrementing the center frequency. The increments depend on the sampling frequency and number of Fast Fourier Transform points in the frequency range chosen which is called ‘the sweep span’. In the spectrum analysers that are based on FFT the sweeping of the radio-frequency (FT) front end is not needed. Instead, FFT achieves the transformation from the time domain moving over to the frequency domain. A series of events happens: first, the memory servers as storage and stores a batch of samples, then the samples that represent time domain measurements are translated into spectrum information. The span frequency of the analyser based on FFT depends on the sample rate. The term ‘sweep time’ is inherited in this case to describe the time that is spent between two consecutive Fast Fourier Transform results, although no sweeping is actually taking place. In other instantaneous, spectrum analysers tend to join or combine the FFT mode and the swept mode. In the end, one sweep results to a combination of several FFT shots that obtained with different frequency centers. This, in other words is called as the swept Fast Fourier Transformation mode. Figure 41 shows how the sweeping process is performed. The FFT-based analyser has one main advantage; one operation can enable you to look at a spectrum on a broader frequency range. However, the acquisition of a batch of samples followed by a step that involves processing is required in the FFT mode. The analyser in turn misses the events that subsequently happen in the acquisition phase (Liu et al., 2013). This problem can be solved if the analyser meets certain conditions that include:

- The speed of processing should be faster than the speed of acquisition,
- The sample acquisition phase and the sample processing phase should occur in parallel.

Spectrum analysers that have the capability to obtain seamless measurements are called real-time spectrum analysers.

3.3.2 SDR devices (Hardware/Software overview)

In this section two SDR devices will be covered, these are: the USRP devices and the RTL-SDR low cost devices.

3.3.2.1 USRP Devices

The Universal Software Radio Peripheral USRP, which was developed formally by Ettus Research, is low-cost and high speed, and it is the best solution for a MATLAB user to implement real time applications. SDR platforms tend to allow basic and traditional radio functions, which include encoding and decoding to be transferred from hardware to software. The USRP consists of an RF section, an IF section, and a baseband section where the RF and IF processing is performed in the hardware in the USRP while the baseband processing is performed in the software in the host computer (H Mohamed et al., 2016a). These sections are implemented on two boards. These boards are a plug-in daughter board (RF front-end and IF), and a fixed motherboard. Figure 35 shows the USRP block diagram.

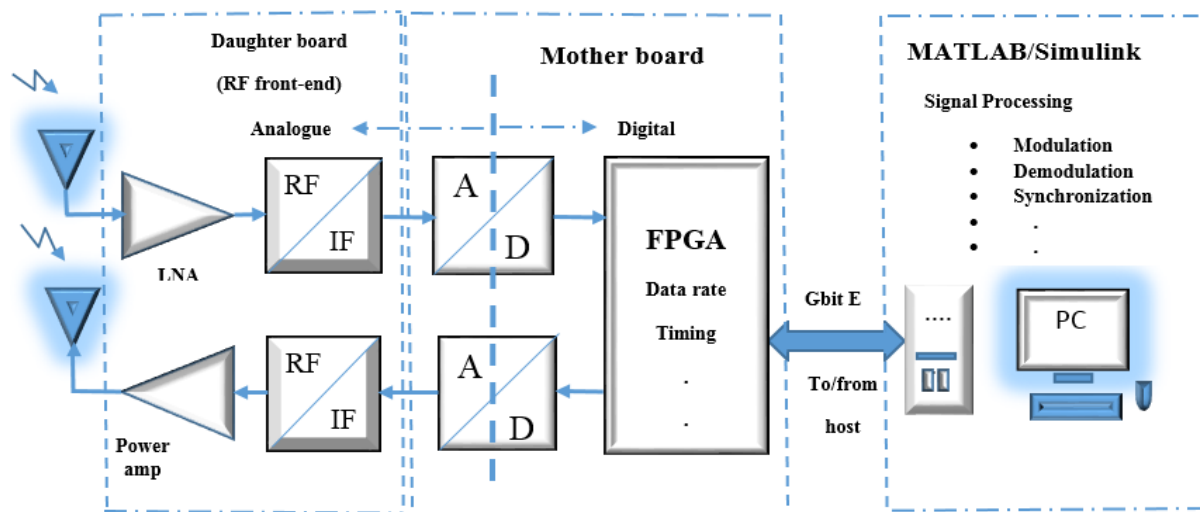


Figure 35. USRP Block diagram

The RF front-end board is responsible for analogue operations, i.e. all of the analogue RF and IF band processing such as filtering and up/down conversion. The motherboard consists mainly of a field-programmable gate array (FPGA), analogue to digital converter (ADC), digital to analogue converter (DAC) and Gigabyte Ethernet connectivity to allow the flow information to and from host processors. The majority of the digital signal processing, such as interpolation, filtering and decimation are performed in the FPGA. On the other side, the host computer is doing the entire baseband specific signal processing (modulation, demodulation, amplification,

mixing, filtering etc.). USRP can be reconfigured to desired specifications by the host computer using software. All the modules make use of a driver software package named USRP Hardware Driver (UHD). UHD is compatible with Windows, Linux and Mac OS. UHD has functions that can control most parameters such as frequency, gain, sample rate, etc. Connecting the USRP to a powerful host machine can compensate for its lack of processing power (H Mohamed et al., 2016a). Some of the specifications of the USRP transceiver are shown in Table 1.

Table 1 Specifications of the USRP N200.	
Feature	Value
Sampling frequency of ADC (Receive)	100 m Sa/s.
ADC Resolution	14 bits
Frequency Accuracy	2.5 ppm
Receiver Noise Figure	5 dB
Dimensions (l x w x h)	22x 16 x 5 cm
Weight	1.2 kg
Frequency range	50-2200MHz
Overall Bandwidth of the device (full duplex)	20 m Sa/s.
Limited by the interface	
Cost	£(1000-2000)

There is also the option of using GNU radio as a third party platform, such that the software is directly implemented just directly above the UHD driver. As a result, this gives a better general performance and efficient sensing capability because the overhead of all function calls is reduced. The device chosen for the work reported here is shown in Figure 36.



Figure 36. USRP N200 hardware.

Figure 36 USRP N200 hardware.

3.3.2.2 RTL-SDR dongles

The RTL-SDR is an inexpensive product and is based on DVB-T TV tuners with RTL2832U ICs. The RTL-SDR can function as a wide band radio scanner. RTL-SDR receivers employ a Realtek RTL2832U quadrature sampling detector, a programmable frequency oscillator, and an RF tuner chip. Research tests show that these devices can operate well without any hardware modifications, using additional software. It is normally feasible to tune in to certain frequency bands using a conventional SDR software program. The advanced versions of RTL-SDR compatible software can directly access the data stream, facilitating real time multimode reception. Figure 37, shows the main components of the NooElec RTL-SDR. RTL2832U ICs can be employed with any of the four tuner chips available: FC0012 – tuner: 22 MHz to 948.6 MHz; FC0013-tuner: 22 MHz to 1100MHz; Elonics E4000: 52 MHz to 2200 MHz, and the Rafael Micro R820T tuner, which has been used in this work, which is capable of tuning from 24MHz to 1766 MHz. The tuner selects a frequency band around a target band centre frequency and performs demodulation within the selected band into the baseband (H Mohamed et al., 2016b).



Figure 37. Key components of the NooElec NESDR Mini RTL-SDR.

In the proposed system, the RTL2832U chip functions as an ADC that samples the baseband signal and outputs to the host computer. In our specific application, the considered dongle is employed to receive and decode PD signals. The chosen SDR has modes that allow for the capturing and transfer of raw samples to the host computer, thus enabling the system to behave like an inexpensive spectrum analyzer. To acquire the spectral information, we rely on RTL-SDR USB dongles and MATLAB code. The selected RTL-SDR dongles are based on

RTL2832U demodulator, which can be modified into cheap SDRs since the chipset allows for the transfer of the captured raw I/Q samples to the computer. The RTL2832U has an ADC that samples at 28.8 MHz. The maximum output rate of the device, due to its USB2.0 interface, is limited to 3.2MHz. In real time operations however, signals that are sampled below 2.4 MHz can be received without any detrimental sample loss. Reducing the sampling rate can often improve the performance of the baseband processing on less powerful computers as well, and setting the sampling rate to 2.4 MHz allows the RTL2832U to decimate by an even factor of 12 (when the ADC samples at 28.8 MHz). Receiving only 1 in every 12 IQ samples, the host computer obtains a signal with the reduced bandwidth of 2.4 MHz (H Mohamed et al., 2016b). Some of the characterizing features of the specifications of the RTL SDR is given as follows:

Table 2 RTL SDR features.	
Features	Specification
Frequency range	24 -1760 MHz
Max sample rate	3.2 M Sa/s (2.8 M Sa/s in practice)
Resolution	8 bits/sample
Noise figure	< 4.5 dB
Cost	Very low ~£(5-10)

Design Objectives.

Some of the main objectives of the proposed system for high bandwidth PD detection are as follows:

- Low-Cost- The cost of the proposed sensing system must not be in excess of £ 5. Low cost is one of the most important factors to be considered while developing inexpensive spectrum sensing devices.
- Small Form-Factor - The sensing system should use a pocket-sized sensing device that could enable easy distribution and deployment scenarios.

- Wideband- The proposed system should be capable of receiving signals within the bandwidth of radiated PD 50-800 MHz.
- COTS Hardware- The sensing system should be built using commercial off-the-shelf (COTS) hardware components.
- Flexible employability- The sensing model must remain flexible enough to adapt to various situations.

The proposed System.

The key feature of the proposed spectral sensing system is a low-cost, portable measurement platform for automatically collecting PD data. The platform has just two hardware components: a PC/laptop and a portable Realtek Software Defined Radio (RTL-SDR) that connects to the PC via a USB interface. A block diagram of the RTL-SDR device is shown in Figure 38. Figure 39 shows the proposed system. The RTL-SDR is required to perform as a spectrum analyzer. The RTL-SDR DVB-T dongle operates in the frequency range of 24-1750MHz. The device was selected due to low cost, availability, portability, and its frequency coverage in the VHF-UHF bands (H Mohamed et al., 2016b).

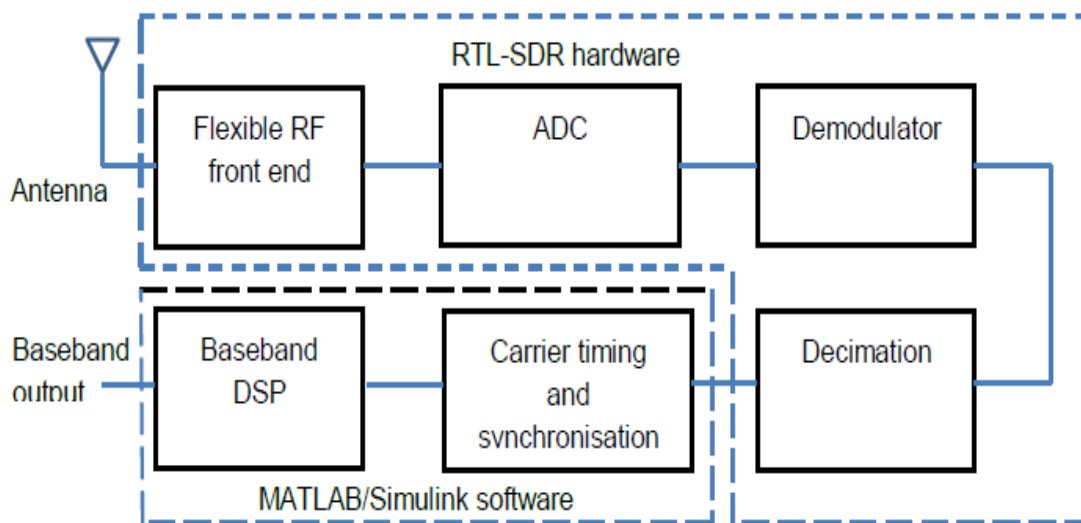


Figure 38. Block diagram of the RTL-SDR receiver chain.

The required software tools have been interfaced with the RTL-SDR modules to allow for real-time control. The tuner selects a frequency band around a target centre frequency and translates the selected band to baseband. The RTL2832U chip functions as an ADC that samples the baseband signal and transfers the raw I/Q samples to the PC. After retrieving the raw I/Q samples the PC calculates the power spectrum using an FFT.

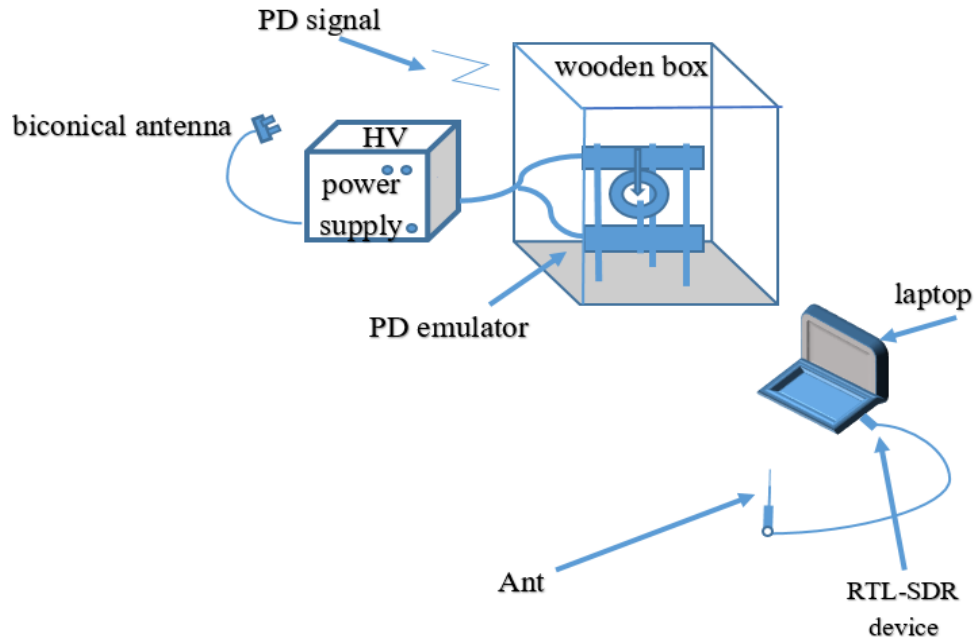


Figure 39. The proposed system.

3.3.3 Summary

Spectrum analysers are a high-cost solution that is usually an overkill for some applications, i.e. most functionalities that are built in spectrum analysers tend to be redundant in case of PD detection. Moreover, spectrum analyzers lack the capability to record seamlessly, long-term data. On the other hand, low-cost SDR devices have less bandwidth; they are flexible, and they have limited processing power. Designing a low-cost solution that has the capability to record seamlessly, and is sufficiently flexible is the only way the situation can be remedied. Table 3 below shows an overview of existing solutions.

Table 3 comparison of existing sensing solutions.			
Metrics	RTL-SDR	USRP	Spectrum analyzer
Cost	Very low	Low	Very high
Size	Very small	Medium	Large
Reliability	Low	High	Very high
Dynamic range	50dB	80 dB for the ADC	90dB
Sensitivity	Low	Medium	High

Freq. Range	24-1700 MHz	DC-6GHz	9KHz -8GHz
Power Consumption	290mA	6V 2.4 A	7.2V 1.5A
Principle advantage	Cost, size	Reliability, Accuracy and cost	Reliability &Accuracy
Dimensions (W x H x D) mm	10x 5 to 315	540 x 22 x 225	194 x 300 x 69
Weight	0.15 kg	1.2 kg	3kg

3.4 USRP as a wide band spectrum analyzer

Several products are based on SDR technology, however not all of them are compatible to work in a sensor network. USRP SDR series are configurable devices and can be connected in a sensor network. One of this series product is the USRP N200. Figure 40 shows Flowchart of USRP N200 for detecting signal energy. Due to the hardware limitations of the USRP N200, the USRP cannot scan a frequency band that is larger than its effective bandwidth (USRP N200 BW is 20MHz) in one time. Instead this can be done in multiple steps hence the swept mode is adopted in this work instead of the FFT mode. This is because the PD band (50-800 MHz) is very wide, and in order to scan the whole PD band, it is required to divide it into sub-bands and to retune until the whole band is covered. In the USRP N200, all samples are sent via the Gigabit Ethernet cable to the PC. These samples are 16-bit I & Q data (complex values). This means 4 bytes per complex sample. The Gigabit Ethernet interface limits the bandwidth to 20MHz in USRP N200 (Hamd Mohamed et al.). There are two important parameters in the swept mode:

Tune delay: it is the required time from the RF front end to tune into a new frequency.

Dwell delay: it is the required time to determine the average values for each center frequency.

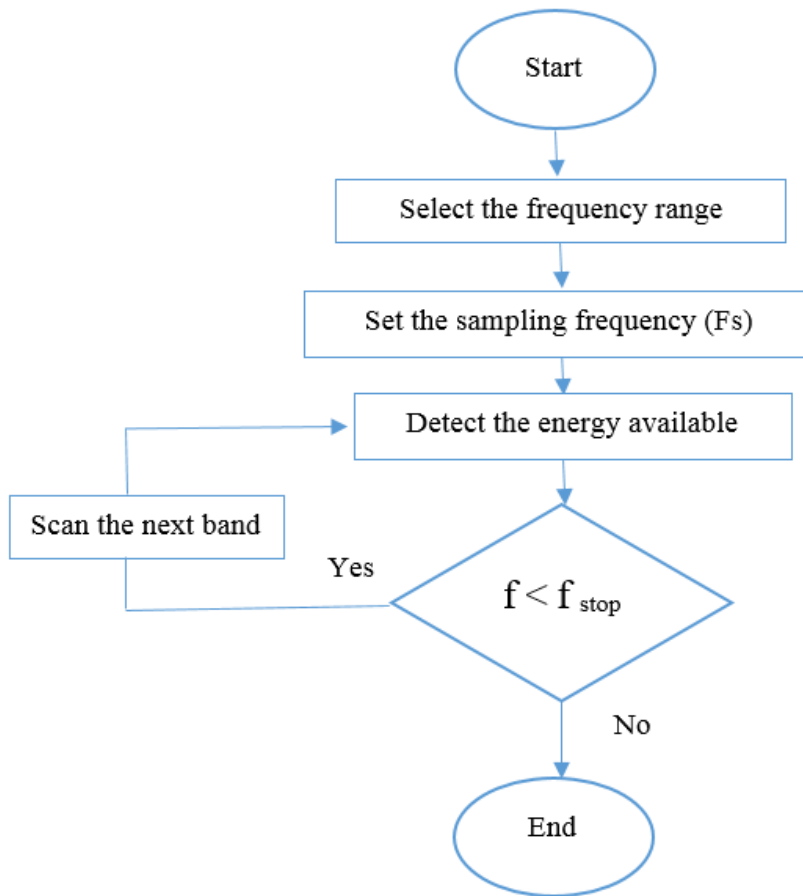


Figure 40. Flowchart of USRP N200 for detecting signal energy.

3.5 The description of the code

This section describes the MATLAB code that sweeps the PD signal a frequency range of 50-800 MHz. The considered USRP is employed to receive and decode the PD signals. The chosen SDR has modes that allow for the capturing and transfer of raw samples to the host computer, thus enabling the system to behave like an inexpensive spectrum analyzer.

To acquire the spectral information, we rely on USRP and MATLAB code. Due to its narrow bandwidth, the device cannot receive data from across the full test band simultaneously. Instead we must rapidly retune the device in order to receive data from multiple center frequencies across the band, and then reconstruct this data on the host computer. The USRP devices, operate in the frequency range of 50-2200 MHz. The device was selected due to its medium cost,

availability, portability, and its frequency coverage in the VHF-UHF bands (Stewart et al., 2015).

The required software tools have been interfaced with the USRP-SDR modules to allow for real-time control. After retrieving the raw I/Q samples from the USRP-SDR sensor, the host computer performs Fast Fourier Transforms (FFT) to obtain spectral information about the received signals. This is carried out multiple times with data from all USRP-SDR retunes, which allows us to construct a full picture of all of the activity across the test band, and produce power spectrum density (PSD) plots.

One key concern is whether the spectral measurements collected by this medium-cost hardware can provide the same level of fidelity and accuracy to those obtained from sophisticated equipment such as high performance spectrum analysers(Stewart et al., 2015).

The term ‘sweeps’ refers to a repetitive process of tuning and retuning the SDR device to different center frequencies in order to obtain spectral information for the full range of the sweep, Figure 41 gives an example of how this process can be used to build up spectral information.

In order to optimize the process, it is better to set the sampling frequency of our SDR to a high value (e.g. 20MHz). Each retune of the USRP-SDR would be 20MHz wide. Each centre frequency, $f_{c, \text{selected}}$ during the retuning process would be 20MHz higher than the previous centre frequency, so in Figure 37, $f_{c(i+1)} = f_{c(i)} + 20\text{MHz}$, and the fifteen retunes would result in a 300MHz band of information with none of the data capture frequency bands overlapping. Using this MATLAB code, it is possible to use the USRP/RTL-SDR device to sweep across a range of the RF spectrum, and produces a MATLAB figure showing all of the PD spectral activity detected(Stewart et al., 2015).

The first section of the code contains a selection of the SDR platform. It is required to select which SDR platform is going to be used weather it is USRP or RTL-SDR, the sdr ID of USRP is set to 1 and RTL-SDR is set to 0. The IP by default is “192.168.10.2” however, it is possible to set it to another value if it is not occupied in the network. The sampling frequency maximum is 25 M Sa/s. And as it takes a higher value as the faster the scan will be. If it is set to 25 MHz, this means that the information bandwidth of the received signal in the MATLAB code is 25 MHz and its spectrum is from $f_c - 12.5 \text{ MHz}$ to $f_c + 12.5 \text{ MHz}$. For the used PD band of 50-800 MHz, it takes about 70 secs to complete the scan process.

Individual 'tunes' of the SDR devices will return bands of spectral information f_s Hz wide

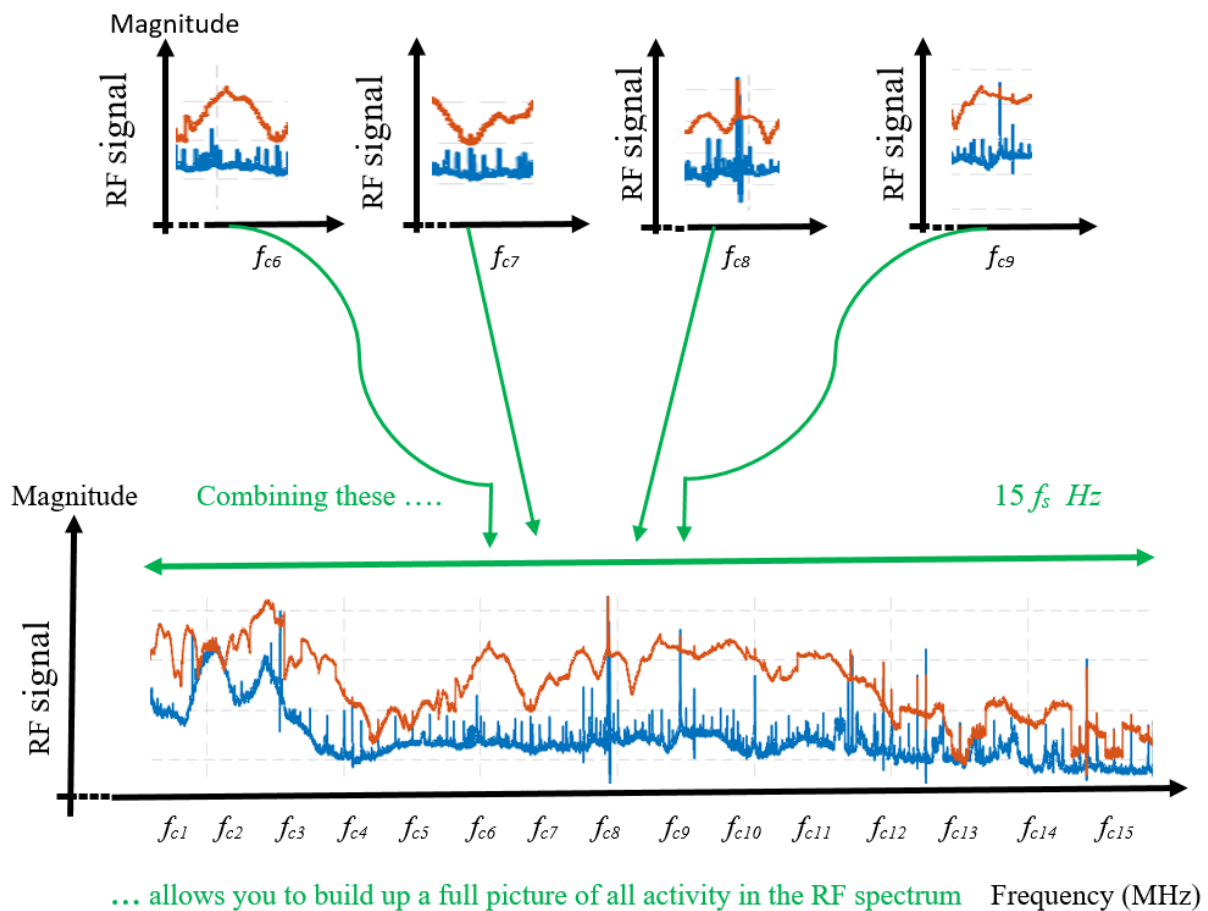


Figure 41. Swept-FFT in spectrum analysis.

```
sdr = 1; % 0=rtlsdr, 1=usrp SELECT SDR
usrp_ipaddress = '192.168.10.2'; % USRP IP address.
sdr_fs = 25 e6; % max is 2.8e6 for RTLSDR, 25e6 for USRP
```

By default, the sampling frequency will be set to value of 2.8 MHz for RTL-SDR. In some cases, when using the RTL-SDR, and to avoid the non-flat frequency response, at some frequencies (beginnings and ends of the band), it is more appropriate to let increment the frequency spectrum with steps less than 2.8MHz (e.g. $f_c - 1.2$ MHz to $f_c + 1.2$ MHz). Therefore, the frequency response will be flatter. Retuning the RTL-SDR in increments of 1.4MHz, then only half of the information is kept. If this process is repeated the full spectrum is obtained.

```
Rtlsdr = 0 % 1=usrp, %sdr = 1 select SDR
sdr_fs = 2.8 e6; % max is 2.8e6 for RTLSDR, 25e6 for USRP.
```


The second section contains the actual code parameters. After selecting the desired SDR platform, it is necessary to set the main parameters to their optimal values. Set the start frequency to the value of 50MHz and the stop frequency to the value of 800MHz (the range of PD of 50 MHz to 800 MHz). The gain can go up to 50dB, however, the optimum value is between 0 and 15 dB. In case that the gain is set to a higher value the USRP device may overload, then the device loses its efficiency and will not be able to distinguish or detect radio signals. The optimum value for the SDR output data frame size which is called `sdr_frmlen` is: 4096×8 . Also this along with other parameters values will be explained later with figures showing the performance according to the range of the values of the parameters.

```
% PARAMETERS (can change)
Location      = 'test';      % location used for figure name
start_freq    = 50e6;        % sweep start frequency Hz
stop_freq     = 800e6;       % sweep stop frequency Hz
sdr_gain      = 10;         % SDR tuner gain in dB
sdr_frmlen    = 4096*8;     % SDR output data frame size
sdr_datatype  = 'single';   % SDR output data type
sdr_ppm       = 0;          % SDR tuner parts per million frequency correction
```

```
% PARAMETERS (can change, but may break code)
nfrmhold      = 20*4;       % number of frames to receive
fft_hold      = 'max';     % hold function "max" or "avg"
nfft          = 2048*8;    % number of points in FFTs (2^something)
dec_factor    = 16;        % output plot downsample
overlap       = 0.5;       % FFT overlap to counter rolloff
nfrmdump      = 100;       % number of frames to dump after retuning (to clear buffer)
```

`nfrmhold` is the number of received frames in every retuning of the USRP N200/RTL-SDR device. This number ideally should be as large as possible, however, increasing it, increases exponentially the required time to execute the code. `fft_hold` describes the method of averaging the received power. Generally, there are two possible settings or configurations: ‘avg’ and ‘max’. If it is set to ‘avg’, the calculation of the mean received power is performed and returned for its spectral component, and when it is set to ‘max’ a MaxHold function will operate to keep the largest power in every spectral component. It is worth mentioning here, that

to detect the PD signal it is required to set the fft-hold function to ‘max’, otherwise the PD signal cannot be detected and observed.

nfft is the number of points in the FFT code. Practically it was found that the optimal value is 8192 points when the number of frames to receive and the output data frame size are set to: 80 and 8192 respectively. dec_factor controls the level of decimation; this is performed before the full sweep is plotted. Here it is set to 16, and this results in an uncrowded plot. ‘overlap’ describes how each retune is overlapped with the next retune. As previously discussed, an adequate overlap ensures not to miss events, and the optimal value is 0.5. This means that the retunes will be in increments of $f_s / 2$, the more overlap is better for accuracy but this will lead to a longer computation time, however, if a maximum overlap of 1 is chosen, then the sweeping will not proceed or retune into the next center frequency. Nfrmdump is the number of dumped frames after each retune. In each retune, 100 frames of IQ samples are required to be dumped until data related to the new center frequency is accessed. Dumping the frames is important so that they do not interfere with the frame averaging process. As discussed earlier, these parameters can be changed, however this may have an undesired effect. The flow of the code as following:

Function: rtl_sdr_rx_specsweep

Function: creat_spectrum

Function: axes_position

Function: resize_spectrum

Function: capture_and_plot

Once the code is run, a connection between the SDR hardware and MATLAB will be established in a few seconds (around 70 seconds if the sampling frequency is set to 25MHz) and it will start receiving frames of data. While this happens, the current center frequency will appear in the MATLAB command window:

```
>> rtl_sdr_rx_specsweep  
  
    f_c = 50MHz  
  
    f_c = 75 MHz  
  
    f_c = 100MHz  
  
    ..    ....
```

MATLAB will continue executing until the full specified frequency range of 50-800MHz is covered, and the frequency spectrum of the PD band is plotted.

3.6 Summary

Partial discharge (PD) is one of the predominant factors to be controlled to ensure reliability and uninterrupted functions of power generators, motors, Gas Insulated Switchgear (GIS) and grid connected power distribution equipment, especially in the future smart grid. The emergence of wireless technology has provided numerous opportunities to optimize remote monitoring and control facilities that can play a significant role in ensuring swift control and restoration of HV plant equipment. In order to monitor PD, several approaches have been employed, however, the existing schemes do not provide an optimal approach for PD signal analysis, and are very costly. In this chapter USRP N200 and an RTL-SDR (Software Defined Radio) based spectrum analyzer have been proposed in order to provide a potentially low cost solution for PD detection and monitoring.

4 Partial discharge detection results

In this chapter the application of Partial Discharge detection using Software Defined Radio technology in the frequency domain is discussed. The proposed system is demonstrated and described, then PD analysis and signal processing are performed. The results obtained using the SDR technology are then validated using a spectrum analyzer. The results are very satisfactory comparing to that of the high cost spectrum analyzers.

4.1 Partial discharge detection using SDR technology

In order to provide reliable operation, the detection of PD is of great significance, and the emergence of wireless technology has provided an alternative to detect and monitor PD events. There are a number of sensing devices available for high frequency signal detection. Some of the solutions, like spectrum analysers, are capable of scanning a wide spectral range, but are not cost effective. A spectrum analyser cannot perform continuous recording for a time period more than a few seconds, and the recorded spectrum requires a higher frequency resolution for better visualization. Furthermore, the unprocessed signal still requires processing to evaluate the energy in a specific band. On the other hand, low-cost SDR spectrum analysers are trimmed for easy and stable recording, but lack flexibility and performance compared to high end commercial types. In order to facilitate distributed spectral or signal sensing, a relatively low-cost sensing platform must be used. Bridging a performance gap between high-end spectrum analysers and the requirement of a low cost spectrum analyser for PD detection, this chapter intends to develop a robust sensing platform for PD detection. In this chapter the application of PD detection using SDR technology in the frequency domain is discussed. The results obtained using SDR technology are then validated using a spectrum analyzer. The results are very satisfactory comparing to that of high cost spectrum analyzers (H Mohamed et al., 2016b).

4.1.1 Partial discharge detection using RTL-SDR dongles

Recently, Realtek RTL2832U demodulator based low-cost USB digital TV tuners have attracted radio scientists and researchers to SDR. SDR can be employed for spectral sensing for wideband signals and hence can be a potential candidate for PD detection. In this work, a study has been conducted for PD detection using a portable spectrum analyser and RTL-SDR dongles, where the spectrum analyser has provided better sensing efficiency at a higher cost, however; the focus of this research is on RTL-SDR based spectral analysis. The performance obtained for RTL-SDR based spectral sensing exhibited certain limitations towards wider bandwidths (H Mohamed et al., 2016b).

4.1.1.1 The Proposed System

The proposed RTL-SDR system has been developed using the RTL2832U IC along with a NooElec NESDR Mini dongle which is supported by open source software. The performance of the proposed RTL-SDR system has been compared with a high-end portable spectrum analyser. Spectral sensing has been analyzed at the following bands: 85 MHz-110 MHz, 600

MHz-700MHz and 50MHz to 800MHz with both a portable spectrum analyser and the RTL-SDR based spectrum analyser. Figure 42 shows the proposed system.

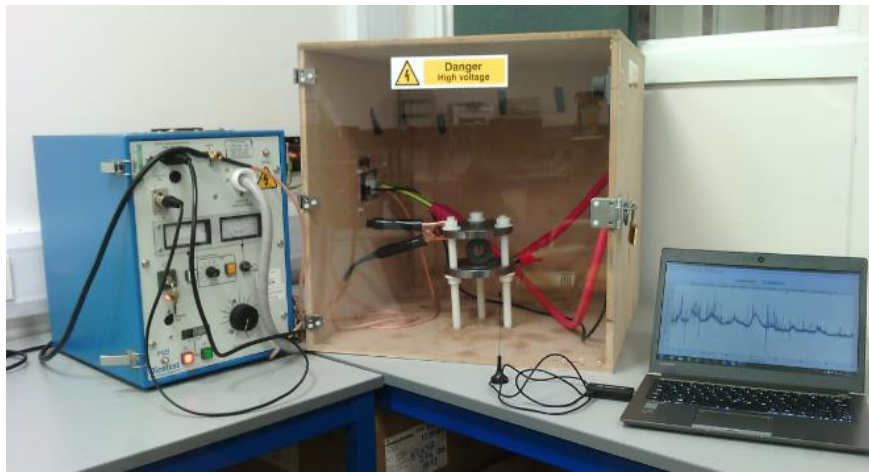


Figure 42. RTL-SDR dongle connected to the laptop via USB port and PD emulator.

4.1.1.2 Results obtained using RTL-SDR device

Figure 43 shows the data taken using the RTL-SDR sensing system for the FM band of (85-110) MHz, while the data obtained using the spectrum analysers are shown in Figure 44.

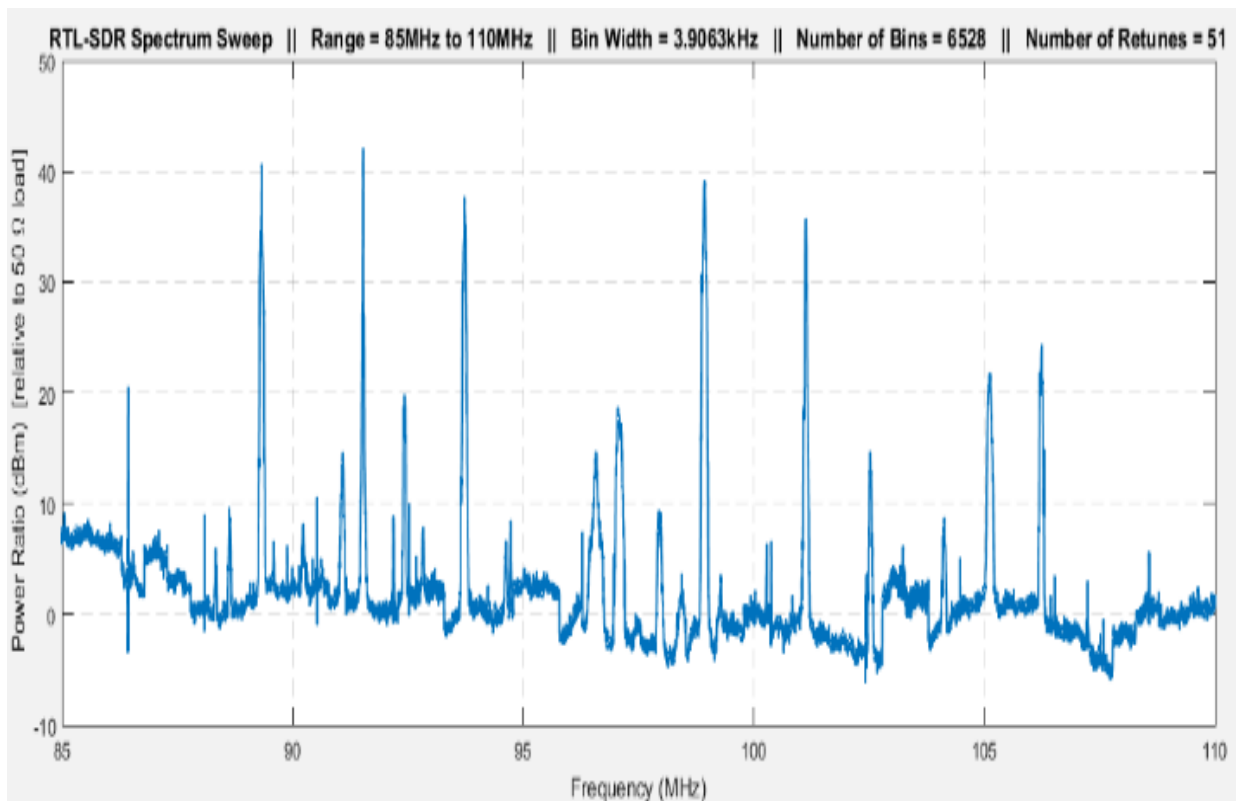


Figure 43. Measured spectrum using the dongle for FM band 85-110 MHz.

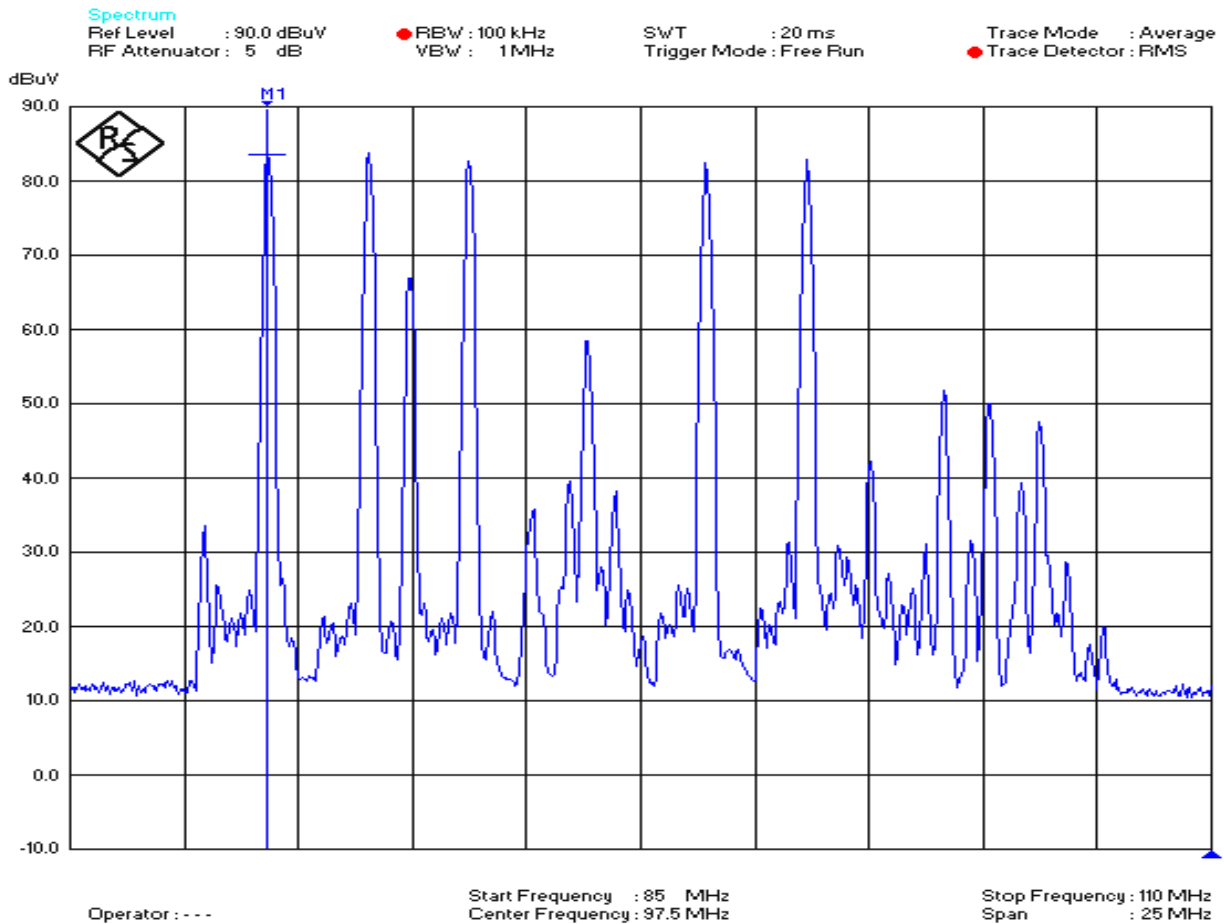


Figure 44. Measured spectrum using an FSH-8 spectrum analyser for the FM band 85-110 MHz.

Figures 45 and 46 show part of the UHF TV band (600-700MHz) using the RTL-SDR dongle and a spectrum analysers respectively. When comparing scans, it is clear that both scans look very similar although the SDR device is not calibrated and it is not indicating the same absolute power levels. The first strong signal is BBC radio 2 at 89.3 MHz. Figures 47 and 48 show the measured spectrum from 50 MHz to 800 MHz using the RTL-SDR dongle in absence of PD and in presence of PD respectively. Similarly, Figures 49 and 50 show the measured spectrum using a spectrum analyser in absence of PD and in presence of PD, respectively. According to both measurement methods the majority of PD occurs at the low frequency band, i.e. from 50MHz to 300MHz. There is a difference of up to 20 dB at some frequencies due to PD radiation, which is a very significant difference. For example, at 125 MHz the difference between the measured spectrum with and without PD using the RTL-SDR dongle is around 19dB, while using the spectrum analyser it is around 21 dB. This yields an error of only 2dB and proves that results obtained by using the SDR device are reliable (H Mohamed et al., 2016b).

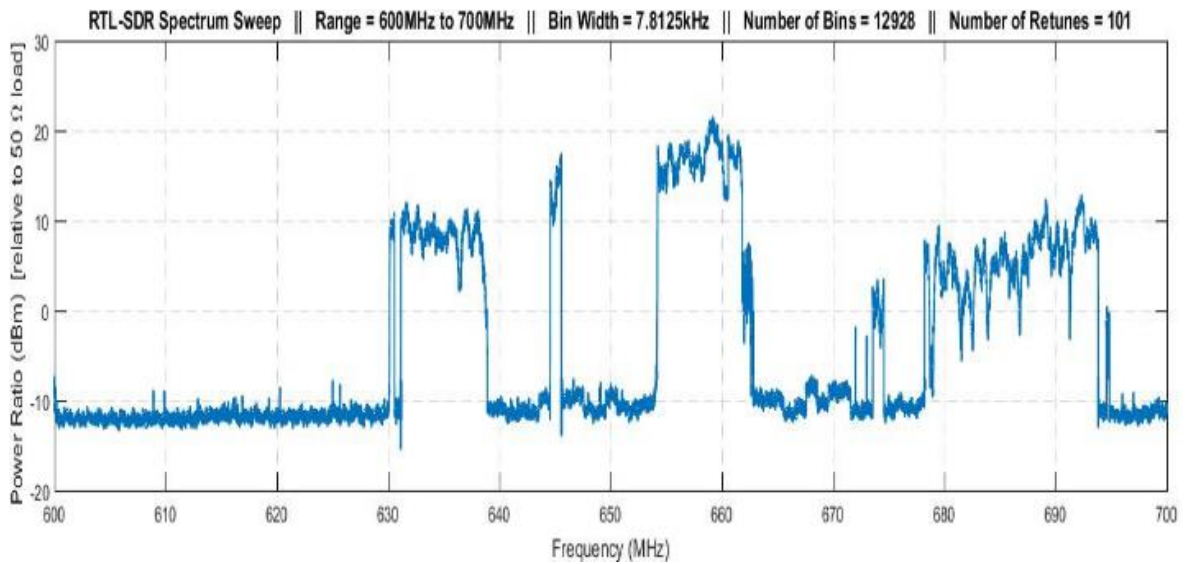


Figure 45. Measured UHF TV band spectrum using the RTL-SDR 600-700 MHz.

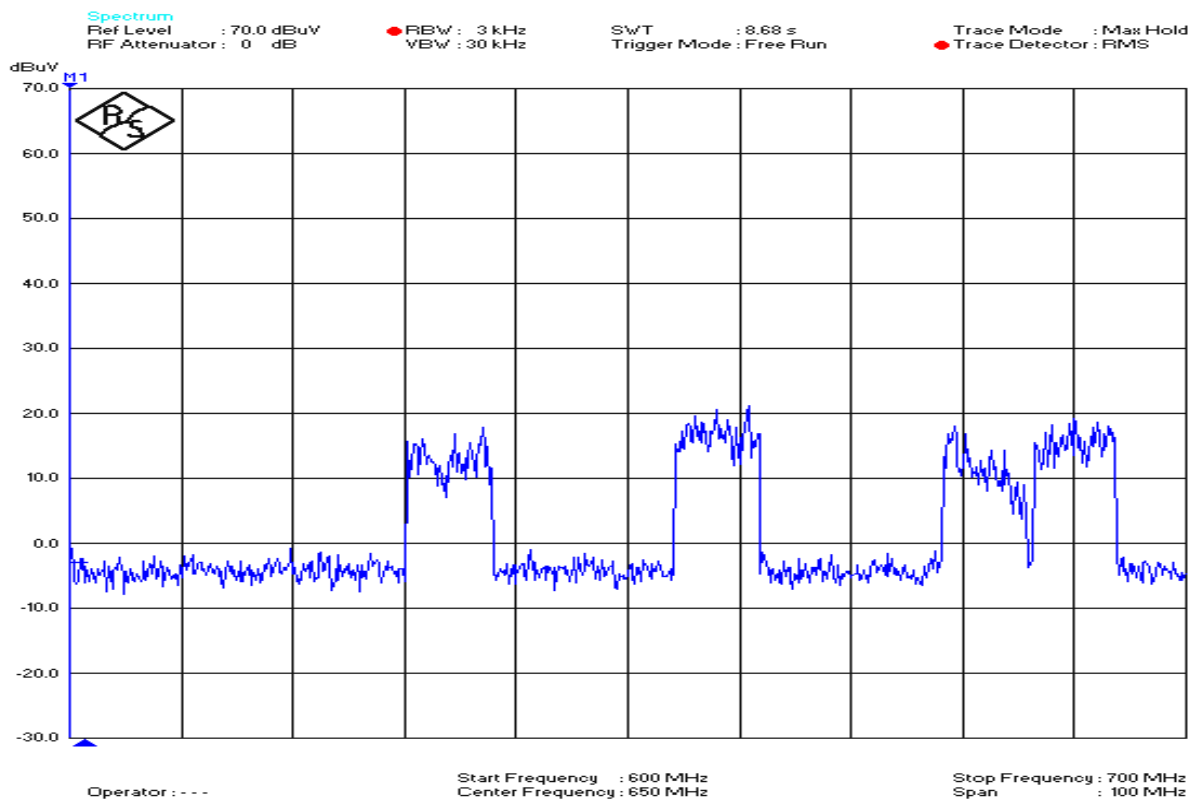


Figure 46. Measured UHF TV band Spectrum using FSH-8 spectrum analyzer 600-700 MHz.

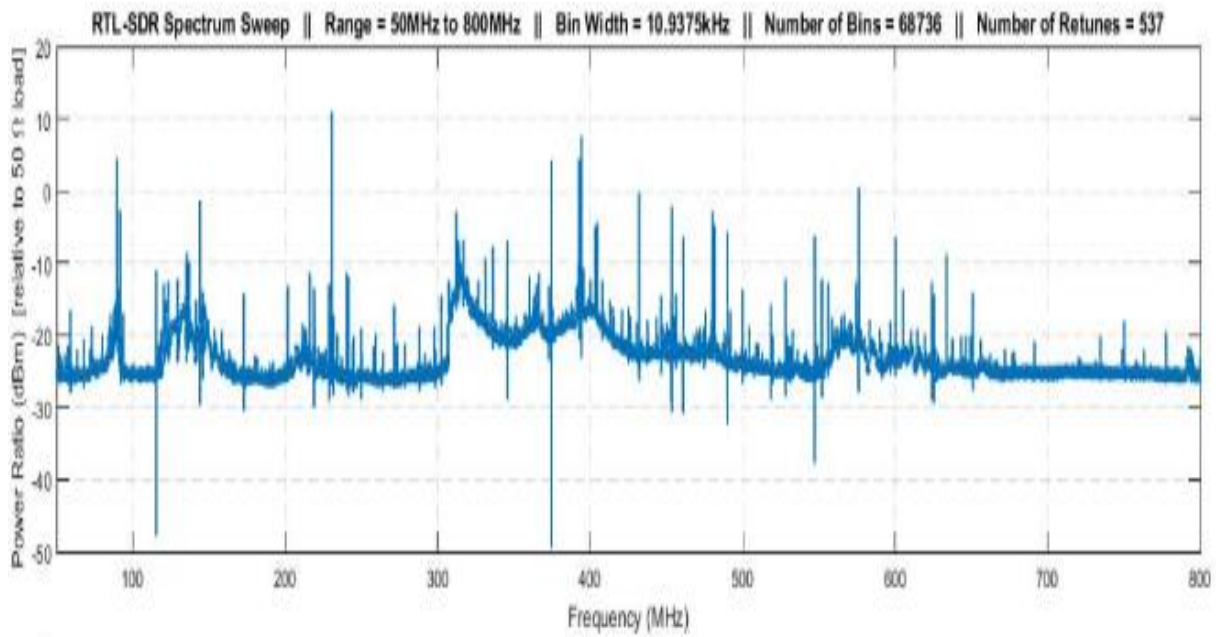


Figure 47. Measured spectrum using the RTL-SDR dongle in absence of PD.

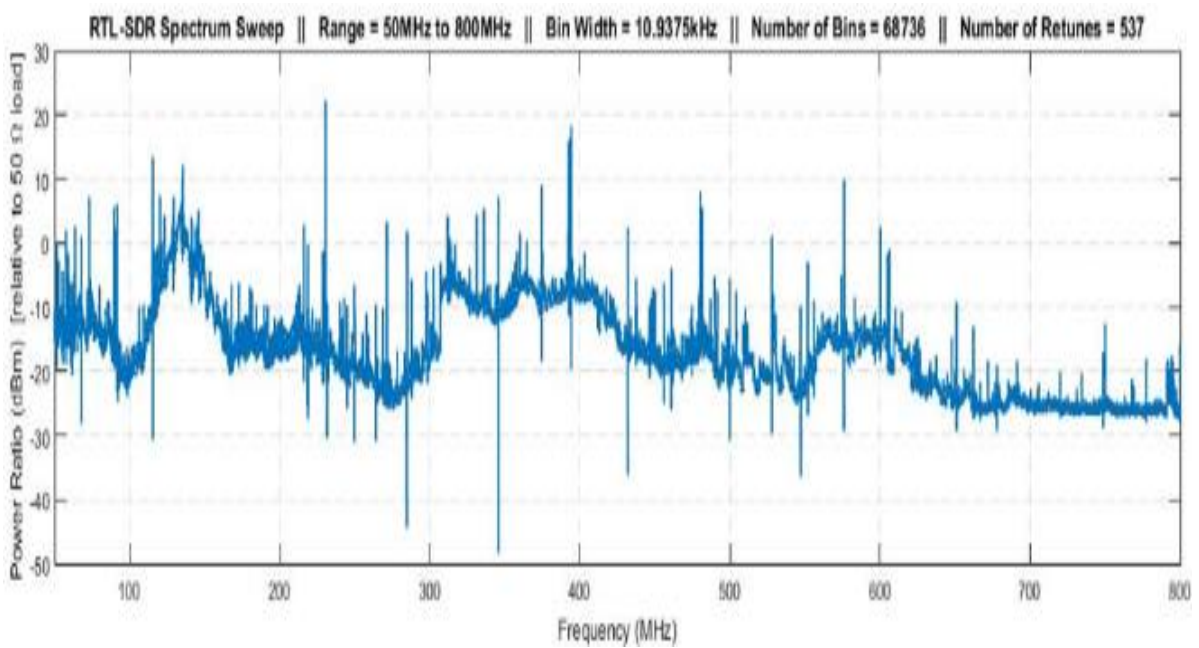


Figure 48. Measured spectrum using the RTL-SDR dongle in presence of PD.

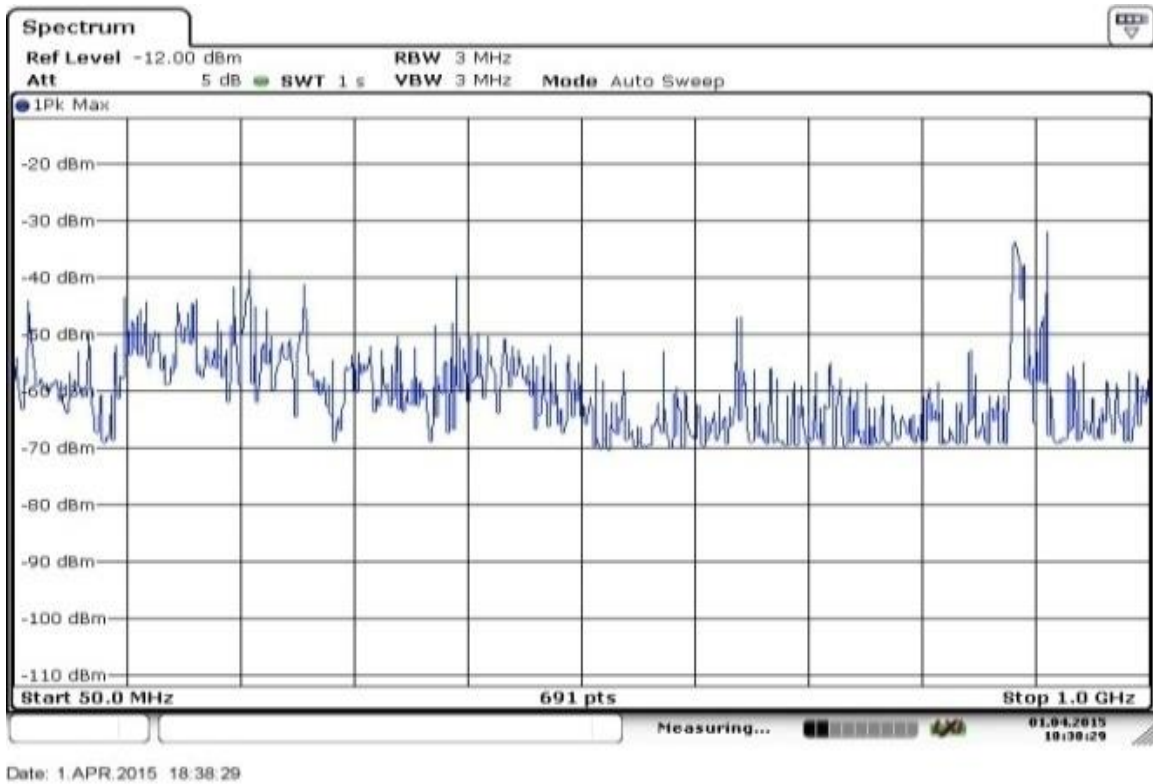


Figure 49. Measured spectrum using a FSV 13.6 GHz R&S Spectrum analyzer in absence of PD.

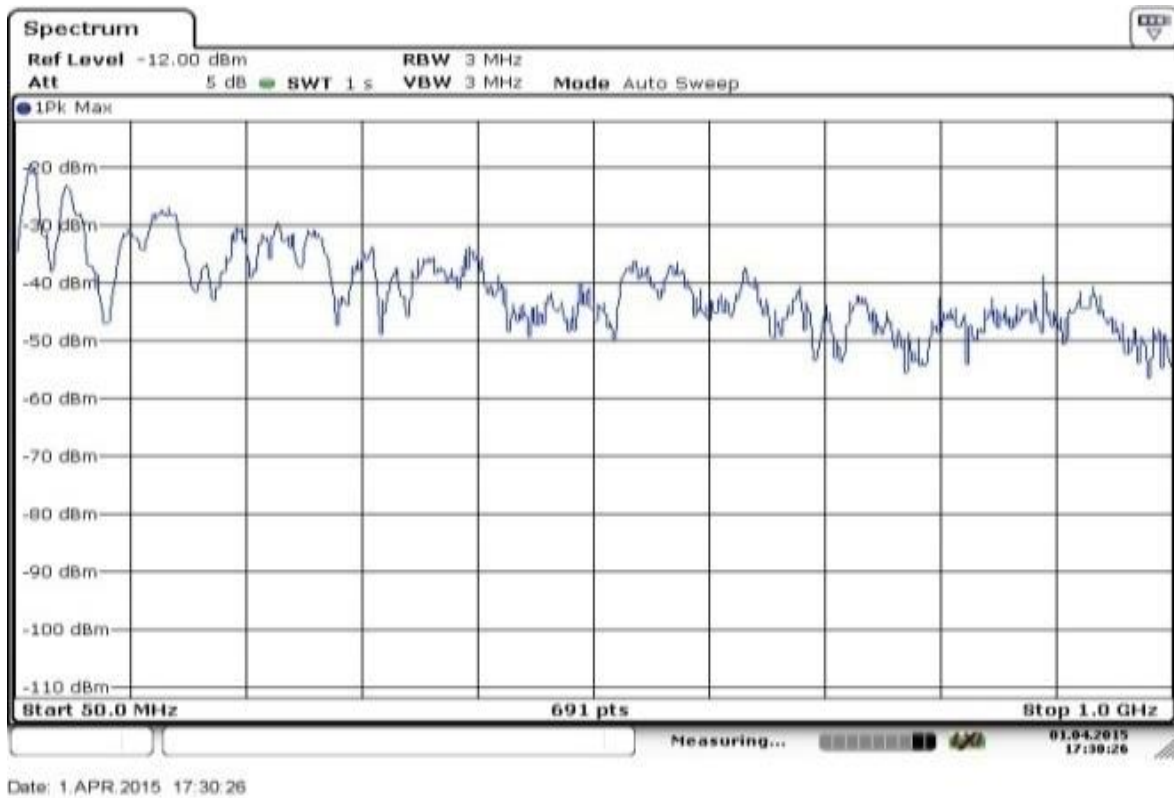


Figure 50. Measured spectrum using a FSV 13.6 GHz R&S Spectrum analyzer in presence of PD.

4.1.2 Partial discharge detection using USRP N200

Recently, researchers from the University of Strathclyde have showed in their work how SDR devices can be used to perform automated sweeps of the RF spectrum. Furthermore, a wideband sensing device called USRP has been developed that possesses better sensing capabilities at higher frequencies and hence it can be a potential candidate for partial discharge detection. The use of USRP SDR can enable low cost and accurate PD detection (H Mohamed et al., 2016a).

4.1.2.1 The experimental set up

The experimental apparatus is shown in Figure 51. The PD emulator is located inside a wooden box with a perspex door to prevent accidental contact with the HV terminals. The detector comprises a USRP N200 transceiver, a laptop and a biconical antenna. The USRP N200 is programmed to measure the spectrum in the 50-800 MHz band while the frequency range of the biconical antenna is 20MHz to 1 GHz, and it has nominal impedance of 50 ohms. The antenna dimensions are 540 mm x 225 mm x 225 mm and its gain at 50MHz is -0.5 dBi. Figure 52 shows the antenna gain in the frequency range of 0-1000 MHz.

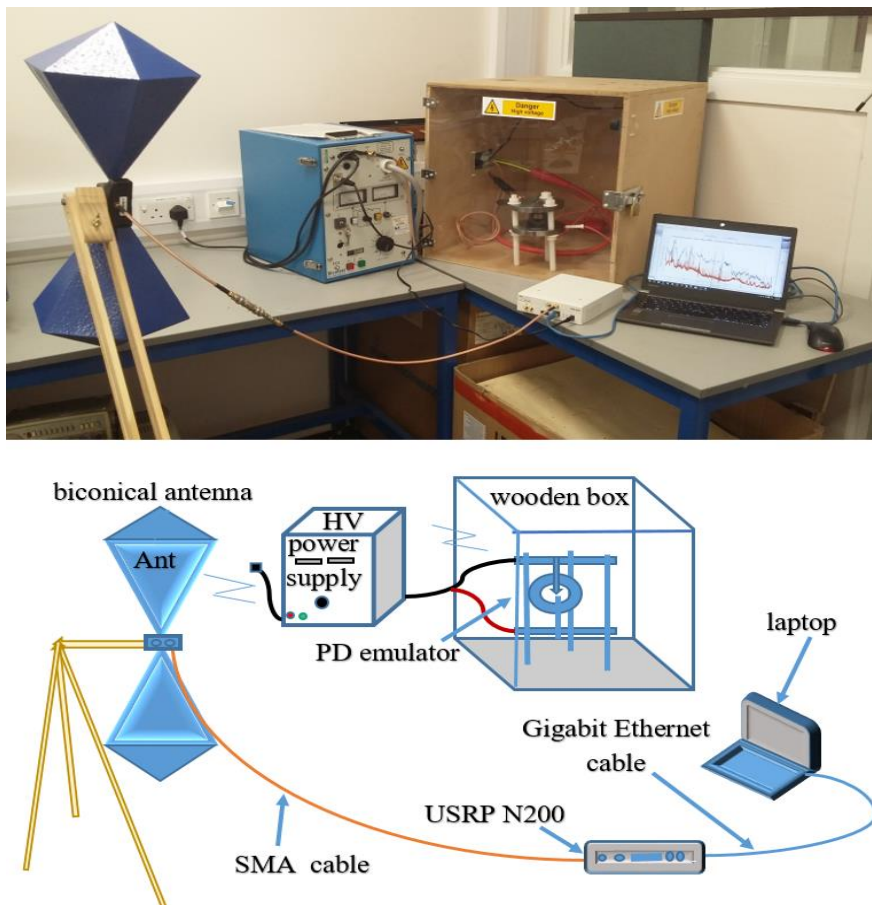


Figure 51. Experimental set up and schematic.

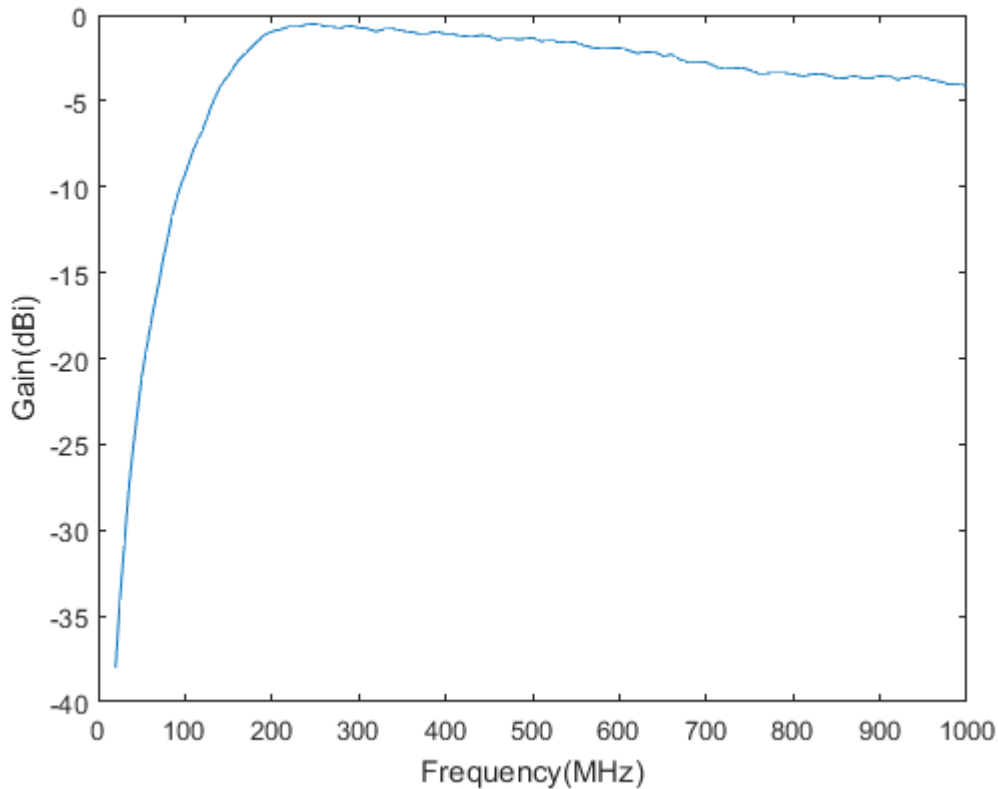


Figure 52. Antenna gain.

PD signal is generated by applying a HV to a PD emulator. PD signals were simultaneously recorded using a spectrum analyzer for validations purposes. Measurements were taken with (i) the HV power supply turned off to obtain the spectrum in the absence of PD, and (ii) with the power supply turned on to obtain the spectrum in the presence of PD. PD signals were recorded using the SDR device and a biconical receiving antenna with USRP N200 followed by spectrum analyser for purposes of validation of the recorded PD data. The USRP N200 transceiver with WBX daughter board has been chosen because the PD band 50-800 MHz is covered with a very good margin. A good feature of USRP is that it allows high speed streaming capability of up to 50 MSa/s in both directions. The high specification of the USRP N200 allowed us to detect the PD signal up to 18 meters away from the source.

Note that here one of the experiments were conducted in the laboratory where the noise level encountered is much less compared to the substation environment. In a practical substation environment, noise or interference mainly consists of continuous sinusoidal-carrier signals (radio frequency) from telecommunication systems and transients caused by thyristor operation or network switching (H Mohamed et al., 2016a).

4.1.2.2 Results Obtained using USRP N200

Figures 53 and 54 show the spectrum when the PD signal is absent (blue curve) and when the PD signal is present (red curve) using the USRP N200 and the spectrum analyzer respectively. This was recorded at distance of 3 meter from the PD emulator in the laboratory. The power spectrum is dominated by low frequencies, particularly the frequencies 50-650 Mhz. However, closer inspection of the power spectrum shows that there is also a small amount of power at higher frequencies 650-800 MHz.

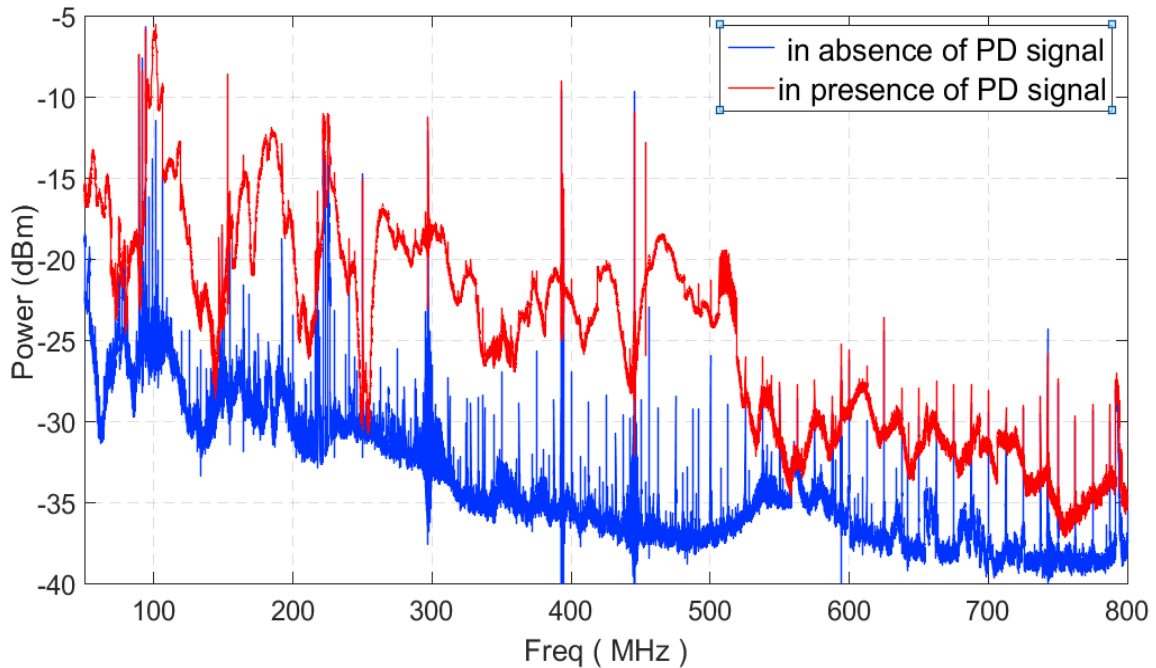


Figure 53. The measured spectra using USRP N200 transceiver.

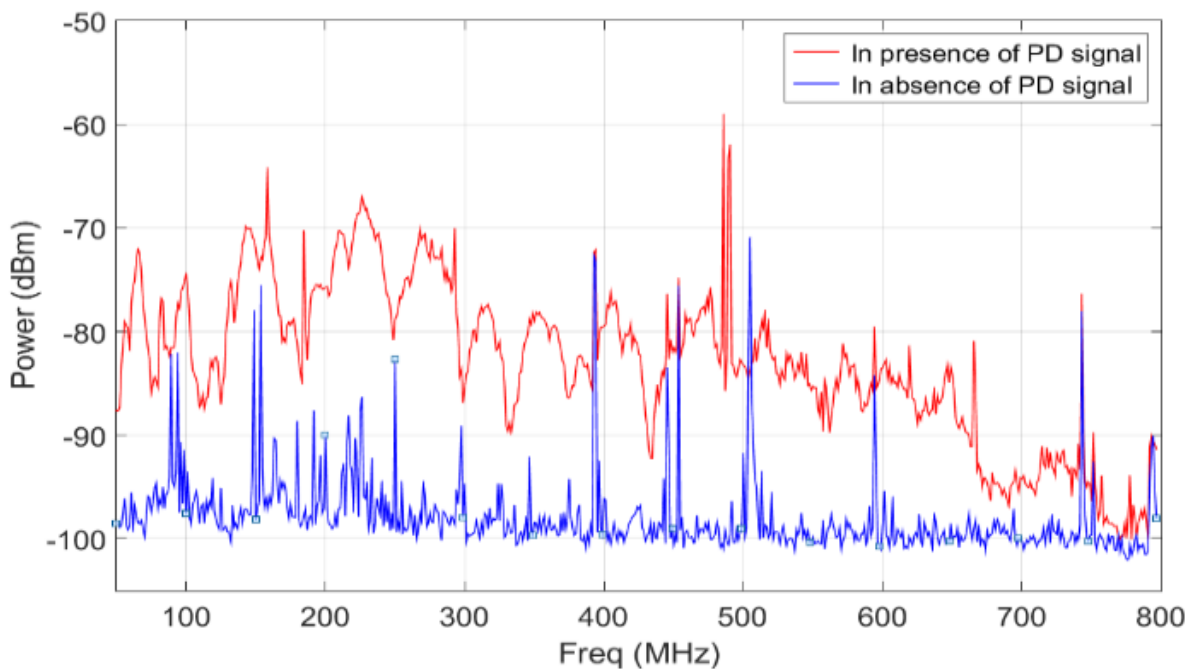


Figure 54 The measured spectra using the FSH-8 spectrum analyzer.

Figure 54 Table 4 Comparison between the measured spectrum using the spectrum analyser and the RTL-SDR dongle and USRP N200.						
Freq. MHz	Measured spectrum using the RTL-SDR dongle dB not calibrated		Measured spectrum using the Spectrum analyser dB calibrated		Measured spectrum using the USRP dB not calibrated	
	In presence of PD	In absence of PD	In presence of PD	In absence of PD	In presence of PD	In absence of PD
50	-10	-25	-88	-99	-21	-28
100	-20	-25	-75	-95	-7	-30
190	-15	-25	-76	-98	-22	-32
225	-16	-23	-67	-90	-17	-37
300	-18	-25	-85	-95	-33	-36
460	-17	-23	-100	-80	-30	-37
700	-25	-25	-100	-95	-37	-40

The other experiment was conducted outside where the interference clearly exists (see Figure 55). Evidence of interference from communication signals can be seen at around 240 MHz for digital radio, also at around 560 MHz to 700 MHz for TV broadcasting. It is clear that the both curves are noisy and especially the curve when the PD signal is absent. Before running the PD localization algorithm signal processing must be implemented in order to obtain an accurate PD location. It is required that several records of PD signal be recorded at different positions.

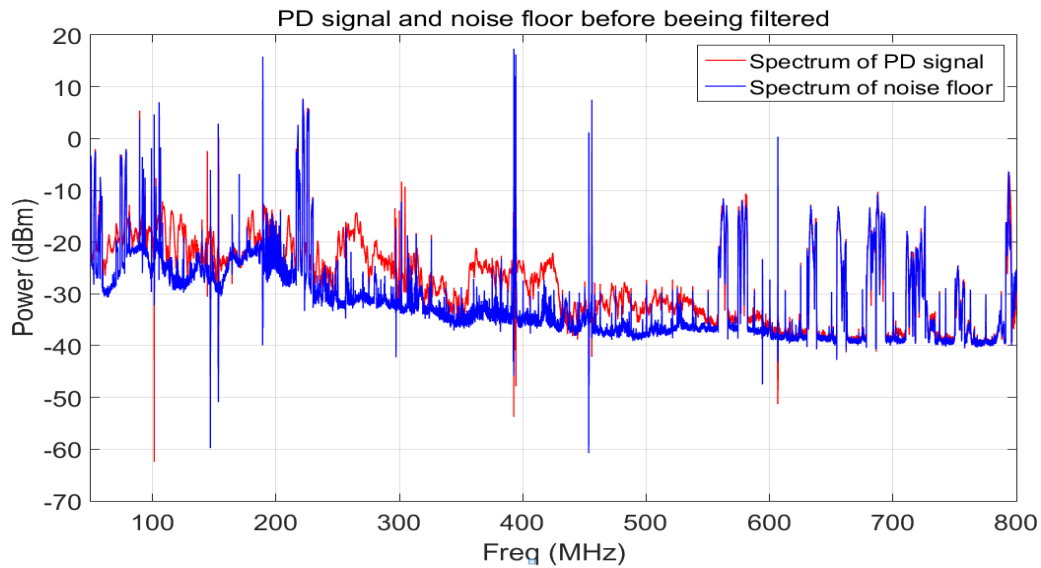


Figure 55 The measured spectra using USRP transceiver (outside the lab).

4.2 Partial discharge analysis

The main difficulty involved in the PD signal analysis is to free the PD signal from surrounding noise and interferences present onsite. The two broad types of interferences that pollute the PD signals are random internal noise and externally coupled disturbances. Random noise results from random fluctuations in electronic devices such as amplifiers, ICs, detection circuit impedance etc. The external interferences are further broadly classified as discrete spectral interferences (DSI), periodic pulse shaped interferences and stochastic pulse shaped interferences. The DSI results from radio transmissions (Satish & Nazneen, 2003) (Meijer et al., 2006). The periodic pulse shaped interferences result from power electronics circuits or during periodic switching of adjustable speed thyristor drives. Stochastic pulse shaped interferences result from infrequent switching operations, arcing between metallic contacts, etc. For rejecting the noise and interferences from the PD signal various de-noising methods are adopted. Among the denoising methods. A median filter is a powerful tool in extracting the PD signal from severe noise and interferences. A median filter is simple and it can filter out the spikes that are caused by an interferer signal from radio communication systems.

4.2.1 The filtering algorithms

4.2.2 Median filter

Median filter is the most commonly used signal processing technique based on statistics. Median filtering is a non-linear, low-pass filtering method that can remove white or salt and pepper noise from an image or an audio signal. It operates directly on samples of acquired signals or images and it has the tendency of edge-preserving smoothing (H.-M. Lin & Willson, 1988). The non-linear function of the median filter can be expressed as:

$$y(n) = \text{med}[x(n - k), x(n - k + 1), \dots, x(n + k - 1), x(n + k)] \quad (5.1)$$

Where $x(n)$ is the input and the $y(n)$ is the output signal. The filter has to do a collection of window containing $N=2k+1$ samples of the signal, then sorts the set of the samples either in ascending or descending order, then selects the mid-value sample (the median). For simplicity, N is commonly odd. But it is possible to take an even number and in this case the median is taken as shown in the equation below. Supposing that x_1 is the smallest value and the x_{2k+1} the largest value.

$$\text{Med}[x_1, x_2, \dots, x_N] = \begin{cases} x_{k+1}, & n \text{ odd} \\ \frac{1}{2}(x_k + x_{k+1}), & n \text{ even} \end{cases} \dots (5.2)$$

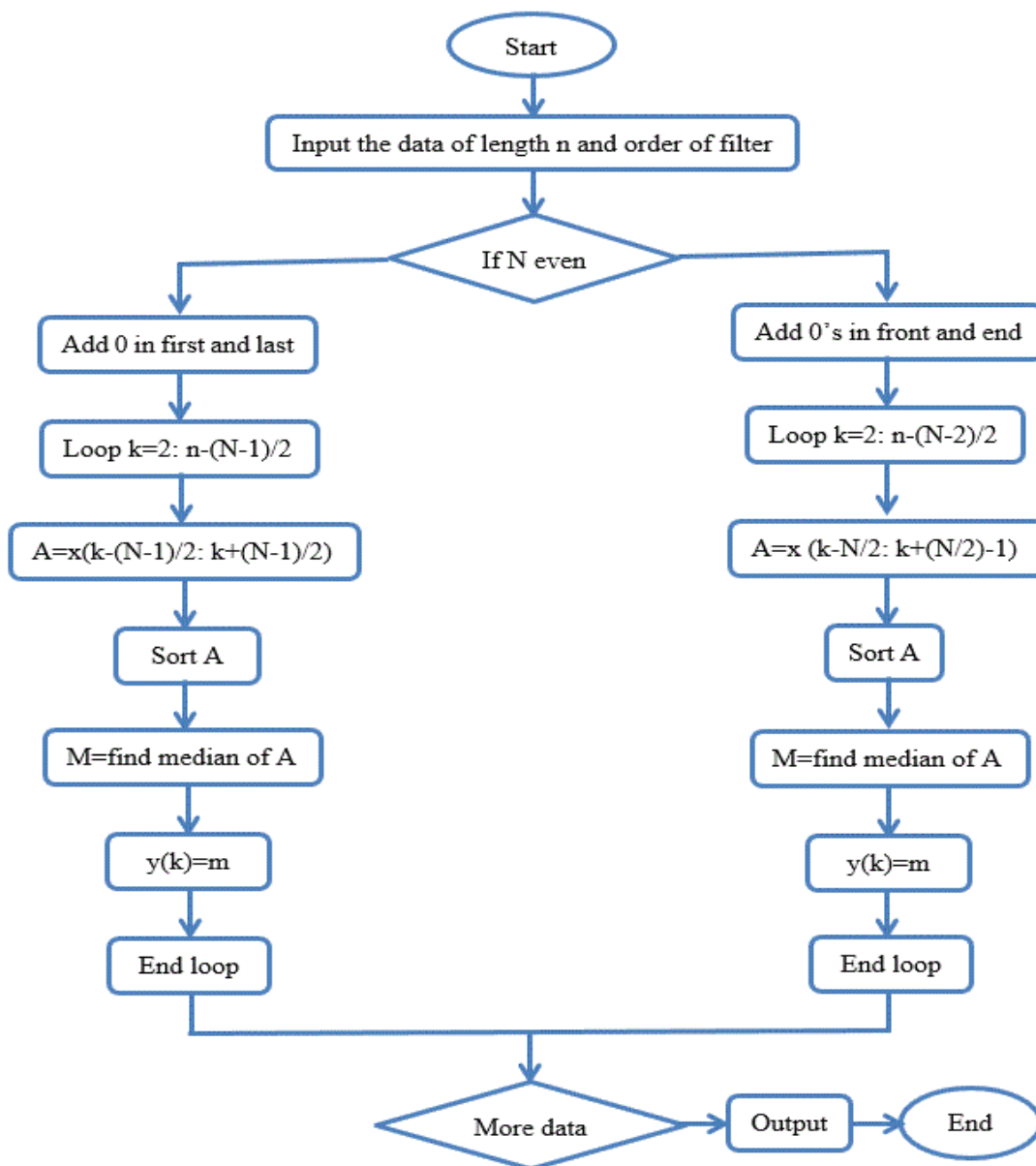


Figure 56. Flowchart of the median filter implementation.

4.2.2.1 Moving Average filter

A moving average filter operates by taking the average of M data points in the input signal to produce a single point as an output signal. It can be expressed as:

$$x_{avg} = \frac{1}{M} \sum_{i=1}^M x(i) \quad (5.3)$$

Where $x(i)$ is the input signal and x_{avg} are the output signal of the moving average filter and M denotes the observation window length. It is worth mentioning here that there is a trade-off between the number of moving average points and the noise, as the more the number of points the less noise and the edges become less sharp. Hence the optimal solution for this problem is the moving average filter specifying the lowest noise possible for a given edge sharpness (Guiñón, Ortega, García-Antón, & Pérez-Herranz, 2007).

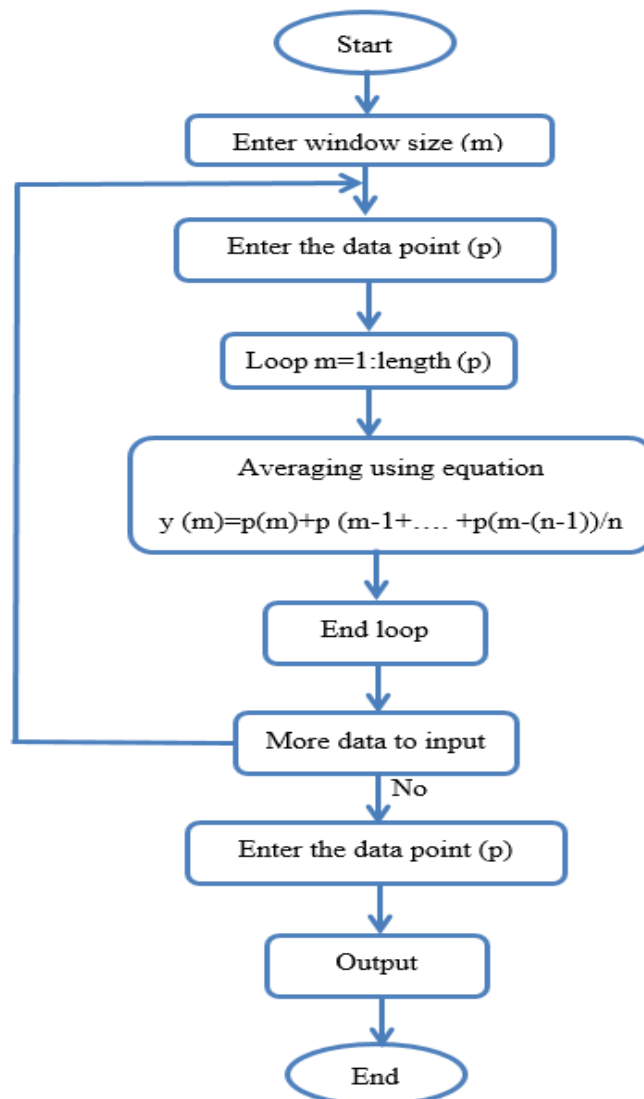


Figure 57. Flowchart of the moving average filter implementation.

4.2.2.2 Spike removal algorithm

The purpose of this algorithm is to eliminate the spikes (the coherent inference mainly from FM and TV broadcasting signals). Thus it is natural to assume that low-pass filtering the raw voltage signal will remove the spikes and that what remains will be a pure estimate of the PD. This resulting signal was obtained by taking the frequency content of the wideband signal obtained from our USRP N200 transceiver, after removing the spikes using the spike removal algorithm presented in the following text. Spike detection and sorting based on the high-pass filtered wideband signal were performed off-line using established methods (HA, Tyagi, Krishnan, & Mallikarjunappa, 2011).

To remove these spikes and obtain reliable and clear spectra, some types of filters must be used, we first selected a median filter followed by a moving average filter.

Command	explanation
medfiltLoopVolt= medfilt1(yin,100);	% applying median filter of order 100 on the signal yin
Plot (xin,medfiltLoop- Voltage,'k')	% applying median filter of order 100 on the signal yin %plotting the signal after applying the filter and smoothing it

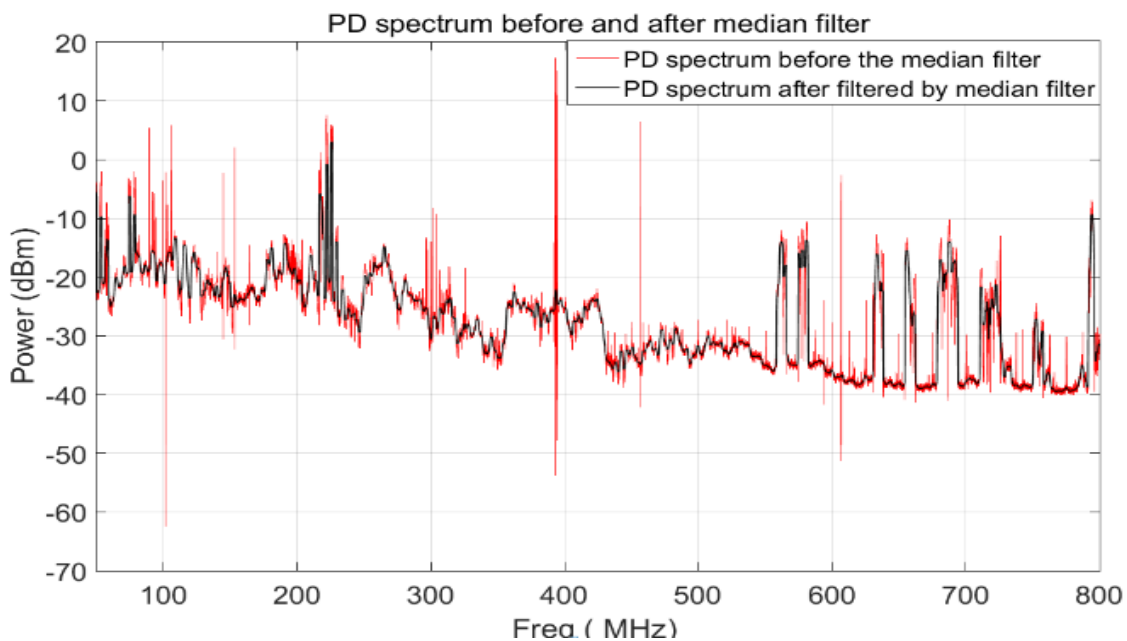


Figure 58. The output of the median filter.

Figure 58 shows the output of the median filter for the original spectrum when the PD is present (red curve) and the filtered spectrum (black curve), by looking at the spikes (in the red curve), it is clear that these spikes have been removed, however at some frequencies there are still some spikes and we need another filter at a second stage. This is shown in Figure 59 Although this filtering reduces the amplitude of the waveform, most of the residual signal remains and this residual retains the basic shape of the original waveform.

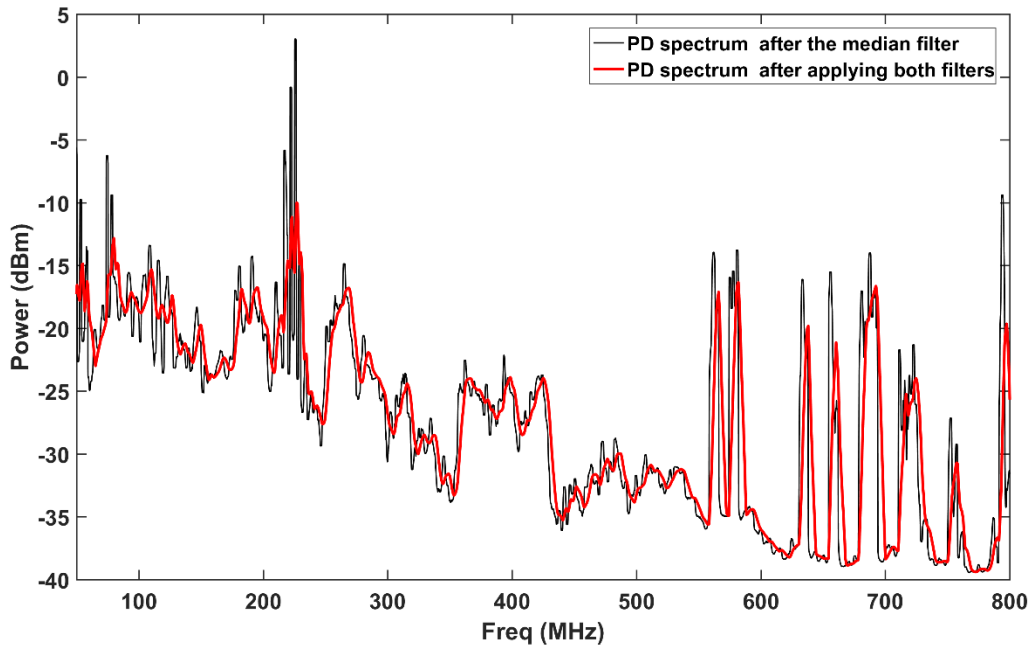


Figure 59. The output of the median filter.

Command	explanation
Range=250;	%range value. It directly affects the output of filtering
r=ones (1, range)/range;	% r is the window for filtering
DS=filter(r,1,medfilt- LoopVolt)	%applying the filter to the output obtained after median filtering

The same process is performed on the noise signal or the spectrum when the PD signal is absent. Figure 60 and 61 show the results after the first filter and the second filter.

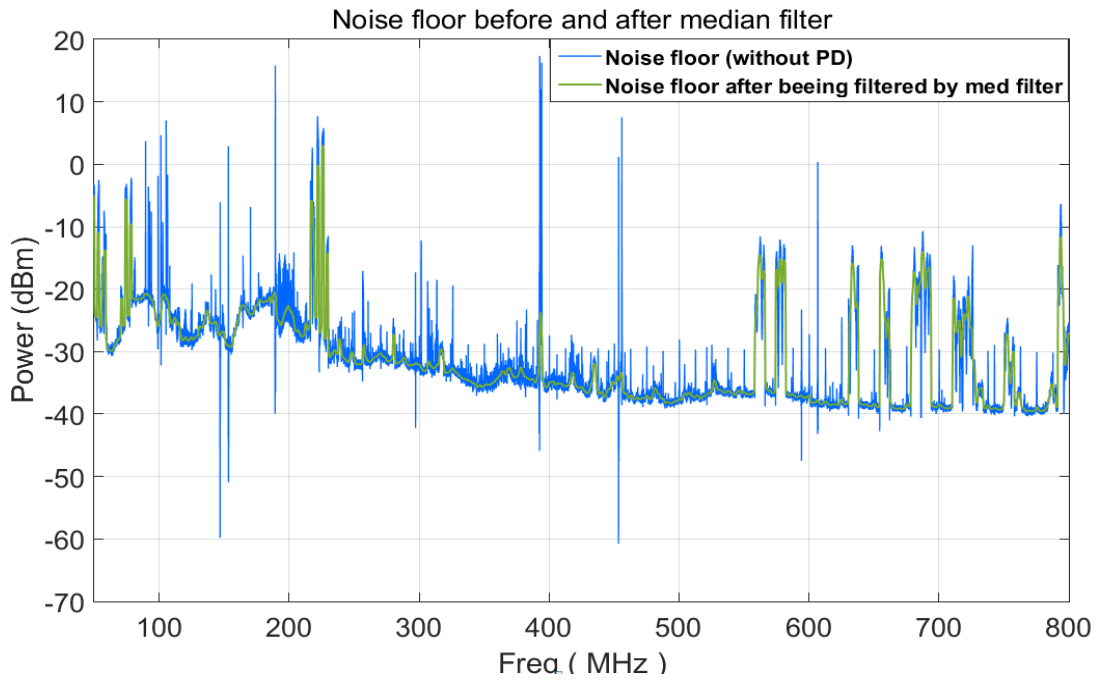


Figure 60. The output of the median filter on the noise signal.

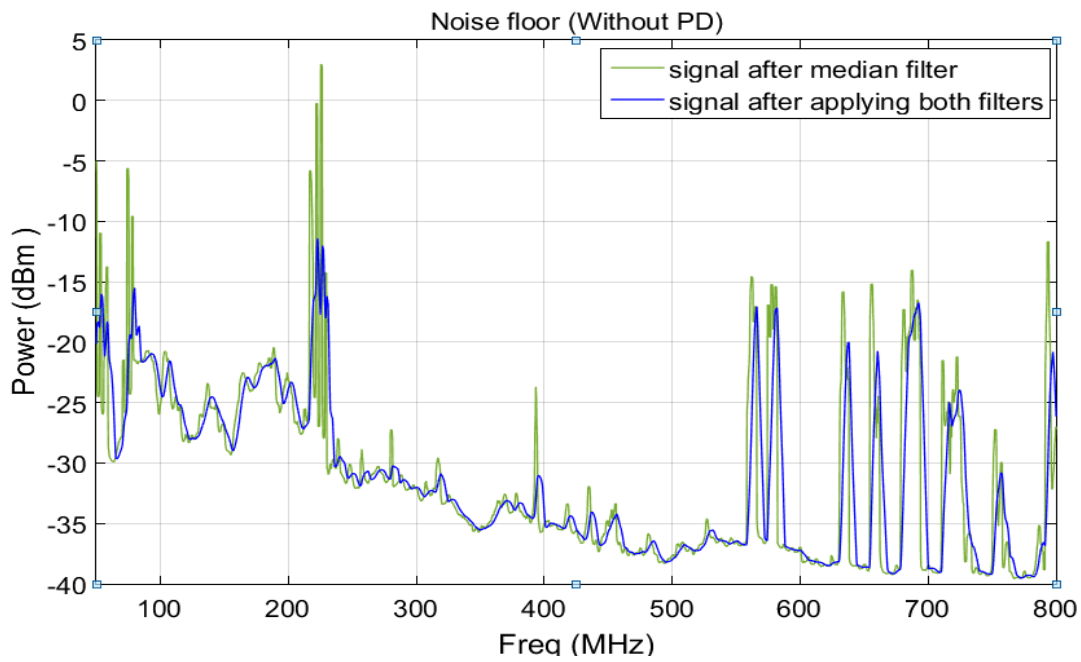


Figure 61. The output of the moving average filter on the noise signal.

The final results after both filters for the PD signal and noise are shown in Figure 62. Comparing it to the spectra shown in Figure 55, it can be mentioned that our simulation results reveal that the final results are clear and the spikes have been removed. Figure 63 shows the difference between two spectra in milliWatts after converting the value from dB into milliWatts (linear scale).

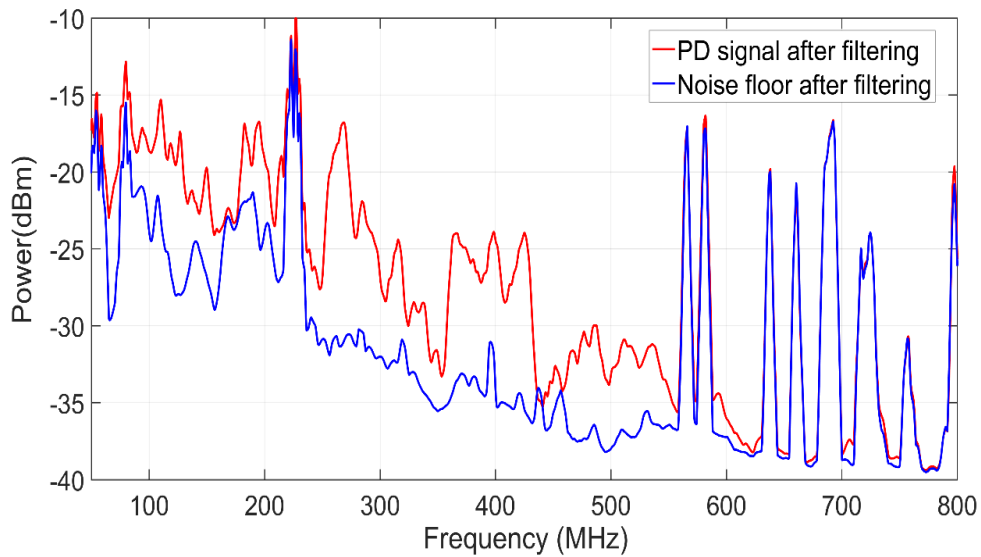


Figure 62 The signals after being filtered.

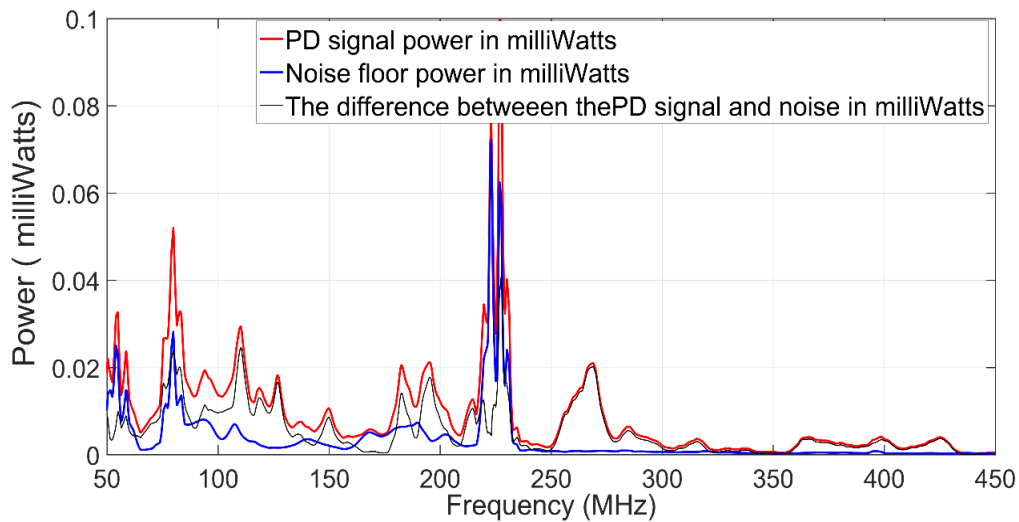


Figure 63. The difference between the PD signal and noise in a linear scale.

4.3 Performance Evaluation

In this section, the evaluation of the performance of the performed research work and assessment for PD detection using the USRP N200 and the conventional RTL SDR model will be discussed. Here it has been intended to explore the limitations of conventional RTL-SDR systems for wideband spectrum analysis and partial discharge sensing and to evaluate the performance of the proposed system for partial discharge detection at a higher bandwidth. Compared to sophisticated hardware like spectrum analyzers and USRP GNU radios, the conventional RTL-SDR device has been found to be limited in the following manner:

4.3.1 Limited Sensing Sensitivity

While generic USRP outputs 14-bit 4-quadrature samples, RTL-SDR outputs 8-bit quadrature signal samples. Because of this resolution difference, RTL-SDR is less sensitive to weak signals and can fail to detect them, especially the detection of partial discharge is very difficult using conventional RTL-SDR sensing systems. But employing the proposed system, the enhanced RTL-SDR system has exhibited better discharge detection and weak signal detection across a wideband spectrum by incorporating MaxHold and resolution bandwidth variation.

4.3.2 Limited Sensing Bandwidth

In this research it has been found that the USRP supports up to 20 MHz bandwidth, while some advanced spectrum analyzers can sense even more bandwidth, but the conventional RTL-SDR can only support up to 2.4 MHz. To monitor a frequency band wider than 2.4 MHz, RTL-SDR requires sweeping the band sequentially. This means that the conventional RTL-SDR can fail to detect certain short-term transmissions or partial discharge that occupies only a small segment of the frequency band. Implementing the variations in resolution bandwidth the sensing capability of the proposed RTL-SDR has been enhanced and partial discharge can be detected even across wideband radio spectrum. The performance analysis made with portable spectrum analyser and two RTL-SDR dongles has exhibited minimal differences, illustrating optimal solution for partial discharge detection in radio range. To achieve better results, the implementation of windowing function, sweeping, MaxHold variation and tuning of resolution bandwidth can be considered in future.

4.3.3 Impact on Sensing Sensitivity

In the employed system, performing quantification of the sensing sensitivity an analysis has been done that distinguishes the sophisticated spectrum analyser and RTL-SDR performance for partial discharge detection and spectrum signal measurements. Initially, the FM spectrum signals were scanned using the proposed RTL-SDR system and a spectrum analyser device individually for a sensing sensitivity for defined bandwidth range (85 MHz-110 MHz, 500 MHz-600MHz and 800MHz to 970MHz respectively). Observing the results, the RTL-SDR based scheme was found to be exhibiting good spectrum sensing for a wideband radio range. In addition, the proposed system can detect partial discharge along with weak signals across a wideband spectrum range of 50 to 800 MHz.

4.3.4 Signal and Noise Measurements

In addition to the spectrum sensing sensitivity, the noise power reported by each sensing model has been analysed when there is no active transmission. As, RTL-SDR and spectrum analyser

both have different noise floors, the emphasis has been put on assessing the variance of the noise power as a function of the sensing duration. Initially, in the employed research it has been observed that in comparison to a spectrum analyser, the RTL-SDRs platforms report a higher noise variance. Furthermore, it has been realized that the increase in noise variance can be compensated by increasing the sensing duration and using the MaxHold function. As soon as the sensing duration increases beyond 1m sec, the RTL-SDR performs in the same manner as a spectrum analyzer, thus providing an optimal solution for low cost wideband spectrum sensing. Observing the respective performance of RTL-SDR and spectrum analyser, we observed that the latter can reliably detect signals with $SNR \geq -2dB$, which increases to 10dB for a RTL-SDR based portable spectrum sensor. In the experimental test with traditional RTL-SDR it was observed that it results into a SNR of 8-13 dB depicting its disability towards sensing weaker signals. In this context the proposed and optimized RTL-SDR system employing windowing, MaxHold function and frequency resolution based tuning has strengthened the proposed system for better sensing of partial discharge (H Mohamed et al., 2016b).

4.4 Summary

Considering the significance of PD detection for HV plant equipment, a low cost, high efficiency PD detection and sensing scheme has been proposed using RTL-SDR receivers. Sophisticated spectrum analyzers provide better accuracy for PD detection, however, this solution is expensive. PD detection has been performed using a portable spectrum analyzer, RTL-SDR devices and USRP N200 devices. It has been found that the SDR based solutions PD detection can give accurate spectrum analysis at higher frequencies. The key limitations of the RTL-SDR dongles have been discussed, especially regarding the non-calibrated relative nature of power measurements and reliability. A PD detection method using SDR software by means of a USRP has been chosen to be employed for further work in this research. The performance of the selected spectrum sensing platform has been verified in experiments conducted using high-end commercial spectrum analysers. When comparing USRP results with spectrum analyser results, a good level of similarity is obtained. The results obtained in this research show that USRP and RTL-SDR can be an attractive low to medium cost solutions for spectral PD detection.

5 Partial discharge localization based on received signal strength

In this chapter a partial discharge detection and localization system using the SDR technique is demonstrated. Firstly, This chapter gives a brief introduction about the localization algorithms that are previously and recently employed for partial discharge detection and localization, then introduces the Received Signal Strength (RSS) algorithm, and how it works. The experimental set-up is demonstrated followed by the localization results. The PD signals are captured using SDR technology (USRP N200) which is connected to a laptop. Due to the limitation of the hardware a single USRP N200 device is used to record PD signals at several locations. The recorded signals then are entered to a MATLAB code and processed offline and hence the PD source is localized. Considering the noisy environment and the simplicity of the system, the estimation error obtained using the selected localization system is satisfactory.

5.1 Introduction

PD occurs when insulation containing voids is subjected to high voltages. If left untreated PD can degrade insulation until, eventually, catastrophic insulation failure occurs. The detection of PD current pulses, however, can allow incipient insulation faults to be identified, located and repaired prior to plant failure (H Mohamed et al., 2016a).

PD pulse detection and monitoring is one of the areas that also requires the use of wireless technology. The PD detection and localization is an important area that did not receive as much attention as it should have to exploit the advantages of available SDR technology. Traditionally PD is detected using galvanic contact methods or sensors that use capacitive/inductive coupling. Recently, however, the use of wireless technology has provided an alternative method to detect and monitor PD. Wireless reception of PD energy has, until now, involved receiving the radiated broadband signals using a broadband receiver. The emergence of wireless network technology and software defined radio has opened new opportunities in PD monitoring. This chapter proposes the use of Software Defined Radio technology for PD detection and localization. Consequently, experimental results show that the proposed system correctly detects PD signals and compares with the results obtained using a spectrum analyzer for validation purposes, implying it may be considered as a simple and reliable candidate for PD detection systems (H Mohamed et al., 2017).

Several localization approaches have been employed to locate a PD source in power stations, these include: time of arrival (TOA), time difference of arrival (TDOA) and angle of arrival (AOA). Classification of these methods is based on the range where they estimate the location of the PD source. However, each one of them has its strengths and weaknesses.

In recent times the received signal strength (RSS) approach has gained importance for indoor and outdoor localization. The RSS algorithm is preferred due to its cost-effectiveness for source localization and where it requires a minimal hardware and software and it does not need the employment of an antenna array or time synchronization as in TOA and TDOA. In general, and according to the need for the receiver coordinates, there are two categories of RSS based source localization: symbolic localization and physical localization, where the coordinates are only required in physical localizations (Xiong et al., 2015; Xu et al., 2014a).

In physical source localization, obtaining the source location is based on the receiver locations and their measurements of the received power. Closer the distance between the source and the receivers, the more accurate the estimation of the source location. Most used algorithms for

RSS-based physical source localization are: gradient, trilateration and centroid methods(Xu et al., 2014a).

In this work, an RSS-based localization physical source localization algorithm has been used to estimate the PD source location in a noisy environment.

5.2 Received Signal Strength algorithm

The main reason behind the RSS algorithm for being selected is its ability to exploit the features of the communications systems that already exist. There is no need to install additional hardware and software which means that the cost and complexity are reduced. The RSS algorithm gives information about the distance between the source and the transmitter, and this distance is obtained by converting the received power into distance. (H Mohamed et al., 2017). The major challenge that is faced in PD localisation is the anonymity of the propagation parameters i.e. the source transmitted power is unknown as well as the path loss index is environment dependent and can vary from node to node due to heterogeneous nature of the environment (H Mohamed et al., 2017). The following equation below describes the RSS model that is based on the common path loss model(Xu, Zhou, & Zhang, 2014b):

$$R_i = R_0 - 10 \log_{10} \left(\frac{d_i}{d_0} \right)^n \quad (6.1)$$

Where,

R_i is the received signal strength (dBm).

R_0 is the radiated power of the PD source (dBm).

d_i is between the i^{th} receiver and the PD source.

d_0 is a reference distance.

n is the path loss exponent ($n=2$ for free space propagation).

In the proposed localization system, the transmitted source power is an unknown as well as the path loss index. As the equation above implies, the received power or the received signal strength is converted into distance. To overcome the problem of unknown parameters, the least

-square approximation is used. It is worth mentioning here that the performance of the RSS algorithm is very low when the geometric conditions are poor, and yields it an estimation error that becomes very large especially at corners (H Mohamed et al., 2017).

The key points to be considered in the algorithm are as below:

- (i) initially assume a plausible path-loss index (e.g. $n = 2$, free space propagation).
- (ii) Calculate the received power ratios at any two nodes to find the locus of possible source location.
- (iii) establish an initial estimate of source location using intersecting loci from all measurements node pairs.
- (iv) calculate an improved estimate of source location using pairs of nodes by varying n . Iterate to converge on a final location estimate and path-loss exponent n .

In a noisy environment, the error should be less than 1 m between the estimated and true location. The main challenge is to optimize the value of an average path loss exponent n used for all links.

Next in Figure 64 is the flowchart of the algorithm and how it works:

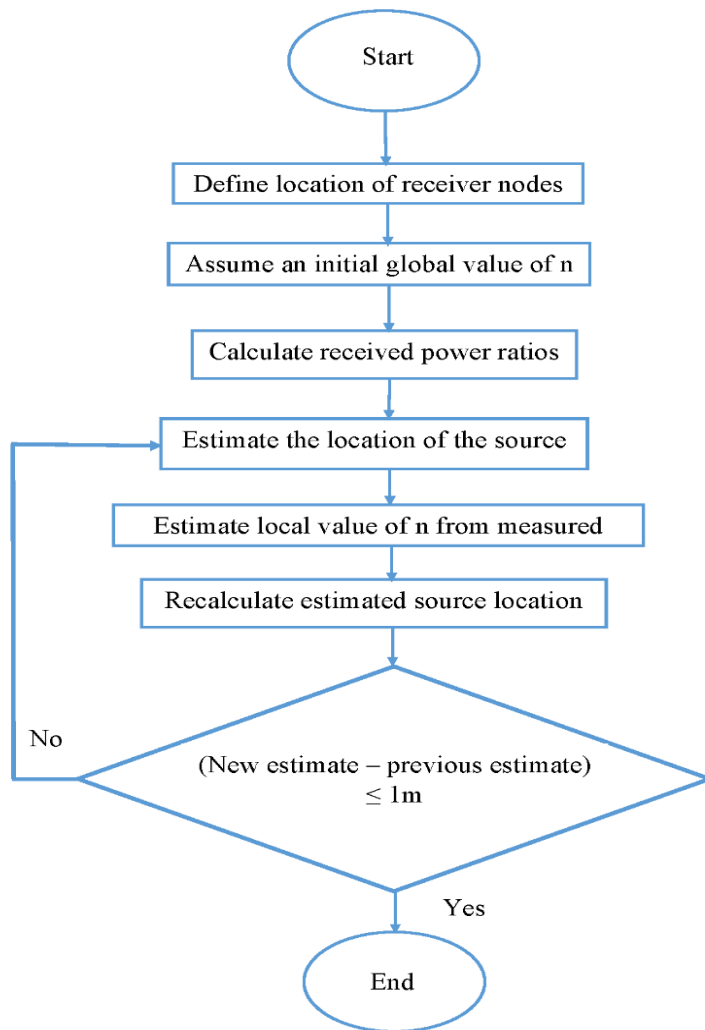


Figure 64. Flowchart of the RSS localization algorithm.

5.3 RSS Localization algorithm description

The RSS algorithm is based on converting the received power into distance. Multiple locations can be approximated by using the multiple receiver nodes that allow trilateration or even multilateration. The main issue that can be associated is the accuracy of the estimated location because of the heterogeneous nature of the radio propagation environment. The major challenge that is faced in PD localisation is the anonymity of the propagation parameters i.e. the source transmitted power is unknown as well as the path loss index is environment

dependent and can vary from node to node due to heterogeneous nature of the propagation model (H Mohamed et al., 2017). The next equation shows the RSS model (Xu et al., 2014b).

$$R_i = R_0 - 10 \log_{10} \left(\frac{d_i}{d_0} \right)^n \quad (6.1)$$

Where,

R_i is the received signal by a node at a point from the source.

R_0 is the unknown transmitted power

d_i is the distance between the source and the i^{th} receiver.

d_0 is the distance of the reference receiver

n is the path loss exponent.

One of the key challenges in such an environment is that both the source transmitted power and the path loss exponent are unknown. This means that equation (1) above remains unsolvable.

The solution to the problem can be found in such a way, that a ratio approach can be used to encapsulate the source transmitting power and hence create a matrix for each of the receiving nodes (Xu, 2014) (Adhikary & Daigle, 2016). This can be done by using one of the receiving nodes as a reference node and re-arrange the equation (1) above and taking the antilog on both sides as shown below.

$$R_0 - R_i = 10 \log_{10} \left(\frac{d_i}{d_0} \right)^n \quad (6.2)$$

$$\frac{R_0 - R_i}{10n} = \log_{10} \left(\frac{d_i}{d_0} \right)^1 \quad (6.3)$$

$$di = d_0 \left(\text{antilog} \frac{R_0 - R_i}{10n} \right) \quad (6.4)$$

$$d_i = d_0 10^{\frac{R_0 - R_i}{10n}} \quad (6.5)$$

Hence

$$d_i = d_0 \frac{10^{\frac{R_0}{10n}}}{10^{\frac{R_i}{10n}}} \quad (6.6)$$

In the above equation (3) the distance of *ith* receiver from the source is computed. To bypass the problem of the unknown received power P_0 , the ratio approach is used in such a way that:

$$P_i = 10^{\frac{R_i}{10n}} \text{ and } P_0 = 10^{\frac{R_0}{10n}} \quad (6.7)$$

Then, it can be written that:

$$\frac{d_i}{d_0} = \frac{P_0}{P_i} \quad (6.8)$$

The source transmitting power can be eliminated by using the ratio method as above.

Then,

$$d_i = d_0 \times \frac{P_i}{P_1} \quad (6.9)$$

But the distance between the source and a node in a two dimensional space can also be calculated as below:

$$d_i^2 = (x - x_i^2) + (y - y_i^2) \quad (6.10)$$

By equating equations (4) and (5) above and expanding the equations, the expressions below are obtained:

$$x_i^2 + x^2 - 2x_i x + y_i^2 + y^2 - 2y_i y = \frac{d_1^2 p_1^{\frac{2}{n}}}{p_i^{\frac{2}{n}}} \quad (6.11)$$

Now multiplying the equations by $p_i^{\frac{2}{n}}$, we obtain:

$$p_i^{\frac{2}{n}}[x_i^2 + x^2 - 2x_i x + y_i^2 + y^2 - 2y_i y] = d_1^2 p_1^{\frac{2}{n}} \quad (6.12)$$

The equations now can be converted as below by multiplying with the common factor:

$$p_i^{\frac{2}{n}} x_i^2 + p_i^{\frac{2}{n}} x^2 - 2p_i^{\frac{2}{n}} x_i x + p_i^{\frac{2}{n}} y_i^2 + p_i^{\frac{2}{n}} y^2 - 2p_i^{\frac{2}{n}} y_i y = d_1^2 p_1^{\frac{2}{n}} \quad (6.13)$$

The distance of the reference node from the source is given by the equation below:

$$d_1^2 = (x_1 - x)^2 + (y_1 - y)^2 \quad (6.14)$$

The distance ratio of the reference node to the i th node is given below:

$$\frac{(x_1 - x)^2 + (y_1 - y)^2}{(x_i - x)^2 + (y_i - y)^2} = \frac{p_i^{\frac{2}{n}}}{p_1^{\frac{2}{n}}} \quad (6.15)$$

$$\frac{x_1^2 + x^2 - 2x_1 x + y_1^2 + y^2 - 2y_1 y}{x_i^2 + x^2 - 2x_i x + y_i^2 + y^2 - 2y_i y} = \frac{p_i^{\frac{2}{n}}}{p_1^{\frac{2}{n}}} \quad (6.16)$$

After expanding the equation, below is the overall set of equations that will be used to determine the matrix equations:

$$\begin{aligned}
& p_1^{\frac{2}{n}}x_1^2 + p_1^{\frac{2}{n}}x^2 - 2p_1^{\frac{2}{n}}x_1x + p_1^{\frac{2}{n}}y_1^2 + p_1^{\frac{2}{n}}y^2 - 2p_1^{\frac{2}{n}}y_1y \\
& = p_i^{\frac{2}{n}}x_i^2 + p_i^{\frac{2}{n}}x^2 - 2p_i^{\frac{2}{n}}x_ix + p_i^{\frac{2}{n}}y_i^2 + p_i^{\frac{2}{n}}y^2 - 2p_i^{\frac{2}{n}}y_iy
\end{aligned} \tag{6.17}$$

By separating all like terms, and writing the equation for each node a matrix equation of AX=b form will be obtained and can be shown below:

$$A = \begin{bmatrix} 2P_2^{\frac{2}{n}}x_2 - 2P_1^{\frac{2}{n}}x_1 & 2P_2^{\frac{2}{n}}y_2 - 2P_1^{\frac{2}{n}}y_1 & P_1^{\frac{2}{n}} - P_2^{\frac{2}{n}} \\ 2P_3^{\frac{2}{n}}x_3 - 2P_1^{\frac{2}{n}}x_1 & 2P_3^{\frac{2}{n}}y_3 - 2P_1^{\frac{2}{n}}y_1 & P_1^{\frac{2}{n}} - P_3^{\frac{2}{n}} \\ 2P_m^{\frac{2}{n}}x_m - 2P_1^{\frac{2}{n}}x_1 & 2P_m^{\frac{2}{n}}y_m - 2P_1^{\frac{2}{n}}y_1 & P_1^{\frac{2}{n}} - P_m^{\frac{2}{n}} \end{bmatrix}, X = \begin{bmatrix} x \\ y \\ s \end{bmatrix}, B = \begin{bmatrix} P_2^{\frac{2}{n}} - P_1^{\frac{2}{n}} \\ P_3^{\frac{2}{n}} - P_1^{\frac{2}{n}} \\ P_m^{\frac{2}{n}} - P_1^{\frac{2}{n}} \end{bmatrix} \tag{6.18}$$

In the above matrices the source related power is eliminated however and, the path loss index (n) still remains unknown; the good thing about the path loss is that it remains between 1 and 7. Hence this constraint can be used to optimize the path loss exponent value between these limits. The path loss exponent can be optimized by considering an initial value and then by optimizing the initial chosen value using the distance ratio based on each of the individual path loss exponent (Adhikary & Daigle, 2016). The path loss exponent optimization is done by using the equation below:

$$n_{MIN} \leq n_{OPT} \leq n_{MAX} \tag{6.19}$$

In an ideal free space environment, the path loss model value is normally 2. An initial value of 2 or any between the constraints is used to optimize the path loss exponent in such a way that each receiving node will have the locus from the source and the intersecting loci of multiple nodes to determine the optimum values of the individual path loss exponents.

5.4 The experimental Set-Up

Figure 65 shows the experimental set-up including its environment. The PD emulator has been used as a PD source. Due to the limitation in the number of receivers, a single receiver (USRP N200 connected to a wideband biconical antenna and a Giga Ethernet cable have been employed to receive the PD signal at several locations and then the signal process and the localizations process are performed in the PC. It is worth mentioning here that the PD emulator is a very HV equipment and it is placed inside a wooden box, for health and safety reasons (H Mohamed et al., 2017).



Figure 65. Experimental setup.

The spectra of the PD signal and the noise background are obtained in the following scenario:

First/ before switching the PD emulator on the noise background spectrum should be obtained.

Second/ the PD emulator is switched on and the PD spectrum is obtained.

This scenario is repeated for every location. Figure 66 shows the results obtained at one of the locations. It can be seen clearly that the spectra of the PD signal and noise background are noisy. Some signal processing is required to take the spikes off from the spectra. Figure 67 shows the spectra after the signal processing.

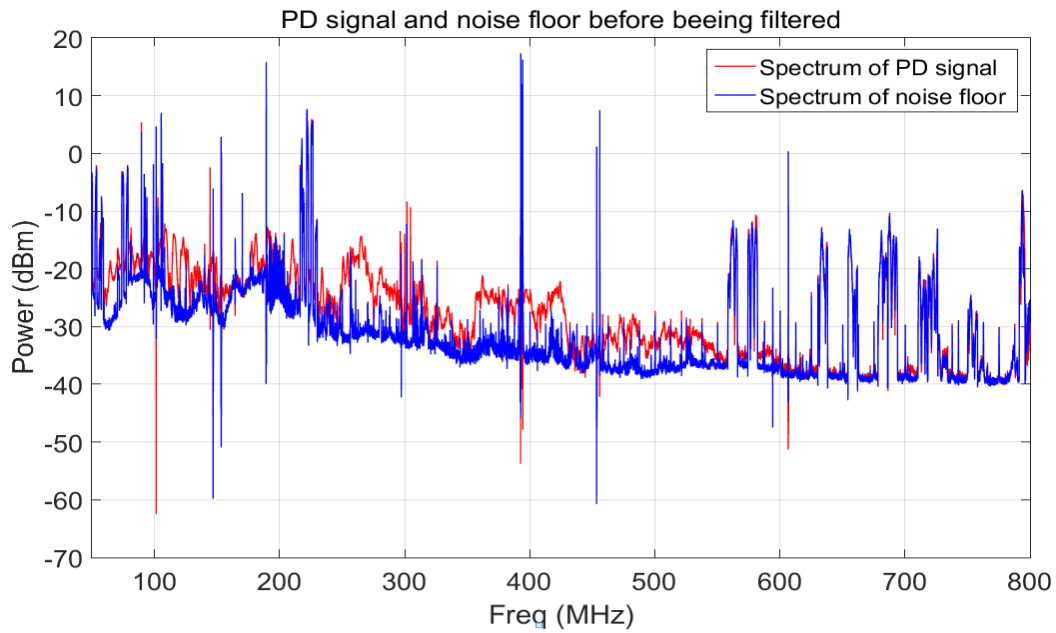


Figure 66. The measured spectra using USRP N200 transceiver (outside the lab.)

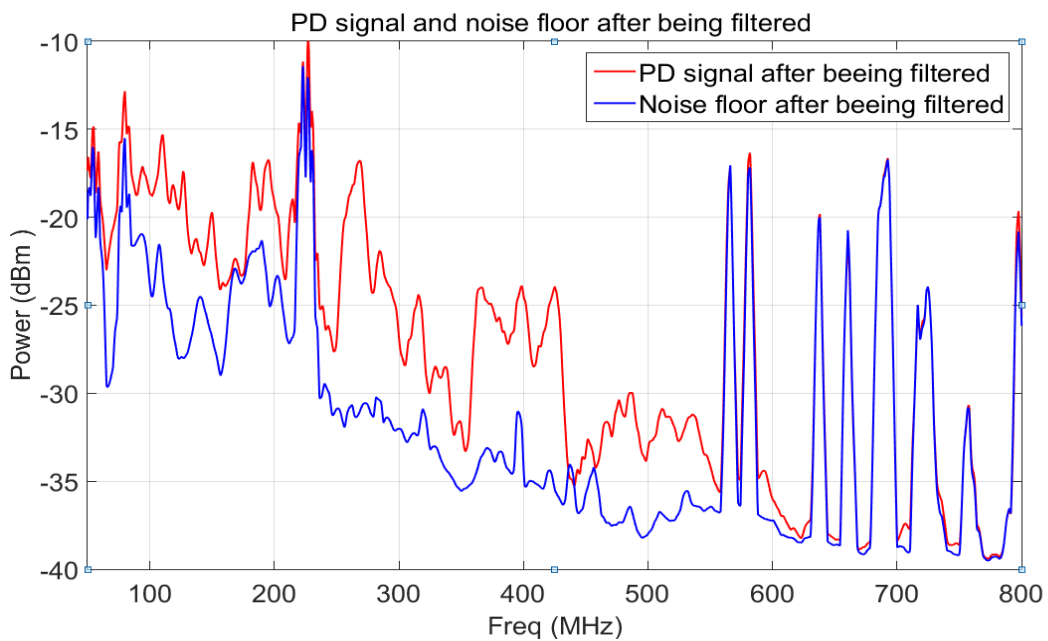


Figure 67. PD signal and noise floor after filtering.

By inspecting Figure 66 it can be clearly seen that some very strong interference caused by TV broadcasting and mobile communications systems in the band of 500-800 MHz is present. To avoid this interference, this band is removed and the new calculated PD band is 50 - 450 MHz. This will not have an important impact as most of the PD energy is at lower frequencies. Figure 68 shows the new PD inspection band.

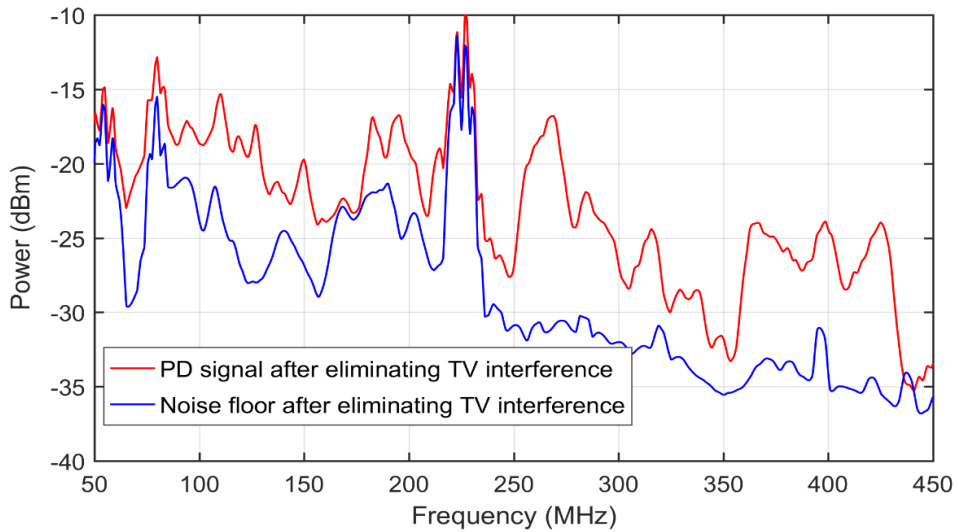


Figure 68. PD signal and background noise plus interference after removing TV interference.

After signal processing is performed, the values of the curves in dBm are converted into a linear scale (milliWatts) and then subtracted from each other at every frequency and integrated to get the average power at each location in milliWatts as shown in the Table 5. It should be noted that received signal power is not calibrated, therefore, this is only a relative estimate of received power and not an absolute value. Figure 69 shows the difference between the PD spectra and noise floor in milliWatts.

Table 5 Power values at the receiver locations (uncalibrated).	
Receiver location	Relative power in milliWatts
1	14.8
2	10.4
3	14.3
4	32.0
5	2.6
6	8.1

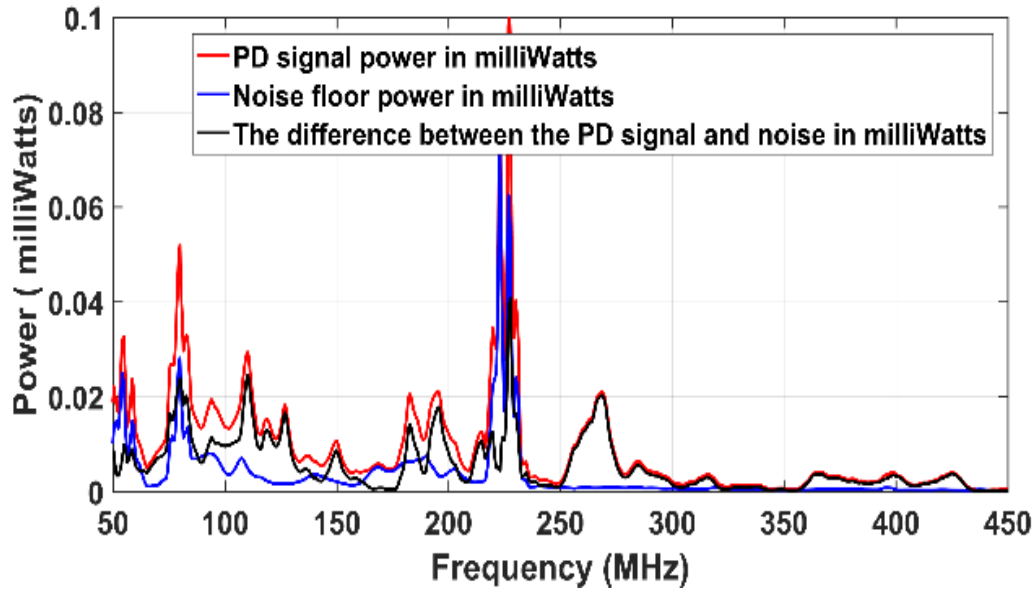


Figure 69. The difference between the PD signal and background noise plus interference.

5.5 The localization results

The localizations algorithm proposed here is based on received signal strength. The power values obtained from the SDR system are entered into the MATLAB code to localize the PD source.

Figure 70 shows the localization results. As it is clear from the figure the estimation error is 5.25 meter. This is not good enough, however the SDR system can be used for PD localizations as a proof of principal. In Figure 71, the estimation error is just 1.3 meter. This improvement due to the fact that as the PD source is getting closer to the centre of the grid is more accurate where the power values at all receivers (6 receivers) are at considerable levels while in the Figure 70 the PD source is located nearly at the edge of the grid and is almost 20 m far from the receiver located at the leftmost of the grid, furthermore the SDR localization system can receive the PD signal up to maximum 20 m. Hence the PD source in Figure 70 is localized by 4 receivers only (after ignoring the receivers at the leftmost) only as can be seen from the Figures 70 and 71. As can be seen in Table 1 and Figure 71, the receivers closer to the PD source receive a higher signal power and based on this principle and the relative strengths of received powers at various locations, the source is localized.

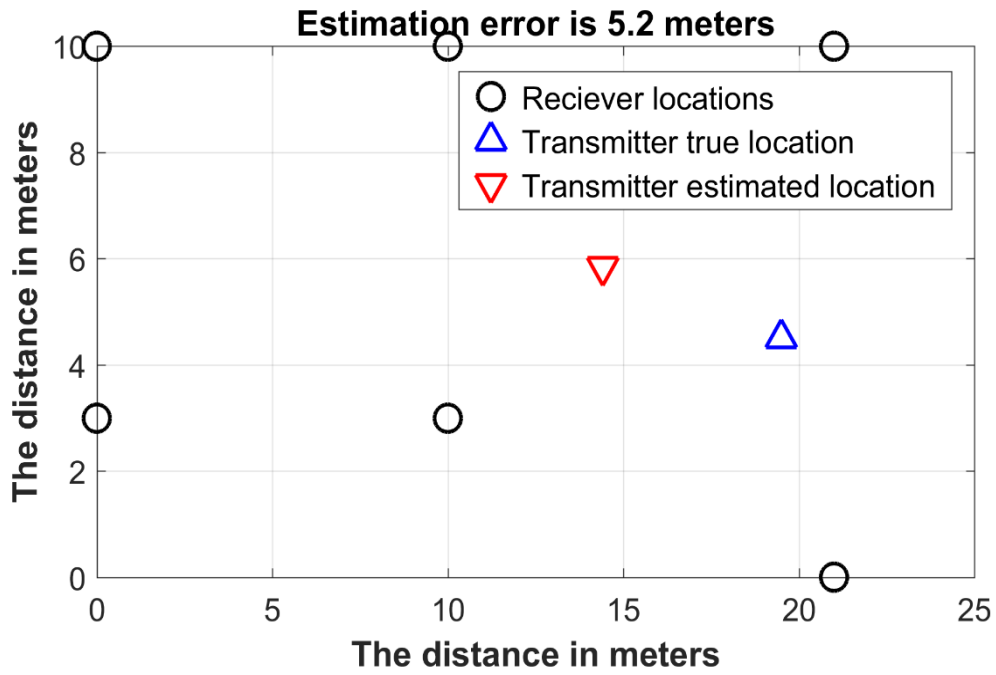


Figure 70. PD source localization set-up and results.

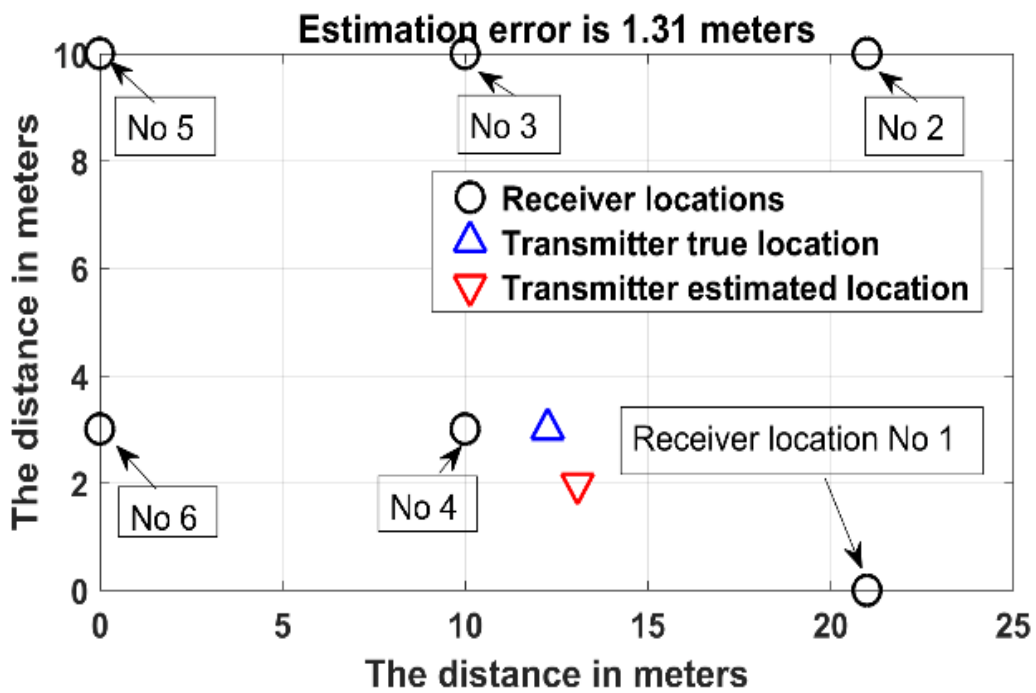


Figure 71. PD source localization set-up and results.

5.6 Summary of the chapter

Partial Discharge (PD) occurs when insulation containing defects or voids is subject to high voltages. If left untreated PD can degrade insulation until, eventually, catastrophic insulation failure occurs. The detection of PD current pulses, however, can allow incipient insulation faults to be identified, located and repaired prior to plant failure. Wireless technology has paved the path for PD detection and monitoring. Software Defined Radio (SDR) is a promising technology. To localize the PD source using the RSS algorithm in an electrical power station, three sensors minimum are required to record the PD signals. Then the power of the recorded signals at each sensor is converted into distance, as the sensors are located at different locations with different distances from the PD source. By solving a system of equations based on a least-squares approximation the PD source is localized. Signals from two PD with good accuracy emulator were received at six outdoors locations using an SDR USRP N200 which is connected to a laptop. PD sources, thereafter, are localized based on received signal strengths.

6 Chapter **Wireless Sensor Networks WSNs**

In this chapter an application of PD detection using SDR technology and radiometric system in the frequency domain are discussed. Also a brief survey of possible WSN technologies along with their comparative advantages and disadvantages is given below. The following sections will mainly discuss Bluetooth, ZigBee and ISA100.11a.

6.1 Introduction

Partial discharge (PD) is an electrical discharge that occurs within part of the dielectric between two HV (High Voltage) conductors. PD causes damage to the dielectric which typically deteriorates with time. If left untreated, PD may result in catastrophic insulation failure destruction of HV equipment, and disruption of power supply. PD detection plays a vital role in electrical power stations, it can help protect HV equipment. In this chapter a comparison between two PD detection systems is presented. These systems are: PD detection system based on SDR technology, and PD detection system based on Radiometric sensors. Both systems can be deployed in a network to perform as wireless sensor network. The results obtained using SDR technology are then evaluated. These results are very satisfactory comparing to those of the Radiometric PD System. SDR system was already described in previous chapters and only PD detection that based on the radiometric system will be described in this chapter and then a comparison between them will be made.

6.2 Wireless Sensor Networks

A Wireless Sensor Network can be defined as “a network of devices, denoted as nodes, which can sense the environment and communicate the information gathered from the monitored field (e.g., an area or volume) through wireless links.” (Buratti et al., 2009). The same authors noted that WSNs can include single-sink or multiple-sink scenarios in terms of routing information within various conditions.

6.3 Requirements for industrial wireless sensor network applications (IWSN)

An IWSN is designed to satisfy various requirements for the industrial domain. These requirements are:

1. Low-cost and small sensor nodes.
2. Scalable architectures and efficient protocols.
3. Application-specific design.
4. Data fusion and localized processing.
5. Resource-efficient design.
6. Self-configuration and self-organization.
7. Adaptive network operation.
8. Time synchronization.
9. Fault tolerance and reliability.
10. Secure design.

6.4 PD detection system based on Radiometric sensor

The whole system comprises of three sub-systems ranging from the detection sensors to the signal processing unit and the front end of the system. The number of sensors that are used can vary however, and the whole network is scalable. Sensors can be added or removed without any issues. Wireless HART transceivers are used that continually receive and log the data that is then processed. The supervisory system deployed will then be utilized to process the data received by the sensors. The overall block diagram of the entire system is illustrated in the figure below:

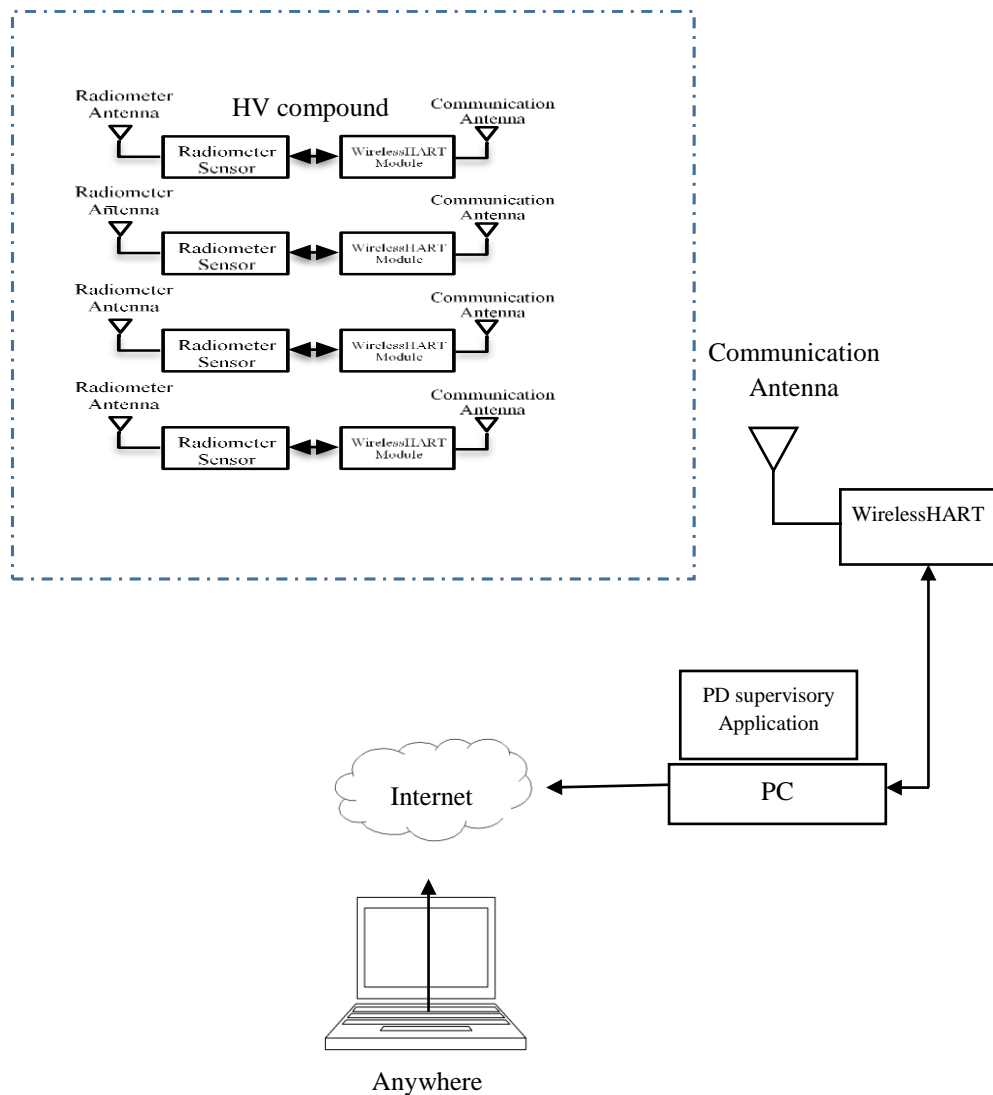


Figure 72 PD detection system based on Radiometric sensor.

6.4.1 PD Radiometer sensor architecture

The PD radiometer sensor utilized is shown in Figure 73:

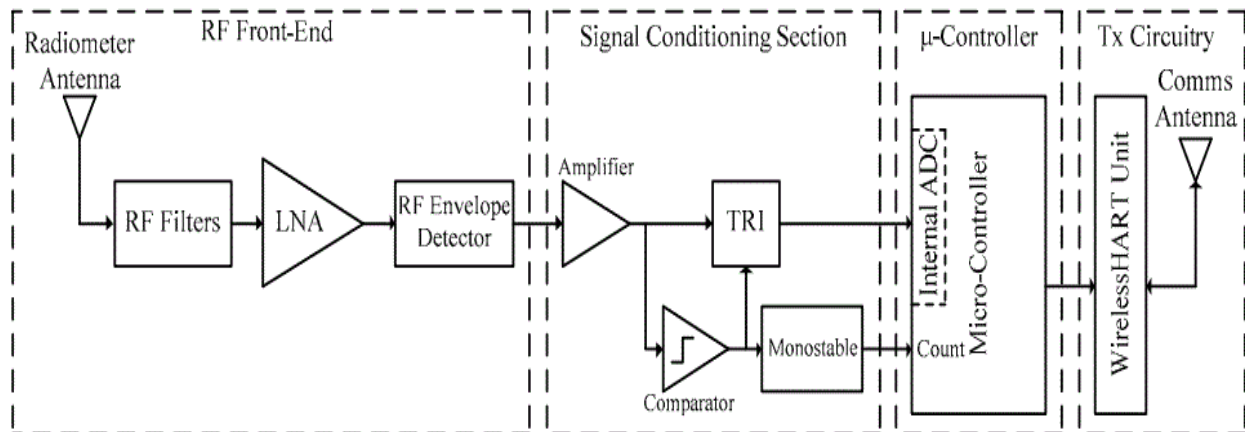


Figure 73. The PD radiometer sensor node block diagram.

6.4.1.1 RF Front-end

The front end of the system is comprised of the dipole antenna which the bandwidth from 20-1000 MHz that easily covers the PD range from 50–800 MHz. The antenna has vertical polarization. When a signal is transmitted by the source that exhibit defects due to any reason, if the signal emitted is within the range from 50-800 MHz it is detected by the antenna. Once the signal is received; it passes through the filtering process by using the band pass roofing and band stop filter after a low noise amplifier (LNA) is utilized. The output of the low noise amplifier is detected by a detector circuit. The detector detects the energy as the emitted signal is in the range of 50-800 MHz, the majority of the energy received at the lower end of the band which is below 300 MHz. RF front-end circuit diagram is shown Figure 74.

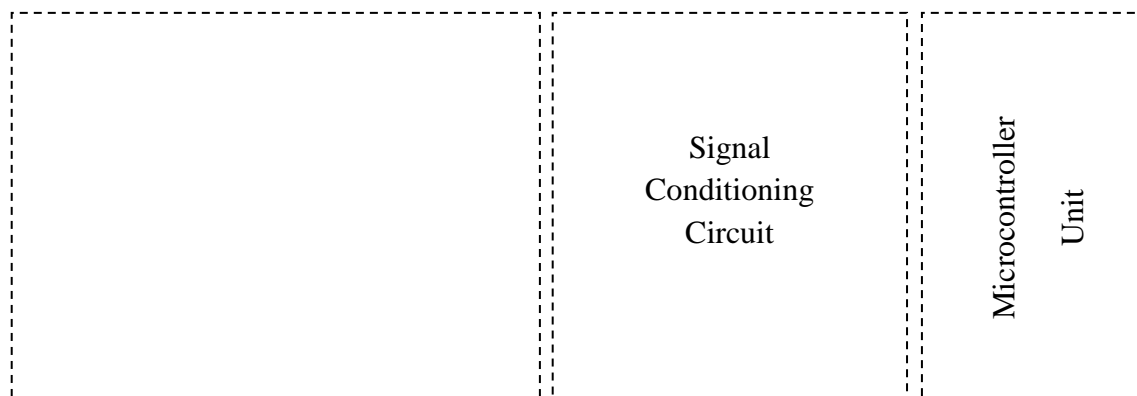


Figure 74. RF front end circuit diagram.

The function of roofing filter in the entire system is to exclude the interferences coming from the environment below or above the required bandwidth typically from 30-320MHz. The

function of the band stop filter is to remove coherent interference in the frequency range from 70-250 MHz. The sensitivity of the sensor is enhanced with the aid of the low noise amplifier utilized within the system. Within the system, the LNA provides a fixed 16.5 dB gain. This will ensure that the sensitivity of the receiver is enhanced.

6.4.1.2 Signal conditional circuit

The signal conditioning is performed by using an envelope detector. When a PD signal is detected it is applied to the signal conditioning part of the system. This means that an envelope detector will receive the PD signal as the input and will amplify the signal further, before it is integrated. A fixed threshold of 3V is set and once the values are reached, the integrator is reset to zero. The integrator is activated by first comparing the signal with the signal of PD interest. A comparator is utilized as part of the whole system to ensure that before the integrator is activated, there is actually a PD signal of interest. The characteristics of the PD signals are identified by using the signal conditioning unit. The comparator circuit is quite useful because it also counts the number of PD pulses.

The voltage values below the threshold will mean that the integrator is not performing its operation and it is at a constant level. The information from the signal conditioning unit is provided to the microcontroller unit. The two inputs that are supplied to the microcontroller unit include the step size of the integrator and the PD pulse count.

6.4.1.3 Microcontroller Unit

The microcontroller unit of the system as mentioned above works on the step size of the integrator and the number of PD pulses received. The main function of the microcontroller is to provide the interface between the PD sensor circuitry and the wireless HART sensors. For this particular system the microcontroller utilized is the PIC24EP512GU810 type. The key features of this microcontroller include that it is fast and has the speed of 70 million instructions per second, the program memory is 512 kB and RAM is 52 MB. The analogue to digital conversion is at satisfactory level providing 1.1 Mega samples per second (Msps) with four simultaneous channels. The features offered by the PIC24EP512GU810 are sufficient to process the received PD signal and to ensure that interface is sufficient.

6.4.1.4 WirelessHART

WirelessHART was developed as a multi-vendor interoperable wireless standard and it was defined for the requirements of process field device networks. It is a wireless sensor networking technology that is based on wired HART protocol which stands for Highway Addressable

Remote Transducer Protocol. The HART Protocol is an implementation of Fieldbus, an industrial automation protocol.

WirelessHART was created to address gaps in industrial wireless standards. It is a centrally-managed mesh network, being designed to be an extension of the commonly-used HART communication protocol. WirelessHART is based on the IEEE 802.15.4 physical layer and adds to it its own Data-Link, Network and Application Layer. It is structured to be user friendly, flexible, reliable, self-organizing, self-healing, secure.

The industrial security and authentication of Wireless HART is extended to 128-bit AES (Advanced Encryption Standard) algorithm that covers end-to-end and hop-to-hop communications. The Medium Access Control (MAC) layer employs TDMA schedule and frequency hopping. Frequency diversity, path diversity and message delivery retrials are used to achieve reliability. Power consumption can be minimized using management of the communication.

The table below compares the distinct features of the most common WSN communication protocols.

Table 6 Comparison of WSN technologies				
The feature	Bluetooth	ZigBee	ISA100.11a	Wireless HART
Standard	802.15.1	802.15.4	802.15.4	802.15.4
Application	Cable replacement	Monitoring and control	Monitoring and control	Monitoring and control
Security	Optional	High	Very High	Very High
Reliability	Low	Very Low	Very High	High
Data rate	Low	Low	Low	Low
Power Consumption	Medium	Low	Very Low	Very Low
Battery Life (days)	1 to 7	100 to 1000	200 to 3000	200 to 3000

Maximum Range (m)	10	100	100+	100+
Ability to cope with very large networks	No	Yes	Yes	Yes
Latency determinism	No	No	Yes	Yes
Success metrics	Cost, convenience	Reliability, power and cost	Reliability power, scalability, security and cost.	Reliability, scalability, security, compatibility, and cost.

WirelessHART compared to Bluetooth, ISA100, ZigBee, is the most economical, robust and complete networking solution for industrial applications. Bluetooth technology can only provide coverage over a limited range. ZigBee can only allow up to 250 kbps connectivity which is slow compared to what WirelessHART can offer. Therefore, WirelessHART is selected as the most appropriate technology for our application.

6.4.1.5 PD supervisory Application

The supervisory system has three parts that include the PD data collector part of the system, the module that monitors and visualizes the PD and the location algorithm to locate the PD source. The function of the data collector module within the supervisory system is to interact with the sensory unit i.e. wireless HART and hence collect and store the data. Data initially is stored in a temporary database. The monitoring and visualization part is the built-in part and utilizes the built-in database. Figure 75 illustrates the visualization and monitoring unit of the supervisory system.

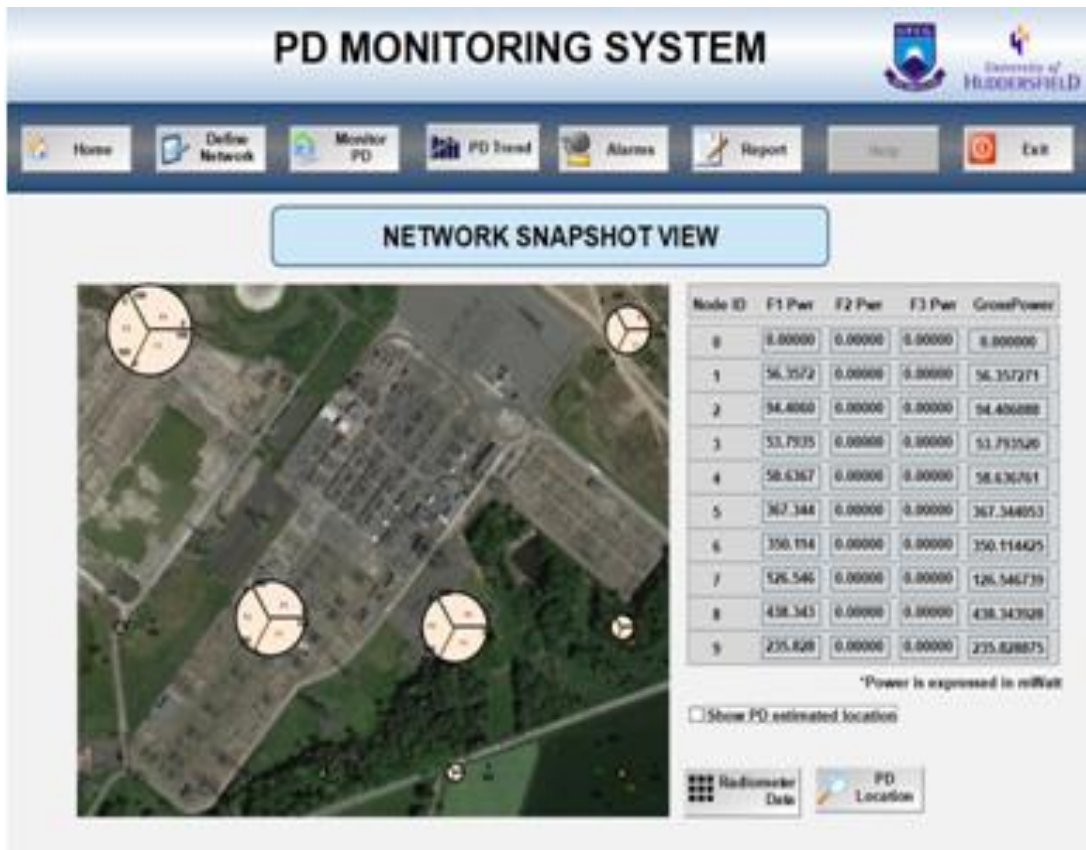


Figure 75. The supervisory system.

The location algorithm part of the system has to locate the source of the emission where the defects occur. The location algorithm is based on the path loss model equation. The location algorithm for PD localization was especially designed implemented as an independent algorithm based on the received signal strength (RSS).

6.5 PD Measurements

Figure 76 shows PD measurements using two systems. (SDR and radiometric). The results obtained from the measurement using both systems are discussed and shown below. Figure 77 Show the results at PD source 1 at (12,4) using the SDR system, the estimation error is just 1 meter. While the estimation error was less about 0.8 meter as shown in Figure 78 With the radiometric system. Both results are very acceptable and are better than expected.



Figure 76. PD measurements using two systems. (SDR and radiometric).

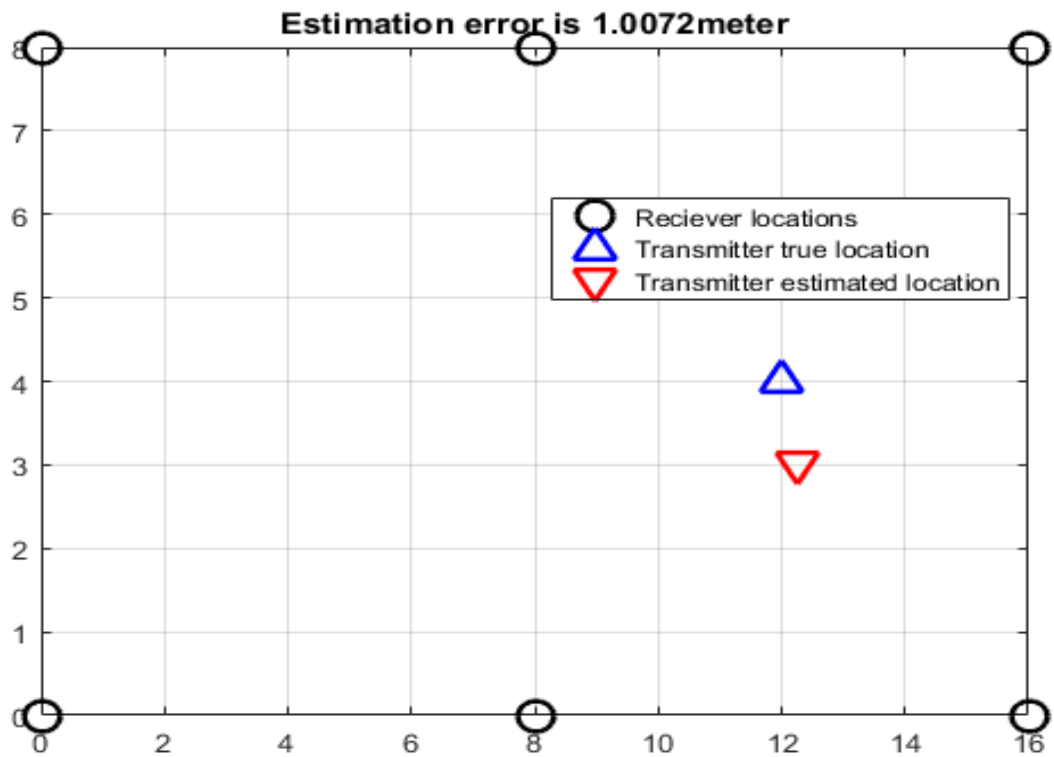


Figure 77. PD results using SDR system at PD source 1 position.

Iteration: 1
 Date: 26-09-2017 10:57
 PD source actual location (12, 4)
 PD source estimated location (12.8, 4.24)
 Estimation error is: 0.8 metre

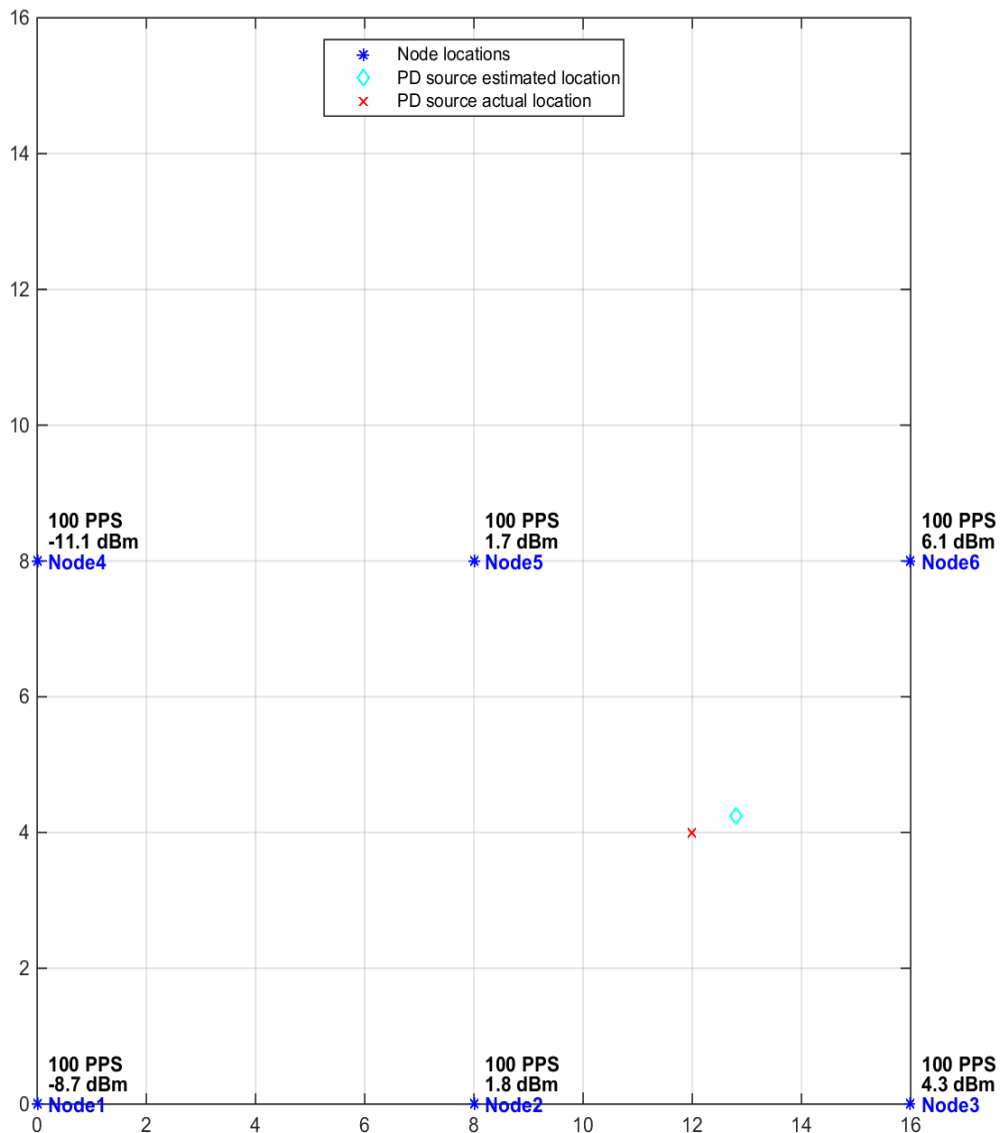


Figure 78. PD results using radiometric sensor system at PD source 1 position.

In Figure 79 the PD source was moved to (15.3, 0.7) located at the edge of the grid more specifically it is at a corner of the grid. The estimation error is 3 meter using the SDR system while using the radiometric sensor it is more than 4.5 meter as shown in Figure 80. It can be seen that the error is quite high and this is due to the fact that the RSS algorithm performs badly at corners.

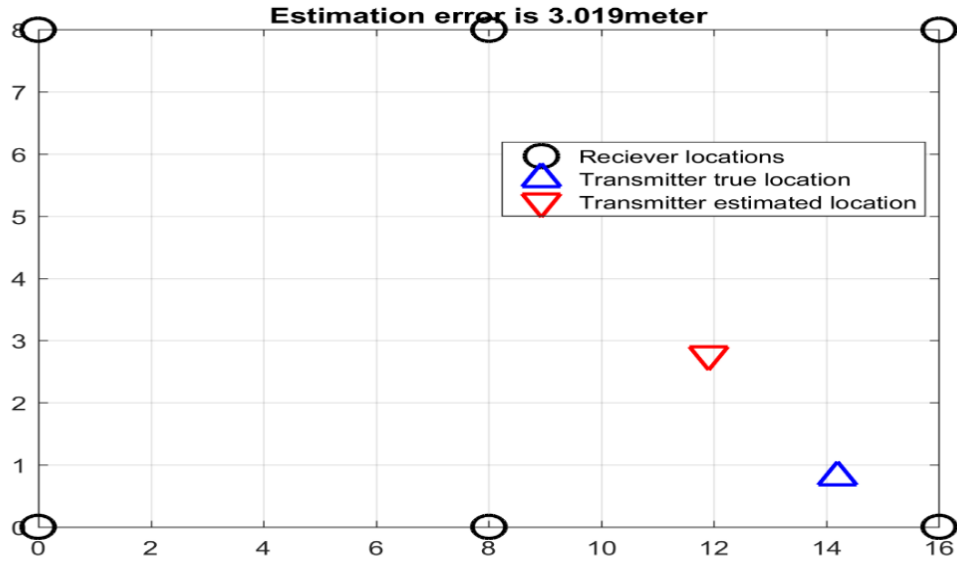


Figure 79. PD results using SDR system at PD source 2 position.

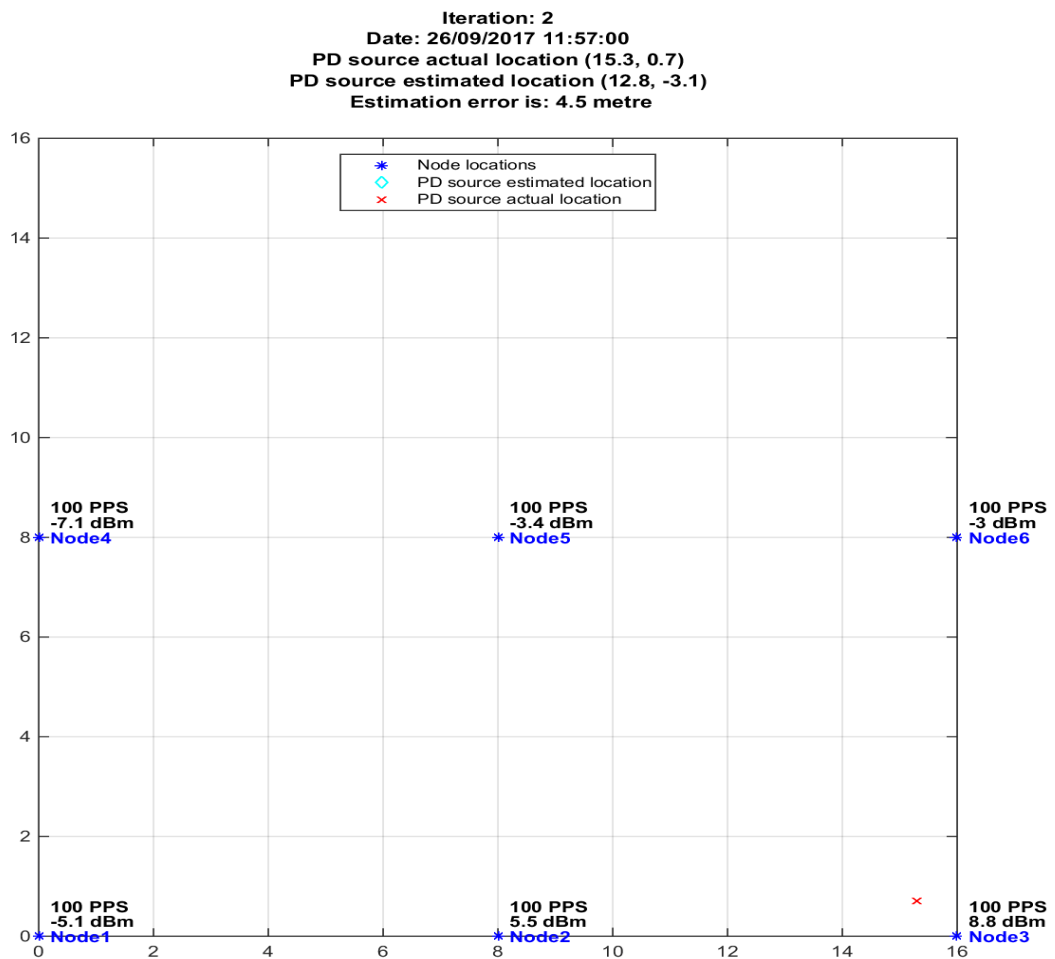


Figure 80. PD results using radiometric system at PD source 2 position

6.6 Summary

In this chapter a comparison between two PD detection systems that both make use of the RSS algorithm shows that the SDR system performs well comparing it to the radiometric system at a similar level of accuracy. These results are very encouragingly and validate both systems.

7 Conclusion and future work

7.1 Conclusion

Insulation of High-Voltage equipment is subject to intense electrical stresses in its operation life; and eventually this can lead to PD to occur especially in the presence of impurities. Partial Discharge is a phenomenon that occurs due to impurities and cracks in the insulation that bridges two conductors in HV systems. The phenomenon starts slowly, however if left unattended, it can lead to a full discharge that totally destroys the insulating material, therefore can become severe and can lead to catastrophic failures. PD can occur in virtually any part of insulation including cables, e.g. in transformers, generators, switchgear, etc. In order to assist in the prevention and effective management of this phenomenon, it is imperative that PD occurrence, modes and types studied extensively. PD detection is critical in HV systems to ensure any PD activity can be monitored and resolved. There are ranges of PD detection mechanisms that have been proposed in the past and are currently used. For example, The IEC 60270 and IEC 62478 standards include common techniques for PD detection such as acoustic emission based methods, galvanic contact measurement methods, and radiometric methods. In galvanic contact measurement methods PD pulses are detected using capacitive coupling while in acoustic emission methods the sound of PD pulses is detected using sensitive directional microphones. Radiometric methods employ a wideband antenna and a fast oscilloscope, or a spectrum analyzer to receive wideband electromagnetic signals radiated by PD pulses.

There are a number of sensing devices available for spectrum sensing. Some of the solutions, like spectrum analyzers are capable of scanning a wide spectrum range, but are too costly. A spectrum analyzer can not perform continuous recording for a time period more than a few seconds, and furthermore, the recorded spectrum requires a higher frequency resolution for better visualization. However, the unprocessed spectrum information still needs further processing. On the other hand, low-cost spectrum analyzers are trimmed for simple and steady recording but are deficient of the flexibility and expected performance, which confine their efficiency to obtain a seamless spectrum sensing for partial discharge and possess a non-configurable frequency span and resolution bandwidth. The predominant requirements for spectrum sensing and assessment in the frequency spectrum sensing context are reliability, flexibility, and the capabilities of continuous recording. Energy per channel with a certain timestamp is the expected output format. In order to facilitate distributed spectrum sensing, the measurement must be accomplished with a relatively low-cost sensing platform. Bridging the research gap between the capacity of high-end spectrum analyzers and the requirement of radio

spectrum sensing, in this study it has been intended to develop an alternative and robust sensing platform for wideband spectrum sensing.

In this research, the work carried out makes use of SDR that can perform as an inexpensive spectrum analyzer. It is a low-cost continuous PD detection mechanism has been proposed based on SDR. Fast Fourier Transform (FFT) and swept mode are common modes in spectrum analyzer nowadays. Spectrum analysers that have the capability to present seamless measurements are called real-time spectrum analysers. The type of device determines the exact features of the real time analysers.

SDR devices can perform as an inexpensive spectrum analyzer and the whole system is a combination of hardware and software. The hardware part of the system consists of two main components that are:

- A portable computer;
- An SRD device that works as a sensor (USRP N200 or RTL-SDR in this research)

The computer provides the platform to the SDR device that is connected to the computer via either a USB port in case of RTL-SDR or via the Ethernet port in case of USRP N200.

The RTL-SDR device

The RTL-SDR is DVB-T TV based tuner, and its prime function is to act as a wideband. The reason to use it as PD detector was that there were no hardware modifications required within the dongle and only software modifications could detect the PD signals. As the PD signal ranges from 50-800MHz, the RTL-SDR primarily covers the given range. This meant that a potential scope of use was identified.

For this work, the RTL 2832U chip was used. It primarily acted as an analogue to digital converter to sample the baseband signal, i.e. PD signal frequency and provide output to the host computer. The operating frequency of the dongle is 25-1750 MHz. The bandwidth of the PD signal is 50-800MHz, thus it is covering the range quite comfortably.

The chosen SDR dongle was programmed by using the MATLAB software, thus capturing and transferring of digitally converted samples to the host computer. In this way, the whole system is working like an inexpensive spectrum analyzer. To allow for real-time control, the interface was performed by using the software tool. To select a baseband frequency, the tuner of RTL-SDR is utilised. The targeted frequency is chosen based on the PD signal characteristics as the whole PD signal is divided into four different bands. Existing experimental study was utilised

and relied upon in order to select the band. The target frequency was converted into the samples by using RTL2832U that acts as ADC. The output of the RTL2832U becomes input to the host computer that accepts the digital data. The host computer performs the calculation for the power spectrum by using the fast Fourier transformation (FFT). This particularly means that the combination of RTL2832U and host computer perform the function of the spectrum analyser. If a spectrum analyser is used to distinguish the characteristics of a PD signal, it will provide a high cost and expensive solution to the problem. However, by utilizing the proposed system a very expensive and practically unfeasible solution can be made feasible.

Although the RTL-SDR dongle was identified as the prospective solution to the problem, it was identified when using practically during modifications of software that its dynamic range and sensitivity were quite low. Considering the intensity of PD signals and based on its characteristics, a better version of the Software Defined Radio was chosen.

The USRP N200

The SDR is a radio system in which some, or all, functions of the physical layer are defined and implemented in software instead of hardware. This means that these functions are programmable which allows users to change the parameters (e.g. center frequency, bandwidth, and modulation) at will. This SDR device uses an FPGA rather than an ASIC. The RF daughter board carries amplification, filtering and down conversion in the receive branch. The motherboard converts the received complex baseband signal from analogue to digital form. The FPGA implements the baseband signal processing (e.g. demodulation and synchronization) before transferring the processed signal to a host computer via an Ethernet cable.

USRP N200 was considered a potential alternative of the RTL2832U. The issues that associated with USRP N200 was that it could not scan more than 20MHz of frequency at a given time due to its own bandwidth limitations, i.e. it has a bandwidth of 20MHz and can't scan more than its own bandwidth. Software modifications were performed in such a way that multistep scans were performed as an alternative to Fast Fourier Transformation. As the PD band is quite wide (50-800MHz), the whole band was divided into multiretunes, and each re-tuning was performed until the whole band was scanned. The communication with pc utilized was the Gigabit Ethernet cable.

7.1.1 PD detection using software defined radio

To make the system work, nothing was changed in terms of hardware. The existing hardware was utilised. The system function was made possible by using software modifications, and all code was written in MATLAB. By using the MATLAB, it was ensured that USRP/RTL-SDR devices sweep across the range of the RF spectrum. A MATLAB figure showing all of the PD spectral activity that it detected was shown. By using MATLAB, the modifications performed were in such a way that based on the used model the maximum sampling frequency was set to be 25Msps due to its maximum capacity. When performing the modifications, it was important to realize that the device input go into overloading. The maximum gain capacity was up to 50dB, but keeping in mind the device capability, it was kept between 1-15 dB. The major consideration was required that if the device gets into overloading, it will be unable to distinguish between radio signals coming from various sources.

To prove the preinciple, there were two separate scans performed at the same time under the same conditions. A spectrum analyser was used at the same time as the SDR. An artificial PD emulator was used to create a PD signal under laboratory conditions. Both scans were performed from 50-800 MHz. Both scans clearly showed the PD activity although there was a slight difference in the quality of scans as obviously SDR scan was not calibrated properly when comparing with the spectrum analyser. Also, both scans were not showing the same levels of absolute power. It was understood and obvious that the spectrum analyser scan was better calibrated due to the sophistication of the device itself. It was concluded that RTL-SDR 2832 was useful and can detect PD, but due to hardware limitations, the PD signal detection may not be very successful if the intensity of the signal is too low or the surrounding environment is too noisy. Under such conditions, it may be that the noise signal will superimpose on the actual signal and hence the SDR will not prove as a useful alternative.

To improve the detection and to overcome the sensitivity issues, the USRP N200 was utilised. The results obtained were far better and encouraging. Although it is a bit expensive solution, but still when considering the performance, it is more far useful than its economic drawback. Signals were measured with and without PD both by using the spectrum analyser and by using the USRP N200 under the same conditions. It was observed that the USRP N200 signal were better than the RTL-SDR results.

While evaluating the performance of all solution , i.e spectrum analyser, RTL-SDR dongle and USRP N200, it can be said that spectrum analyser provided the better results. This is due to its specifications and dedicated use for frequency domain measurements of electromagnetic

signals at a given frequency range. The solution, however, is expensive and will not be feasible to use for continuous monitoring of PD signals. When comparing the portable spectrum analyser with the USRP N200, the results show that accurate PD detection can be made by using SDR at higher frequencies. The key limitations of the RTL-SDR dongles are that it has a non-calibrated relative nature of power measurements. The comparison of results obtained from USRP with spectrum analyser shows a similarity to a great extent which is very encouraging.

7.1.2 PD localization using RSS algorithm

The PD localisation was performed by using the received signal strength intensity (RSSI). The location algorithm was based on the sensors nodes receiving the signal and the conversion of the signal into the distance. There was no need for node synchronization as used in traditional localisation algorithms, e.g. TOA, TDOA, AOA etc. A ratio approach was adopted to deal with the anonymous environment and the unknowns involved. RSS is a simple and cost effective approach but its main disadvantage is low accuracy especially at the corners of the measurement grid. This proved that received signal strength could be a useful approach for PD detection and considering its benefits over the tradition localisation schemes; it is even more useful as it has less complexity and economic benefits are higher.

The measurements were made indoors and outdoors. The recorded results were obtained using the same receiver in 6 different locations. By entering the power values that were obtained at every node into the MATLAB code, the PD source location is estimated, and the results obtained show that the estimated location of the source was quite satisfactory about 1.3 meters, considering the environment could be noisy especially outdoors. The location estimation showed that there was an error of fewer than 3 meters for all positions measurements. In some instances the error was even less than a meter which can be considered as very good. The recorded power values at six locations range between (2.6 to 32) milliWatts. It is worth mentioning here that these are not absolute powers, and these are only a relative estimate of received power as the received signal power by the USRP N200 is not calibrated. The RSS alorithem does take very short time to perform the computation, a few seconds, however spectrum scanning can take tens of seconds which is significantly longer. The range of the SDR system is affected by some key variables, these are: the type of SDR device and antenna, also the strength of PD signal, in addition to the site location, and the range can vary significantly from one site to another depending on the surrounding environment. However, all these variables can affect the SDR system detection range. It has been proved experimentally

that the SDR localization system can detect PD signals at a maximum range of around 20m, and this very encouraging for further work.

7.2 Future work

The SDR devices employed in this research are expected to cover the whole PD frequency band 50-800 MHz. Both devices follow the same principle of operation and they differ only in their capabilities. Some further investigations include:

- 1- To calibrate the employed SDR devices and to use the absolute power and not the relative received power.
- 2- To use or employ better signal processing algorithms and better localization algorithms for PD localization and select the most accurate algorithm.
- 3- It is also suggested that one of the future directions is to increase the range and accuracy of the SDR devices as PD detection system.
- 4- To make use of other SDR products, especially those with high specifications.
- 5- As the RTL-SDR dongle is very low cost device, it is recommended to further work on the RTL-SDR dongle and try to overcome its limitations.
- 6- Due to the rules in the power station it was not possible to test the SDR technology in the real environment in power stations. It is recommended to test the system in a real environment.
- 7- Further investigate how to build a sensor network to be employed in electrical power stations.

8 References

- Adhikary, R., & Daigle, J. N. (2016). *RSS based localization in Rayleigh fading environment*. Paper presented at the Wireless Communications and Networking Conference (WCNC), 2016 IEEE.
- Agoris, P. D. (2009). Sensitivity verification of radio frequency partial discharge detection in high voltage equipment.
- Baigent, D., Adamiak, M., Mackiewicz, R., & SISCO, G. M. G. M. (2004). *IEC 61850 communication networks and systems in substations: an overview for users*. Paper presented at the Proceedings of the VIII simposio iberoamericano sobre proteccion de sistemas electricos de potencia, Monterey, Mexico, Citeseer.
- Baker, P., Judd, M., & McArthur, S. (2010). A frequency-based RF partial discharge detector for low-power wireless sensing. *IEEE Transactions on Dielectrics and Electrical Insulation*, 17(1).
- Bartnikas, R. (2002). Partial discharges. Their mechanism, detection and measurement. *IEEE Transactions on Dielectrics and Electrical Insulation*, 9(5), 763-808.
- Bilén, S. G., Wyglinski, A. M., Anderson, C. R., Cooklev, T., Dietrich, C., Farhang-Boroujeny, B., . . . Reed, J. H. (2014). Software-defined radio: a new paradigm for integrated curriculum delivery. *IEEE Communications Magazine*, 52(5), 184-193.
- Bojovschi, A., Rowe, W., & Wong, K. (2009). *Radiation spectra of partial discharge in dielectrics*. Paper presented at the Power Engineering Conference, 2009. AUPEC 2009. Australasian Universities.
- Bruno, L., Adesso, P., & Restaino, R. (2014). Indoor positioning in wireless local area networks with online path-loss parameter estimation. *The Scientific World Journal*, 2014.
- Buratti, C., Conti, A., Dardari, D., & Verdone, R. (2009). An overview on wireless sensor networks technology and evolution. *Sensors*, 9(9), 6869-6896.
- Chang, H.-C., Gu, F.-C., Chen, H.-C., & Kuo, C.-C. (2011). *Partial discharge measurement and pattern recognition in gas insulated switchgear*. Paper presented at the Lightning (APL), 2011 7th Asia-Pacific International Conference on.
- Chen, H.-C., Yen, M.-Y., & Chang, K.-J. (2015). Searching for spectrum holes: A 400–800 MHz spectrum sensing system. *IEEE Transactions on Very Large Scale Integration (VLSI) Systems*, 23(12), 2842-2851.
- Coenen, S., Tenbohlen, S., & Markalous, S. Detection of Partial Discharges in Power Transformers using UHF PD Measurements and Acoustic Measurements: University of Stuttgart.
- Cupp, J. G., & Beehler, M. E. (2008). Implementing smart grid communications. *Burns & McDonnell TECHBriefs*.
- Dantas, J. P., Figueredo, M. G., & da Cruz, J. H. (2013). *Evaluation methodologies for cooperative spectrum sensing: Towards a real time performance*. Paper presented at the 2013 SBMO/IEEE MTT-S International Microwave & Optoelectronics Conference (IMOC).
- Desai, U. B., Jain, B., & Merchant, S. (2007a). *Wireless Sensor Networks: Technology Roadmap. A Project supported by Department of Information Technology, Ministry of Information and Communication Technology*.
- Desai, U. B., Jain, B., & Merchant, S. (2007b). *Wireless sensor networks: technology roadmap*. Paper presented at the Workshop on Wireless Sensor Networks at IITB on April.
- EATechnology. What is PD? Partial Discharge. Retrieved from <http://www.partial-discharge-academy.com/what-is-partial-discharge>
- Energy, U. D. o. (Feb 2012). SMART GRID SYSTEM REPORT. Retrieved from www.oe.energy.gov
- Gallagher, T. J., & Pearmain, A. (1983). *High voltage: measurement, testing and design*: Wiley.
- Gellings, C. (2011). Estimating the costs and benefits of the smart grid: a preliminary estimate of the investment requirements and the resultant benefits of a fully functioning smart grid. *Electric Power Research Institute (EPRI), Technical Report (1022519)*.
- Ghassemi, A., Bavarian, S., & Lampe, L. (2010). *Cognitive radio for smart grid communications*. Paper presented at the Smart Grid Communications (SmartGridComm), 2010 First IEEE International Conference on.

- Gibson, J. D. (2012). *Mobile communications handbook*: CRC press.
- Guiñón, J. L., Ortega, E., García-Antón, J., & Pérez-Herranz, V. (2007). Moving average and Savitzki-Golay smoothing filters using Mathcad. *Papers ICEE, 2007*.
- HA, V. H. V., Tyagi, B., Krishnan, V. K. V., & Mallikarjunappa, K. M. K. (2011). Removal of interferences from partial discharge pulses using wavelet transform. *TELKOMNIKA (Telecommunication Computing Electronics and Control)*, 9(1), 107-114.
- Hampton, B., & Meats, R. (1988). *Diagnostic measurements at UHF in gas insulated substations*. Paper presented at the IEE Proceedings C (Generation, Transmission and Distribution).
- Harada, H. (2008). *A feasibility study on software defined cognitive radio equipment*. Paper presented at the New Frontiers in Dynamic Spectrum Access Networks, 2008. DySPAN 2008. 3rd IEEE Symposium on.
- Harada, H., Murakami, H., Ishizu, K., Filin, S., Saito, Y., Tran, H. N., . . . Kato, S. (2007). *A software defined cognitive radio system: cognitive wireless cloud*. Paper presented at the Global Telecommunications Conference, 2007. GLOBECOM'07. IEEE.
- He, X., Xie, G., & Jiang, Y. (2011). Online partial discharge detection and location system using wireless sensor network. *Energy Procedia*, 12, 420-428.
- Hettiwatte, S. N., Wang, Z., & Crossley, P. A. (2014). *Estimating transformer parameters for partial discharge location*. Paper presented at the Power Engineering Conference (AUPEC), 2014 Australasian Universities.
- Huang, L., Deng, Q., Qiao, X., Gu, D., Wang, W., & Yang, H. (2009). *SDR implementation of cognitive radio: Sensing and disjoint spectrum access*. Paper presented at the Communications and Networking in China, 2009. ChinaCOM 2009. Fourth International Conference on.
- IEC-TS, P. (2016). 62478: 2016 High Voltage Test Techniques—Measurement of Partial Discharges by Electromagnetic and Acoustic Methods. *BSI: London, UK*.
- IEC, I. S. (2000). 60270, High Voltage Test Techniques-Partial Discharge Measurements. *International Electrotechnical Commission*.
- Isomäki, P., & Avessta, N. (2004). *An overview of software defined radio technologies*: Turku Centre for Computer Science.
- Johnson, H. N. (2009). O, "Propagation of High Frequency Partial Discharge Signal in Power Cables". *School of Electrical Engineering and Telecommunications*.
- Judd, M., & Farish, O. (1998). *High bandwidth measurement of partial discharge current pulses*. Paper presented at the Electrical Insulation, 1998. Conference Record of the 1998 IEEE International Symposium on.
- Judd, M. D., Yang, L., & Hunter, I. B. (2005). Partial discharge monitoring of power transformers using UHF sensors. Part I: sensors and signal interpretation. *IEEE Electrical Insulation Magazine*, 21(2), 5-14.
- Kaemarungsi, K., & Krishnamurthy, P. (2004). *Modeling of indoor positioning systems based on location fingerprinting*. Paper presented at the INFOCOM 2004. Twenty-third Annual Joint Conference of the IEEE Computer and Communications Societies.
- Karmakar, S. (2012). An Experimental Study of Air Breakdown Voltage and its Effects on Solid Insulation. *Electrical Systems, Setif*, 212.
- Khayam, U., & Vauzia, F. (2014). *Design, fabrication, and testing of double layer printed bow-tie antenna as partial discharge sensor in gas insulated switchgear*. Paper presented at the Power Engineering and Renewable Energy (ICPERE), 2014 International Conference on.
- Kim, K., Xin, Y., & Rangarajan, S. (2010). *Energy detection based spectrum sensing for cognitive radio: An experimental study*. Paper presented at the Global Telecommunications Conference (GLOBECOM 2010), 2010 IEEE.
- Kitsunezuka, M., & Pister, K. S. (2015). Cross-Correlation-Based, Phase-Domain Spectrum Sensing With Low-Cost Software-Defined Radio Receivers. *IEEE Trans. Signal Processing*, 63(8), 2033-2048.

- Ko, J., Terzis, A., Dawson-Haggerty, S., Culler, D. E., Hui, J. W., & Levis, P. (2011). Connecting low-power and lossy networks to the internet. *Communications Magazine, IEEE*, 49(4), 96-101.
- Kreuger, F. (1991). Industrial high voltage: electric fields, dielectrics, constructions. *Delft University Press, Delft, The Netherlands*.
- Kreuger, F. H. (1989). *Partial discharge detection in high-voltage equipment*: Butterworth-Heinemann.
- Krivda, A. (1995). Automated recognition of partial discharges. *IEEE Transactions on Dielectrics and Electrical Insulation*, 2(5), 796-821.
- Kuffel, J., & Kuffel, P. (2000). *High voltage engineering fundamentals*: Elsevier.
- Le, B., Rondeau, T. W., Reed, J. H., & Bostian, C. W. (2005). Analog-to-digital converters. *IEEE Signal Processing Magazine*, 22(6), 69-77.
- Lin, D. T., Chae, H., Li, L., & Flynn, M. P. (2012). A 600MHz to 3.4 GHz flexible spectrum-sensing receiver with spectrum-adaptive reconfigurable DT filtering. Paper presented at the Radio Frequency Integrated Circuits Symposium (RFIC), 2012 IEEE.
- Lin, H.-M., & Willson, A. N. (1988). Median filters with adaptive length. *IEEE Transactions on Circuits and Systems*, 35(6), 675-690.
- Lin, L., & So, H.-C. (2011). *Best linear unbiased estimator algorithm for received signal strength based localization*. Paper presented at the Signal Processing Conference, 2011 19th European.
- Liu, W., Pareit, D., De Poorter, E., & Moerman, I. (2013). Advanced spectrum sensing with parallel processing based on software-defined radio. *EURASIP Journal on Wireless Communications and Networking*, 2013(1), 228.
- Lokhanin, A., Shneider, G., Sokolov, V., Chornogotsky, V., & Morozova, T. (2002). Internal insulation failure mechanisms of HV equipment under service conditions. *Cigre Report 15, 201*, 1-6.
- Lonngren, K. E., Savov, S. V., & Jost, R. J. (2007). *Fundamentals of Electromagnetics with MATLAB*: Scitech publishing.
- Machado-Fernández, J. R. (2015). Software Defined Radio: Basic Principles and Applications. *Facultad de Ingeniería*, 24(38), 79-96.
- Madani, V., Vaccaro, A., Villacci, D., & King, R. L. (2007). *Satellite based communication network for large scale power system applications*. Paper presented at the Bulk Power System Dynamics and Control-VII. Revitalizing Operational Reliability, 2007 iREP Symposium.
- Mate, A., Lee, K.-H., & Lu, I.-T. (2011). *Spectrum sensing based on time covariance matrix using GNU radio and USRP for cognitive radio*. Paper presented at the Systems, Applications and Technology Conference (LISAT), 2011 IEEE Long Island.
- Meijer, S., Agoris, P. D., Seitz, P., & Hermans, T. J. (2006). *Condition assessment of power cable accessories using advanced VHF/UHF PD detection*. Paper presented at the Electrical Insulation, 2006. Conference Record of the 2006 IEEE International Symposium on.
- Mohamed, H., Lazaridis, P., Upton, D., Khan, U., Mistry, K., Saeed, B., . . . Atkinson, D. (2017). *Partial discharge localization based on received signal strength*. Paper presented at the Automation and Computing (ICAC), 2017 23rd International Conference on.
- Mohamed, H., Lazaridis, P., Upton, D., Khan, U., Saeed, B., Jaber, A., . . . Barlee, K. (2016a). *Partial discharge detection using software defined radio*. Paper presented at the Students on Applied Engineering (ICSAE), International Conference for.
- Mohamed, H., Lazaridis, P., Upton, D., Khan, U., Saeed, B., Jaber, A., . . . Barlee, K. (2016b). *Partial discharge detection using low cost RTL-SDR model for wideband spectrum sensing*. Paper presented at the Telecommunications (ICT), 2016 23rd International Conference on.
- Mohamed, H., Lazaridis, P. I., Khan, U., Saeed, B., Mistry, K., Upton, D., . . . Glover, I. A. Partial Discharge detection in smart grid using Software Defined Radio.
- Moore, P. J., Portugues, I. E., & Glover, I. A. (2006). Partial discharge investigation of a power transformer using wireless wideband radio-frequency measurements. *IEEE Transactions on Power Delivery*, 21(1), 528-530.

- Muhr, M., Strehl, T., Gulski, E., Feser, K., Gockenbach, E., Hauschild, W., & Lemke, E. (2006). Sensors and sensing used for non-conventional PD detection. *CIGRE, Paris*, 1-7.
- Muslim, J., Susilo, A., Nishigouchi, K., Kozako, M., Hikita, M., Arief, Y. Z., & Khayam, U. (2013). *Enhanced bowtie UHF antenna for detecting partial discharge in gas insulated substation*. Paper presented at the Power Engineering Conference (UPEC), 2013 48th International Universities'.
- Neto, J. M., Zhang, Y., Jaber, A., Zhu, M., Judd, M., Atkinson, R., . . . Glover, I. A. (2014). *Radiometric location of partial discharge sources for the future smart grid*. Paper presented at the General Assembly and Scientific Symposium (URSI GASS), 2014 XXXIth URSI.
- Orr, P. J., Reid, A. J., & Judd, M. D. (2008). *Sensor response characteristics for UHF location of PD sources*. Paper presented at the Condition Monitoring and Diagnosis, 2008. CMD 2008. International Conference on.
- Oughstun, K. E., & Sherman, G. C. (2012). *Electromagnetic pulse propagation in casual dielectrics* (Vol. 16): Springer Science & Business Media.
- Oussalah, N., Zebboudj, Y., & Boggs, S. A. (2007). Partial discharge pulse propagation in shielded power cable and implications for detection sensitivity. *IEEE Electrical Insulation Magazine*, 23(6), 5-10.
- Paysarvi-Hoseini, P., & Beaulieu, N. C. (2011). Optimal wideband spectrum sensing framework for cognitive radio systems. *IEEE Transactions on signal processing*, 59(3), 1170-1182.
- Portugues, I. E., Moore, P. J., Glover, I. A., & Watson, R. J. (2008). A portable wideband impulsive noise location system. *IEEE Transactions on Instrumentation and Measurement*, 57(9), 2059-2066.
- Rahimi, F., & Ipakchi, A. (2010). *Overview of demand response under the smart grid and market paradigms*. Paper presented at the Innovative Smart Grid Technologies (ISGT), 2010.
- Reid, A. J., Judd, M. D., Stewart, B. G., & Fouracre, R. A. (2006). Partial discharge current pulses in SF6 and the effect of superposition of their radiometric measurement. *Journal of Physics D: Applied Physics*, 39(19), 4167.
- Samat, S., Musirin, I., & Kusim, A. (2012). *The effect of supply voltage on partial discharge properties in solid dielectric*. Paper presented at the Power Engineering and Optimization Conference (PEDCO) Melaka, Malaysia, 2012 Ieee International.
- Sarijari, M. A., Marwanto, A., Fisal, N., Yusof, S. K. S., Rashid, R. A., & Satria, M. H. (2009). *Energy detection sensing based on GNU radio and USRP: An analysis study*. Paper presented at the Communications (MICC), 2009 IEEE 9th Malaysia International Conference on.
- Satish, L., & Nazneen, B. (2003). Wavelet-based denoising of partial discharge signals buried in excessive noise and interference. *IEEE Transactions on Dielectrics and Electrical Insulation*, 10(2), 354-367.
- Shan, Q., Glover, I., Moore, P., Portugues, I., Judd, M., Rutherford, R., & Watson, R. J. (2008). *Impulsive noise environment of high voltage electricity transmission substations and its impact of the performance of ZigBee*. Paper presented at the Proc. Int. Conf. Wireless Commun. Mobile Comput.
- Sheffield, J., Froula, D., Glenzer, S. H., & Luhmann Jr, N. C. (2010). *Plasma scattering of electromagnetic radiation: theory and measurement techniques*: Academic press.
- Shihab, S., & Wong, K. (2000). *Detection of faulty components on power lines using radio frequency signatures and signal processing techniques*. Paper presented at the Power Engineering Society Winter Meeting, 2000. IEEE.
- Shuhong, J., Xicai, S., & Fanru, K. (1998). *A time-of arrival location algorithm for maneuvering target on two-dimensional surface*. Paper presented at the Signal Processing Proceedings, 1998. ICSP'98. 1998 Fourth International Conference on.
- Sinaga, H. H. (2012). Detection Identification And Localization Of Partial Discharges In Power Transformers Using UHF Techniques. *The University of New South Wales Austrailia. FhD Thesis*.

- So, H. C., & Lin, L. (2011). Linear least squares approach for accurate received signal strength based source localization. *IEEE Transactions on signal processing*, 59(8), 4035-4040.
- Sohraby, K., Minoli, D., & Znati, T. (2007). *Wireless sensor networks: technology, protocols, and applications*: John Wiley & Sons.
- Stewart, R. W., Barlee, K. W., & Atkinson, D. S. (2015). *Software defined radio using MATLAB & Simulink and the RTL-SDR*: Strathclyde Academic Media.
- Tabassam, A. A., Suleman, M. U., Khan, S., & Tirmazi, S. H. R. (2011). *Spectrum estimation and spectrum hole opportunities prediction for cognitive radios using higher-order statistics*. Paper presented at the Wireless Advanced (WiAd), 2011.
- Taflove, A., & Hagness, S. C. (2005). *Computational electrodynamics: the finite-difference time-domain method*: Artech house.
- Tian, Y., Kawada, M., & Isaka, K. (2009). Locating partial discharge source occurring on distribution line by using FDTD and TDOA methods. *IEEJ Transactions on Fundamentals and Materials*, 129(2), 89-96.
- U.S. Department of Energy, N. E. T. L. A Vision for the Modern Grid. Retrieved from www.smartgrid.gov/document/vision_modern_grid
- Vaccaro, A., & Villacci, D. (2005). Performance analysis of low earth orbit satellites for power system communication. *Electric power systems research*, 73(3), 287-294.
- Wong, K. L. (2007). *Method and apparatus for detecting an event*. Deakin University.
- Xiong, H., Chen, Z., An, W., & Yang, B. (2015). Robust TDOA localization algorithm for asynchronous wireless sensor networks. *International Journal of Distributed Sensor Networks*, 11(5), 598747.
- Xu, Y., Zhou, J., & Zhang, P. (2014a). RSS-based source localization when path-loss model parameters are unknown. *IEEE communications letters*, 18(6), 1055-1058.
- Xu, Y., Zhou, J., & Zhang, P. (2014b). RSS-based source localization when path-loss parameters are unknown *IEEE communication letters* 18(6), 1055-1058.
- Yu, R., Zhang, Y., Gjessing, S., Yuen, C., Xie, S., & Guizani, M. (2011). Cognitive radio based hierarchical communications infrastructure for smart grid. *Network, IEEE*, 25(5), 6-14.
- Yucek, T., & Arslan, H. (2009). A survey of spectrum sensing algorithms for cognitive radio applications. *IEEE communications surveys & tutorials*, 11(1), 116-130.
- Zhang, Y., Upton, D., Jaber, A., Ahmed, H., Saeed, B., Mather, P., . . . Atkinson, R. (2015). Radiometric wireless sensor network monitoring of partial discharge sources in electrical substations. *International Journal of Distributed Sensor Networks*, 11(9), 438302.

9 Appendices

Appendix-A1

Testing the USRP N200 and comparing it with Spectrum analyzer.

An experiment has been conducted to modulate a square signal generated by a pulse generator with AM carrier generated by a signal generator, this **AM signal** has a frequency of **100MHz** and modulation depth of **90%** when the frequency spectrum is recorded by both the USRP Transceiver and the Rohde& Schwarz signal analyser where the frequency range is **(99.5-100.5) MHz**, and **the centre frequency at 100MHz**. The experiment is done in two manners:

First) the time period- let's call it-'**T**' is kept constant at **67 μ s**; where the pulse duration- let's call it-'**t**' took the following values:

Pulse duration of $t=7.5 \mu$ s

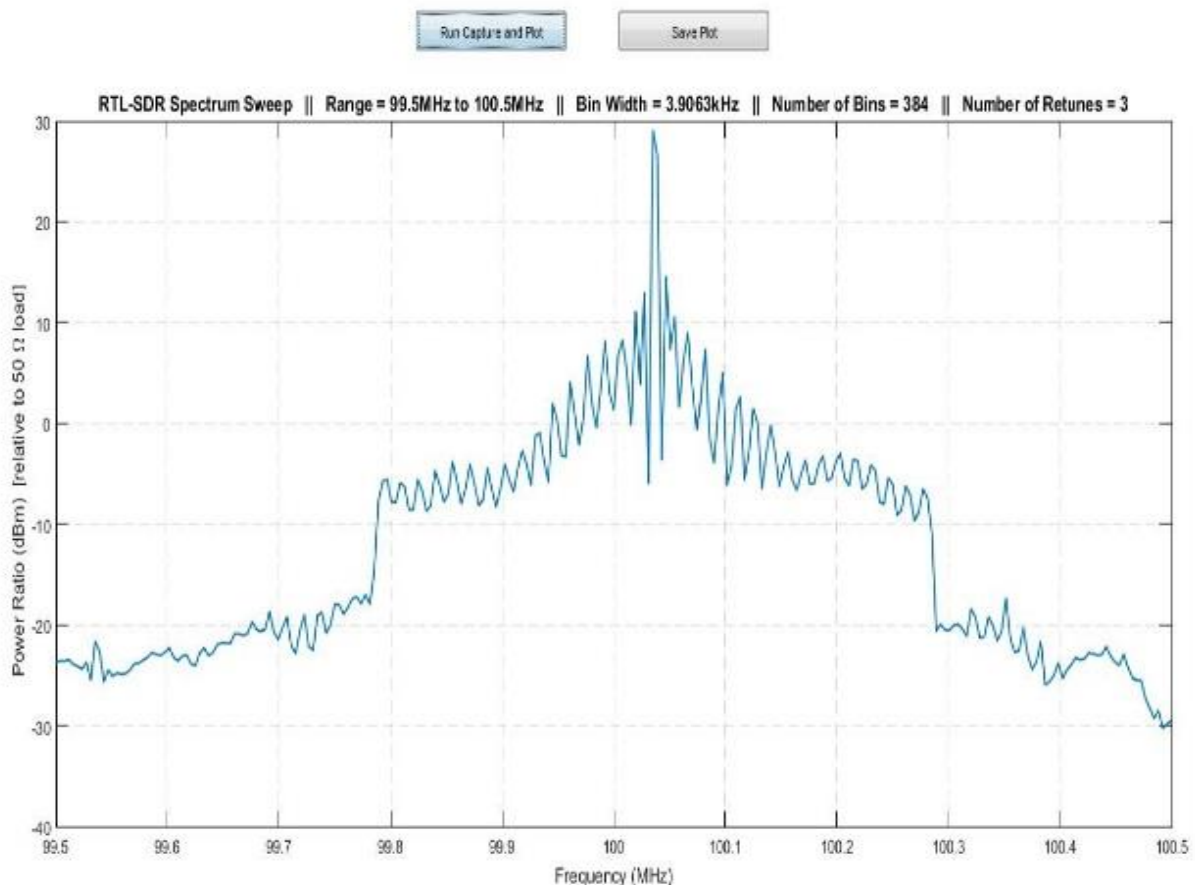
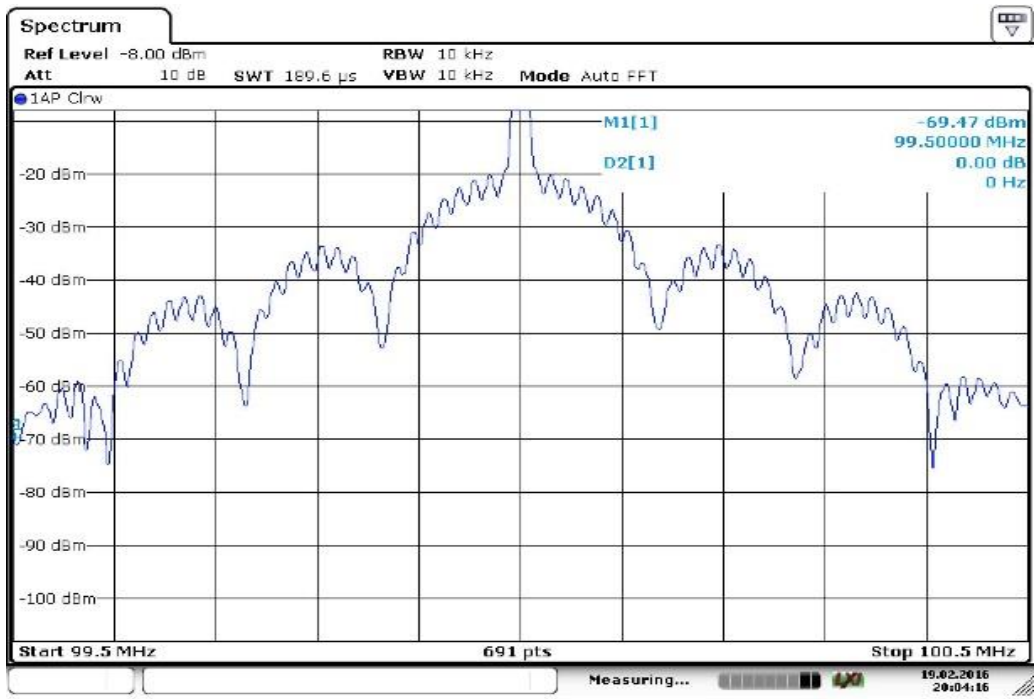


Fig. (1a) the measured Spectrum by the USRP transceiver



Date: 19.FEB.2016 20:04:17

Fig. (1b) the measured Spectrum by the R&S signal analyser

Pulse duration of $t=10 \mu\text{s}$.

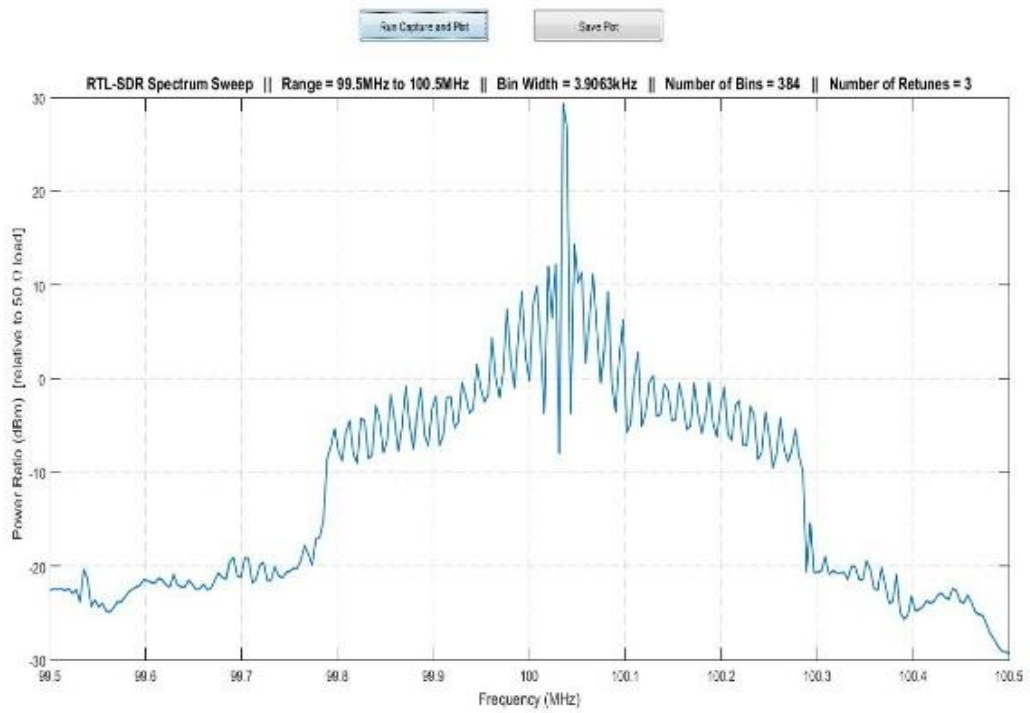


Fig. (2a) the measured Spectrum by the USRP transceiver.

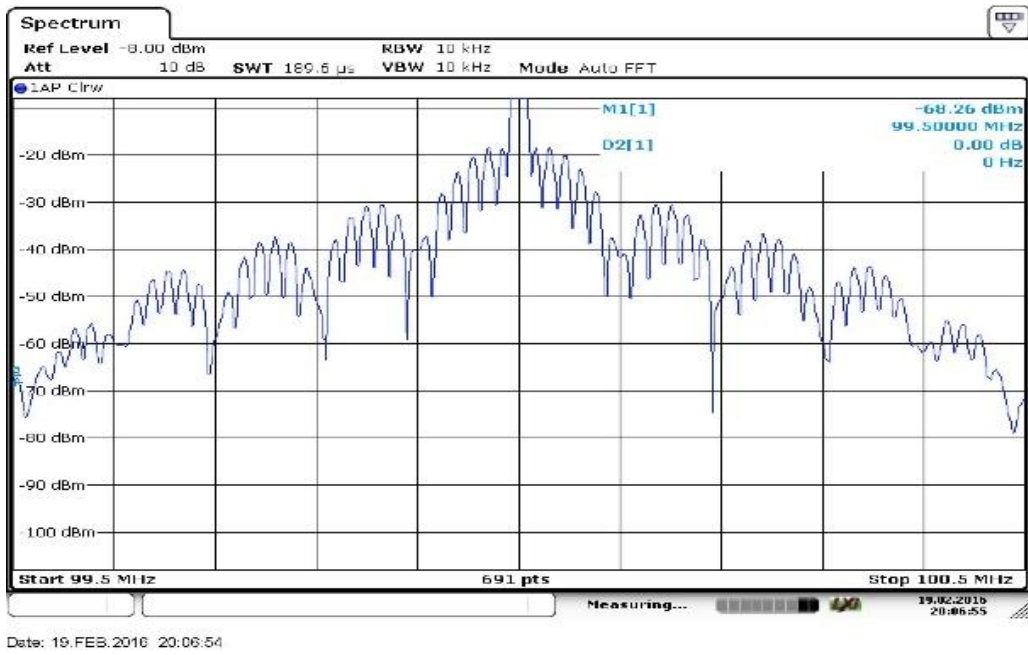


Fig. (2b) the measured Spectrum by the R&S signal analyser

When Pulse duration has value of 15 μ s. ($t=15 \mu$ s)

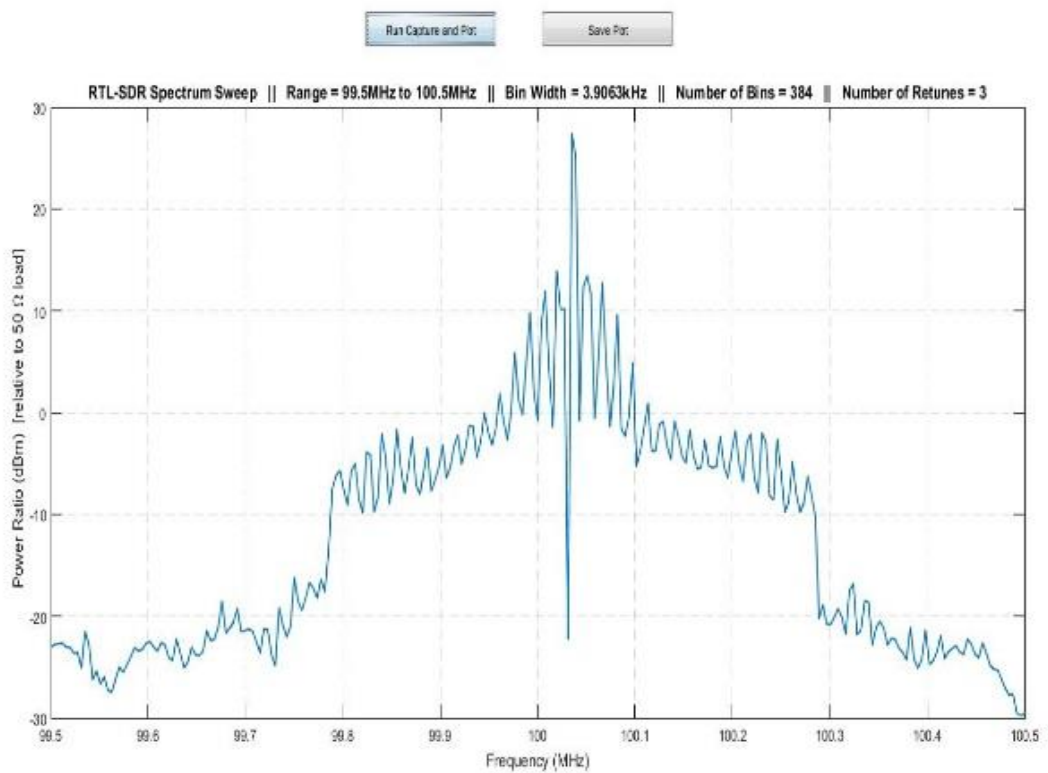
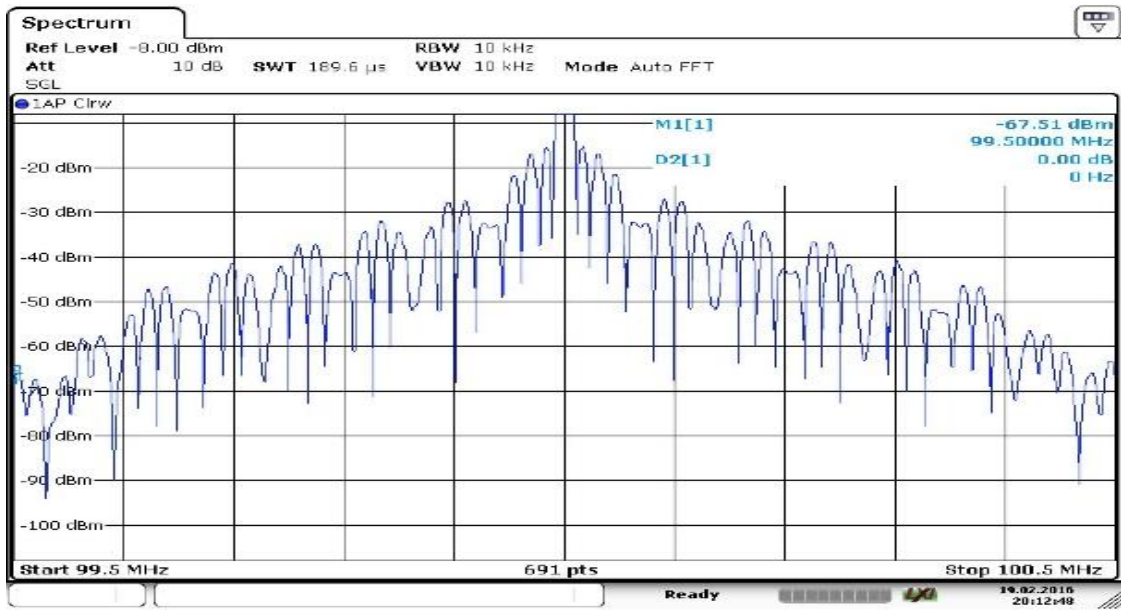


Fig. (3a) the measured Spectrum by the USRP transceiver



Date: 19.FEB.2016 20:12:48

Fig. (3b) the measured Spectrum by the R&S signal analyser.

Pulse durations of $t=20 \mu$ s.

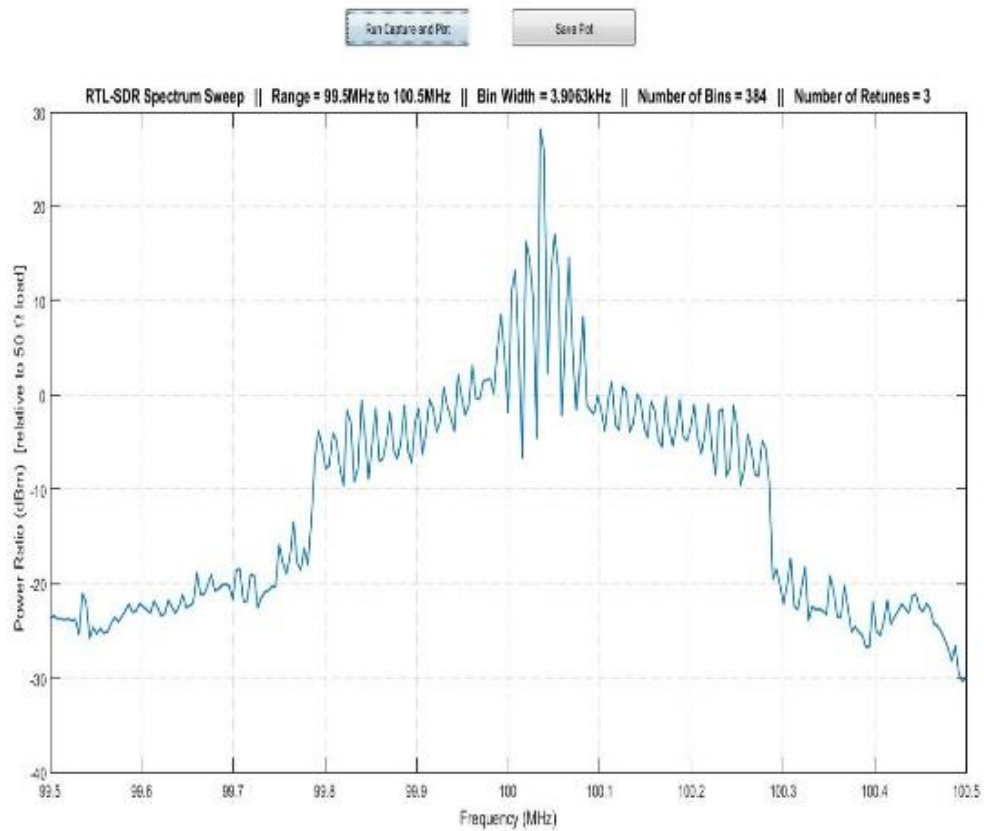


Fig. (4a) the measured Spectrum by the USRP transceiver

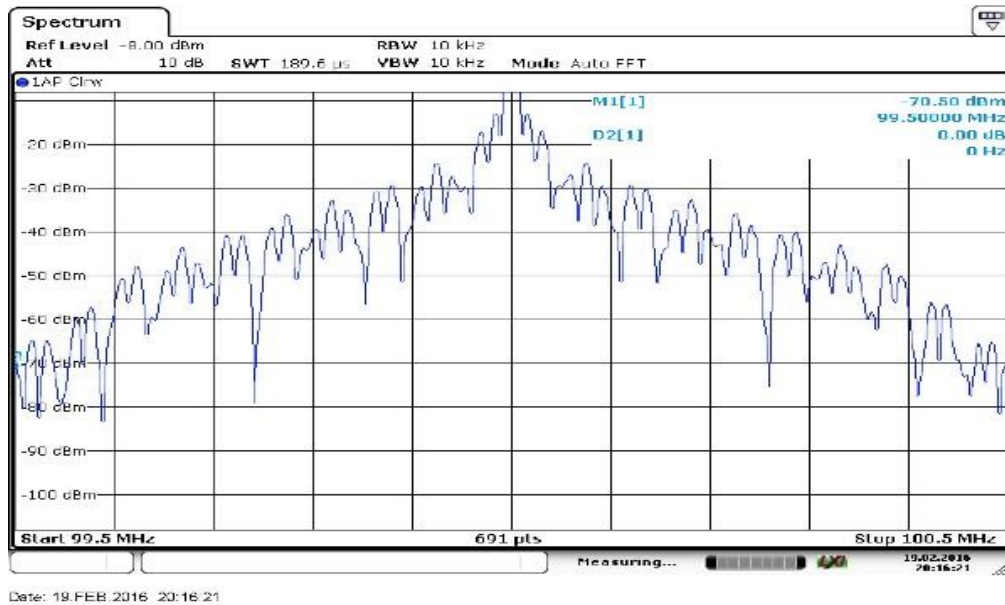


Fig. (4b) the measured Spectrum by the R&S signal analyser

Second) the Pulse duration "t" is kept constant at **0.5us**; where the time period '**T**' took the following values:

Time period of $T=1.5\mu s$.

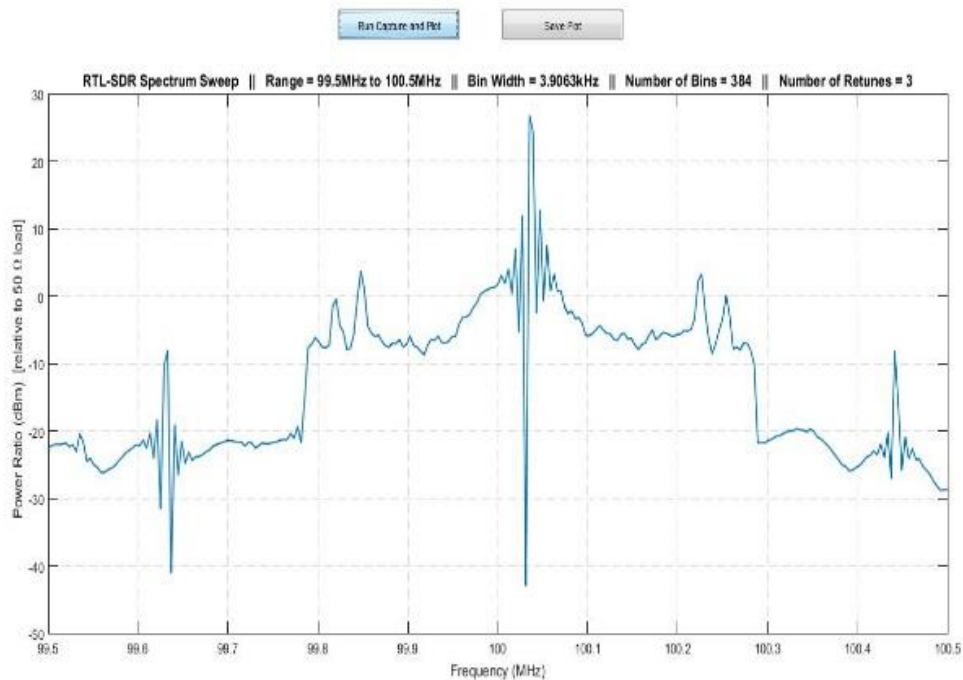
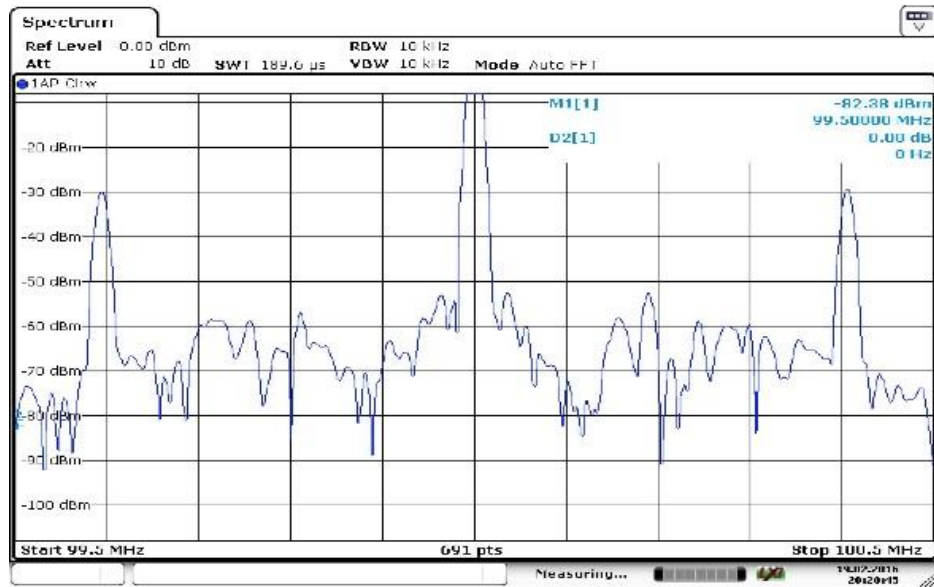


Fig. (5a) the measured Spectrum by the USRP transceiver



Date: 19 FEB 2016 20:20:45

Fig. (5b) the measured Spectrum by the R&S signal analyser

Time period of $T=2.5 \mu\text{s}$

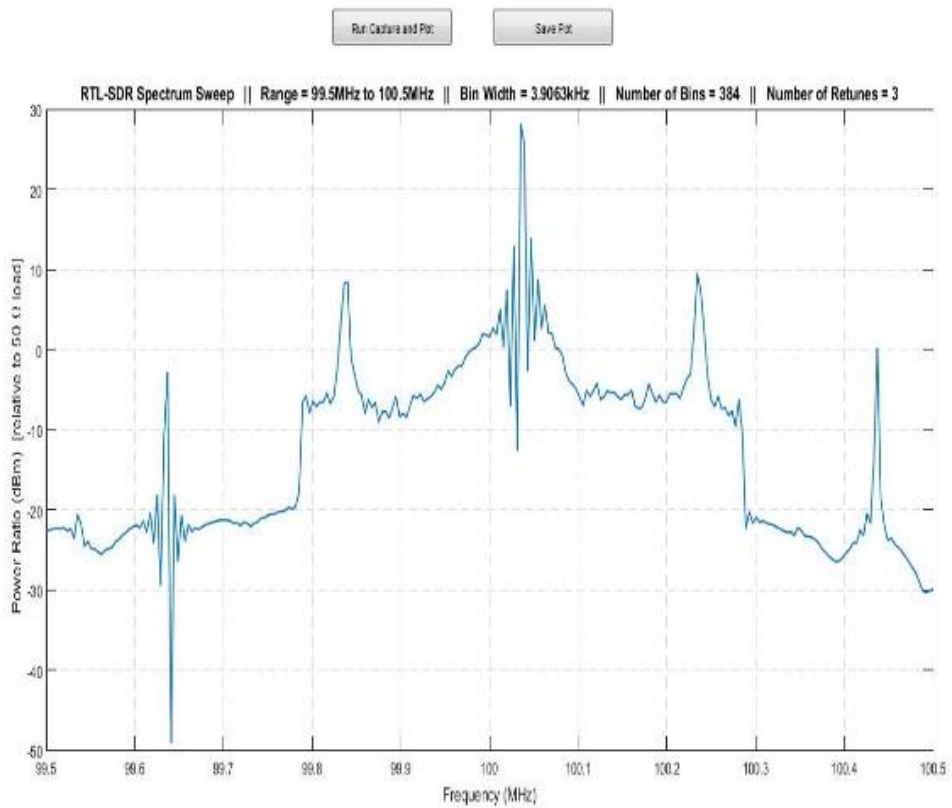


Fig. (6a) the measured Spectrum by the USRP transceiver

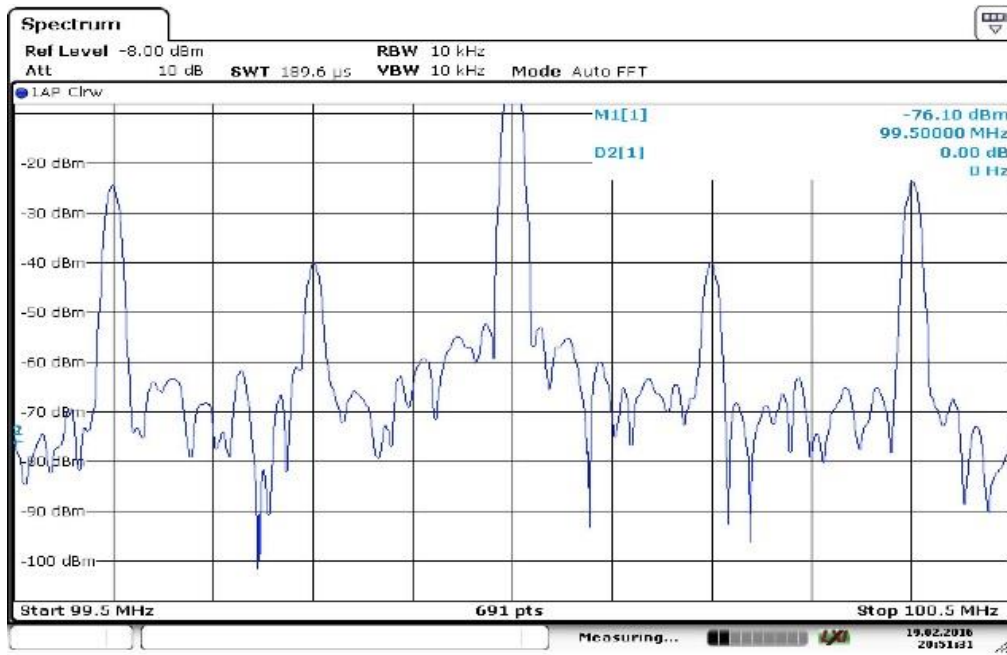


Fig. (6b) the measured Spectrum by the R&S signal analyser

Time period of $T=5.5\mu s$.

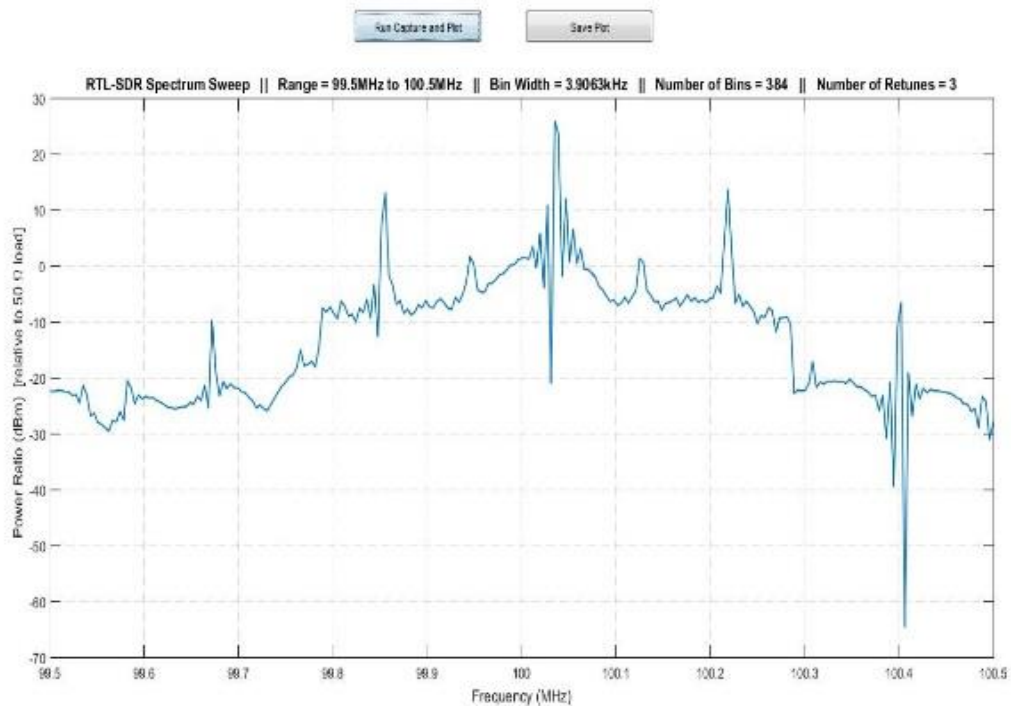


Fig. (7a) the measured Spectrum by the USRP transceiver

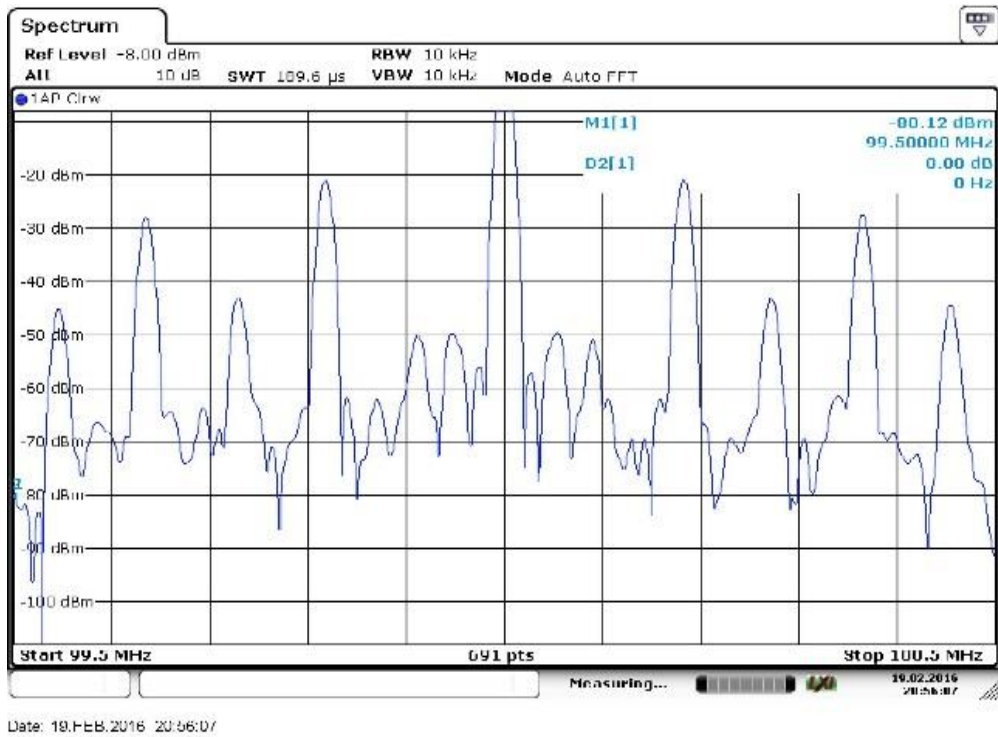


Fig. (7b) the measured Spectrum by the R&S signal analyser.

Time period of $T=9.5 \mu\text{s}$.

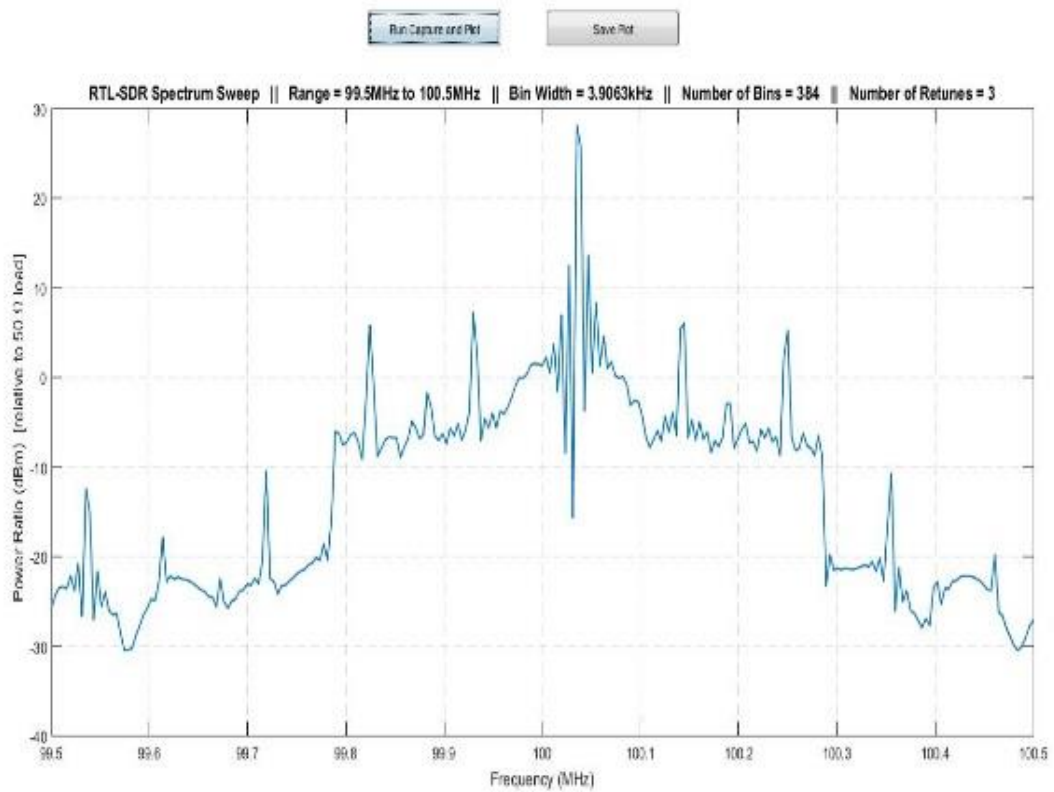


Fig. (8a) the measured Spectrum by the USRP transceiver

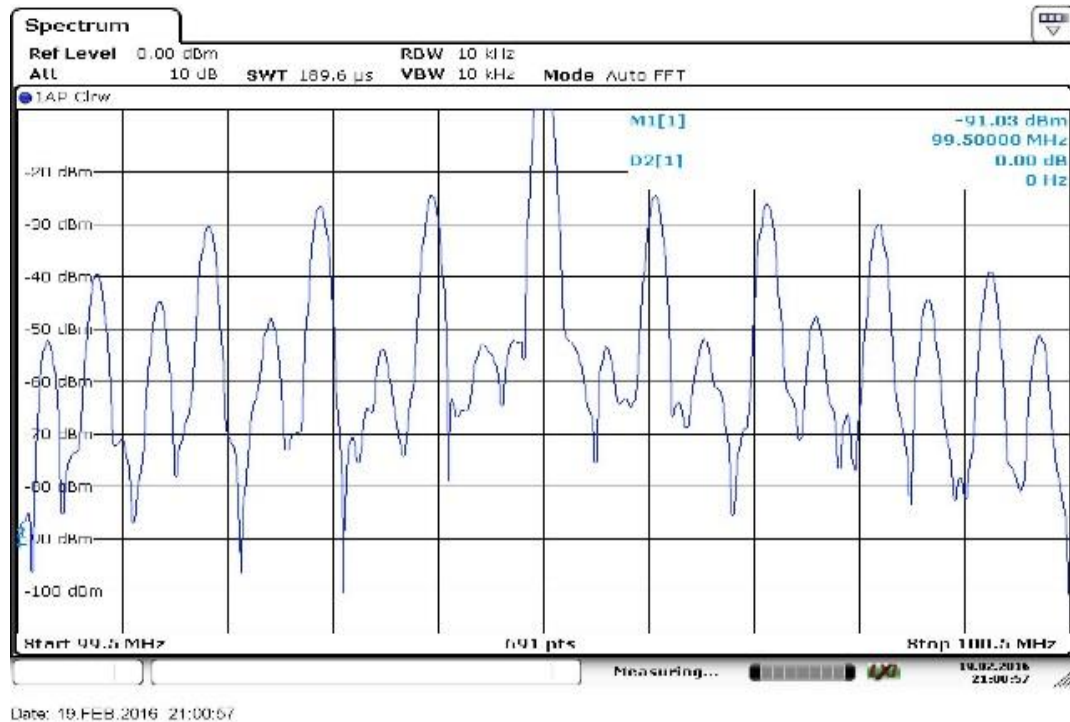


Fig. (8b) the measured Spectrum by the R&S signal analyser.

Result discussion:

From the figures shown above, and although the resolution bandwidth of the USRP transceiver is a bit less than the resolution of the signal analyser, the measured spectra by the USRP transceiver in the all figures, i.e {1a, 2a, 3a, 4a, 5a, 6a, 7a and 8a} the spectra seem that as the average of the fft points is taken and do not change up and down as quick as of that of the signal analyser, leading to getting inaccurate spectrum, in addition to that, the centre frequency is shifted by about **45KHz** in all the measured spectra by the USRP transceiver.

The following are the figures of the square signal and the modulated signal as shown by the oscilloscope ((please note that the figures below are not for the above figures but similar, in case you want to calculate the power I can do the experiment again to get the shape of signals in time domain by the oscilloscope and send them to you))

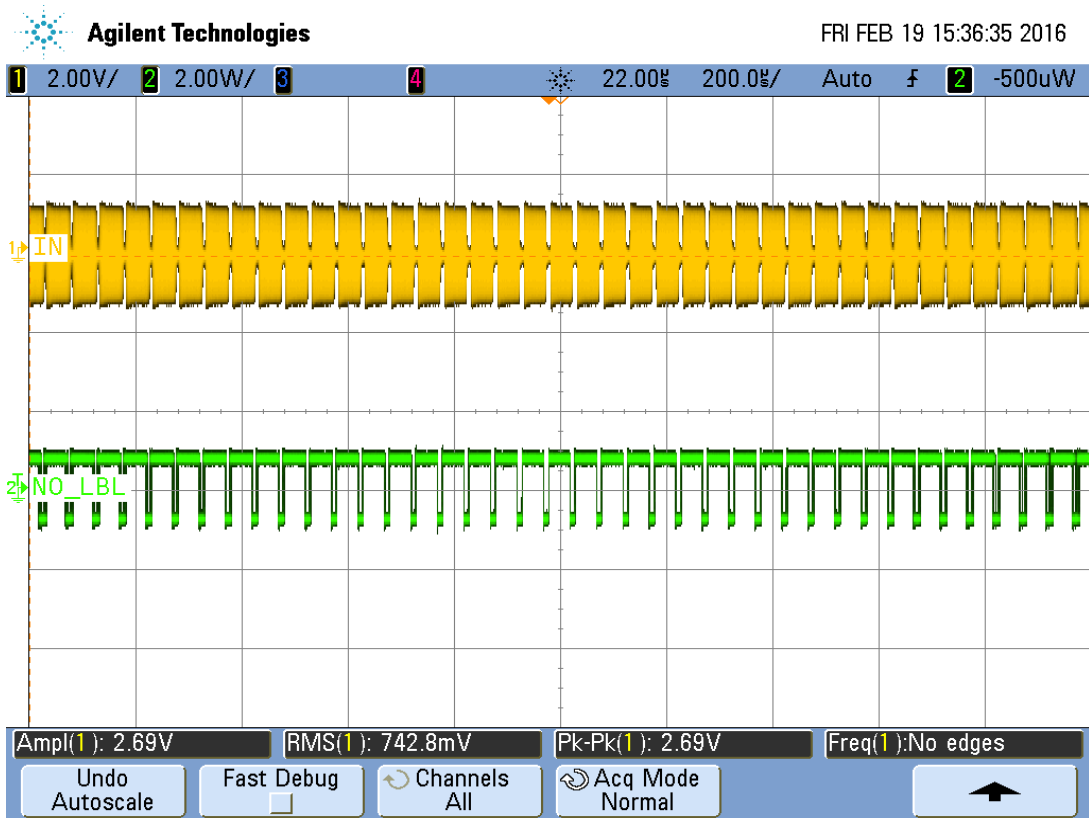


Fig. 9 AM carrier generated by a signal generator

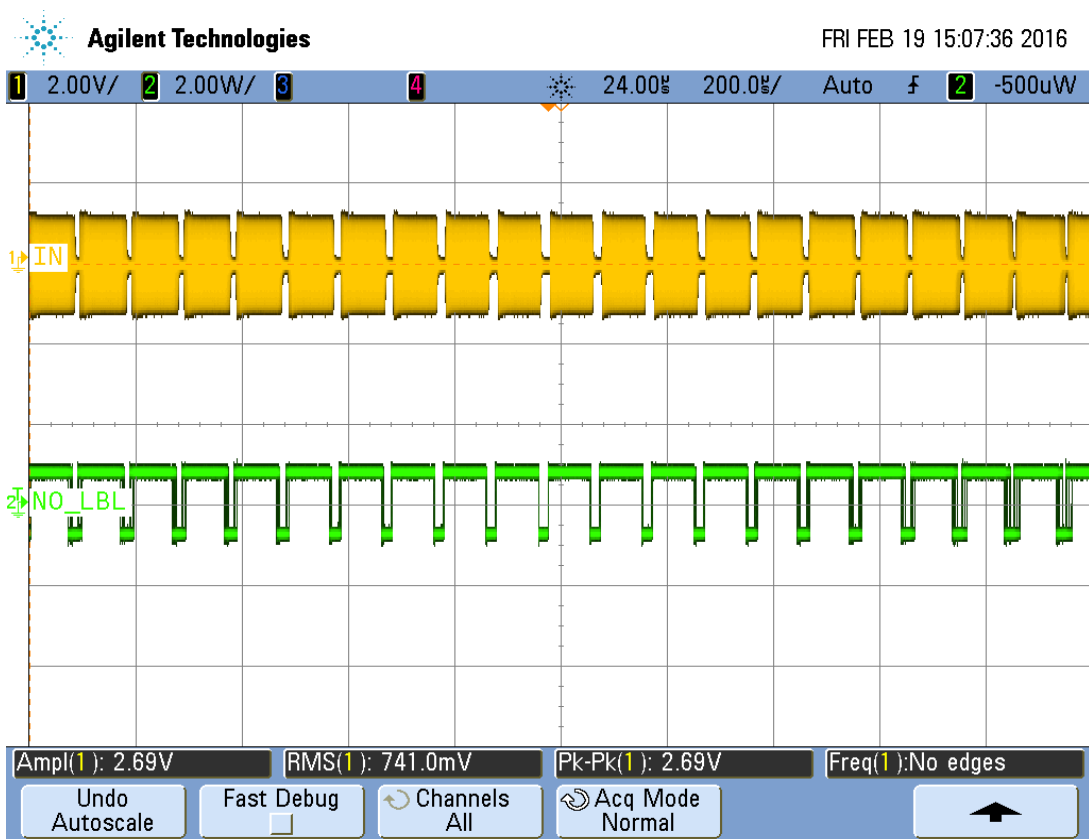


Fig. 10 AM carrier generated by a signal generator with different modulation depth

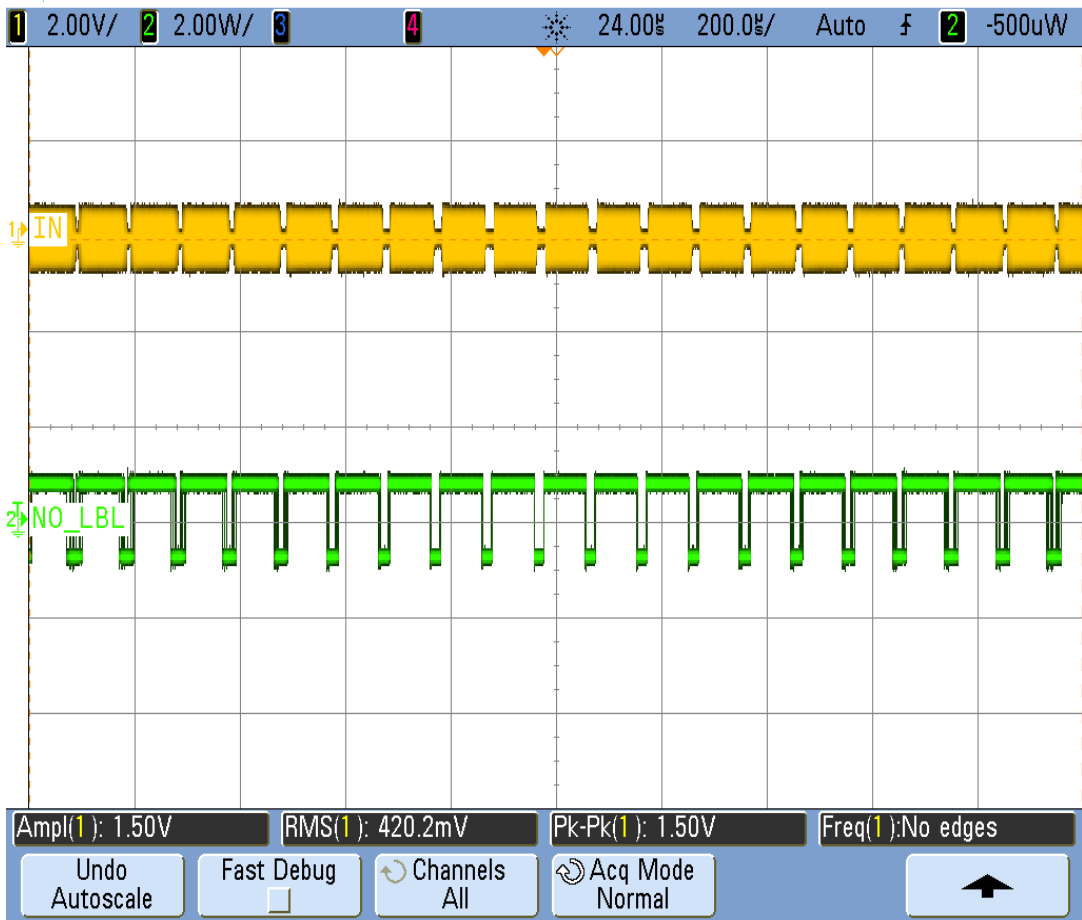


Fig. 11 AM carrier generated by a signal generator with different modulation depth

Appendix-A2

Tests of signal processing to remove the spikes and some strong interference signals:

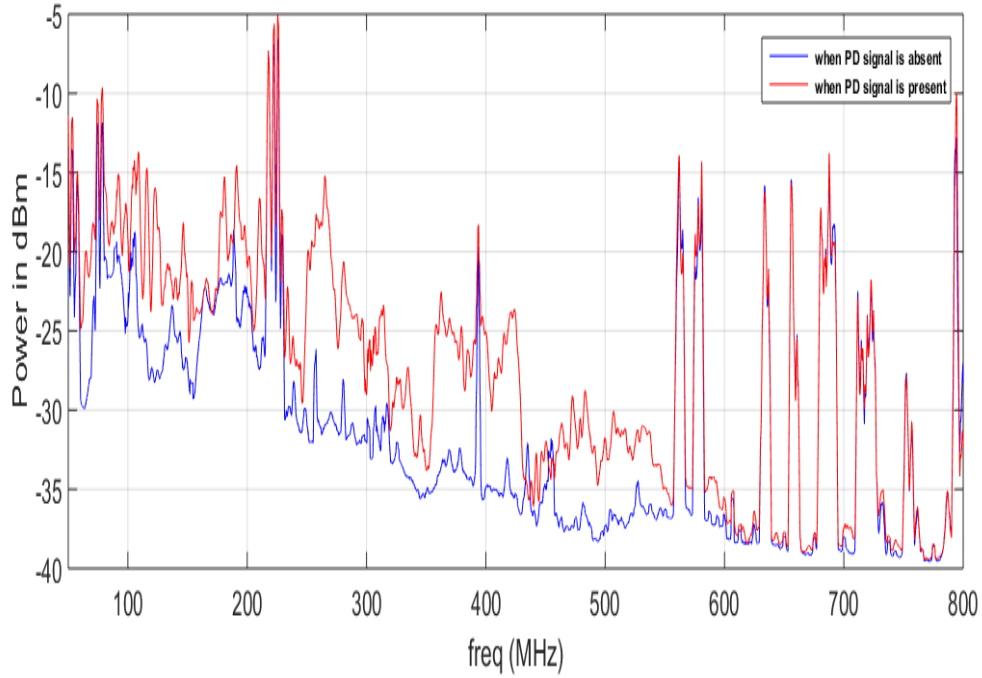


Fig. 12. Before removing spikes from the spectra

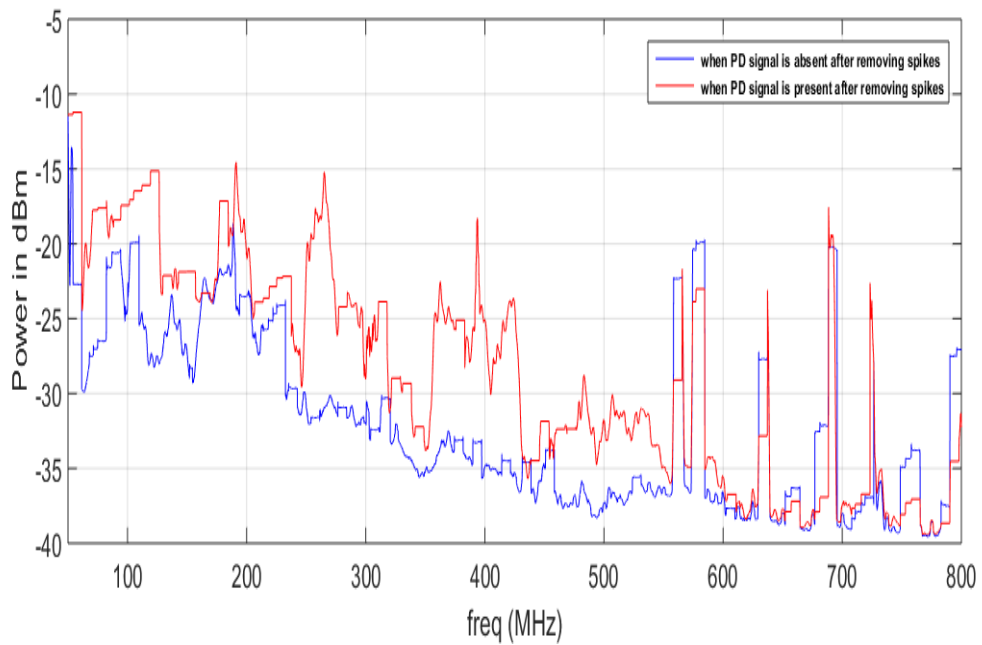


Fig. 13. After removing some spikes from the spectra

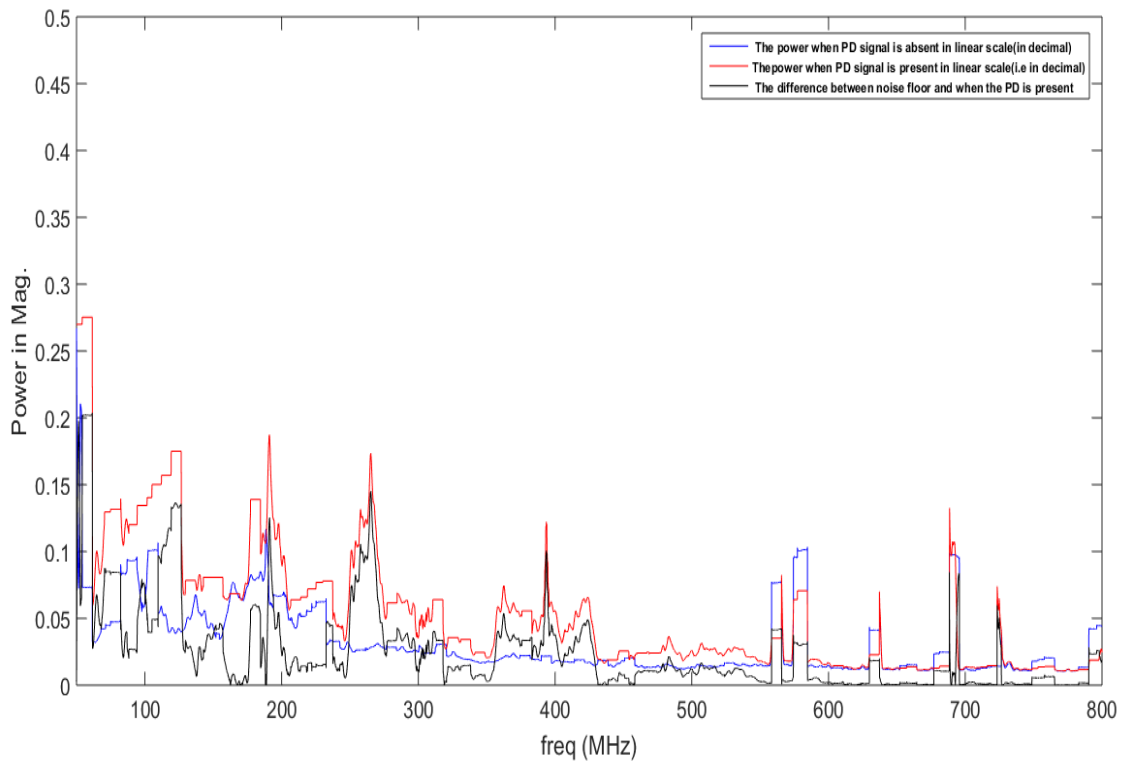


Fig. 14 The power in watts (the black curve is the difference between the red curve and the blue curve)

Appendix –A3

Network mote

Motes and manager are pre-supplied with security and information, which can form a network by themselves once powered up. The manager CLI is capable to of tracing all motes that joins the network automatically after the motes are turned on by a couple of minutes. Therefore, the CLI manager is an important interface for diagnostics and debugging.

Before any data can be sent, several pieces of software need to be installed and to verify whether the software installed can connect to both the mote and the manager. In order to verify this, it involves first to prepare the Hardware. With regard to connections concerning the mote; the DC9003A-C (left in figure 14) need to be connected using board-to-board connector with the DC9006 (right in figure 15).



Figure 15 Layout of mote boards

Sliding the side switch on board DC9003 will power on the mote, connection between the computer and the mote is done through the USB port integrated on board DC9006, but before doing this; serial drivers need to be installed on the computer in order that the computer can identify it. Once the computer identifies the mote, the USB port used should be the same for all future use with this computer unless similar steps for the previous port were repeated for the new additional port. Four virtual COM ports should be added automatically thereafter; otherwise an installation of Future Technology Devices International (FTDI) drivers is needed. The APIExplorer can be employed to find out the API port and then the CLI port can be identified.

Preparing the system

Certain specific software tools are required to allow the smart mesh Wireless Hart sensor network users to interact with the API and CLI of the mote and manager. Following mentioned are few tools which can be used by the user for certain cases.

- In order to interact with the CLI and API of the Mote through a serial-to-USB link FTDI drivers are installed.
- In order to interact with the CLI of the Mote and the Manager, a serial terminal client, “Putty” is installed.
- The user can visualize and configure the whole network with Admin Toolset which resides on the Manager, by using a web-browser.
- To analyse the Mote and Manager API’s features Python-based tool set, “Smart Mesh SDK” can be used.

Installation of SDK Software

Another software interface with the network manager is the Application Programming Interface (API). Interaction with the network is conducted through the programming interface provided by the WirelessHART manager XML-RPC API, which is defined as an Extensible Mark-up Language (XML) that allows a client application send Remote Procedure Call (RPC) requests to the manager and receive back responses in addition to other data from the manager via XML-RPC. The API constitutes of a Control Channel, used to establish connection and exchange commands and information about the network, and a Notification Channel, used to send data and network events to the client Host program. The Python Developer SDK is used for experimenting and communicating with the Manager API.

While the CLI is deployed for direct human interactions through text input, the API is a device interface for interacting with other processors. The SDK contains applications which perform various functions exercising the APIs through a GUI interface.

The following steps are followed in series to complete the software set-up.

1. Installing FDTI Serial Driver for the DC9006A board.
 2. This serial driver enables the serial communication between the device and the computer through a USB.
- Connect USB Cable between the Mote/Manager and the computer.
 - A pop-up window for found new hardware wizard opens on the screen

- The software must be installed from the CD that comes with the USB-serial converter cable. Once the software is installed, four ports will be added to the ports (COM) list of device manager as shown in figure 16.

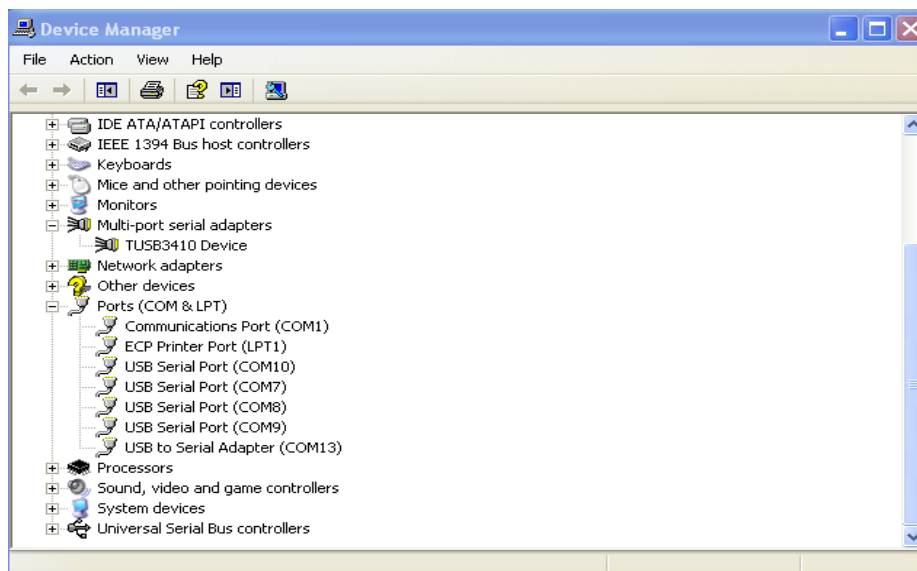


Figure 16 Device Manager and the added ports

COM Ports Configuration

- Post the installation of DC9006 (Wireless Harte Mote), all four of the new COM ports must be configured as shown in the below screen in figure 17:

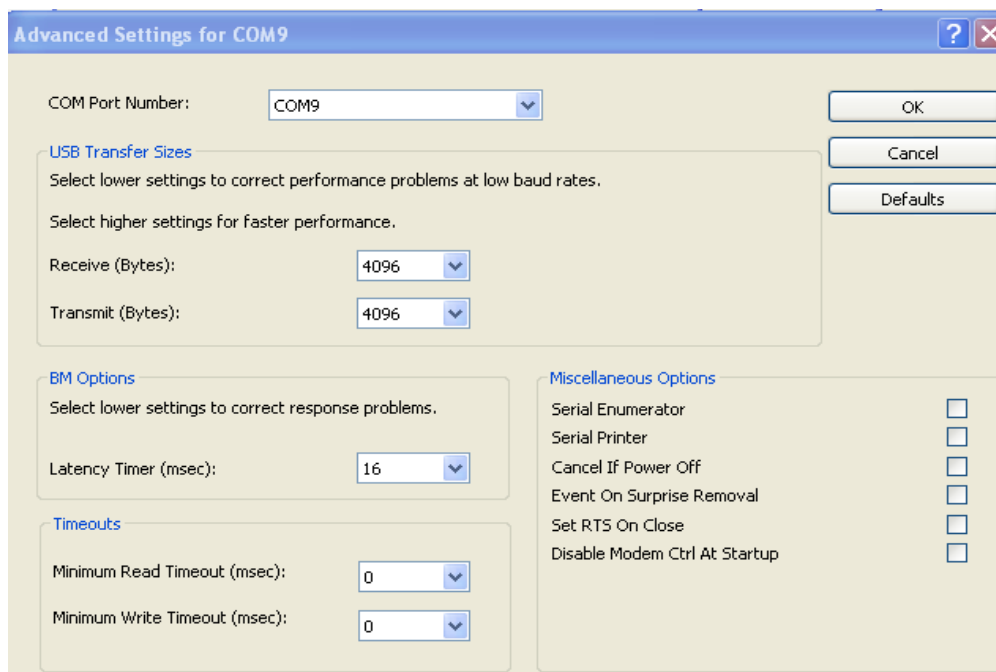


Figure 17 Parameters settings for serial port

Once ports are configured as shown above, the Wireless Hart can be accessed with two different serial ports.

3. InstallTest.Py executable which resides on the "src/bin/InstallTest" directory of the Smart Mesh SDK folder is used to test and verify the installation.

The Smart Mesh SDK is a python-based tool which is used to interact and analyse different aspect of Wireless Hart Mote and Manager APIs.

- The latest version of Smart Mesh SDK is downloaded from Dust Networks of the Linear Design Tools site.
- Latest version of python and its relevant version of “Pyserial” are installed. Version compatibility is important as Pyserial adds serial port support to the python.
- Once installation is completed successfully, test script “src/bin/InstallTest” will display the following text

```
C:\Python27\python.exe
Installation test script - Dust Networks SmartMeshSDK v1.0.4.110
Testing installation of Python...
PASS!
You are running Python 2.7.6
on platform: Windows-XP-5.1.2600-SP3, x86
Testing installation of PySerial...
PASS!
You have PySerial 2.7
Testing installation of PyWin32...
PASS!
You have PyWin32 build 219
Press Enter to exit.
```

Figure 18 Test script

Establishing connection to the manager and mote

Establishing connection to the mote CLI

The software terminal “putty” is used to interact with the mote through the CLI serial port. When the mote were plugged in, there are four COM ports were added. The COM port settings are 9600 baud, 8data bits, no parity, 1 stop bit and no flow control. The motes are pre-configured to be in master mode, but they can be changed to be in slave mode.

Following are putty configuration settings to interact serially with the mote.

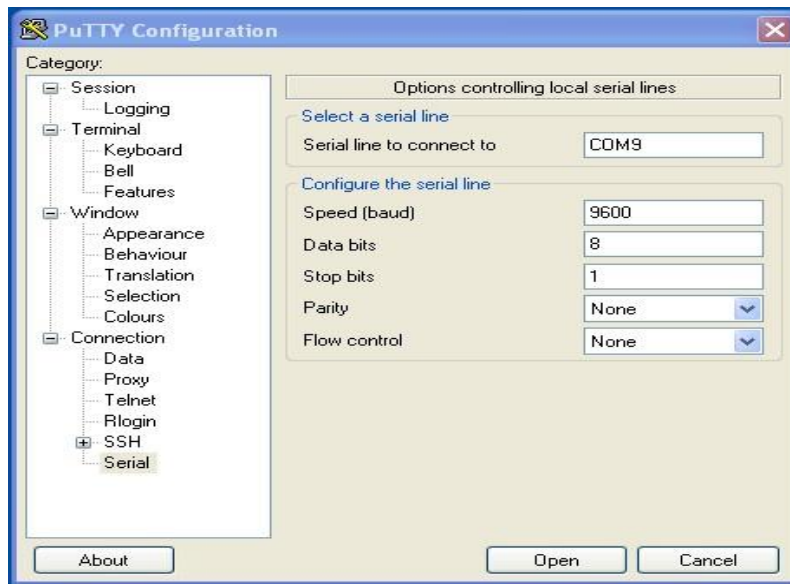


Figure 19 serial port parameters

Motes can be configured in either of two ways:

- Master Mode.
This is the automatic mode for the mote; it automatically connects to the network when the mote is switched on.
- Slave Mode.
In order to connect to the network in slave mode the API –“join” command should be issued to the mote.

Following are a few illustrations of commands used in the Mote.

- In order to see information about the mote attached to the DC9006A board the CLI: ”minfo” command is used, the Figure. 20 show an illustration.

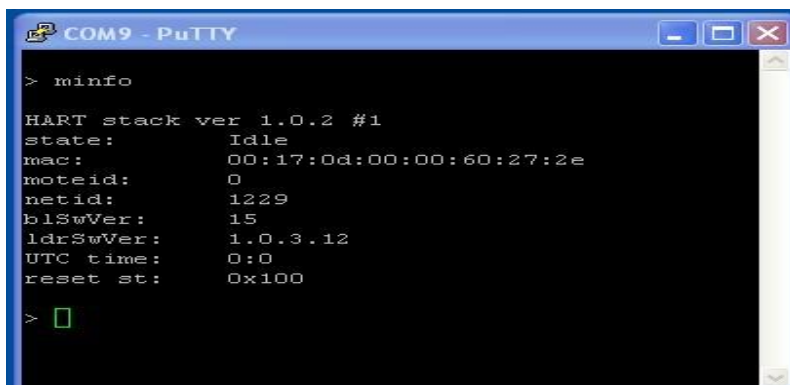


Figure 20 “minfo” command

- In order to view the mode of the mote, the “get mode” command is used as shown below in the figure 21.

```

COM9 - PuTTY

> minfo

HART stack ver 1.0.2 #1
state:      Idle
mac:        00:17:0d:00:00:60:27:2e
moteid:     0
netid:      1229
blSwVer:    15
ldrSwVer:   1.0.3.12
UTC time:   0:0
reset st:   0x100

> get mode
slave
> █

```

Figure 21` “get mode” command

- "Set mode variable" variable= master/slave is used to change the mode of the mote as shown in figure 22.

```

COM9 - PuTTY

blSwVer:    15
ldrSwVer:   1.0.3.12
UTC time:   0:0
reset st:   0x100

> get mode
slave
> set mode
cli: Received command is incomplete

Usage:
set mode [master|slave]

> set mode master
> █

```

Figure 22 “set mode master” command

- When API: “Join” command is issued to the idle in slave mode and idle state, the status of the mote changes to “search” as shown in figure 23.

```
COM9 - PuTTY
HART Mote 1.0.2-14
> minfo
HART stack ver 1.0.2 #1
state:      Search
mac:       00:17:0d:00:00:60:27:2e
moteid:    0
netid:    1229
blSwVer:  15
ldrSwVer: 1.0.3.12
UTC time: 4:4
reset st: 0x400
> 
```

Figure 23 Mote searching state

- Then the mote negotiates a connection with the manager and status convert to connect, as shown in figure 24.

```
COM9 - PuTTY
netid:    1229
blSwVer:  15
ldrSwVer: 1.0.3.12
UTC time: 93040:93040
reset st: 0x400
> minfo
HART stack ver 1.0.2 #1
state:    Conn
mac:     00:17:0d:00:00:60:27:2e
moteid:  9
netid:   1229
blSwVer: 15
ldrSwVer: 1.0.3.12
UTC time: 93060:93060
reset st: 0x400
> 
```

Figure 24 Mote connect state

- Post negotiation the mote enters the join state, as shown in figure 25.

```
COM9 - PuTTY
netid:      1229
blSwVer:   15
ldrSwVer:  1.0.3.12
UTC time:  93039:93039
reset st:  0x400

> minfo

HART stack ver 1.0.2 #1
state:     Join
mac:       00:17:0d:00:00:60:27:2e
moteid:    0
netid:     1229
blSwVer:   15
ldrSwVer:  1.0.3.12
UTC time:  93040:93040
reset st:  0x400

>
```

Figure 25 Mote Join state

- While the mote is in “join” status, it shares the joining key with the manager. Once the key is validated and matches with that of the manager, the mote enters the operational mode; as shown below in figure 26.

```
COM9 - PuTTY
netid:      1229
blSwVer:   15
ldrSwVer:  1.0.3.12
UTC time:  93060:93060
reset st:  0x400

> minfo

HART stack ver 1.0.2 #1
state:     Oper
mac:       00:17:0d:00:00:60:27:2e
moteid:    9
netid:     1229
blSwVer:   15
ldrSwVer:  1.0.3.12
UTC time:  1404830824:1404830824
reset st:  0x400

>
```

Figure 26 Mote Operational state

Joining a mote to the manager with the API

The manager and the mote should now be connected to the computer through the CLI program.

The next step is to connect simultaneously to the API of the mote.

The Smart Mesh SDK is a "Python" based tool used to interface with the device's application programming interface.

Once the Smart Mesh SDK is installed following four sub-directories are created:

- arc: It contains the source code.

- win: it contains pre-compiled versions of the sample applications generated using the “py2exe” utility.
- doc: It contains HTML based documentation.
- api: It contains the C header file and sample code.

Following shows the status of the APIExplorer in various scenarios.

- Once the APIExplorer application is accessed from its pre-compiled executable from “win” sub directory, the prompt as shown in figure 27 appears.



Figure 27 API Explorer Prompt

- Once the mote gets connected through the API, the port area turns green to indicate successful connection as shown in figure 28.

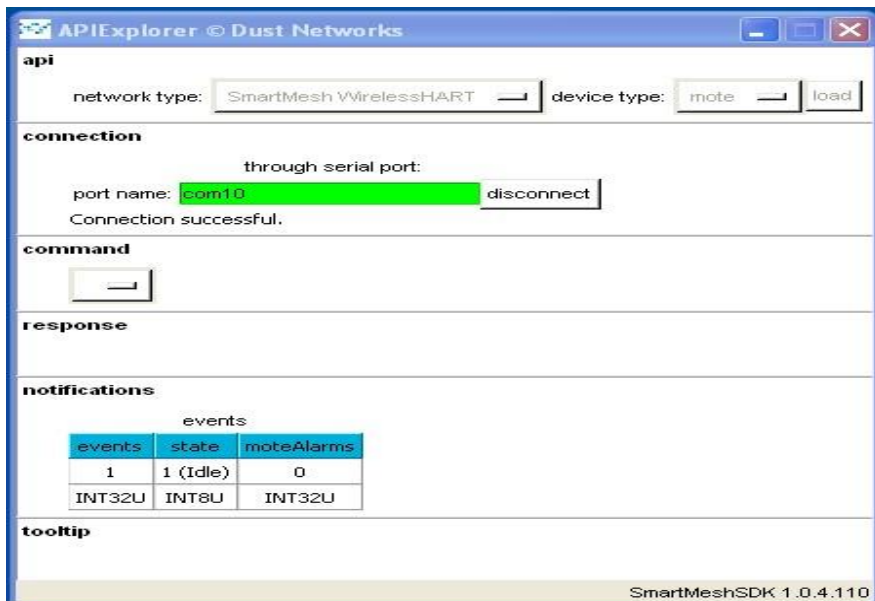


Figure 28 PI Explorer establishing mote connection

- The figure 29 shows all the commands supported by the mote API.

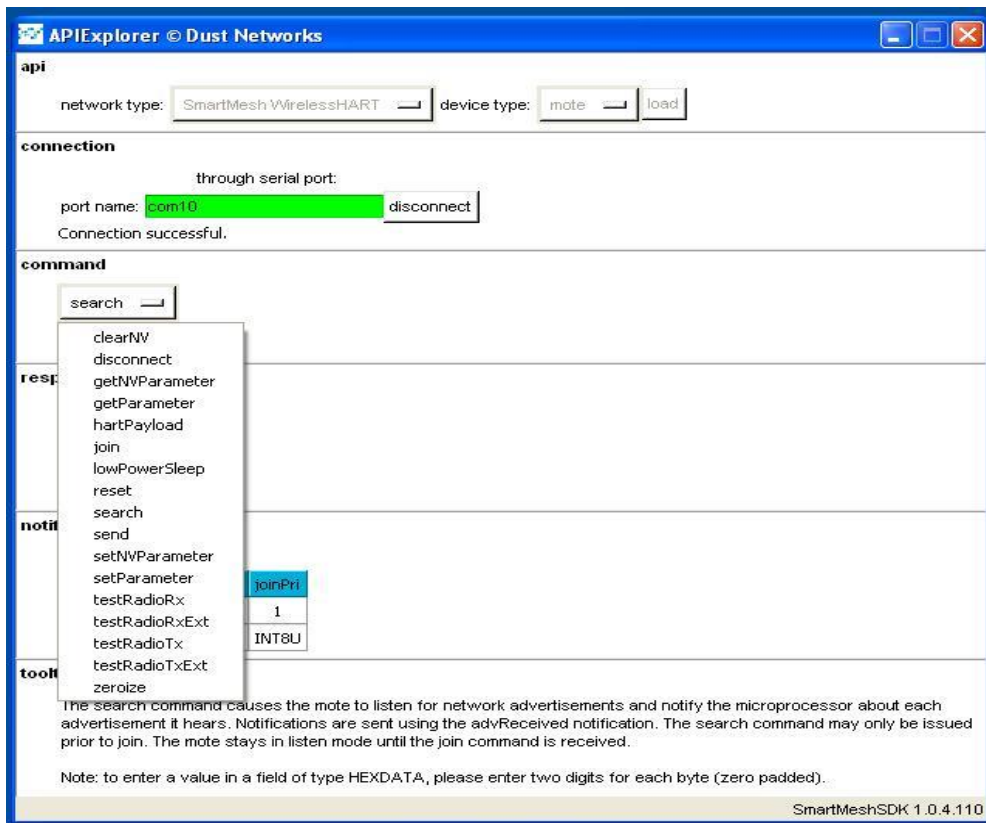


Figure 29 Mote commands set

Connecting with the Manager through CLI

The manager is connected through the serial terminal software “putty”, it can be connected in following two ways:

- Through Com Port (com 13; this case).
- Through SSH protocol by port 22 and IP address of the manager as shown in figure 30.

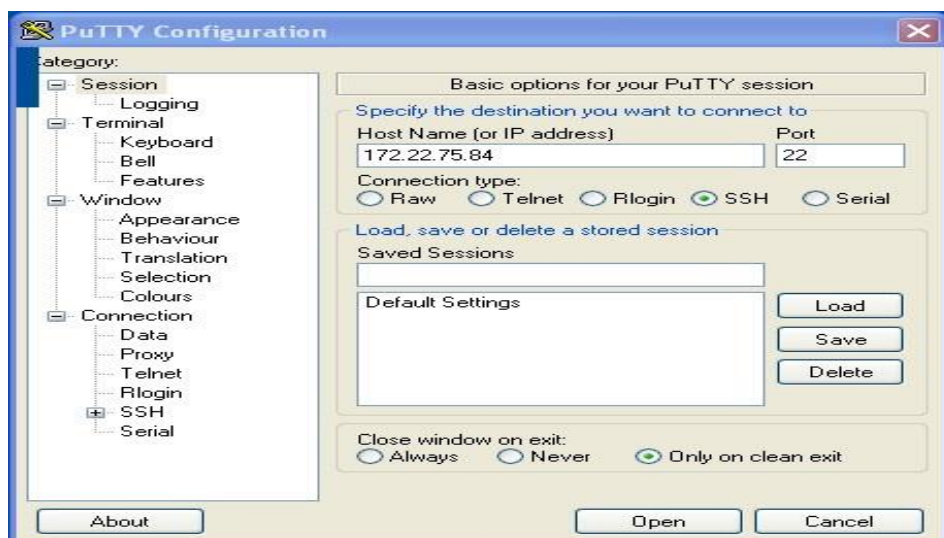


Figure 30 Manager Connection through SSH

- Once connected; the command prompt needs user authentication, at the beginning it will ask login as following:

Manager login: dust

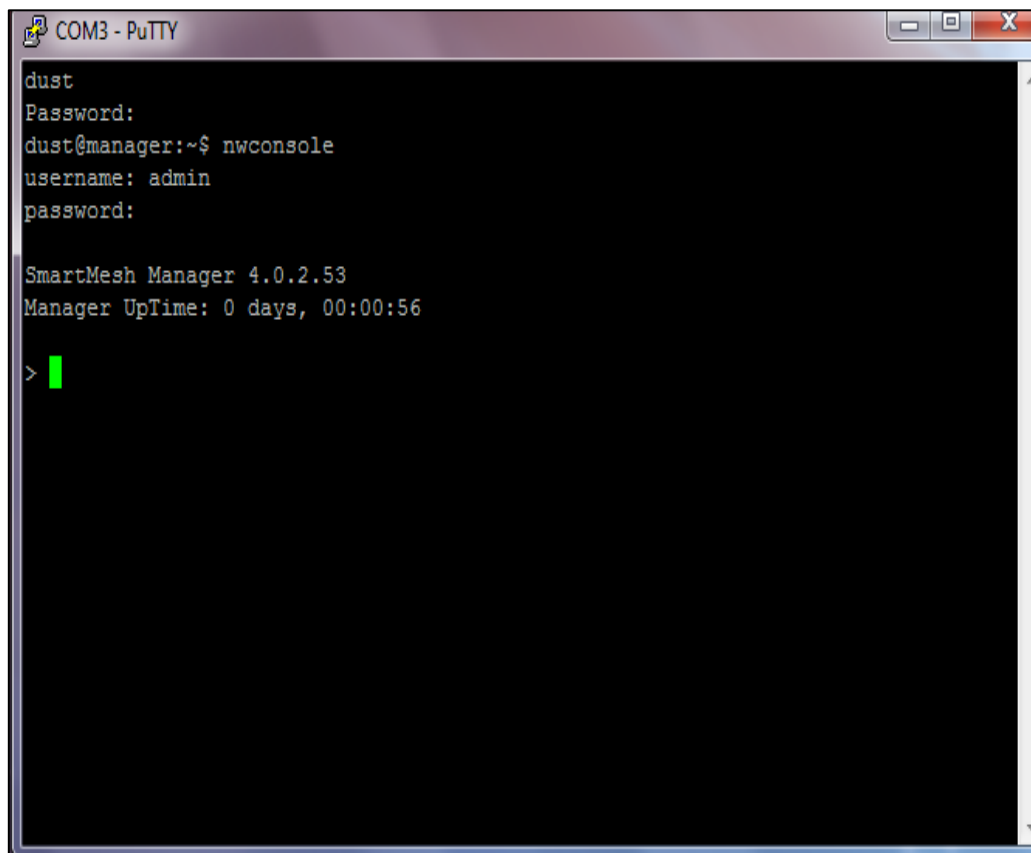
Password: dust

Then a prompt will appear with (dust@manager :~>), so type 'nwconsole', this will lead to login step as following:

User name: admin

Password: admin

Figure 31 shows prompt after authentication.



```
COM3 - PuTTY
dust
Password:
dust@manager:~$ nwconsole
username: admin
password:

SmartMesh Manager 4.0.2.53
Manager UpTime: 0 days, 00:00:56

> █
```

Figure 31 Wireless Hart Manager CLI Prompt

“sm” command on the CLI prompt lists all the motes associated with the manager as illustrated in figure 32.

```

COM3 - PuTTY
Current time: 03/31/14 21:13:43 ASN: 571870
Elapsed time: 0 days, 01:35:29
  MAC                MoteID  Age  Jn      UpTime   Fr  Nbrs  Links  State
00-17-0D-00-00-20-C3-BE  ap  1    1      01:35:18  6  5     92  Oper
00-17-0D-00-00-60-1E-19   10  27  1      00:46:28  2  2     12  Oper
00-17-0D-00-00-60-1E-FD   11  2  2      00:01:05  2  2     11  Conn
00-17-0D-00-00-60-23-C8    7  0  1      01:30:18  2  4     45  Oper
00-17-0D-00-00-60-27-2C    8  1  1      01:25:03  2  2     38  Oper
00-17-0D-00-00-60-27-2E    9  2  1      00:46:32  2  3     13  Oper
>
> sm
Current time: 03/31/14 21:14:49 ASN: 578502
Elapsed time: 0 days, 01:36:35
  MAC                MoteID  Age  Jn      UpTime   Fr  Nbrs  Links  State
00-17-0D-00-00-20-C3-BE  ap  1    1      01:36:25  6  5    120  Oper
00-17-0D-00-00-60-1E-19   10  4  1      00:47:35  2  2     12  Oper
00-17-0D-00-00-60-1E-FD   11  5  3      00:02:11  2  2     38  Oper
00-17-0D-00-00-60-23-C8    7  0  1      01:31:24  2  4     46  Oper
00-17-0D-00-00-60-27-2C    8  1  1      01:26:09  2  2     38  Oper
00-17-0D-00-00-60-27-2E    9  26  1      00:47:38  2  3     13  Oper
>

```

Figure 32sm command

The mote id for any mote in Idle or search state will take number ‘0’ When a mote converts from Idle state to operation state will take its specific number as in the figure shown below:

```

COM6 - PuTTY
state:      Search
mac:       00:17:0d:00:00:60:27:2c
moteid:    0
netid:     1229
blSwVer:   15
ldrSwVer:  1.0.3.12
UTC time:  283492:283492
reset st:  0x400

> minfo
error: unknown comm'

error: unknown comm'
> minfo

HART stack ver 1.0.2 #1
state:     Oper
mac:       00:17:0d:00:00:60:27:2c
moteid:    8
netid:     1229
blSwVer:   15
ldrSwVer:  1.0.3.12
UTC time:  1402856908:1402856908
reset st:  0x400

```

Figure 33 mote in search star and oper state

Next figure shows the stages of a mote being operator as shown mote9 start negotiating then convert to operator state.

```

COM3 - PuTTY
MAC MoteID Age Jn UpTime Fr Nbrs Links State
00-17-0D-00-00-20-C3-BE ap 1 1 3-06:16:17 6 2 59 Oper
00-17-0D-00-00-60-1E-19 10 0 1 3-06:03:35 2 2 38 Oper
00-17-0D-00-00-60-1E-FD 11 4 1 3-06:13:55 2 2 15 Oper
00-17-0D-00-00-60-23-C8 7 76237 3 21:13:47 2 2 38 Lost
00-17-0D-00-00-60-27-2E 9 69591 4 20:59:59 2 3 68 Lost
> Mote #9 changed state to Negot1
Mote #9 changed state to Negot2
Mote #9 changed state to Conn
Mote #9 changed state to Oper

> sm
Current time: 06/15/14 18:07:28 ASN: 28231222
Elapsed time: 3 days, 06:25:19
MAC MoteID Age Jn UpTime Fr Nbrs Links State
00-17-0D-00-00-20-C3-BE ap 1 1 3-06:25:08 6 3 91 Oper
00-17-0D-00-00-60-1E-19 10 0 1 3-06:12:26 2 3 40 Oper
00-17-0D-00-00-60-1E-FD 11 5 1 3-06:22:46 2 2 15 Oper
00-17-0D-00-00-60-23-C8 7 76768 3 21:22:38 2 2 38 Lost
00-17-0D-00-00-60-27-2E 9 0 5 00:08:20 2 2 39 Oper
>

```

Figure 34 mote negotiating

In the figure 35, three commands are shown to interact with the network.

```

COM3 - PuTTY
1 7 -44 -42 0( 0) 2 33( 0) 36 100%
> delete sessions
usage: delete { acl #<MAC> | mote (<ID>|#{<MAC>}) | user <userName> }
Delete configuration object

>
> get mote
get <object> <args>
objects:
acl #<MAC> -- get all ACL devices
acl #<MAC> -- get ACL device with EUI-64 <MAC>
alarms -- get all alarms
blacklist -- get channel blacklist
motes -- get all motes
mote (<ID>|#{<MAC>}) -- get mote with ID <moteID> or EUI-64 <MAC>
network -- get network
otapstatus -- get OTAP status
otapfiles -- get OTAP files
otapmotes -- get OTAP motes
paths -- get all paths
path <MAC> <MAC> -- get path between specified motes
security -- get security
sla -- get service level agreement
system -- get system
users -- get all users

> get all motes
get <object> <args>
objects:
acl #<MAC> -- get all ACL devices
acl #<MAC> -- get ACL device with EUI-64 <MAC>
alarms -- get all alarms
blacklist -- get channel blacklist
motes -- get all motes
mote (<ID>|#{<MAC>}) -- get mote with ID <moteID> or EUI-64 <MAC>
network -- get network
otapstatus -- get OTAP status
otapfiles -- get OTAP files
otapmotes -- get OTAP motes
paths -- get all paths
path <MAC> <MAC> -- get path between specified motes
security -- get security
sla -- get service level agreement
system -- get system
users -- get all users

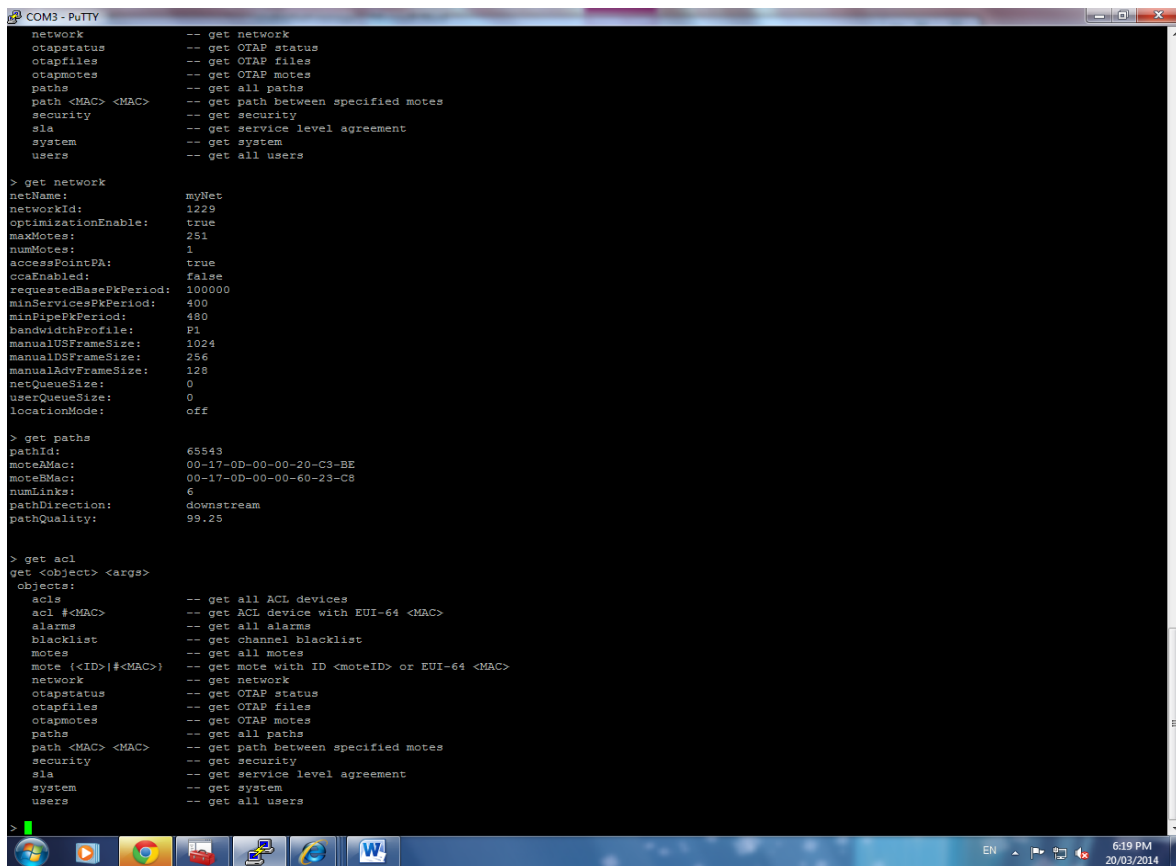
> get system
systemName: Dust
location: dust
swRev: 4.0.2.53-1
hwModel: LTP5903
hwRev: 002
serialNumber: 00170d801c98
time: 1395338842433
startTime: 1395312621000
cliTimeout: 120
controllerSwRev: 4.0.2.53

> get all users

```

Figure 35 get mote and get system command

If information about the network is needed, type get network as in the figure 36.



```
COM3 - PuTTY
network          -- get network
otapstatus       -- get OTAP status
otapfiles        -- get OTAP files
otapmotes        -- get OTAP motes
paths            -- get all paths
path <MAC> <MAC> -- get path between specified motes
security         -- get security
sla              -- get service level agreement
system          -- get system
users            -- get all users

> get network
netName:          myNet
networkId:        1229
optimizationEnable: true
maxMotes:         251
numMotes:         1
accessPointPA:    true
ccaEnabled:       false
requestedBasePkPeriod: 100000
minServicePkPeriod: 400
minPipePkPeriod: 480
bandwidthProfile: P1
manualUSFrameSize: 1024
manualDSFrameSize: 256
manualRSFrameSize: 128
netQueueSize:    0
userQueueSize:   0
locationMode:    off

> get paths
pathId:           65543
moreMac:          00-17-0D-00-00-20-C3-BE
moteBMac:         00-17-0D-00-00-60-23-C8
numLinks:         6
pathDirection:   downstream
pathQuality:      99.25

> get acl
get <object> <args>
objects:
acls              -- get all ACL devices
acl #<MAC>        -- get ACL device with EUI-64 <MAC>
alarms            -- get all alarms
blacklist         -- get channel blacklist
motes             -- get all motes
mote (<ID>|#<MAC>) -- get mote with ID <moteID> or EUI-64 <MAC>
network          -- get network
otapstatus       -- get OTAP status
otapfiles        -- get OTAP files
otapmotes        -- get OTAP motes
paths            -- get all paths
path <MAC> <MAC> -- get path between specified motes
security         -- get security
sla              -- get service level agreement
system          -- get system
users            -- get all users

>
```

Figure 36 get network command

To show event, type 'show events' and to prevent one mote from joining the network add it to the blacklist and to test it whether there is a connection or not type ping mote 1 as in the figure 37.

```

COM3 - PuTTY
network          -- get network
otapstatus       -- get OTAP status
otapfiles        -- get OTAP files
otapmotes        -- get OTAP motes
paths            -- get all paths
path <MAC> <MAC> -- get path between specified motes
security         -- get security
sla              -- get service level agreement
system           -- get system
users            -- get all users

> show events
show <subcommand> <args>
subcommands:
cli-sessions     -- show cli user names and login times
events <last> <num> -- show event with eventID <last> and preceding <num>
events. if <last> = 0, show latest <num> events.
frame [frID]     -- show frame information (if no frID given, show all)
ap [-a]          -- show gateway (-a: include unused paths)
linksmapi        -- show links map
mote {<ID>|#<MAC>} [-l] [-a] -- show mote with ID <moteID> or EUI-64 <MAC>
(-l: show links, -a: include unused paths)
motes [-a]       -- show all motes (-a: include 'unused' motes)
moteall          -- show all motes (required superuser privilege)
msg [-v]         -- show number of commands SMM sent (-v: verbose)
optimization     -- show current optimization parameters
sessions         -- show info on XML sessions
stat <args>      -- show statistics info
status           -- show SMM status
time [ASN]       -- show time (current or specified ASN)
ver [hw]         -- show motes/gateway sw / hw version

> set blacklist
set <object> [objectId | #MAC] {<field>=<value>}...
objects:
acl              -- set ACL device
blacklist        -- replace channel blacklist
mote             -- set mote
network          -- set network
security         -- set security
sla              -- set service level agreement
system           -- set system
user             -- set user

> ping mote 1
Invalid mote: 'mote'
> [11:14:34] Ping mote 1: reply #1: 0.019s 0 hops [29.0C 2.941V]
[11:14:34] Ping mote 1: sent 1, rcvd 1, 0% lost. Ave.roundtrip: 0.019s hops: 0
ping motel
Invalid mote: 'motel'
> ping mote 7
Invalid mote: 'mote'
> [11:14:54] Ping mote 7: reply #1: 3.209s 1 hops [22.0C 2.906V]
[11:14:54] Ping mote 7: sent 1, rcvd 1, 0% lost. Ave.roundtrip: 3.209s hops: 1
get sla
minNetReliability: 99.00
maxNetLatency: 12500
minNetPathStability: 50.00
apRdntCoverageThreshold:70.00
>

```

Figure 37 show events, set black list and ping mote commands

Connecting with the manager through API

- The APIExplorer can be used to access the manager using the Wireless Hart manager IP address and port 4445 as shown in figure 38.

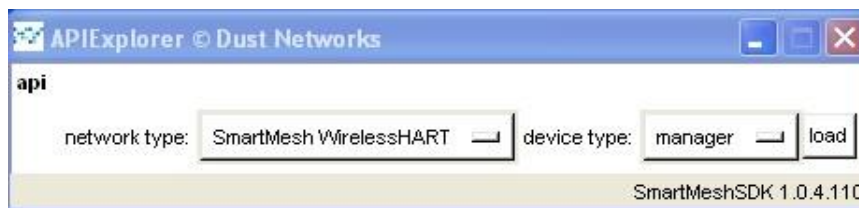


Figure 38 API Explorer Prompt

- Once the connection is established the IP address and the port area turns green to indicate successful connection as shown in the figure 39.

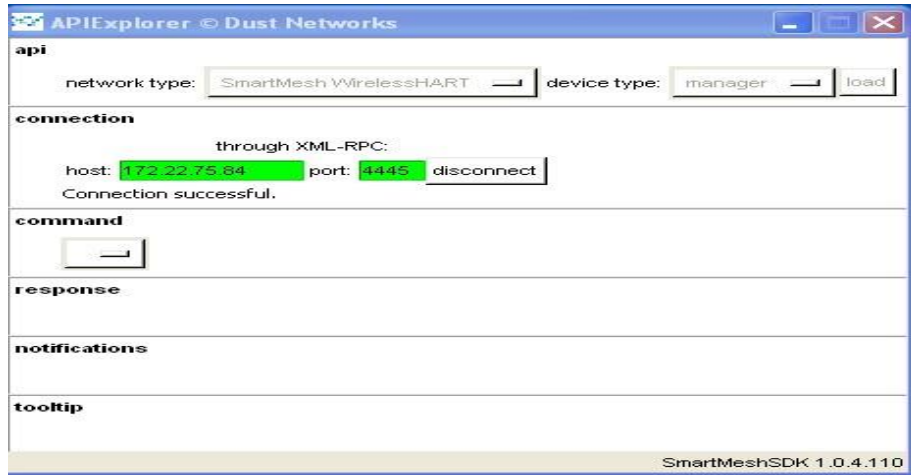


Figure 39 API Explorer establishing manager connection

- The command drop-down menu as shown in figure 40 shows some commands that can be applied to the manager.

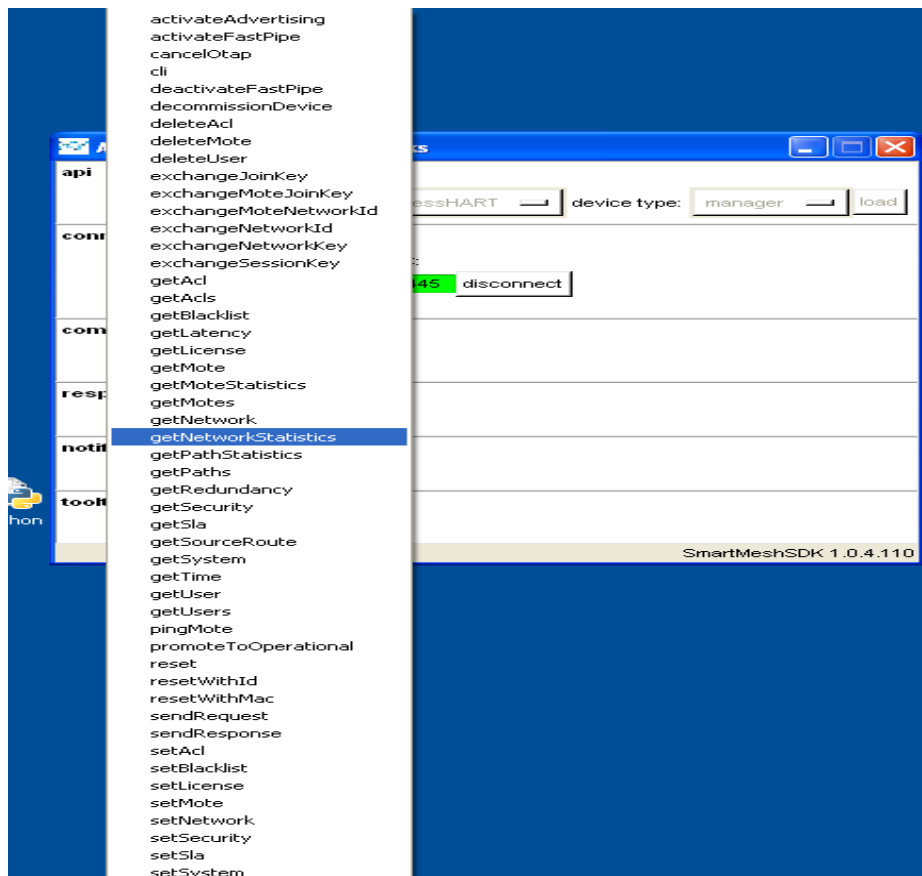


Figure 40 API Explorer manager commands list

- Once a command is selected from the command drop-down menu and the “Send” button is pressed, the command is applied to the manager and the response area shows the associated responses of the manager, as shown in figure 41.

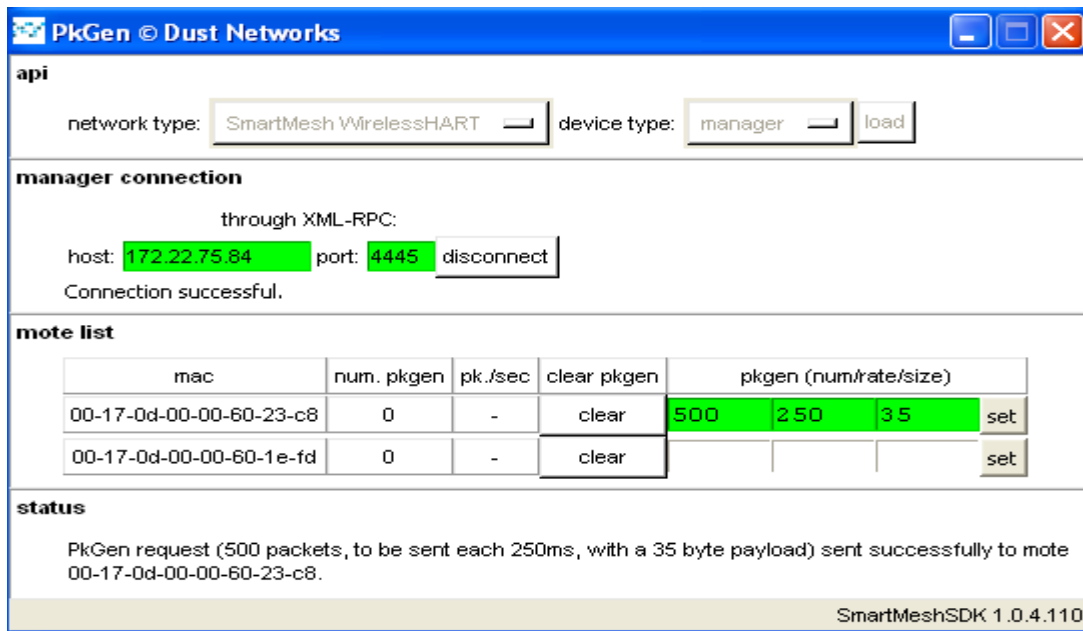


Figure 41 API Explorer executing a command

Admin Toolset and Smart Mesh SDK Applications

Admin Toolset

The Admin Toolset sits on top of the manager and provides an access to the user to interact with the manager through the web browser. The users can perform various functions through this toolset:

- Visualize various network parameters.
- Enhance security at application layer.
- Visualize network topology.

The users can access these resources by typing in a web browser the IP address of the manager through the secure hyper-text transfer protocol. The authentication can be completed through default username; “system” and the default password, “system”.

Figure 42 shows the snapshot of the Admin Toolset main window.

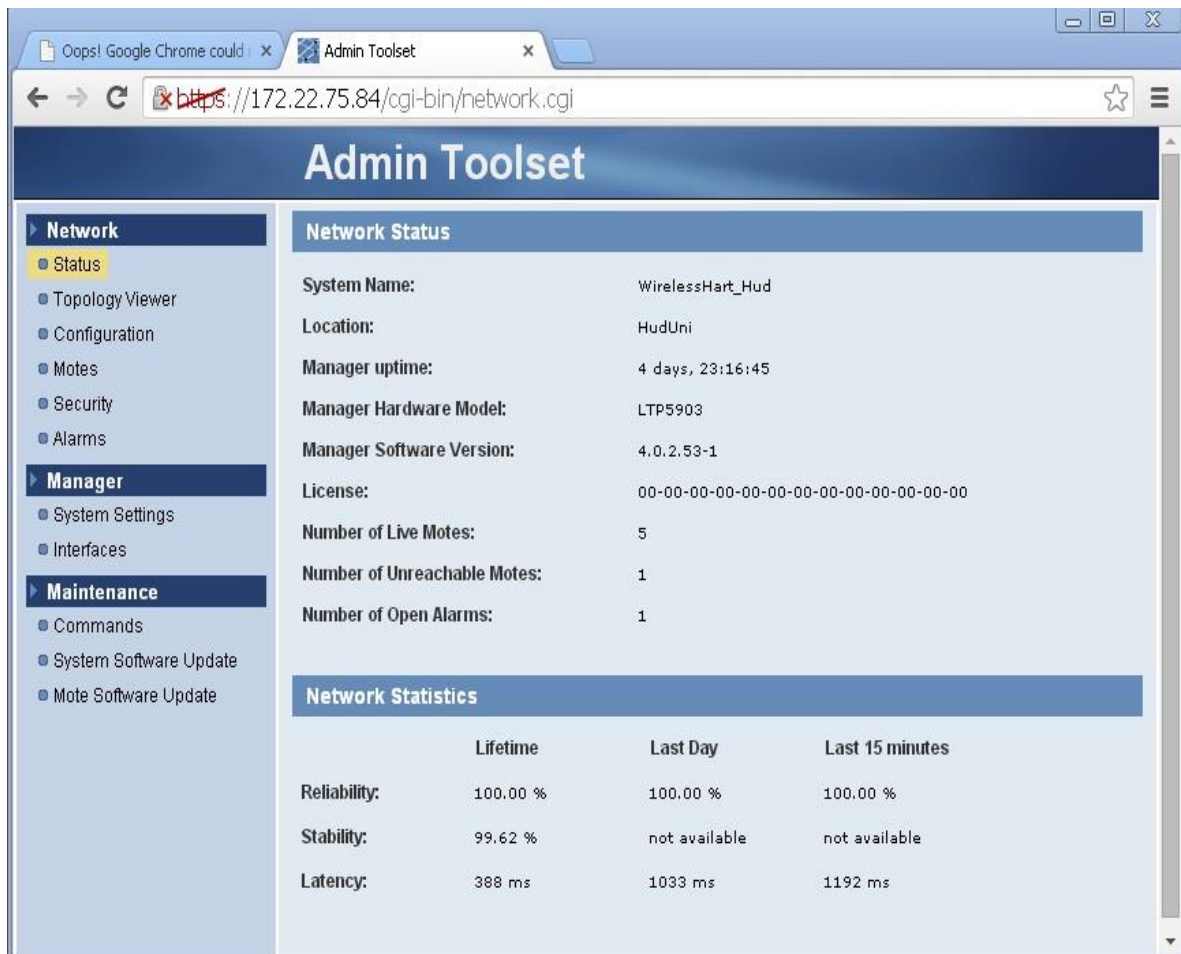


Figure 42 Admin Toolset status menu

- Figure 43 shows configuration window, which allows user to change following parameter:
- Network-wide minimum bandwidth
- The maximum number of motes
- The maximum bandwidth limit for a single mote and pipe
- The location mode
- The optimization
- The access point mode
- CCA
- Bandwidth profile
- Upstream
- Downstream
- Advertising bandwidth.

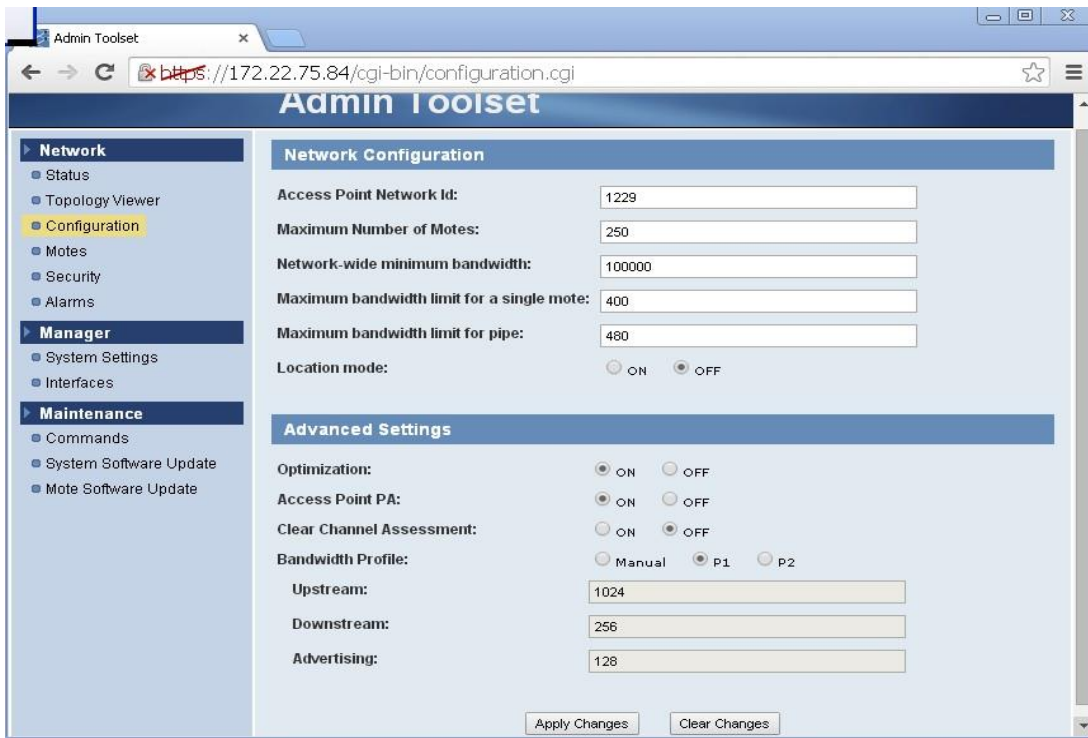


Figure 43 Admin Toolset Configuration menu

- Figure 44 shows the mote list, MAC address, Name, S/W Rev, status, Join Time, Joins and Location.

MAC address	Name	S/W Rev	State	Join Time	Joins	Location
00-17-0D-00-00-20-C3-BE	Access Point	3.0.3-0	Operational	07/07/14 13:55:47	3	not supported
00-17-0D-00-00-1A-54-2E			Idle	not available	0	not supported
00-17-0D-00-00-19-F6-42			Idle	not available	0	not supported
00-17-0D-00-00-18-C5-DC			Idle	not available	0	not supported
00-17-0D-00-00-19-D8-9C			Idle	not available	0	not supported
00-17-0D-00-00-19-28-D6			Idle	not available	0	not supported
00-17-0D-00-00-60-23-C8		1.0.2-14	Operational	07/08/14 16:12:59	8	supported
00-17-0D-00-00-60-27-2C		1.0.2-14	Operational	07/08/14 16:08:33	4	supported
00-17-0D-00-00-60-27-2E			Lost	not available	8	supported
00-17-0D-00-00-60-1E-19	10	1.0.2-14	Operational	07/08/14 16:08:13	4	supported
00-17-0D-00-00-60-1E-FD		1.0.2-14	Operational	07/08/14 16:07:51	5	supported

Figure 44 Admin Toolset Mote menu

- The Topology viewer shows network topology and nodes connection. In figure 45, which shows a mesh network (upstream paths), the green color indicates that the connections are successful, while the red color indicates the bad connection.

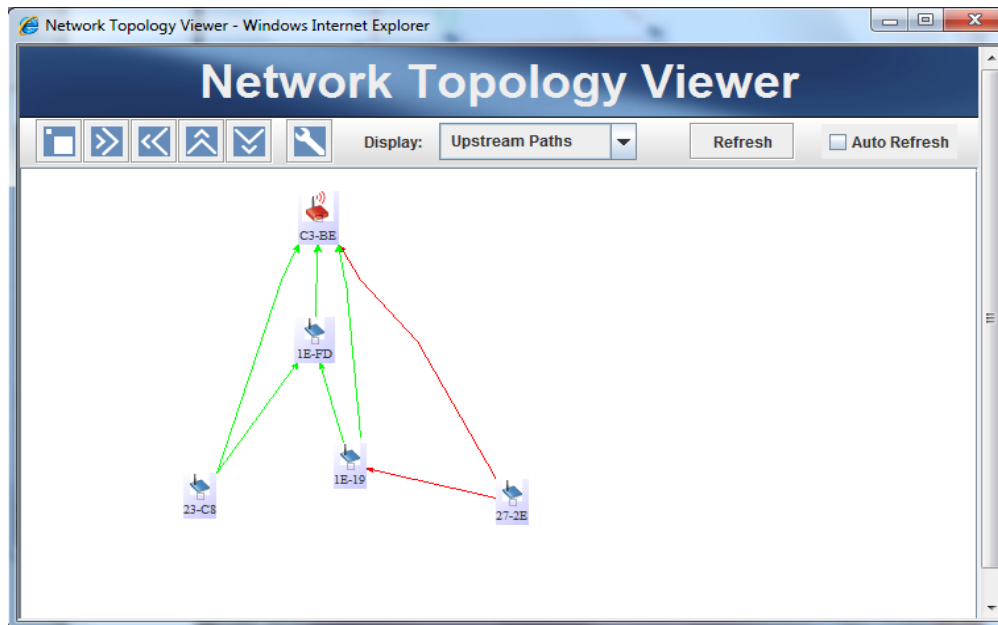


Figure 45 Admin Toolset Topology view (upstream paths)

Next figure shows the topology viewer for downstream paths.

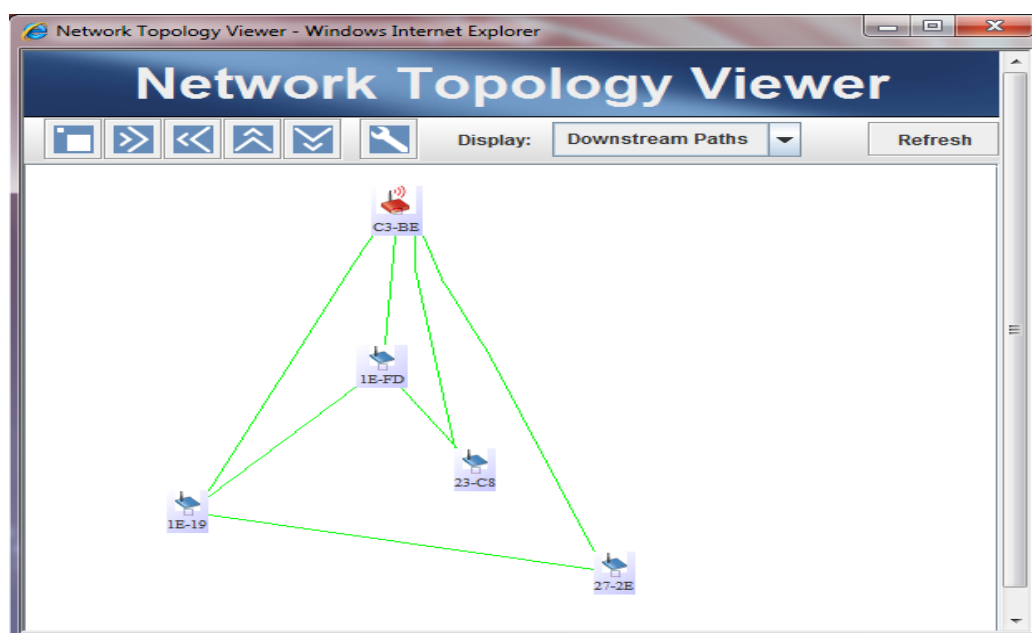


Figure 46 Admin tool set view (downstream paths)

Smart Mesh SDK applications

A: Temperature Monitor tool:

Smart Mesh SDK has a temperature monitor application to show the temperature reading by the sensor of each mote as shown in figure 47.

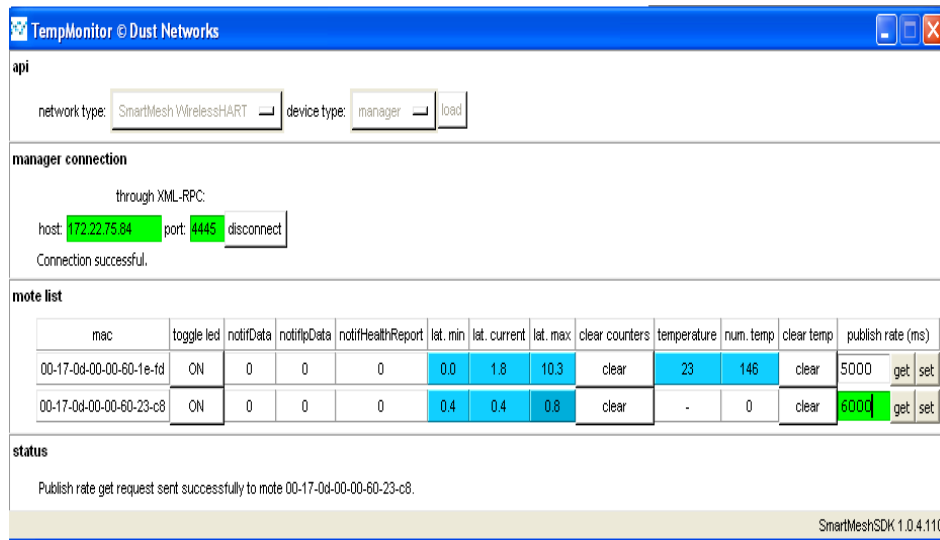


Figure 47 Temperature Monitor

B: Packet generator tool:

Packet generator tool shown in figure 48 is another application available for the network analysis.

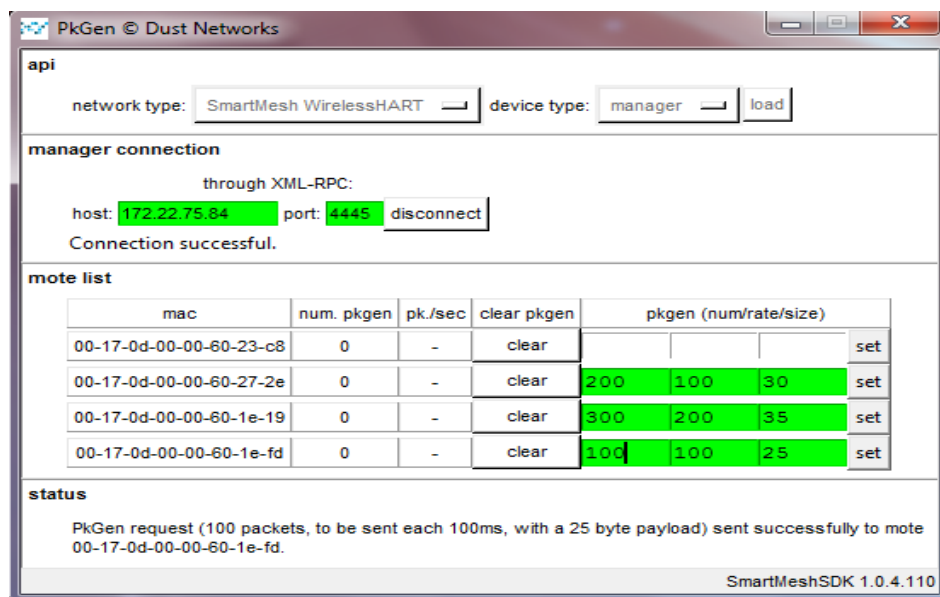


Figure 48 Packet Generators

